MILLENNIAL- TO CENTENNIAL-SCALE VEGETATION DYNAMICS IN RELATION TO OTHER ENVIRONMENTAL PROXIES DURING THE MIOCENE IN AND AROUND THE PARATETHYS SEA AND LAKE PANNON

Dissertation

zur Erlangung des Doktorgrades der Naturwissenschaften

an der Karl-Franzens-Universität Graz

Institut für Erdwissenschaften

vorgelegt von

Mag. rer. nat. Andrea Kern

Graz, Mai 2012

Contents

Preface **7**

Acknowledgements 8

Abstract **10**

Chapter 1 **14**

Introduction to the study area and applied methodology

1.1. Introduction 13

1.2. Regional situation - part 1: Paratethys Sea and Lake Pannon 16

1.3. Regional situation - part 2: Vegetation and climate 18

1.4. Vegetation and climate reconstruction based on paleobotanical records 20

1.5. Solar cycles and their reflection in geological archives 23

Chapter 2 **27**

Millennial-scale vegetation dynamics in an estuary at the onset of the Miocene Climate Optimum

2.1. Introduction 28

2.2. Geological setting 29

2.2.1. The Korneuburg Basin 29

2.2.2. The SPK-C + SPK-C1 Stetten section 30

2.2.3. Dating and time/sedimentation rate model 31

2.3. Material and Methods 33

2.4. Results 34

2.5. Discussion 37

2.5.1. Palaeoenvironments 37

2.5.1.1. Autochthonous brackish-marine depositional environments 38

2.5.1.2. Terrestrial environments 39

2.5.2. Palaeoclimate 41

2.5.3. The pace of environmental change 43

2.6. Conclusions 44
2.7. References 45

Chapter 3 **51**

Precipitation driven decadal scale decline and recovery of wetlands of Lake Pannon during the Tortonian

3.1. Introduction 52
3.2. Geological Setting 53
3.2.1. Stratigraphy, dating and age model 54
3.3. Material and methods 54
3.4. Results 55
3.4.1. Dinoflagellates – composition and patterns 55
3.4.2. Pollen and spores 58
3.5. Discussion 61
3.5.1. Palaeoclimate 61
3.5.2. Lake ecology and dynamics 63
3.5.3. Vegetation dynamics 66
3.6. Conclusions 69
3.7. References 71

Chapter 4 **81**

Strong evidence for the influence of solar cycles on a Late Miocene lake system revealed by biotic and abiotic proxies

4.1. Introduction 82
4.2. Geological setting 84
4.3. Methods 85
4.3.1. Sampling 85
4.3.2. Data analysis 86
4.4. Results 86
4.4.1. Natural gamma radiation (GR) 86
4.4.2. Magnetic susceptibility (MS) 90
4.4.3. Ostracods 91
4.4.4. Similarities and dissimilarities in the proxy records 93

4.5. Discussion 93
4.5.1. From depth to time domain – a hypothesis 94
4.5.2. Holocene solar cycles 95
4.5.3. Solar cycles in Miocene and Holocene times – a comparison 98
4.5.4. Ecological interpretation 99
4.6. Conclusions 101
4.7. References 103

Chapter 5 **109**

High resolution analysis of Upper Miocene lake deposits suggests the influence of Gleissberg-band-solar forcing
5.1. Introduction 110
5.2. Geological Setting 112
5.3. Methods 113
5.4. Results 114
5.4.1. Pollen 114
5.4.2. Dinoflagellate cysts 117
5.4.3. Ostracod and mollusc abundance 118
5.4.4. Geochemistry 119
5.4.5. Geophysics 120
5.5. Discussion 120
5.5.1. General paleoclimate 120
5.5.2. Vegetation reconstruction 120
5.5.3. Pollen zonation 121
5.5.4. Surface water conditions deduced from dinoflagellate cysts 123
5.5.5. The lake bottom 124
5.5.5.1. Ostracods and molluscs 124
5.5.5.2. Geochemistry and geophysics 125
5.5.6. General trends 126
5.5.7. Presence of solar cycles 129
5.5.7.1. Periodicities 129
5.5.7.2. Filtered records 123
5.5.7.3. Modulation of the Gleissberg cycles 134
5.6. Conclusion 135
5.7. References 137

Chapter 6 **146**

Millennial- to centennial-scale vegetation dynamics in relation to other environmental proxies during the Miocene along the Paratethys Sea and in and around Lake Pannon – a synopsis

6.1. Short-term environmental changes 147
6.2. Consideration of paleoclimatic estimates 149
6.3. Presence of sub-Milankovitch cycles in the Late Miocene 150
6.4. Conclusion 152

Chapter 7 **153**

References and supplementary material

7.1. Referenes 153
7.2. Supplementary Material Chapter 2 167
7.2.1. Pollen countings (Table 2.1) 167
7.2.2. Coexistence Approach climatic data (Appendix 1) 171
7.3. Supplementary Material Chapter 3 174
7.3.1. Pollen and dinoflagellate cysts counting (Table 3.1) 174
7.3.2. Coexistence Approach climatic data (Table 3.2) 190
7.4. Supplementary Material Chapter 4 193
7.4.1. Data set: magnetic susceptibility, natural gamma radiation, ostracod abundance (Table 4.1) 193
7.5. Supplementary Material Chapter 5 207
7.5.1. Collection of all measurements and countings (Table 5.1) 207
7.5.2. Coexistence Approach climatic data (Table 5.2) 219

Preface

This thesis combines several high-resolution multi-proxy studies, which focus on the short-term paleoenvironmental and paleoclimatological evolution during the Early and Late Miocene of Central Europe. Thanks to funding of the Austrian Science Fund (FWF Project P21414-B16), it was possible to examine specific questions, which can be summed up as follows:

(1) Which time resolution can be achieved beyond the ^{14}C range in previously well studied and dated localities by applying spectral analysis to high-resolution records.
(2) How do different environments react to changing conditions? Can a common trigger cause delayed response in different habitats?
(3) In which pace is the fossil vegetation changing on decadal to centennial scale?
(4) Are these environmental variations linked to shifting climatic parameters?
(5) Do short-term repetitive changes detected in the proxy records fit to any known sub-Milankovitch cycles, such as solar cycles?

Herein, four different studies are presented, one from the Early Miocene (~16.5 Ma; Korneuburg Basin) and three from the Late Miocene (~11.4 and ~10.5 Ma; Styrian and Vienna basins, respectively). The first study discusses the vegetation dynamics in an Early Miocene estuary at the western coast of the Paratethys Sea at the onset of the Mid-Miocene Climatic Optimum. The thematic priority was on documenting shifts within the subtropical vegetation during one 21-kyr-precessional cycle. The three other studies treated Late Miocene deposits of the paleo-Lake Pannon. Here, a much higher time resolution down to a decadal scale was achieved. Thus, aside from describing the environmental and paleoclimatological variations, one key aspect was to detect repetitive patterns in the high-frequency records.

The doctoral candidate performed all vegetation analyses and palaeoclimate reconstructions, including collecting in the field and sampling of the cores as well as partly preparing them in the laboratory. Further, she assisted in taking geophysical measurements. She performed the data analysis, applied various statistic methods and summarized the scientific results for publication. All results are already published or submitted to international, peer-reviewed, journals.

Chapter 1

An introduction into the topic and the applied methods is given.

Chapter 2

Kern, A., Harzhauser, M., Mandic, O., Roetzel, R., Ćorić, S., Bruch, A.A., Zuschin, M., 2010. Millennial-scale vegetation dynamics in an estuary at the onset of the Miocene Climatic Optimum. Palaeogeography, Palaeoclimatology, Palaeoecology 304, 247–261.

Chapter 3

Kern, A.K., Harzhauser, M., Soliman, A., Piller, W.E., Gross, M., 2012. Precipitation driven decadal scale decline and recovery of wetlands of Lake Pannon during the Tortonian. Palaeogeography, Palaeoclimatology, Palaeoecology 317–318, 1–12.

Chapter 4

Kern, A.K., Harzhauser, M., Piller, W.E., Mandic, O., Soliman, A., 2012. Strong evidence for the influence of solar cycles on a Late Miocene lake system revealed by biotic and abiotic proxies. Palaeogeography, Palaeoclimatology, Palaeoecology 329–330, 124–136.

Chapter 5

Kern, A.K., Harzhauser, M., Soliman, A., Piller, W.E., Mandic, O., submitted. High resolution analysis of Upper Miocene lake deposits suggests the influence of Gleissberg-band-solar forcing. Palaeogeography, Palaeoclimatology, Palaeoecology

Chapter 6

Millennial- to centennial-scale vegetation dynamics in relation to other environmental proxies during the Miocene in and around the Paratethys Sea and Lake Pannon – a synopsis

Chapter 7

References and supplementary material

Acknowledgement

First, I want to thank Mathias Harzhauser and Werner Piller for supervising my PhD project, Thanks for trusting in my skills to research these complex topics and for giving me the freedom to work in my way and speed. Further, to give me the possibilities to attend international meetings and likewise highly supporting me at the beginning of my scientific career. Additional, I want to thank all members of the Paleontological-Geological Department of the Natural History Museum of Vienna and the Department of Geology and Palaeontology, Institute od Earth Sciences of the University of Graz for support; in particular, Oleg Mandic and Patrick Grunert helped a lot. Of course, I thank Ali Soliman for cooperation in this project by sharing his insight into the dinoflagellate perspective and performing most of the lab work than me. I thank Martin Gross for cooperation concerning the Mataschen locality and Angela Bruch for introducing me into the Coexistence Approach as well as making me aware of its use/misuse. Also, I thank Johanna Eder for specific discussions and Gonzalo Jiménez-Moreno for numerous informations and helpful reviews and comments as well as colleagues at the Geological Survey for cooperation.

In the end I want to thank my family for supporting me.

Abstract

The presented thesis integrates key studies of high-resolution environmental changes of different Miocene time slices and depositional environments. A combination of different proxies, such as geochemistry, geophysics, palynology and benthic fauna (ostracods and molluscs), was used to detect short-term processes, which were compared to paleoclimatological estimates based on the Coexistence Approach.

1. The first investigated section formed in a paleo-estuary along the western coast of the Paratethys Sea. The age of the deposits ranges around 16.5 to 16.7 Ma, representing the late Burdigalian (Karpatian), when the Mid-Miocene Climatic Optimum began (Zachos et al., 1994; Böhme, 2003; Sun and Zhang, 2008). Based on a continuous 1.8-km-long section, the presence of astronomically forced sedimentary cycles could be outlined, which allowed to establish an age- and sedimentationrate-model for this section. To test the influence of the Milankovitch cycles on vegetation in a subtropical estuary, a certain 21-kyr-precession cycle was chosen for high resolution analysis of palynomorphs. The achieved sample resolution for this study ranged around 1-kyr per sample. Still, vegetation switched from salt marsh to a clearly freshwater dominated swamp forest of mainly Taxodioideae within few millennia. Soon after a rapid transgression flooded the estuary, establishing marine conditions. Several centuries later this was followed by further deepening, where dinoflagellates and other algae bloomed in the nutrient rich environment. The subsequent regression is immediately reflected by the expansion of non-forested wetland vegetation. All these changes happened on a millennial scale within an otherwise rather stable subtropical climate. Estimates show a pronounced seasonality of 9.6–13.3°C in the coldest month (CMT) and 24.7–27.9°C during the warmest month (WMT) with a mean annual temperature (MAT) of 15.7–20.8°C. Although the mean annual precipitation of 823–1372 mm (MAP) fits the previously assumed subtropical climate, the clear expression of a very dry phase with only 9–24 mm rainfall (MPdry), opposed by a wet season with 79–172 mm (MPwet), was rather surprising. Nevertheless, this manifestation of distinct seasons was recently correlated by stable isotope data on oystershells from the same locality (Harzhauser et al., 2010).
Hence, while environmental changes were rapid and the oscillations of the sea level influenced the vegetation of the estuary on Milankovitch-cycle scale, the overall composition remained the same. This suggests that the astronomically forced cyclicity of the sea level was not coupled with a climatic cyclicity in case of the investigation area. This misfit might be explained by the fact that the climatic amplitude is below the methodological resolution of the

Coexistence Approach due to the broad climatic range of c. 5°C for the MAT and of c. 500 mm for the MAP of the subtropical vegetation of the Early Miocene Korneuburg Basin.

2. A much higher sample density (1 cm) and likewise temporal resolution was achieved for the Late Miocene records. The first study was conducted on a 98-cm-long core from the Styrian locality Mataschen. It represents a coastal lagoonal setting along the shores of Lake Pannon.

Integrated stratigraphy suggests an early Tortonian age (early Pannonian) of ~11.3 Ma and a sedimentation rate of 7–14 years/cm (Gross et al., 2011). Aside from pollen, dinoflagellates were included to describe the surface water conditions within an interval of less than 1400 years of Late Miocene time. During this very short period, major change of climate is highly doubtful and consequently also no significant temperature variation could be observed (MAT 17.2–20.5 °C; CMT 9.6–13.3°C; WMT 24.7–27.9°C). Nevertheless, a shift in the mean annual precipitation is documented within decades forcing the vegetation to adapt. A drop of MAP to slightly less than 1000 mm resulted in different inundation periods of the lake surrounding marshes. This is reflected in a change in the dominating grasses from Poaceae and *Sparganium/Typha* to Cyperaceae. A subsequent increase of MAP towards ~1200 mm followed within only ~70 years. This higher precipitation caused a rise of the lake level but occurred with a slight lag of 4–6 decades. This transgression is clearly indicated by the takeover by the “open-marine” dinoflagellate taxon *Impagidinium* and a rapid dieback of the marsh vegetation. In the next hundred years, the non-forested wetlands could recover; either by a slow-down of the transgression or an adaptation of the plants to the ongoing lake level rise.

This study clearly shows climate as a main driving force even of small-scaled environmental changes. While the overall temperature is not significantly changing very much on such time scales and short periods in the Late Miocene, mean annual precipitation is less stable and fluctuates on a centennial scale. Moreover, the temporal resolution is comparable to Holocene records and thus the Miocene climate history could – hypothetically – be resolved with an identical precision.

3. Identical methods and the same sample density of 1 cm were applied by the second study on Upper Miocene deposits from Hennersdorf in the Vienna Basin. The sediments formed accordingly in Lake Pannon but are slightly younger (10.4–10.5 Ma; middle Tortonian/Pannonian) and in a more offshore setting. Contrary to Mataschen, where a very early stage of lake is preserved, the Hennersdorf core represents the phase of its maximum extension (Harzhauser et al., 2008). The investigated core is 6 m long and was taken without

core break. This resulted in a set of 600 evenly-spaced data points of magnetic susceptibility, natural gamma radiation and total abundance of ostracods.

These large data sets allow detecting sub-Milankovitch-scale cyclicities. Such cycles were already supposed to be present in the Mataschen record (Kern et al., 2012) and in a previous study on a 37-cm-long core from Hennersdorf (Harzhauser et al., 2008) but the sample number was too low in both cases to achieve statistical significant results. A combination of spectral analysis (Lomb-Scargle and REDFIT periodograms), wavelet analysis and the application of Gaussian filters to the raw data revealed prominent peaks within all three proxies. The ratios between the most prominent frequencies are strikingly similar to those between the most dominant solar cycles from Holocene ^{14}C and ^{10}Be data (Solanki et al., 2004). Based on the assumption that the observed peaks correspond to solar cycles, a best fit sedimentation rate was calculated ranging around ~13.7 years/cm, which is only slightly higher than previous offshore estimations of equal time (e.g. Lirer et al., 2009). Based on this estimate, the investigated core corresponds to ~8220 years. Converting the frequency peaks from depth domain into time domain results in a perfect correlation to the lower and upper Gleissberg cycle, the deVries/Suess cycle, the unnamed 500-year and ~1000-year-cycle and the 2400-year Hallstatt cycle. Striking similarities appear also in the wavelets of the magnetic susceptibility and the Holocene isotope data of Solanki et al. (2004), suggesting a comparable modulation of the cycles. Significant differences, however, are the presence of a 350-year-cycle in the Holocene record and the appearance of a 1500-year-periodicity in all three fossil records. This suggests influence of the 1500-year "Earth-system-immanent-cycle" that is not directly linked to a known solar cycle but is well documented from other climate archives (Debret et al., 2007).

4. Based on this correlation and time model, a shorter part of the core was chosen for detailed palynological (pollen and dinoflagellates) and geochemical analyses (total carbon, total organic carbon, carbonate and total sulfur). In addition to the presence and abundance of benthic ostracods, molluscs were evaluated. The studied interval was limited to ~2000 years and a sedimentary sequence of 1.5 m. This length limited the possibility to detect statistically significant cycles to the lower and upper Gleissberg cycles and the deVries/Suess cycle.

Climate estimates based on the Coexistence Approach suggest a stable climate with a wide range between 15.6–20.8°C MAT (CMT 5–13.3°C; WMT 24.7°C–27.9°C) and a MAP of 823–1529 mm (MPdry 9–24 mm; MPwet 79–172 mm). Similar to the Mataschen core, no major temperature shift can be deduced from the core data as well as a stable precipitation level. The overall vegetation composition did not change significantly during the 2 millennia of Late Miocene time. Nevertheless, pollen spectra suggest distinct changes in the contribution by

certain taxa, which indicate mainly variations in transport mechanism and/or intensity. A detailed analysis of all proxies revealed a rapid fluctuation of lake bottom and lake surface water conditions, which are related to a decrease of fluvial input and the onset of wind dominated matter flux. Phases of low bottom water oxygenation and lake stratification led to a collapse of the ostracod populations and are usually outlined by low TOC/TS ratios and higher magnetic susceptibility values, which may point to prolific conditions for sulfur bacteria. Towards the top of the core, the contribution by wind transport seems to decline and phases of high hinterland input alternate with intervals of predominant contribution from the close by wetlands.
Several of these observed changes occur simultaneously in many proxies and display repetitive patterns. These appear in frequencies of 123–114, 82–67 and 55–48 years, which point towards the influence of the upper and lower Gleissberg cycles. The observed changes in wind intensity and probably also direction, as revealed by the pollen spectra, might document the influence of these solar cycles on prevailing weather conditions. This could partly be explained by feedback mechanisms between solar energy and cloud formation. Moreover, both frequency bands of the Gleissberg cycle are modulated by higher order cycles such as 1000-years-cycle and the quasi-periodic Earth-system-immanent 1500-years-cycle. Especially, the long trend in windiness fits to the 1000-years-modulation and might explain its prevalence in hinterland proxies.

All these Miocene data are absolutely comparable with Holocene case studies in resolution and modulation. Further, the presence of solar cycles is proven for pre-glacial records. Overall, however, the results show also very convincingly that the various proxies respond to a certain solar cycle in a very individual way and that straightforward predictions are difficult. Moreover, the non-parallel developments of many lake surface, lake bottom and hinterland proxies suggest a non linear environmental response to solar forcing.

Chapter 1

Introduction to the study area and applied methodology

1.1. Introduction

During the last decade, new techniques allowed scientists to analyze Earth's deep time with increasing resolution and precision. Especially the cooperation between earth science and astronomy resulted in unexpected synergies and now provides the fundament for astrochronology (Laskar et al., 2011). Similarly, the understanding of isotope chemistry increased the possibilities to interpret geological archives in terms of paleoenvironment and paleoclimate. This led to a well resolved model of global Cenozoic climate history (e.g. Zachos et al., 2001). Although most long term trends were deduced from deep marine cores also shallow marine and terrestrial ecosystems mirror equal global climatic trends (e.g. Utescher et al., 2000; Bruch et al., 2007; Brandano et al., 2010 and references therein). Observations of the modern climate system and many Holocene records show, the interaction of atmosphere and temperature is complex and climate models reported important inter-hemispheric differences (Gordon, 1992; Jones et al., 2011). These regional distinctions are often neglected when global climate models are generated, but are prominent in models focusing on this phenomenon (Flato and Boer, 2001). Nevertheless, the situation of each certain site is always influenced by local conditions, which may be modulated by special wind situations, precipitation and/or current patterns. To understand the climate system in more detail and also to test models, the fossil climate archives can be utilized. Past climate changes are usually discussed in terms of Milankovitch cycles (Hays et al., 1976; Milankovitch, 1941), which have been influencing the climate potentially throughout Earth's history (de Boer and Smith, 2009). In 1930 Milutin Milankovitch proposed regular changes of the Earth's movement around the Sun, which he described as eccentricity, obliquity and precession. Their periodicities are quite different in duration (eccentricity 400,000 and 100,000 years; obliquity 41,000 years; precession 19,000 and 21,000 years), and thus, their impact on the climate is different as well. The long eccentricity changes directly result in a diverse intensity of sunlight reaching the earth and thus affect temperature of all latitudes more or less equally. Obliquity refers to the variation of the earth axis between 22.1° and 24.5°, which results into a different dispersal of sunlight and likewise controls the expression of seasonality. The dissimilar intensities of each season along the latitudes are additionally controlled by precession (Laskar et al., 1993). Pleistocene and Holocene records revealed further repetitive patterns with even shorter durations. So-called Dansgaard-

Oeschger (e.g. Dansgaard et al., 1969; Dansgaard,1985; Grootes et al., 1993; Bond and Lotti, 1995) cycles happen within app. 1470 years, coinciding with an abrupt warming, followed by a slow cooling phase (Alley, 2000). During the last glacial period, these processes could later be linked to stronger cold events, called Heinrich events (e.g. Heinrich, 1988; Bond and Lotti, 1995; Bond et al., 1997; Hemming, 2004), which led to a greater number of ice rafted debris to be brought into more southern latitudes. One explanation is the interruption of the thermohaline circulation in the Atlantic, which mainly affected the northern hemisphere (Hinnov et al., 2002; Sanchez-Goni et al., 2002; Debret et al., 2009).

Such observations of re-appearing climatic shifts can only be collected by using high resolution analyses. For continental records, aside from geochemistry, especially pollen analyses are a suitable tool to reconstruct vegetation dynamics and climate with a high temporal resolution. The most suitable archives for high resolution palynological analyses are long-lived lakes or bogs, where drilled cores easily provide a high sample density. Within the Late Pleistocene and Holocene, the resolution of these palynological studies reach down to decadal- and centennial-scale (e.g. Sanchez-Goni et al., 2002; Jiménez-Moreno et al., 2007; 2008; Gonzalez and Dupont, 2010). While these studies are usually backed by ^{14}C datings, such basis is missing for older records. Beyond, astronomical tuning often emerged as a useful tool to evaluate sedimentation rates and to estimate how much time is represented in a certain sequence. Among the earliest successful attempt to apply this astronomical tuning to a continental succession was performed in the Early Pliocene Ptolemais Basin in northern Greece. There well preserved sedimentary cycles are crop out showing a pattern triggered by precession and obliquity. Kloosterboer-van Hoeve et al. (2006) observed one of these precession cycles in more details, showing distinct millennial scale alternations within the vegetation (11–10 and 2.5–1.5 ka). Although no extensive glaciations of the Arctic occurred during the Early Pliocene (e.g. Zachos et al., 2001; Moron et al., 2006; Micheels et al., 2009), these frequencies agree well with cyclicities known from the Pleistocene glacial. Shorter periodicities were not detected by Kloosterboer-van Hoeve et al. (2006) due to the low sampling density. This study, however, documented sub-Milankovitch cycles were influencing Earth’s climate prior to the ice ages and can therefore not be limited to feedback mechanism of the thermohaline circulation as previously expected (Bond et al., 1997; Kloosterboer-van Hoeve et al., 2006).

To explore the existence of such short-term cyclic climatic changes also in the Miocene, we decided to focus on localities from the Late Miocene with a greater focus. The Late Miocene stage of the Tortonian is of special interest as it represents a past counterpart to near future climate scenarios (Meehl et al., 2007). The prevailing climate was several degrees warmer (e.g. Bruch et al., 2006; Böhme et al., 2008; Utescher et al., 2009; Micheels et al., 2009;

Pound et al., 2011). While the South pole was permanently covered with ice, the Northern glaciation was currently setting in (e.g. Lear et al., 2003; Moron et al., 2006; Utescher et al., 2009; Micheels et al., 2009). Model experiments additionally tried to solve the prevailing atmospheric CO_2 conditions, which varied between 360 and 460 ppm (McFadden, 2005; Micheels et al., 2009). This may not be significantly higher than at the moment, but a simple CO_2 rise cannot explain warm global conditions alone (Steppuhn et al., 2007; Micheels et al., 2009). Hence, studying small scale climatic variations in the past may support recent climatic change studies by providing information of environmental response within such a globally warmer system. During this warm Tortonian phase, the Eastern Austrian basins were characterized by a huge lake called Lake Pannon, which covered the entire Pannonian Basin System. Well-log analysis and 3D seismic allows a good correlation and dating of these lake deposits (Kosi et al., 2003; Harzhauser et al., 2004). Further, the presence of Milankovitch cycles was proven by Lirer et al. (2009), Paulissen et al., 2011 and Paulissen and Luthi (2011), as well as cycles on smaller scale have been discussed already by Harzhauser et al. (2008) and Paulissen and Luthi (2011) in these deposits. Still, a clear link to known sub-Milankovitch cycles was missing so far.

1.2. Regional situation - part 1: Paratethys Sea and Lake Pannon

The idea of this study is to resolve small-scale vegetation and climate changes within the frame of an already well studied paleogeographic settings of the Paratethys Sea and Lake Pannon.

A. The Paratethys Sea was a mainly epicontinental sea that formed during the terminal Eocene (Baldi, 1980; Rusu, 1988). Marine conditions prevailed but were repeatedly interrupted by hypo- and hypersaline phases, which were caused by disconnections from the world's oceans (Rögl, 1998). A detailed overview of the paleogeography and paleoecology of this sea is given in Rögl (1998), Popov et al. (2004) and Harzhauser and Piller (2007). An account on the regional stratigraphy and the correlation with global stages is presented in Piller et al. (2007). One of the herein presented study focuses on the late Karpatian, which corresponds to the late Burdigalian of the Early Miocene. At this time, the Korneuburg Basin in Austria was part of an estuary that formed at the onset of the Mid-Miocene Climatic Optimum. The only c. 20 km long and 7 km wide basin is part of the Alpine-Carpathian thrust belt and originated as a sub-basin of the Vienna Basin during its early piggy-back stage. Reactivation of thrusts as strike-slip faults in the Early Miocene caused a rapidly subsiding pull-apart type basin. The depositional environments of this basin are documented by several hundreds of meters of shallow marine sediments (Wessely, 1998). Its paleoecology and fossil content was described in great detail in numerous papers published in Sovis & Schmid (1998; 2002). The studied Stetten section is part of a c. 120-m-thick section comprising lignites, clay, silt, sand and rare pebble layers with abundant coquinas. For this study, 21 m of the section (N48°21'47.82'' - E016°22'0.12'') were measured and sampled in more detail to achieve quantitative data on the vegetation and climate fluctuations surrounding this estuary.

B1. The ongoing continentalisation of central Europe during the latest Middle Miocene and Late Miocene caused the Central Paratethys to retreat to the east and gave rise to the formation of Lake Pannon within the Pannonian Basin Complex (Rögl, 1998; 1999; Magyar et al., 1999). This change is also reflected in the regional stratigraphy and the beginning of the Tortonian is coeval with the onset of the Pannonian (Harzhauser et al., 2004; Piller et al., 2007; Harzhauser and Mandic, 2008; Paulissen et al., 2011). In this lake, salinity strongly declined to brackish and slightly alkaline conditions, causing a distinct turnover in its biota (Müller et al., 1999; Harzhauser and Piller, 2007). Based on the endemic evolution of the molluscs, Papp (1951) defined a division into ecozones (A to H), which were later revised by Magyar et al. (1999) and Harzhauser et al. (2004).

Magyar et al. (1999) illustrate the evolution of Lake Pannon focusing mainly on its paleogeography. The initially very low lake level led to an exposition of many large islands. Even a separation of the lake into smaller water bodies was suggested, this phase may have been very short as no form of endemism appeared (Magyar et al., 1999). Deposits of this phase are outcropping especially in the eastern Styrian Basin (Austria) and are well exposed at the locality Mataschen where c. 30 m of pelitic to psammitic deposits of the Feldbach Formation were studied in great detail (Gross et al., 2008; 2011). The Styrian Basin formed as a subbasin of the Pannonian Basin Complex during Miocene and Pliocene at the eastern margin of the Eastern Alps. It is about 100 km long and about 60 km wide and contains up to 4000 m of Neogene sediments (Kollmann, 1965; Sachsenhofer, 1996). The Pannonian basin fill is well resolved by seismics and sequence stratigraphy (Kosi et al., 2003) and integrated stratigraphy allowed a dating of the studies interval to ~11.42 to ~11.26 Ma (Gross et al., 2011). High sedimentation rates of ~0.7 to ~1.5 mm/yr and minor bioturbation revealed the studied core as perfect candidate for high-resolution studies.

B2. First transgressive pulses of Lake Pannon started during the early Pannonian and large areas surrounding the lake became flooded. Its maximum extension was achieved later during the middle Pannonian at around 10.5–10.0 Ma (Korpás-Hódi, 1983; Sütő-Szentai, 1991; Magyar et al., 1999; Harzhauser et al., 2004). This phase is reflected in most basins by the formation of thick layers of blue green clay, which are included in the Bzenec Formation in the Vienna Basin. This basin was formed during the Neogene as a rhombohedral pull-apart basin with a SSW-NNE orientation of 200 km length and 55 km width (Royden, 1985; Wessely, 1988; Harzhauser et al., 2004). It formed during the Miocene between the Alps and

the Carpathians along sinistral fault systems, enabling extrusion of crustal blocks from the Eastern Alps (Neubauer and Genser, 1990; Linzer et al., 2002; Ratschbacher et al., 1991). A detailed overview of the evolution of the Vienna Basin and its depositional environments, including an extensive list of references, is presented in Royden (1985), Wessely (1988) and Kováč et al. (2004). The Pannonian basin fill of the Vienna Basin was described by Harzhauser et al. (2004) based on well-log data. Lirer et al. (2009) and Paulissen et al. (2011) performed spectral analyses on geophysical well-log data and were able to detect several astronomical cycles. Due to a new magnetostratigraphy, it was possible to tune the logs to astronomical target curves and to establish a well constrained age-model for the Pannonian of the Vienna Basin. Based on these data, the herein studied Hennersdorf section was correlated and dated indicating an age of ~10.5 to ~10.4 Ma. A very high sedimentation rate of ~0.73 mm/yr and largely dysoxic bottom conditions during deposition suggested the locality as promising section for high-resolution studies.
Afterwards the lake retreated from the Vienna Basin and established its shores in western Hungary (Magyar et al., 1999). From 9 to 8 Ma the alluvial plains and wetlands developed in the Vienna Basin and sedimentation was restricted to small areas (Harzhauser et al., 2004). Accordingly, samples from the Gbely Formation were barren of pollen and could not be analyzed within this thesis.

1.3. Regional situation - part 2: Vegetation and climate

The overall Cenozoic climate development was outlined by Zachos et al. (2001) based on stable oxygen data from deep sea cores and refined in countless contributions thereafter. The most salient phases are the long and very warm climate optimum from the late Paleocene to the Eocene, followed by the distinct Eocene/Oligocene cooling. The next and last global temperature optimum started during the late Early Miocene and had a dramatic influence on early Middle Miocene biota. This Mid-Miocene Climatic Optimum is followed by a stepwise decrease in global temperatures which finally culminated in the Pleistocene glacials. The large scale Cenozoic climate history is mainly based on marine records, often deriving from deep-water data. As a consequence, continental records are important to compare the marine trends with the terrestrial sphere. Moreover, the established vegetation is an important factor for regional climate as it controls distinct climatic factors such as albedo and evaporation (Bonan et al., 1992; de Noblet et al., 1996; Hoffmann and Jackson, 2000). Generally the large scale climatic trends, deduced from continental records, are in good agreement with those based on marine data (e.g. Utescher et al., 2000; 2009; Mosbrugger et al., 2005; Bruch et al., 2006). From the end of the Oligocene, a slight warming took place, peaking into the Mid-Miocene Climatic Optimum, followed by an overall cooling

(Utescher et al., 2000; 2009; Böhme et al., 2007). The Mid-Miocene Climatic Optimum is mirrored in the paleo-vegetation by the presence of taxa, which nearest living relatives are found in areas characterized by distinctly warmer climate (Mai, 1995). A high percentage of broadleaved evergreen plants (more than 30%) within the forest vegetation and mangroves at the sea-shores are typical (Kvaček et al., 2006; Kovar-Eder et al., 2008). Following Mai (1964) this vegetation type was called "Younger Mastixoid Flora" due to the high percentages of Mastixiaceae. Additionally, among the thermophiles, Lauraceae, Theaceae, Symplocaceae, Sapotaceae, *Engelhardia* and several evergreen Fagaceae were ubiquitous (Kvaček et al., 2006). Modern counterparts of this flora are mainly found in Southeast Asia or Florida, where the temperatures remain above the freezing level during the cold months (Kvaček et al., 2006; Utescher et al., 2009). Specifically, the evergreen oak-laurel forests in southern parts of China, Burma, Vietnam, and southern islands of Japan and on Taiwan are considered as modern analogues (Kovar-Eder and Hably, 2006).

With the onset of the Middle Miocene Climate Transition (Shevenell et al., 2004; Lewis et al., 2007), distinct changes of the prevailing vegetation happened as the thermophile plants started to move towards refuge areas in south-east Europe (Givulescu, 1957; Stuchlik et al., 1999; Kovar-Eder et al., 2006). A major turnover occurred on the Asian continent. Due to the rise of the Himalaya, the Asian monsoon system intensified (e.g. An et al., 2001) and less humidity was transported towards the continent (e.g. Liu et al., 2009). Botanically, this is mirrored by an expansion of C_4 grasses, which out-competed the C_3 grasses by their better adaptation to dry conditions (Pegani et al., 1999; Molnar, 2005; Tripple and Pagani, 2007). Additionally, the rise of the Tibetan Plateau lead to the exposure of a wide area of silicate-rich sediments, which caused a higher evaporation rate and reduced atmospheric CO_2 (Quade et al.,1989; Guo et al., 2002; Spicer et al., 2003; Harrison and Yin, 2004; Sun and Wang., 2005). In Europe, this downward trend caused a migration of the evergreen plants to the south (e.g. Utescher et al., 2000; 2009; Kovar-Eder et al., 2008). The resulting forest assemblage is compared to a Mixed Mesophytic forest, which is only rarely preserved in natural vegetation today. Few examples may be found along the Appalachian Mountains (USA) (McCarthny et al., 2001) or Eastern Asia (Wolfe, 1979; Kvaček et al., 2006) or the Chinese humid subtropical forests (Kovar-Eder et al., 2006). There, Neogene taxa such as *Pinus* and *Cathaya* are growing together with Ericaceae on the rocky slopes, associated with evergreen and deciduous taxa such as *Castanopsis*, *Quercus*, *Cunninghamia* and different Lauraceae.

The paleobotanic and paleoclimatic evolution of Europe during the Miocene was illustrated on paleo-vegetation/climate-maps by Bruch et al. (2006; 2007), Kovar-Eder et al. (2006) and Kvaček et al. (2006). A collection of coeval sites was combined, often by using an interpolation to decipher gradients over Europe and various time-slices (Bruch et al., 2006).

These maps give further information on precipitation trends. Especially during the Tortonian, rainfall in Europe was higher than today, also referred as “washhouse climate” by Böhme et al. (2008). Similar to the modern situation, northern Europe was wetter and precipitation decreased towards the south but with a less steep gradient than today (Bruch et al., 2006). The overall cooling trend is accompanied by a decrease in precipitation (Utescher et al. 2000; Bruch et al., 2006), leading to more and more dry conditions in the south. Another important factor for the European climate today is the differentiation between the warmer and wetter oceanic climate, which is strongly influenced by the Gulf Stream, and the dry areas inside the continent. There, a stronger seasonality of temperature and low precipitation are characteristic. Although the development towards a pronounced seasonality and latitudinal gradients was described by several authors before (e.g. Utescher et al., 2000; Mosbrugger et al., 2005; Bruch et al., 2006; 2007), focus lay on summer and winter temperatures only, but the annual range of rainfall was often neglected. Bruch et al. (2011) tried to scrutinize the existing data and documented that very wet conditions prevailed during the Mid-Miocene climatic optimum in Europe as well. Latitudinal differences remained weak to absent up to Tortonian times, when annual precipitation was clearly higher all over Europe by a presumed higher summer rainfall than today. During the Tortonian a distinct intensification of the seasonality developed. This climate evolution caused a partly opening up of the vegetation firstly in the southern part of Europe and is also indicated by the mammal assemblages (Augustí et al., 1999; Fortelius et al., 2006). From the Messinian on, distinct gradients developed between the western, the eastern and southern part of Europe (Kovar-Eder et al., 2008; Bruch et al., 2011).
Concluding, the data on seasonality, precipitation and vegetation dynamics parallel the large-scale trends revealed from the marine sphere but usually remain within a time resolution of millions of years.

1.4. Vegetation and climate reconstruction based on paleobotanical records

Different approaches were developed during the last decades to quantify paleoclimate based on plant fossils. In the marine system, climate reconstructions are frequently based on stable isotopes ($\delta^{18}O$ and $\delta^{13}C$) (e.g. Zachos et al., 2001; Lear et al., 2003). For botanical marcofossils, such as wood, a comparable method could be applied as well, but usually no long and continuous records are available. Further, the data often resulted in problematic interpretations (Birks and Birks, 1980; Guiot, 1994) and are also highly regional (Mosbrugger and Utescher, 1997). A more promising attempt is based on plant physiognomy, which was introduced by Wolfe (1979; 1993) as the CLAMP analysis (Climate Leaf Analysis Multivariate Program). This method utilizes various morphological features of a leaf and compares these with modern counterparts and their ecological requirements. It simply relies on morphology and does not focus on detailed taxonomic identifications (e.g. species, genus or family level). This taxonomic vagueness, which can be seen as major drawback of the method, provides the possibility to apply this method to geologically old floras which lack close relatives in the modern flora.

Another widely used method is the Coexistence Approach (CA), which is based on comparing fossil taxa with their nearest living relatives. This idea is long known, and basically assumes, that these closely related plants occupy the same climatic range as well as ecological conditions in their natural distribution today, as their fossil counterpart did in the past (discussion in Mosbrugger and Utescher, 1997). The basic idea is a comparison of each fossil taxon with its nearest living relatives to gain information of its climatic range based on its distribution today. Thus, for each plant of the fossil assemblage a climatic interval can be described, which is limited by the data collected from recent flora.

Considering the whole assemblage, a climatic range appears, in which all these fossil taxa hypothetically could have lived. This is named the Coexistence Interval and represents the paleoclimatic estimate expressed in a range of temperature, warmest and coldest month temperature as well as annual rainfall and the precipitation of the warmest, wettest and driest month. Outliers of this interval can appear which are mainly caused by misidentifications or problems with the comparability of the ecological requirements of the suspected living relative. As the climate database of the CA relies on real climatic measurements, also estimates on seasonality can be given (Mosbrugger and Utescher, 1997). A clear weakness of the Coexistence Approach, however, is that it only evaluates the presence or absence of taxa but neglects their abundance. Further, it does not consider taphonomy and in the case of palynology, it is often unable to distinguish between species or even certain genera, it may unite plants living in different areas including higher elevated environments. These elements can be excluded for each study manually, which introduces some degree of subjectivity. Also, the nearest living relative of a fossil plant may not always be clear or may be doubted by other specialists. Comparisons between the different methods usually reveal a good overlap in results. The CLAMP method gives more precise values in cases, where the Coexistence Interval has a wide range (Kvaček, 2007) but often estimates slightly lower temperatures (e.g. Uhl, 2006; Uhl et al., 2006). Hence, the Coexistence Approach is the best method to reconstruct paleoclimate from palynological data.

Nevertheless, the reconstruction of paleoconditions based on pollen/spores has to consider several intricacies. Although their walls are built up by sporopollenin, which counts to one of the most stable materials in nature (Klaus, 1987; Wiermann und Gubatz, 1992), the preservation of pollen grains is limited to fine grained sediments, mainly silt and clay. This results from the fact that the sporopollenin-wall is resistant against acids but is easily

damaged by basic solutions. Therefore, clay and silt are favored for palynology as they reduce the amount of pore waters to a minimum (Klaus, 1987) and likewise avoid oxidation. Further, several plants produce thin walled pollen grains with very low preservation potential. Unfortunately, this includes the families of Lauraceae, Theaceae and some Magnoliaceae, which rank along the most important components of Miocene forests according to leaves and diaspores (Hofmann and Zetter, 2005; Kovar-Eder and Kvaček, 2006). Pollen identification with the light microscope is limited usually to the family and genus level. To distinguish species of the same genus is usually only possible by a combination of light and scanning electron microscopy (Zetter, 1989; Zetter and Ferguson, 2002). This method is extremely time-consuming and impossible to be applied for huge sample sets as used in the herein presented studies. Thus, the taxonomic composition of an assemblage and the identification level of its taxa are better resolved in the fossil leaf record than with pollen/spores or fruits/seeds. A drawback of the leave-floras, however, is that they mainly represent the azonal vegetation (Kovar-Eder and Kvaček, 2007), which in turn can be etected by palynology due to the wide dispersion of pollen grains and spores.
Further, the amount of produced pollen is a factor obscuring the results. Each taxon is different concerning its pollen productivity. Principally, plants, which pollen are dispersed by wind produce more pollen than animal-pollinated ones (Klaus, 1987). Even within the anemophilous plants, there are large differences in how far pollen grains usually are transported. This leads to an overrepresentation of certain taxa in the fossil assemblages, especially of Pinaceae. Also several angiosperms display a very high pollen production and a far-distance dispersal mechanism, e.g. *Alnus* or *Corylus* (Kvavadze and Stuchlick, 1990).

These plant based reconstruction should further be compared with other terrestrial climate indicators. A good index was developed by Fortelius et al. (2002; 2006) and Eronen (2006) using hypsodont large mammals to reconstruct precipitation. Basically, the drier the area, the higher teeth are developed by specific mammals, which complements the difficulties in reconstructing low precipitation values from plant fossils as these conditions are often unfavorable for plant preservation. Another application is the reconstruction of climate based in the occurrence of amphibians and reptiles (Böhme et al., 2006). Reptile species richness is directly linked to temperature and rainfall as well as sunlight as heat source. Therefore, different groups were created referring to ecophysiolocial strategies, which give information on precipitation, correlating especially dry-climate-interpretations based on paleobotanical records.

1.5. Solar cycles and their reflection in geological archives

Throughout the human history, phases of colder and warmer climate occurred and influence the cultural development (Schimmelmann et al., 2003; Versteegh, 2005; Grey et al., 2010). The repetitive nature of some of these climatic changes during the Holocene called for an explanation by an external forcing mechanism as provided by the variations of solar activity. While ancient Chinese and Korean astronomers (Bray and Loughhead, 1965) already had observed changes in the solar activity by naked eye observation, western scientists considered the emitted energy of the Sun to be roughly constant. The first recognition of changes on the sun's surface by a European goes back to the German astronomer Samuel Heinrich Schwabe, who studied the presence of sunspots and recognized a periodicity of c. 11 years in their appearance and abundance (Schwabe, 1844). A sunspot appears as a dark area on the solar surface. Although small parts of the sun likewise release less energy, the total sun emits more energy during phases of intense sunspot presence due the development of extremely highly energetic solar flares (Wilson et al., 1981; Grey et al., 2010). Satellite measurements of the total solar irradiance since 1976 and NASA pictures verified the near-regular 11-years-change in the number of sunspots (Hoyt and Schatten, 1998). Although the repetitive behavior is obvious and accepted by the scientific community, the origin of the sunspots is still discussed (see e.g. Grey et al., 2010 for an overview). The well documented 22-years-periodicity was named Hale cycle. Since its duration is the double of a Schwabe cycle a link between both is obvious. The trigger mechanism of the Hale-cycle is mainly understood: due to the rotation of the sun, its magnetic field is turned over within that period, affecting the amount of emitted energy (Hale et al., 1919; Babcock, 1961; Benevolenskaya, 1998). Another postulated solar cycle is the Gleissberg cycle (Wolf, 1862; Gleisserg, 1939; 1965; Peristykh and Damon, 2003). At first, most studies discussed a duration of about 88-years with a very broad frequency variation. In consequence, this cycle appeared rather instable concerning length and intensity. Orgutsov et al. (2007) were able to document that this cycle in fact comprises two main bandwidths of 50–80 and 90–140 years, respectively. Hence, these are now referred to as lower and upper Gleissberg cycles. Both were also detected in the Miocene records (see chapters 4 and 5). The next cyclicity is called deVries or Suess cycle by a duration of 200 to 210 years (Damon and Sonett, 1991; Stuiver and Brazinas, 1993), whose expression in numerous Holocene records is striking (Schimmelmann et al., 2003; Raspopov et al., 2008; Tarrico et al., 2009; Di Rita, 2011). Several additional solar cycles with longer frequencies have been described, but their detection relies on proxy data only as their long duration cannot be significantly described by direct observations (Beer et al., 1990; Hoyt and Schatten, 1998). A ~350-years-cycle (Solanki et al., 2004; Yin et al., 2007), a 500 to 550-years-cycle (Stuiver et al., 1995; Chapman and Shackleton, 2000), a ~1000-years-cycle (Stuiver et al., 1995; Chapman and

Shackleton, 2000; Debret et al., 2007) and the ~2400-years-Hallstatt-cycle (Damon and Sonett, 1991; Charatova, 2000; Nederbragt and Thurov, 2005) are statistically significant and well documented from various geochemical and sedimentological archives. According to the ^{14}C records from tree rings, the ~200-year (160–210) and the 2400-year-cycle (2200–2600) are most prominent (e.g. Suess, 1980; Sonett and Finney, 1991; Damon and Sonett, 1990). A clear astronomical documentation of solar cycles was reported by Jose (1965), who pointed out re-occurring long-term changes of 178.7 years, fitting more or less to the strong ~200-years-cycle (verified by Fairbridge and Sanders, 1987; Jakubcova and Pick, 1987). Proxy-based studies are common, but the requirement of having either a high sample density to reveal short cycles or covering a time span long enough to detect a significant repetition of the longer cyclicities, is still problematic (Charatova, 2000). Although the origin of the very short solar cycles seems to be solved, the cause of longer cyclicities is still unexplained (Versteegh, 2005). As the sun behaves like a typical star, the energy output is constantly varying (Tsiropoula, 2003). Further, the movement of the big planets of our solar system (Jupiter, Uranus and Neptune) influences the rotation of the sun, which is circling within a diameter of $3*10^6$ km around the center or mass of the solar system, resulting likewise in different solar input of the Earth. Beer et al. (2000) summarized some sun-related processes, which may lead to energy variations, e.g. the nuclear fusion in the core of the Sun or the transport through the radiative and convective zone of the sun. On the other hand, also the magnetic activity of the sun may contribute to such changes (Gray et al., 2010).

For a long time it was assumed, that these solar variations are too weak to influence the Earth’s climate. Nevertheless, the periodicity of the deVries/Suess cycles agreed well with cold phases during the human history’s last millennium (Wagner et al., 2001; Solanki et al., 2004), which are further expressed as long phases or low sunspot activity. To explore the connection of climate and solar activity, a comparison between different approximations and historical records was conducted (Versteegh, 2005). Most suitable records are the measurements of cosmogenic radioactive isotopes such as ^{14}C or ^{10}Be (Rainsbeck and Yiou, 1980; Beer et al., 1983; 1990). These are produced by interaction in the Earth’s atmosphere with cosmic-ray particles, which intensity are modulated by solar activity (Beer et al., 1990). Details between the relationship of solar activity and cosmic ray flux are not well understood, but their anti-correlation was obvious (Beer et al., 1990). ^{14}C and ^{10}Be are produced by nuclear reaction in the atmosphere. Later, ^{14}C is oxidized into CO_2 and transferred into the carbon cycle. Unlike, ^{10}Be is mainly attached to aerosols, where it is brought to the Earth’s surface to a large extent by precipitation. Therefore, ^{10}Be records always have to be considered with care, as rainfall may reflect a very local signal only (Beer et al, 1990). Main source for ^{14}C analyses are tree rings (e.g. Suess, 1980; Sonett and Suess, 1984; Raspopov et al., 2004; Nordemann, 2005; Rigozo et al., 2008; Wang and Zhang, 2011) or speleothems

(Neff et al., 2001; Niggemann et al., 2003). Due to normal atmospheric circulation, ^{14}C can be found in tree rings, allowing in combination with dendrochronology a documentation of solar activity during more than 10,000 years (Gray et al, 2010). The longest published record by Solanki et al. (2004) summarized data from ^{14}C and ^{10}Be over almost 12,000 years of Holocene solar activity. ^{10}Be is only measured in ice cores (e.g. Beer et al., 1990) providing much longer continuous sequences. Comparative measurements showed that ^{10}Be behaves inverse to solar activity with a short phase lag of one year (Gleissberg, 1965; Beer et al., 1990). The interplay of all solar cycles is hard to decipher and still unresolved. The Schwabe and the Hale cycle have a direct connection and, additionally, the Gleissberg cycle seems to modulate the Schwabe cycle (Gleissberg, 1939).

To demonstrate a direct connection of solar cycles and climate dynamics is even more difficult since measured climate data such as temperature and precipitation are inaccurate before 1850 (Versteegh, 2005). Nevertheless, several climatic events during the last millennia of human history could be linked to a rough cyclicity (e.g. Vos et al., 1997; von Rad et al., 1999; Schimmelmann et al., 2003; Taricco et al., 2009). The best known example is the coincidence of the Little Ice Age with minima of solar spot activity (Eddy, 1976; Robock, 1979). Initially, interpreted as an undifferentiated cooler period lasting from 1430 to 1850 (Robock, 1979), this phase was shown to comprise distinct events, named Dalton (1830–1790), Maunder (1715–1645) and Spörer (1550–1460) minima, which were heralded by the Oort and Wolf minima around 650 and 950 years BP (Eddy, 1976; Komitov and Kaftan, 2004). Especially during the Maunder Minimum no sunspots were detected for more than half of its duration (Eddy, 1976). The Medieval Warm Period (Jones et al., 2001; Cubash et al., 2006) on the other hand marks times characterized by a high solar activity and therefore a warmer climate. Additional evidence for the coincidence between solar cycles and paleoclimate was documented in numerous $\delta^{18}O$ studies on stalagmites and speleothems (e.g.: Neff et al., 2001; Taricco et al., 2009). The solar connection to these climate phenomena was tested and verified also by climate models (e.g. Perry and Hsu, 2000; Cubasch et al., 2006). A very convincing causality between solar cycles and climate was shown by model experiments of Svensmark and Friis-Christansen (1997) and later by Marsh and Svensmark (2003; 2004). Unlike many other climate models (Houghton et al., 1992; 1995), they considered the effect of clouds as climate forcing. Thus they could show a strong correlation between the total cloud cover and the incoming cosmic ray flux, which was essential for all further environmental interpretations. Cloud formation, as crucial parameter, explains at least partly why solar cycles have regionally different expressions, as physiogeography and water availability will have a major effect (Li et al., 2010). Nevertheless, the potential influence of solar activity on the environment is usually neglected. A solar-like forcing of Pleistocene records was postulated first by Hagelberg et al. (1994), who also introduced the term sub-Milankovitch cycles. Although they reported millennial-scale cycles, their time resolution was still too rough to detect distinct solar cycles. Schimmelmann et al. (2003) reported a connection of solar cycles to drought and flood events, but did not discuss any environmental response. Recently, furthermore, Di Rita (2011) recognized a significant coincidence between salt marsh vegetation expansion and the ^{10}Be curve during the last 6000 years and linked it with the 200-years-cycle. Beyond the Holocene, the documentation of solar cycles is scare with exceptions of key studies on annually preserved sediments such as rhymites (Muñoz et al., 2002; Rodrígez-Tovar and Pardo-Igúzquiza, 2003; Lenz et al., 2010). Such deposits allow an accurate time model based on varve counting and a high temporal resolution, which allows detecting even shortest solar and climate-feed-back cycles. Unfortunately, most of the published records are too small to cover the whole spectrum of known cycles in solar radiation. The herein presented Miocene records do not allow counting annually deposited varves. This considerable limitation, however, is partly counterbalanced by the high sedimentation rates at all studied sections. A very dense sample protocol is thus necessary to approach an at least decennial to centennial resolution as presented in the following chapters.

Chapter 2

Millennial-scale vegetation dynamics in an estuary at the onset of the Miocene Climate Optimum

Andrea Kern [a*], Mathias Harzhauser [a], Oleg Mandic [a], Reinhard Roetzel [b], Stjepan Ćorić [b], Angela A. Bruch [c], Martin Zuschin [d]

[a] Natural History Museum Vienna, Geological-Paleontological Department, Burgring 7, 1010 Vienna, Austria.

[b] Geological Survey of Austria, Neulinggasse 38, 1030 Vienna, Austria.

[c] Senckenberg Research Institute and Natural Museum, Senckenberganlage 25, 60325 Frankfurt am Main, Germany.

[d] University of Vienna, Department of Palaeontology, Althanstrasse 14, 1090 Vienna, Austria.

[*] Corresponding author. Fax: 0043-1-52177-459; E-mail address: andrea.kern@nhm-wien.ac.at

Abstract

Pollen analyses have proven to possess the possibility to decipher rapid vegetational and climatic shifts in Neogene sedimentary records. Herein, a c. 21-ky-long transgression-regression cycle from the Lower Austrian locality Stetten is analyzed in detail to evaluate climatic benchmarks for the early phase of the Middle Miocene Climate Optimum and to estimate the pace of environmental change.

Based on the Coexistence Approach, a very clear signal of seasonality can be reconstructed. A warm and wet summer season with c. 204–236 mm precipitation during the wettest month was opposed by a rather dry winter season with precipitation of c. 9–24 mm during the driest month. The mean annual temperature ranged between 15.7–20.8 °C, with about 9.6–13.3 °C during the cold season and 24.7–27.9°C during the warmest month. In contrast, today's climate of this area, with an annual temperature of 9.8°C and 660 mm rainfall, is characterized by the winter season (mean temperature: -1.4°C , mean precipitation: 39 mm) and a summer mean temperature of 19.9°C (mean precipitation: 84 mm).

Different modes of environmental shifts shaped the composition of the vegetation. Within few millennia, salt marshes with abundant Cyperaceae rapidly graded into Taxodiaceae swamps. This quick but gradual process was interrupted by swift marine ingressions which took place on a decadal to centennial scale. The transgression is accompanied by blooms of dinoflagellates and of the green alga *Prasinophyta* and an increase in *Abies* and *Picea*. Afterwards, the retreat of the sea and the progradation of estuarine and wetland settings was a gradual progress again.

Despite a clear sedimentological cyclicity, which is related to the 21-ky precessional forcing, the climate data show little variation. This missing pattern might be due to the buffering of the precessional-related climate signal by the subtropical vegetation. Another explanation could be the method-inherent broad range of climate-parameter estimates that could cover small scale climatic changes.

Keywords: pollen, palaeoenvironment, palaeoclimate, late Burdigalian, Karpatian, Paratethys Sea

2.1. Introduction

Lower Miocene deposits of Austria are mainly represented by marine sediments of the Paratethys Sea, whereas well dated terrestrial strata are rare. An exception is the Korneuburg Basin in the north of Vienna (Fig. 2.1). This basin formed during the Burdigalian in the latest Early Miocene. The geology and palaeoecology of the Korneuburg Basin has been studied intensively within the last few years and presented in two monographs (Sovis and Schmid, 1998, 2002). During these studies a total of more than 650 taxa of fossil animals and plants have been described from this small basin. This enormous dataset allows a relatively detailed reconstruction of the palaeoenvironments (Harzhauser et al., 2002). Additional data on the palaeoecology were published by Zuschin et al. (2004) and Latal et al. (2005). According to these studies, the basin was strongly cut off from the open sea, where an estuary was formed in its southern part and more marine depositional environments prevailed in the north. There, the only small connection to the Paratethys was established. In the south, separated from the marine part by a tectonically induced swell, a broad array of coastal-terrestrial habitats became established, ranging from patches of an impoverished *Avicennia* mangrove via Taxodiaceae swamps to riparian forests (Hofmann et al., 2002). The coastal mudflats were inhabited by biostromes of the giant oyster *Crassostrea gryphoides*, which formed colonies of several thousands of individuals with shell sizes of up to 80 cm length. One of these biostromes was excavated during 2005–2008 by the Natural History Museum Vienna and is now part of the Geopark “Fossilienwelt Weinviertel”. Contemporaneously, a major road construction project, the S1 motorway (Wiener Außenring-Schnellstraße) between the Tradenberg tunnel and the city of Korneuburg, was undertaken in the year 2008, allowing an exceptionally complete geological logging of a continuous section of the Miocene basin fill. The coincidence of both projects – providing palaeoecologic, stratigraphic and geologic backbones - gave rise to a sampling campaign on the palyno-assemblage studied in this paper.

Still, the mode of vegetational shifts in such Miocene estuaries is poorly studied, due to the usually very spotty preservation of accessible sediments. Moreover, as absolute datings and clear correlations with astronomical parameters are so far missing in the Lower Miocene deposits of central Europe, no estimation of the pace of the changes can be given. Herein, we try to quantify the observed vegetational shifts and to integrate the data in a hypothetic time/sedimentation rate model.

2.2. Geological setting

2.2.1. The Korneuburg Basin

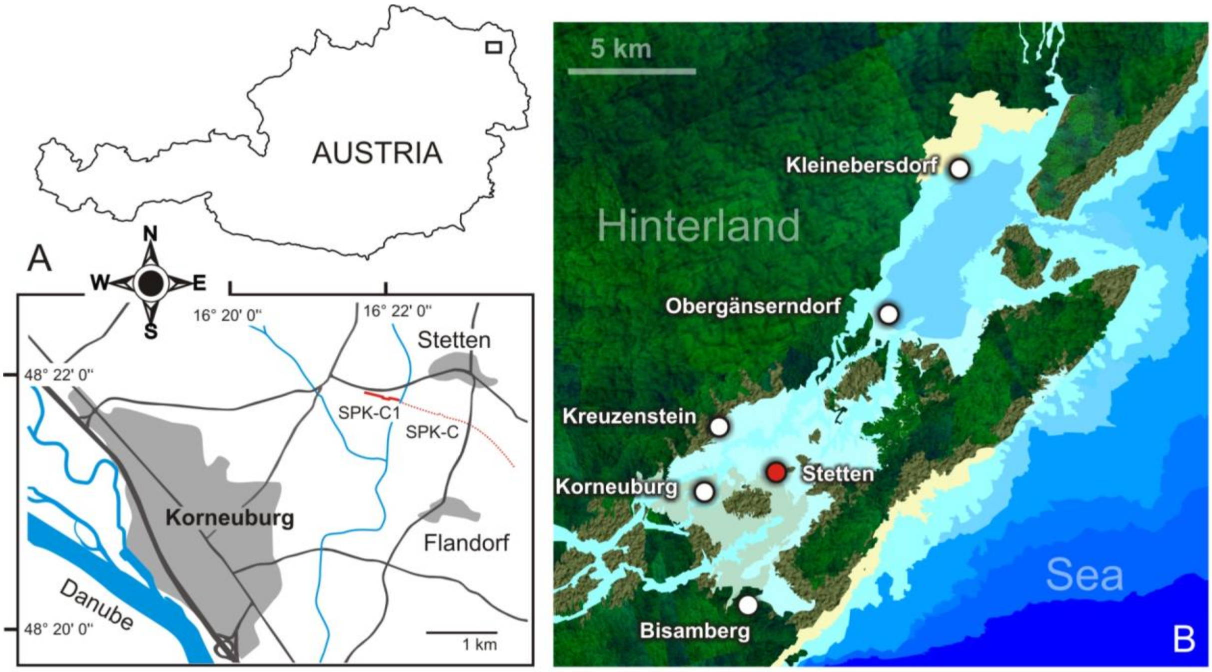

Fig. 2.1.
A: Geographic setting of the investigated section. The insert in the upper map indicates the position of the study area in north-eastern Austria. Full red line: SPK-C1, dotted red line: geologically documented section SPK.
B: A strongly simplified paleogeographic reconstruction of the late Burdigalian Korneuburg Basin based on palaeoecological and sedimentological data (after Harzhauser et al., 2003; 2009). The red dot shows the position of the SPK-C1 section at the time of deposition. The sketch is an idealized illustration representing a phase when the Paratethys Sea reached far into the estuary corresponding more or less to the situation as represented by the samples SPK-C1 5 to 16.

The Korneuburg Basin (Fig. 2.1) is part of the Alpine-Carpathian thrust belt. It originated as a sub-basin of the Vienna Basin during its early stage. Reactivation of thrusts as strike-slip faults in the Lower Miocene caused a rapidly subsiding pull-apart type basin. The onset of the pull-apart phase of the Vienna Basin during the Middle Miocene, resulted in tilting of the Lower Miocene strata. The asymmetric SSW-NNE-oriented basin is c. 20 km long and attains a maximum width of 7 km, but is strongly narrowed in its northern extension. A central high separates the basin fill into two depocenters (Fig. 2.1B), the southern part with a sediment thickness of c. 880 m deep and a northern part of c. 530 m (Wessely, 1998). This

swell was already active during the Early Miocene and caused a separation into a marine embayment in the north and an estuary in the south (Harzhauser et al., 2002). The basin margins are formed in the north by the Waschberg Unit and towards the south by the Rhenodanubian Flysch Unit. These Alpine-Carpathian nappes are underlain by the autochthonous basement formed mainly by Cretaceous and Jurassic units and by the crystalline of the Bohemian Massif. Sedimentation began during the Early Miocene (Eggenburgian) and comprised shallow marine marls and sands (Ritzendorf Formation). The main phase of deposition, however, started in the late Early Miocene (late Burdigalian = Karpatian in regional stratigraphy; Piller et al., 2007), represented by marly silts and fine to medium sands of the Korneuburg Formation. Rarely, gravel and boulder may occur in close position to the Flysch Zone; thin lignites of <1 m may occur as well.
According to palaeomagnetic measurements, a rather southern position of the area at c. 34° latitude was calculated by Scholger (1998) for the late Burdigalian Korneuburg Basin. Although this interpretation, requiring a northward movement of c. 1400 km since the late Burdigalian, seems to be an overestimation, a considerable northward shift is in accordance with other studies (Márton, 2008).

2.2.2. The SPK-C + SPK-C1 Stetten section

Due to c. 25° western tilting of the Karpatian deposits, during the Middle Miocene or later, the basin fill can be followed along a W-E transect. A c. 1.8 km long transect was geologically documented in detail in the southern part of the basin in the year 2008 (Fig. 2.1A). 324 sediment-samples, 118 molluscs-samples, 17 samples for diaspores and 118 palynosamples were taken for palaeontological, mineralogical and sedimentological analysis.
The c. 120-m-thick section comprises lignites, clay, silt, sand and rare pebble layers with abundant coquinas (Fig. 2.2A). The lower 30 m are characterized by pelitic sedimentation; its middle part between 30–75 m represents an intense alternation of pelites and psammites, whereas the top is dominated by sand. Internally, it may be divided into at least 6 coarsening-fining upward cycles. For this study, the lower 21 m of the section (N48°21'47.82'' E016°22'0.12''), representing one of these cycles were measured and sampled in more detail (Fig. 2.2B).
It starts with c. 6 m clay and clayey silt with two prominent lignites of up to 50 cm thickness. Rootlets below the lignite indicate in-situ preservation. Above the lignite follows a 9-m-thick coarsening upward sequence of clay, clayey silt, silt, fine sand and medium sand (Fig. 2.2). An in-situ mass occurrence of the gastropod *Turritella gradata* occurs in the lower part. This coquina is a local marker bed and can be traced, without change of density and atructure,throughout the construction area. The silty middle part bears in-situ occurrences of

the razor clam *Solen marginatus* along with scattered mollusc debris. This pattern changes completely in the 2-m-thick sandy unit which bears 2 prominent tempestitic coquinas consisting mainly of disarticulated bivalves. Two thin pebble lags accompany the coquinas. The top part is represented by a fining upward sequence of silt and clay with scattered plant debris and rare coquinas.

2.2.3. Dating and time/sedimentation rate model

The Karpatian deposits are of latest Early Miocene age. The correlation of the mammal fauna with palaeomagnetic data allowed a dating into the early mammal zone MN 5, spanning a time of about 16.5–16.7 Ma (Daxner-Höck, 1998; Harzhauser et al., 2002). Due to the co-occurrence of calcareous nannoplankton zonal markers *Helicosphaera ampliaperta* Bramlette and Wilcoxon, 1967 and *Sphenolithus heteromorphus* Deflandre, 1953 the investigated samples can be placed into Zone NN4 (Martini, 1971). Early Miocene nannofossil assemblages contain *Coccolithus pelagicus* (Wallich, 1871) Schiller, 1930, *Cyclicargolithus floridanus* (Roth and Hay, 1967) Bukry, 1971*, Helicosphaera carteri (*Wallich, 1877) Kamptner, 1954, *Reticulofenestra excavata* Lehotayová, 1975, *Reticulofenestra gelida* (Geitzenauer, 1972) Backman, 1978, *Reticulofenestra pseudoumbilica* (Gartner, 1967) Gartner, 1969*,* and high percentages of reworked Cretaceous and Paleogene taxa. See Piller et al. (2007) for the correlation of the regional stages of the Paratethys realm with the standard stages.

The complete 1.8 km long section has been measured by a hand-held gamma-radiometer to evaluate the character and interpret the cause of cyclic changes observed during sedimentological logging. The final data-set grew to more than 17,000 measurements, all with fixed stratigraphic positions in the lithological column. Throughout the succession, the spectral analysis of the gamma-log data detected prominent, highly significant periodicities with a stratigraphic distance ranging from 17.5 m to 22.5 m (Fig. 2.2C). Lithologically, these periodicities are also well expressed by coarsening-fining upward rhythms, culminating in shore-sand units separated by clay or sandy clay (Fig. 2.2A). A detailed analysis of the total succession will be given elsewhere; for this study, however, the detailed palynological analysis of the lower 21 m of the section is discussed. The working hypothesis is that the observed cycles are either pure autocycles triggered by subsidence or that they are expressions of the 21-kyr-precession signal – or a combination of both. An interpretation of the sedimentary cycles as expression of the 100-kyr-eccentricity signal is ruled out as it would result in a 2-My-long phase of sedimentation. This, however, is far too long for the late Karpatian with a duration of less than 1 Ma (Piller et al., 2007).

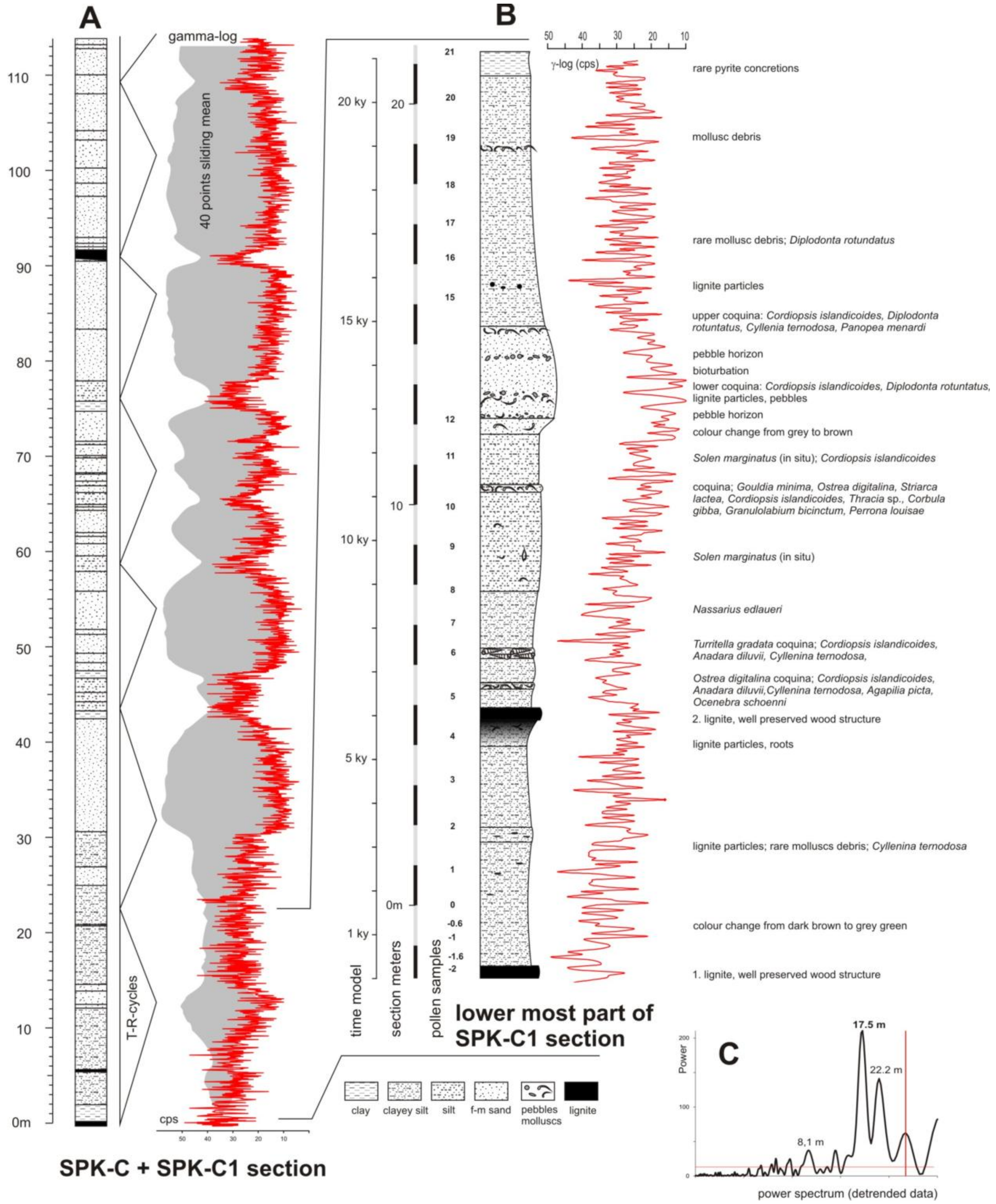

Lithology of the SPK C+ SPK-C1 section (A) and detailed log of the lower part (B). A: The gamma-log and the sedimentary features reflect distinct coarsening-fining upward cycles which correspond to transgressive-regressive cycles (T-R-cycles). B: The lower part of the SPK-C1 section with typical mollusc assemblages and the position of the palynological samples. C: The spectral analysis performed on the gamma-log data, proves the existence of cycles which are interpreted as an expression of precessional forcing. Thus, the lowermost part of SPK-C1, spanning one of these cycles, might cover about 19-21 ky.

Considering the cycles as 21-kyr-precession signal would result in an average sedimentation rate of roughly 0.8–1.1 mm per year. This sedimentation rate fits well to the basin type with rapid subsidence and is therefore somewhat higher than in the later pull-apart phase of the Vienna Basin, when sedimentation rates between 0.4–0.6 mm per year are typical (Hohenegger et al., 2008; Lirer et al., 2009). Although the proposed Miocene sedimentation rates in the Korneuburg Basin are higher than in the neighbouring Vienna Basin, they are comparable with modern values in estuarine and lagoonal settings. Tropical to subtropical estuaries with rates of 1-10 mm/yr are documented from Western Africa (Debenay et al., 1994), Brazil (Patchineelam and Smoak, 1999; Behling et al., 2001) and South East Asia (Li et al., 2006; Ellison, 2005). Comparably high values of 0.5-1.8 mm/yr are also known from the precolonial Chesapeake Bay (Donoghue, 1989). Such high sedimentation rates are especially well documented from tropical mangals, ranging from 1.2–2.4 mm/yr (Lynch et al., 1989; Smoak and Patchineelam, 1999; van Santen et al., 2007) up to c. 11 mm/yr (Kamaruzzaman and Ong, 2008). Moreover, high sedimentation rates were supported by synsedimentary tectonic activity generating a depocenter in the Korneuburg Basin. Increasing relief energy in the Alpine hinterland and the North Alpine Foreland Basin caused high sediment supply to fill the newly generated accommodation space (Wessely, 1998). Thus, the investigated cycle should reveal patterns related to autocyclic mechanisms or astronomic forcing spanning roughly 21,000 years, which may represent one full precession cycle. The sample density (one sample each meter) should thus account for a time resolution of c. 800–1000 years per sample.

2.3. Material and Methods

The samples were taken during the highway construction close to Stetten in Lower Austria. For this investigation, 24 palyno-samples were processed to evaluate preservation, diversity and composition of the palynomorph assemblages. Except for the sand unit at m 12–14 (Fig. 2.2B), where preservation is too poor for analysis, all samples derive from clay and silt parts. The samples were processed with hydrochloric acid (HCl conc.) and HF (hydrofluoric acid conc.) to eliminate all silica and calcareous matter. Afterwards the preparation followed the procedure of Klaus (1987) using glacial acidic acid (CH_3COOH conc.) before acetolysis was preformed (Erdtman, 1954). Finally, after washing and sieving the samples with a 6µm nylon sieve, the material was transferred into a glass tube and kept in glycerin. Between sample SPK-C1 -2 and 4 at least 150 pollen were counted due to bad preservation, for the rest an amount of more than 200 were identified (excluding *Pinus*). All samples are stored in the collection of Natural History Museum Vienna (NHMW Inv. 2009B0004/001 – 2009B0004/064).

The software “Past” was used for cluster analyses and non-metric Multidimensional Scaling (nMDS) (Hammer et al., 2001). The pollen diagram was created by Tilia and Tilia-Graph (Grimm, 2004).
Climatic reconstructions were based on the counted pollen data, which were analyzed by using the Coexistence Approach (Mosbrugger and Utescher, 1997). For the calculation of the climatic intervals, climatic data of the most appropriate nearest living relative of each taxon were considered. Taxa, which are today only limited to a much retreated area, such as *Cathaya* or *Sciadopitys*, were excluded from the analysis, because their recent distribution might not reflect their Miocene habitat requirements. Also, if they were limiting an interval, the Pinaceae pollen and the rare taxon *Ephedra* were not considered. Because of the ability of their pollen to spread over long distances their presumable living environment may have been far away.
For the remaining taxa, the natural worldwide distribution was considered to reflect the interval of their possible climatic viability. Taking all taxa into account, a climatic interval can be deduced, in which all these taxa can survive and “co-exist”. This is called the Coexistence interval and is presented here as the climatic interval, in which the fossil taxa are most likely to have existed.

2.4. Results

In total, 24 samples were investigated; all samples contain pollen, spores and dinoflagellate cysts (Table 2.1; Figs. 2.3, 2.4). In addition, spores of fungi, chitinous inner tests of foraminifera and lignite particles are abundant. High amounts of pyrite characterize all samples.

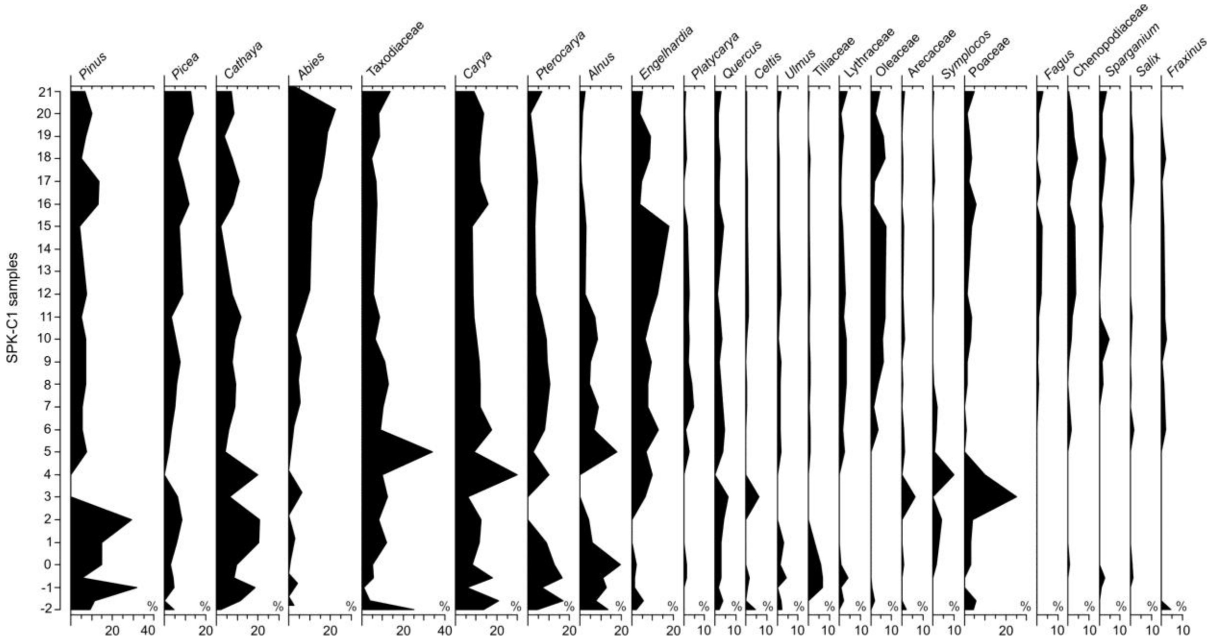

Fig. 2.3 . Pollen diagrams reduced to the most significant angiosperms and gymnosperms.

Samples from the lower most part of the section (SPK-C1 -2 to 4), situated between the prominent lignites, are poorly preserved. Here the assemblages are low diverse as a result of taphonomic bias (only thick-walled pollen and spores are preserved). Starting with sample SPK-C1 6, the number of taxa increases and the preservation improves. All samples contain small fragments of lignite, which are most abundant between the two lignite layers (SPK-C1 -2 to 5).

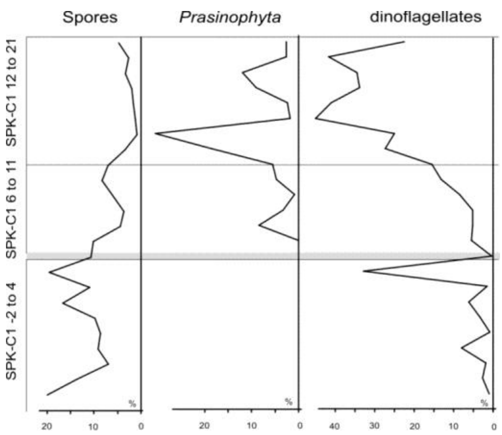

Fig. 2.4. Frequencies of spores, *Prasinophyta* and dinoflagelltes in the samples in percent. Spores and dinoflagellates display an opposing trend. The green flagellate *Prasinophyta* has a remarkable peak in the upper part of the section close to the foreshore and shoreface interval.

In most samples (SPK-C1 4–16, 18, 21) angiosperms are more abundant than gymnosperms. The angiosperms *Carya, Engelhardia, Pterocarya, Alnus*, *Quercus, Sparganium*, Oleaceae, Lythraceae and Poaceae attain percentages over 10%. Tiliaceae, Chenopodiaceae, *Fagus*, Symplocaceae, *Ulmus, Fraxinus* and *Salix* appear with more than 5%. Among the gymnosperms no family is

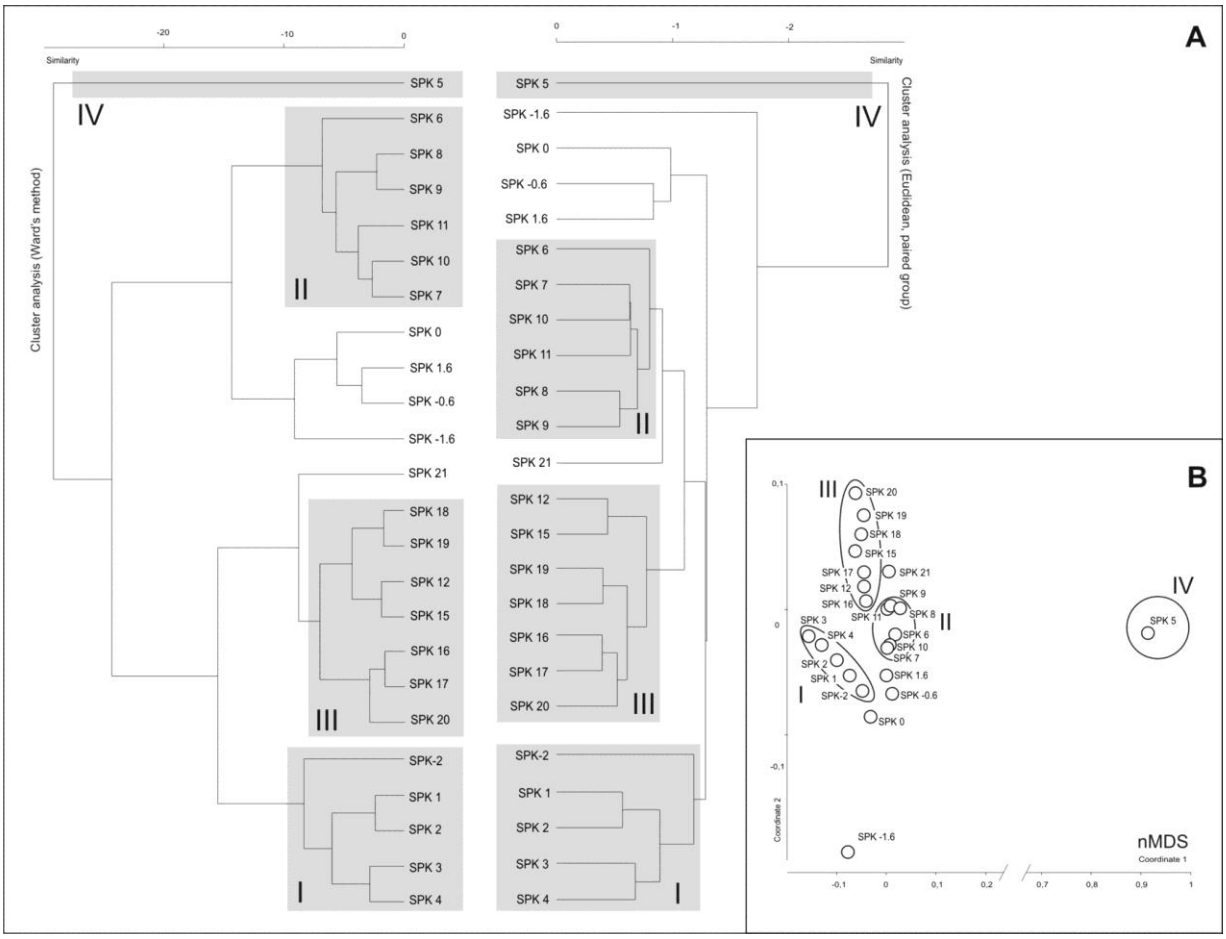

Fig. 2.5.
A: Q-mode Cluster analyses of the data (left: Ward's method, right: paired group) revealing several robust groupings of samples, which are also evident in the nMDS plot (B); see text for discussion. SPK -2 to 21 samples in the cluster refer to SPK-C1 -2 to 21.

clearly dominant unlike among the angiosperms, where *Carya, Pterocarya* and *Engelhardia* are the most abundant elements.

A cluster analysis (Ward's method and paired group) of the data set (excluding undetermined counts, undetermined Pinaceae and extremely rare cluster I unites samples from the lowermost part of the section (SPK-C1 -2 to 4). These samples are rich in *Carya, Cathaya, Pinus, Pterocarya, Alnus,* Pteridaceae, Schizaeaceae and Tiliaceae. Cluster II encompasses samples SPK-C1 6–11. This cluster is characterized by coincident high abundances of *Carya, Cathaya, Engelhardia,* Taxodiaceae, *Pterocarya, Platycarya* and *Alnus* accompanied by Oleaceae, *Sparganium, Quercus, Lonicera* and Lythraceae. No group dominates the spectra. Cluster III is formed by samples SPK-C1 12 to 20. Although*, Carya, Engelhardia, Cathaya* and Taxodiaceae are still well represented, the increase of *Abies* and *Picea* is characteristic. Additionally Chenopodiaceae, *Sparganium*, Poaceae and Oleaceae are important constituents of the samples. In contrast, *Alnus, Symplocos, Platycarya,* Rutaceae and Arecaceae become rare elements.

Within this main cluster, a subcluster (samples SPK-C1 16, 17, 20) forms which is characterized by comparably lower levels of *Engelhardia* and Oleaceae but increased occurrences of *Pinus* and *Cathaya*. This interval is also characterized by a distinct increase of dinoflagellates and a decrease of spores (Fig. 2.4). Above sample SPK-C1 12, the dinoflagellates are the dominating group of the playno-assemblage with up to 63.5 %. Along with the dinoflagellates, the green algae *Prasinophyta* appears with a prominent peak in SPK-C1 15. It starts in low numbers in SPK-C1 7, and rises significantly in samples SPK-C1 12 and 15, thus spanning the barren sandy interval.

Sample SPK-C1 5 forms the cluster IV; it is an outlier in all cluster analyses and also in nMDS plots (Fig. 2.5B), caused by abundance peaks of Taxodiaceae, *Glyptostrobus* and *Alnus*.

Finally, several samples tend to form poorly supported clusters or, depending on

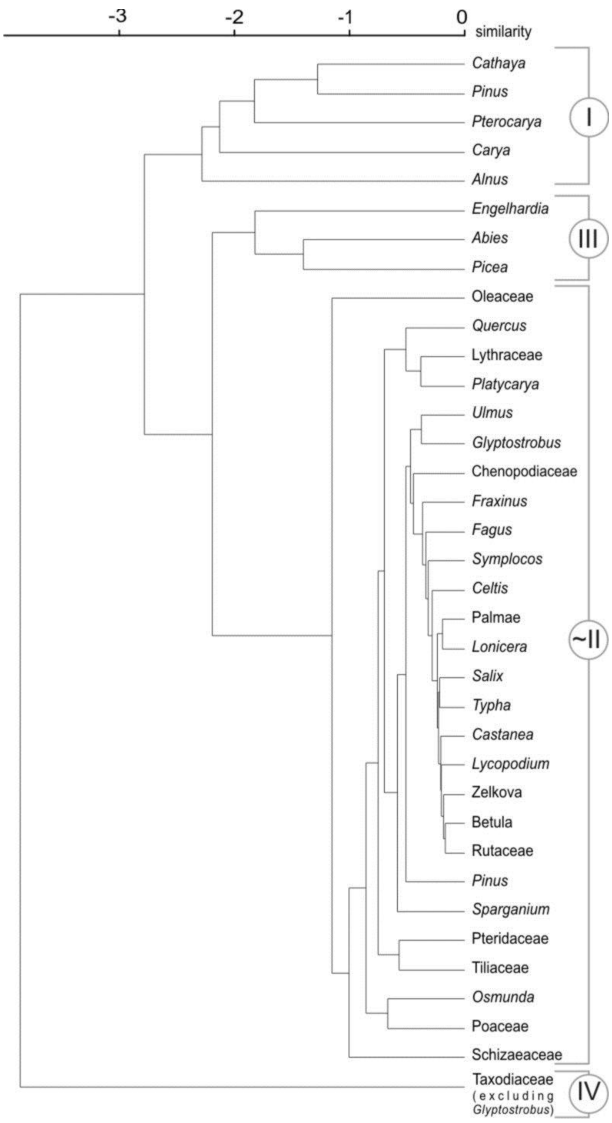

Fig. 2.6. A percentage-based R-mode cluster analysis of the data set was performed to test which taxa unite sample-groupings defined in Fig. 2.5.

method, group differently. These are especially those samples with poor preservation and low numbers of counts. Only SPK-C1 21 is an exception. Although generally close to samples of cluster III, it differs by a distinct drop of *Abies* and a slight increase in Taxodiaceae. The nMDS plot reveals a similar pattern (Fig. 2.5B). The outliers SPK-C1 5 and SPK-C1 -1.6 are both lignite-related samples. Cluster I, II and III group within distinct regions and tend to be arranged along a stratigraphic axis. The clusters are also robust in a cluster analysis based on percentages of taxa (Fig. 2.6), which are also clearly dominant in different parts of the section (Fig. 2.7). Now the uniting elements of cluster I are *Cathaya, Pinus, Pterocarya, Carya* and *Alnus. Engelhardia, Abies* and *Picea* group within cluster III. Taxodiaceae still represent a maverick position corresponding to cluster IV. Thus, despite the supposed short time interval represented by the samples, statistically robust quantitative and qualitative differences of the palyno-assemblages suggest major shifts in ecological parameters.

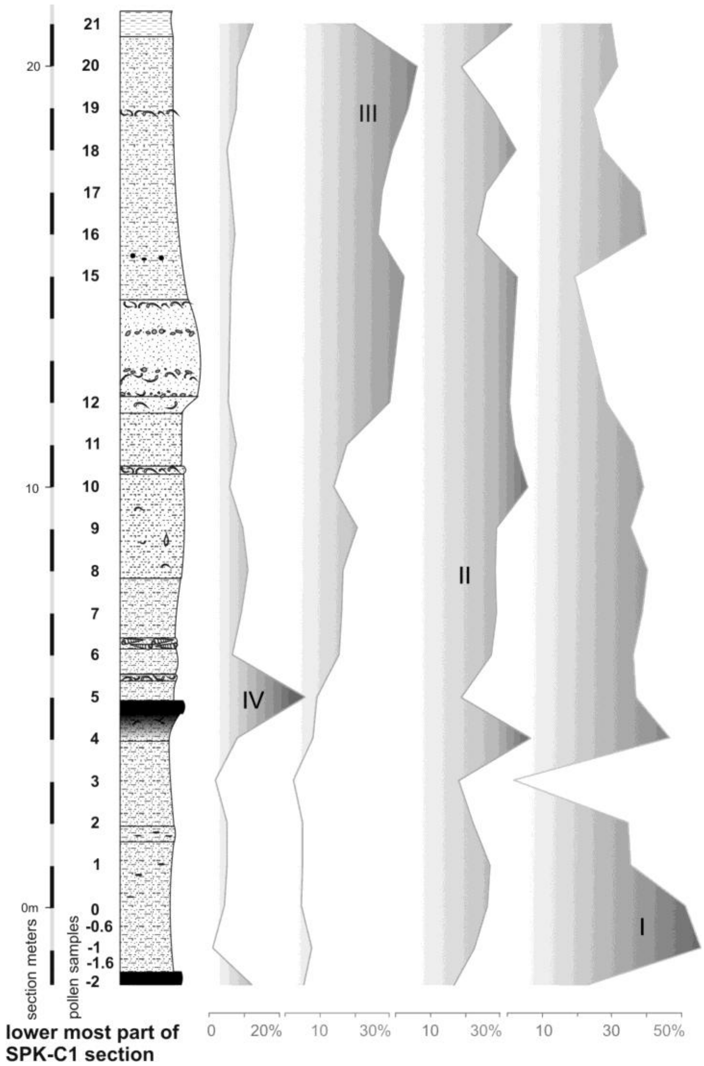

Fig. 2.7. The abundance of pollen and spore taxa, grouped according to the clusters shown in Fig. 2.6 (lithological details are given in Fig. 2.2B).

2.5. Discussion

2.5.1. Palaeoenvironments

The southern part of the Korneuburg Basin was interpreted by Harzhauser et al. (2002) and Latal et al. (2005) as an estuary (Fig. 2.1B). A high number of biota were reconstructed ranging from shallow sublittoral shore face settings, mudflat coasts, *Crassostrea* biostromes, *Avicennia* thickets, coastal Taxodiaceae swamps, riparian forests to mixed-mesophytic forests in the hinterland. For the investigated part of the SPK-C1 section an interpretation of the depositional environments can be performed on the autochthonous invertebrate faunas and sedimentary features. This may serve as base for further interpretations of the par-autochthonous or allochthonous palyno-assemblages.

2.5.1.1. Autochthonous brackish-marine depositional environments

The lower part of the section, covered by the samples SPK-C1 -2 to 4, bears rare brackish-marine molluscs such as the nassariid gastropod *Cyllenina ternodosa*. These are usually confined to extremely shallow sublittoral to intertidal mud flat environments (Zuschin et al., 2004). The decrease of mollusc hash towards the lignite at 4.4–4.8 m and the low diversity of the mollusc assemblage indicate a gradual shift towards brackish or freshwater conditions which peak in the formation of a Taxodiaceae swamp. In correlative parts of the section, the occurrence of unidentifiable planorbid gastropods supports the interpretation of a freshwater swamp.

Marine conditions became re-established soon after. Above sample SPK-C1 5, a thin *Ostrea digitalina* coquina with neritid, nassariid and muricid gastropods (*Agapilia pachii, Cyllenina ternododsa, Ocenebra schoenni*) and disarticulated bivalves such as *Cordiopsis islandicoides* and *Anadara diluvii* formed at 5.4 m. Throughout the Late Oligocene and Early Miocene, such assemblages are highly indicative for estuaries and brackish lagoons (Baldi, 1973; Harzhauser and Mandic, 2002; Mandic et al., 2004). At 6.2 m, a second coquina appears, consisting mainly of *Turritella gradata*, a large sized turritellid gastropod. The shells are more or less in life-position and lack any post-mortem orientation by currents. Articulated valves of the venerid *Cordiopsis islandicoides* are additional indicators for such calm conditions. Elements of the asteroid starfish *Luidia?* sp. point to a strong marine influence in the estuary at that time. Starfishes like *Luidia* prefer normal marine conditions and only rarely tolerate salinities of less than 20 ppt (Hendler et al., 1995). Therefore, this part of the section is interpreted as a calm, soft-bottom lagoonal environment which initially was settled by *Ostrea digitalina* colonies in littoral settings which soon became replaced by subtidal environments with huge *Turritella* populations. The section interval between 8 up to 11.8 m is characterized by a coarsening upward trend and a change in the mollusc fauna. Intertidal elements such as *Nassarius edlaueri* are replaced by the large razor clam *Solen marginatus*, typical for shoreface environments (Mandic et al., 2008). The solenoids are found in life position in the silty and sandy sediment. A first tempestite was formed at 10.4 m, pointing to a gradual increase of water energy. The mollusc assemblage with *Ostrea digitalina, Striarca lactea, Gouldia minima, Cordiopsis islandicoides, Thracia* sp., *Corbula gibba, Granulolabium bicinctum* and *Perrona louisae* represents a mixture of intertidal and sublittoral elements and reflects the proximity of mudflats and sandy foreshore settings.

This trend culminates in the sandy unit between 11.8 m and 14.4 m. Tempestites, shell and pebble lags indicate high wave energy in foreshore and shore settings. A color change from green-blue-grey towards ochre–yellow suggests an increased aeration of the sediment by repeated reworking by waves and by intense bioturbation. This is documented by poorly preserved, rare *Ophiomorpha-Thalassinoides*-like traces. The estuarine-marine character of the assemblages is obvious from elements such as the ungulinid *Diplodonta rotundata* and the geoduck *Panopea menardi.* The latter genus forms large populations in the subtidal zone and is extremely deep burrowing, attaining depths of more than 1 m (Gribben et al., 2004). The absence of deeply burrowed in-situ shells and the occurrence of disarticulated shells in the coquina may thus point to heavy wavy agitation leading to considerable reworking of the sediments. Upsection, the water energy decreases distinctly. Silty clayey sediments prevail; molluscs are represented by rare shells of *Diplodonta rotundata* and shell fragments. Even mudflat species are missing. A single thin coquina consisting of unidentifiable shell hash formed at 19.0 m. The low diversity and the predominance of a single species point to restricted environmental conditions which did not allow the establishment of marine taxa. Moreover, a poor oxygenation of the bottom is indicated by the increase of pyrite. This development points to a late phase of the marine ingression, heralding the progradation of lagoonal environments and the end of this sedimentary cycle.

2.5.1.2. Terrestrial environments

The cluster analysis already documented considerable vegetation shifts within the sedimentary cycle. The lowermost section (SPK-C1 -2 to 4; cluster I), characterized by a low pollen grain concentration, where only thick walled pollen are preserved. This part is interpreted as (salt) marshes comparable to the modern Everglades in the SE of North America. Graminoids, mostly of the family Cyperaceae, dominate the wetlands above peat layers (Willard et al., 2001), similar to the lignite layer found at the base of the section. Because these marshes occasionally fall dry, either periodically or during single events, the soils get oxidized, which may explain the bad preservation of the palynological remains and the absence of the thin-walled Cyperaceae pollen. The high amount of fern spores and the distribution of *Quercus*, *Celtis* and *Alnus* also fit to this modern equivalent. Tree islands with these taxa are frequently formed between the marshes (Willard et al., 2001; Denk et al., 2001).

Upsection, the fluvial influence is increasing, indicated by the contribution of hinterland taxa such as *Alnus, Symplocos, Carya*, Poaceae and especially Taxodiaceae (SPK-C1 -1 to 5). The trend climaxes in sample SPK-C1 5 (cluster IV) where Taxodiaceae are predominant and formed swamps (Fig. 2.7). This vegetation led to the formation of the second lignite layer. Clear freshwater conditions are further verified by the occurrence of freshwater gastropods, which shows that, at this time, the marine influenced part of estuary had retreated towards the basin. The establishment of large Taxodiaceae swamps can be a

relatively rapid process, comparable to the modern Everglades, which formed in less than 5000 years (Gleason and Stone, 1994).
Afterwards, the environmental conditions quickly shift back to brackish and marine environments as obvious from the mollusc fauna. Consequently, the palynosamples show a constant increase of dinoflagellate cysts, dominated by the genus *Spiniferites* sp., which is a neritic element of eutrophic environments (Harland, 1983; Turon, 1984; Zonneveld, 1995). Along with the dinoflagellates, the green alga *Prasinophyta* is an important brackish water indicator and points towards rich nutrient content within the surface water. Today, *Prasinophyta* blooms are known from the Black Sea after heavy rainfall, which cause a decrease of the salinity of coastal waters and lead to eutrophic conditions (Vershinin, 2007). During this interval (cluster II and III), the pollen assemblage clearly reflects the surrounding and hinterland vegetation. Typical plants dwelling next to salt water drained soils surrounding the shores of estuaries are Cyperaceae, Poaceae and Chenopodiaceae (Grigore and Toma, 2007; Jiang and Ding, 2008; González and Dupont, 2009). Alongside the tributaries and ponds within the wetlands, *Sparganium* and *Typha* were distributed (Britton and Crivelli, 1993), probably associated with the Lythraceae *Decodon*. This genus is common in the Miocene and has also been detected in the close-by locality Teiritzberg by SEM analysis (Kvaček and Sakala, 1999; Hofmann et al., 2002). The swamp vegetation is still represented by Taxodiaceae, such as *Taxodium* and *Glyptostrobus,* along with *Nyssa,* Tiliaceae and *Craigia* (Kvaček, 2003). These wetlands were sometimes overgrown by Pteridaceae, Arecaceae, Apiaceae, but also trees like Arecaceae, *Alnus, Fraxinus* or Oleaceae were inhabitants of this environment (cf. Utescher et al., 2009).
Some distance along the tributaries, riparian vegetation with abundant angiosperms developed. *Engelhardia*, *Carya* and *Pterocarya* are found along with other riparian plants such as *Salix*, *Fraxinus*, *Liquidambar* and the Ulmaceae *Ulmus* and *Zelkova* because of their ability to tolerate longer phases of inundation as are typical in such wetlands (Britton and Crivelli, 1993; Wilen and Tiner, 1993; Denk et al., 2001). The rest of the palyno-assemblages indicate forests with some open habitats in between, where Poaceae, other grasses and herbs were growing. A “Younger Mastixioid Flora” sensu Mai (1964) was developed including a high amount of broad-leaved evergreen and thermophilous elements. *Quercus* and *Fagus* were growing associated with Euphorbiaceae, Rutaceae, Sapotaceae and *Symplocos* (Jarvis and Clay-Poole, 1992). At somewhat higher elevations, *Abies* and *Picea* were common (cf. Jiménez-Moreno et al., 2008). Such low mountainous areas might have been formed by the Flysch-sandstone ridges bordering the Korneuburg Basin or by the young Alps in the south-west. The changing sea-level during the marine ingression caused slight alternations in the lateral distributions of these plant assemblages, but no taxon is dominating or disappearing within this part of the section.

At the top, the marine influence decreases again and dinoflagellates and Pinaceae pollen are replaced by angiosperms again. Additionally, especially Taxodiaceae pollen become more frequent again, indicating the re-establishment of swamp environments, due to the retreat of the sea from this part of the estuary.

2.5.2. Palaeoclimate

During the middle Burdigalian (regional Ottnangian and early Karpatian age) the tropical Early Miocene climate of central Europe experienced a first cooling phase in the Miocene. This is recorded in the marine sphere by a distinct turnover of the mollusc fauna and a switch in the carbonate sedimentation towards a temperate bryomol facies (Harzhauser and Piller, 2007; Piller et al., 2007). Simultaneously, the frequency of tropical plant taxa declines and several tropical elements such as Sapotaceae disappear for a period of time (Planderová, 1990). Soon after, during the late Burdigalian (late Karpatian), the climate switched back towards subtropical conditions. Thermophilic molluscs display a distinct northward extension of their distribution area and Tethyan molluscs appear in the Paratethys Sea (Harzhauser et al., 2003; Harzhauser and Piller, 2007). In the terrestrial record, this warm phase is documented by the high number of thermophilic elements such as *Engelhardia*, *Platycarya*, Myricaceae and certain Fagaceae, Fabaceae and ferns (Doláková and Slamková, 2003). This trend indicates the onset of the Middle Miocene Climatic Optimum (MMCO) (Jiménez-Moreno et al., 2005).
The herein studied section represents a short, c. 21 kyr spanning interval of that early phase of the MMCO. Consequently, thermophile taxa such as *Engelhardia* and *Platycarya* are present in all samples and *Engelhardia* is even the most frequent angiosperm at all. Especially the abundant occurrence of *Engelhardia*, together with Mastixiaceae and Sapotaceae, point towards a warm and frost-free climate. Rutaceae, Areaceae, *Osmunda*, Schizaeaceae and *Ilex* are irregularly present, Rubiaceae and Araliaceae only sporadic, but their nearest living relatives today live all in tropical to subtropical climates. *Nyssa* and *Lonicera* indicate also a warm and mild climate (Fauquette et al., 2006; Kovar-Eder et al., 2006).

First climatic interpretations for the late Burdigalian of the Korneuburg Basin have already been performed based on various proxies: thermophilic ectothermic vertebrates suggest a humid subtropical climate with a minimum value of the mean annual temperature (MAT) of 17°C, and the minimum cold month temperature (minCMT) ranging from at least 3°C to about 8°C (Böhme, 2003). The mean annual precipitation was estimated to range around 2000 mm (Meller, 1998). The marine gastropod fauna indicates minimum sea surface temperature values around 14–15°C (Harzhauser et al., 2002). This estimate was supported by $\delta^{18}O$ studies, which document a range from 14°C to 25°C in coastal marine waters (Latal et al., 2005).

These estimates can now be tested and refined based on the palyno-assemblages. Herein we use the Coexistence Approach of Mosbrugger and Utescher (1997) which allows several palaeoclimate benchmarks such as the mean annual temperature (MAT), the mean temperature of the coldest and warmest months (CMT, WMT), the mean annual precipitation (MAP), the mean precipitation of the wettest and driest months (MPwet, MPdry) and the mean precipitation of the warmest month (MPwarm) to be estimated. Results of the entire data set indicate a MAT of 15.7–20.8 °C, a CMT of 9.6–13.3 °C, and a WMT of 24.7–27.9 °C. Precipitation data comprise a MAP of 823–1372 mm, a MPwet of 204–236 mm, a MPdry of 9–24 mm and a MPwarm of 79–172 mm. This describes a much warmer and wetter climate that can be found today in this area (climatic data of Vienna). Each season is definitely colder, resulting in a MAT of 9.8°C and a MAP of 660 mm. The colder season clearly shows frosts by a CMT of -1.4°C but a higher rainfall of 39 mm. In contrast the warm season is colder (WMT: 19.9°C), too, but also dryer (MPwarm: 84 mm) (Müller, 1996).

The temperature estimates based on the Coexistence Approach indicate a warm subtropical climate. A clear improvement to existing data is the evaluation of the coldest month temperature with c. 10°C. This lower boundary is mostly defined by the common occurrence of *Mastixia* sp. A second important improvement is the rather low MAP which is about half of previous estimates. Moreover, a completely new and surprising aspect is the clear evidence of seasonality in these data. Up to now, the onset of the MMCO was assumed to correlate with an overall wet subtropical climate without marked seasonality (Kovar-Eder et al., 1998; Meller et al., 1999).

Our data, calculated with the Coexistence Approach and the Nearest Living Relatives concept, suggest that during the late Burdigalian, there was a wet season with a precipitation of 200 to 240 mm per month. In respect to the high precipitation results of the warmest month, it is likely that this wet season was the summer season. *Engelhardia*, *Symplocos* and Taxodiaceae occur today in similar climates with clear seasonality. Especially the mixture of *Symplocos,* together with *Betula* and *Quercus,* points to the existence of a warm and wet season. This was contrasted by a quite dry season, lasting at least one month, with a rainfall of less than 30 mm (Fig. 2.8), which is suggested mostly by the occurrence of *Celtis*, *Sparganium* and the subtropical taxon *Platycarya*.

Comparable climate parameters were proposed for the more continental late Burdigalian settings in southern and north-western Germany by Böhme et al. (2007) and Utescher et al. (2000). Therefore, this climate pattern with dry and slightly cooler winter seasons and humid and warm summer seasons seems to have characterized Central Europe at the onset of the MMCO. These data suggest similarities with the modern Cwa climate of Koeppen (1936). Today this climate covers parts of northern India extending into south-eastern Asia (south Nepal, Myanmar, northern Thailand) to East China and in central south Africa (east Angola, Zambia, north Zimbabwe, north Mozambique) (Peel et al., 2007).

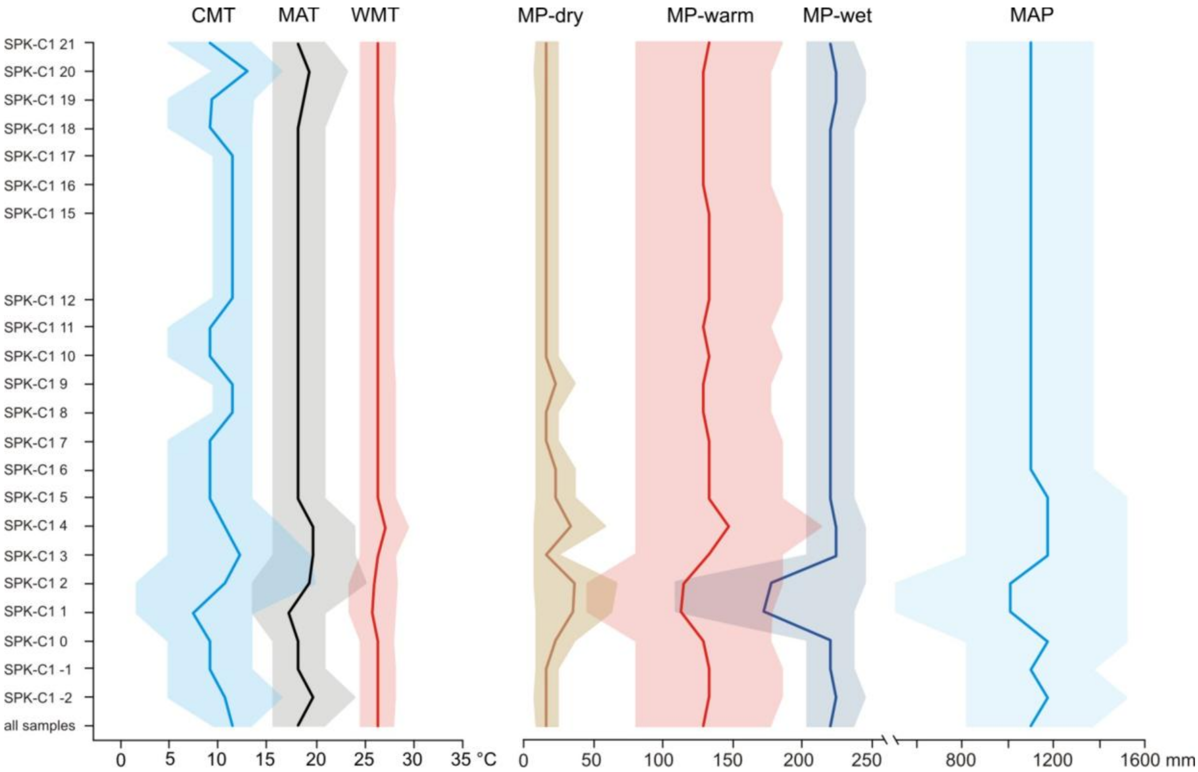

Fig. 2.8. Climate signals revealed by the Coexistence Approach of Mosbrugger and Utescher (1997). Shaded areas indicate the total range; middle line represents average values. The data suggest rather stable climatic conditions during the c. 21-ky-interval. Nevertheless, shifts within the ranges would be unresolved due to the method used.
Abbreviations: CMT: Coldest month temperature, WMT: warmest month temperature, MAT: mean annual temperature, MAP: mean annual precipitation, MPwet, MPdry MPwarm: precipitation of the wettest, driest and warmest month.

2.5.3. The pace of environmental change

Although the suggested 21-kyr-precessional cyclicity is supported by power spectra analysis of the entire SPK-C + SPK-C1 sections, the conversion into a time model for the investigated part of the SPK-C1 section is difficult. Sedimentation will not have been completely constant throughout the interval. In-situ occurrences of *Turritella* coquinas and of bivalves in life-position are good indicators for undisturbed sedimentation in large parts of the section. In contrast, pebble lags and tempestitic coquinas in the sand layers at 12–14 m point to winnowing and re-sedimentation. Despite these uncertainties, the conversion of the average sedimentation rate of 800–1100 cm per ky into a time model will allow a rough estimation of the pace of environmental change.

Hence, the basal formation of salt marshes and peat bogs characterized the locality for about 5000–6000 years. As in the modern Everglades, these environments graded into

Taxodiaceae swamps which seem to have developed very quickly within less than 2000 years. The subsequent marine ingression was not a gradual process but rather a very swift take-over. The swamps drowned within a few decades and made way for lagoonal marine mollusc assemblages. The transgressive pulse culminated within c. 8000 years in the establishment of highly dynamic shore and foreshore environments. Within another 5000–7000 years, the fully marine conditions switched gradually back and a progradation of swampy conditions took place.
Despite the very clear cyclicity in the sedimentary record, the analysis of the palaeo-vegetation provides no hint of major cyclic climate changes. Therefore, we suggest that the rhythm in the sea-level record was not coupled with a climatic cyclicity in the investigation area. This result, however, may also be an artifact, if the amplitudes of the climatic parameters are too low to be resolved by the Coexistence Approach. On the other hand, the factors influencing the relative sea-level of the huge early Miocene Eurasian Paratethys may not be expressed in the investigation area, which was only a minor appendix.

2.6. Conclusions

The onset of the Middle Miocene Climate Optimum during the late Burdigalian in Central Europe coincided with considerably seasonality. A warm and wet summer season with a precipitation of 204–236 mm during the wettest month was opposed by a rather dry winter season with very low precipitation of c. 9–24 mm in the driest month and temperatures which did not drop significantly below 10°C. The vegetational dynamics in this late Early Miocene estuary were rapid. Major marine ingressions which drowned the marshes and swamps happened within few decades or centuries. The establishment of Taxodiaceae swamps was a rapid process as well which took few millennia. Only the regression of the sea and the coinciding progradation of estuarine and wetland settings was a gradual progress.
The assumption that the statistically significant sedimentary rhythm of the section is related to the 21-kyr-precession cycle is supported by several Middle Miocene wells in the Vienna Basin which document a clear reflection of the precessional and eccentricity cycles (Hohenegger et al., 2008; Lirer et al., 2009). Despite the clear cyclicity in the sedimentary record, however, the palyno-spectra reflect rather stable climatic conditions during the investigated interval (Fig. 2.8). Quantitative changes in the composition of the palyno-assemblages, as obvious in the cluster analysis, seem to be triggered only by shifting local environments bound to periodic marine ingressions into the wetlands of the Korneuburg Basin. This in turn, suggests that the – probably astronomically forced – cyclicity of the sea-level was not coupled with a climatic cyclicity in the investigation area. This misfit might be explained by the fact that the Central Paratethys was just an appendix of the Western Tethys

Ocean during the late Burdigalian (Rögl, 1998). Therefore, the mechanisms forcing the hydrological budget of the huge Western Tethys Ocean are not necessarily visible in its northern embayment on a regional scale. A second explanation might be that the climatic amplitude is below the methodological resolution of the Coexistence Approach due to the broad climatic range of c. 5°C for the MAT and of c. 500 mm for the MAP of the subtropical vegetation of the Korneuburg Basin.

Acknowledgements

The study was supported by the FWF-grants P21414-B16 (*Millennial- to centennial-scale vegetation dynamics and surface water productivity during the Late Miocene in and around Lake Pannon)* and the Geological Survey of Austria. It contributes to the NECLIME network. Many thanks to Andreas Kroh (NHM) for identifications of the starfish remains.

2.7. References

Baldi, T., 1973. Mollusc fauna of the Hungarian Upper Oligocene (Egerian). Akadémiai Kiado, Budapest.

Behling, H., Cohen, M.C.L., Lara, R.J., 2001. Studies on Holocene mangrove ecosystem dynamics of the Bragança Peninsula in north-eastern Pará, Brazil. Palaeogeography, Palaeoclimatology, Palaeoecology 167, 225–242.

Böhme, M. 2003. Miocene Climatic Optimum: evidence from Lower Vertebrates. Palaeogeography, Palaeoclimatology, Palaeoecology 195, 389–401.

Böhme, M., Bruch, A., Selmeier, A., 2007. The reconstruction of Early and Middle Miocene climate and vegetation in Southern Germany as determined from the fossil wood flora. Palaeogeography, Palaeoclimatology, Palaeoecology 253, 91–114.

Britten, R.H., Crivelli, A.J., 1993. Wetlands of southern Europe and North Africa: Mediterranean wetlands. In: Whigham, D.F., Dykyjová, D., Hejný, S. (Eds.), Handbook of vegetation science, Wetlands of the world I: Inventory, ecology and management. Kluver Academic Publishers, Dordrecht, Bosten, London, pp.129–194.

Daxner-Höck, G., 1998. Säugetiere (Mammalia) aus dem Karpat des Korneuburger Beckens. 3. Rodentia und Carnivora. Beiträge zur Paläontologie 23, 367–408.

Debenay, J.-P., Pages, J., Guillou J.-J., 1994. Transformation of a subtropical river into a hyperhaline estuary: the Casamance River (Senegal) – paleogeographical implications. Palaeogeography, Palaeoclimatology, Palaeoecology 107, 103–119.

Denk, T., Frotzler, N., Davitashvili, N., 2001. Vegetational patterns and distribution of relict taxa in humid temperate forests and wetlands of Georgia (Transcaucasia). Biologocal Journal of the Linnean Sociaty 72, 287–332.

Doláková, N., Slamková, M., 2003. Palynological Characteristics of Karpatian Sediments. In: Brzobohatý, R. Cicha, I., Kovác, M., Rögl, F. (Eds.), The Karpatian - a Lower Miocene Stage of the Central Paratethys. Masaryk University, Brno, pp. 325–345.

Donoghue, J.F., 1989. Trends in Chesapeake Bay sedimentation rates during the late Holocene. Quaternary Research 34, 33–46.

Ellison, J., 2005. Holocene palynology and sea-level change in two estuaries in Southern Irian Jaya. Palaeogeography, Palaeoclimatology, Palaeoecology 220, 291–309.

Erdtman, G., 1954. An introduction to pollen analysis. Chronica Botanica Company, Waltham, Massachusetts.

Fauquette, S., Suc, J.-P., Bertini, A., Popescu, S.-M., Warny, S., Bachiri Taoufiq, N., Perez Villa, M.-J., Chikhi, H., Feddi, N., Subally, D., Clauzon, G., Ferrier, J., 2006. How much did climate forace the Messinian salinity crisis? Quantified climatic conditions from pollen recods in the Mediterranean region. Palaeogeography, Palaeoclimatology, Palaeoecology 238, 281–301.

Gleason, P.J., Stone, P., 1994. Age, origin, and landscape evolution of the Everglades peatland. In: Davis, S.M., Ogden, J.C. (Eds.), Everglades: The Ecosystem and its Restauration. St.Lucie Press, Delray, Florida, pp.149–197.

González, C., Dupont, L.M., 2009. Tropical salt marsh succession as sea-level indicator during Heinrich events. Quaternary Science Reviews 28, 939–946.

Gribben, P.E, Helson, J., Millar, R., 2004. Population abundance estimates of the New Zealand geoduck clam, *Panopea zelandica*, using North American methodology: Is the technology transferable? Journal of Shellfish Research 23, 683–691.

Grigore, M.N., Toma, C., 2007. Histo-anatomical strategies of Chenopodiaceae halophytes: adaptive, ecological and evolutionary implications. WSEAS Transaction on Biology and Biomedcine 12/4, 204–218.

Grimm, E.C., 2004. Tilia and TG View Version 2.0.2. Illinois State Museum, Research and Collector Center.

Hammer, Ø., Harper, D.A.T., Ryan, P.D., 2001. PAST; Palaeontological Statistics software package for education and data analysis. Palaeontologica Electronica 4(1), 9 pp.

Harland, R., 1983. Distribution map of recent Dionflagellate cysts in bottom sediments from the North Atlantic Ocean and adjaceted seas. Palaeontology 26, 321–387.

Harzhauser, M., Mandic, O., 2002. Late Oligocene Gastropods and Bivalves from the Lower and Upper Austrian Molasse Basin. In: Piller, W.E., Rasser, M. (Eds.), The Paleogene of Austria. Österreichische Akademie der Wissenschaften, Schriftenreihe der Erdwissenschaftlichen Kommission 14, Vienna, pp. 671–795.

Harzhauser, M., Piller, W.E., 2007. Benchmark data of a changing sea – Palaeogeography, Plaeobiogeography and events in the Central Paratethys during the Miocene. Palaeogeography, Palaeoclimatology, Palaeoecology 253, 8–31.

Harzhauser, M., Mandic, O., Zuschin, M., 2003. Changes in Paratethyan marine molluscs at the Early/Middle Miocene transition - diversity, paleogeography and paleoclimate. Acta Geologica Polonica 53, 323–339.

Harzhauser, M., Sovis, W., Kroh, A., 2009. Das verschwundene Meer. Naturhistorisches Museum, Wien, ISBN 978-3-902421-42-5.

Harzhauser, M., Böhme, M., Mandic, O., Hofmann, Ch.-Ch., 2002. The Karpatian (Late Burdigalian) of the Korneuburg Basin – A Palaeoecological and Biostratigraphical Synthesis. Beiträge zur Paläontologie 27, 441–456.

Hendler, G., Miller, J.E., Pawson, D.E., Kier, P.M., 1995. Sea Stars, Sea Urchins, and Allies. Smithsonian Institution Press, Washington, DC.

Hofmann, Ch.-Ch., Zetter, R., Draxler, I., 2002. Pollen- und Sporenvergesellschaftungen aus dem Kapatium des Korneuburger Beckens (Niederosterreich). Beiträge zur Paläontologie 27, 17–43.

Hohenegger, J., Coric, S., Khatun, M., Pervesler, P., Rögl, F., Rupp, C., Selge, A., Uchman, A., Wagreich, M., 2008. Cyclostratigraphic dating in the Lower Badenian (Middle Miocene) of the Vienna Basin (Austria): the Baden-Sooss core. International Journal of Earth Sciences 98, 915–930.

Jarvis, D.I., Clay-Poole, S.T., 1992. A comparison of modern pollen rain and vegetation in southwestern Sichuan Province, China. Review of Palaeobotany and Palynology 75, 239–258.

Jiang, H., Ding, Z., 2008. A 20 Ma pollen record of East-Asian summer monsoon evolution from Guyuan, Ningxia, China. Palaeogeography, Palaeoclimatology, Palaeoecology 265, 30–38.

Jiménez-Moreno, G., Fauquette, S., Suc, J.-P., 2008. Vegetation, climate and palaeoaltitude reconstructions of the Eastern Alps during the Miocene based on pollen records from Austria, Central Europe. Journal of Biogeography 35, 1638–1649.

Jiménez-Moreno, G., Rodríguez-Tovar, F.I., Pardo-Igúzquiza, E., Fauquette, S., Suc J.P., Müller, P., 2005. High-resolution palynological analysis in the late early-middle Miocene core from the Pannonian Basin, Hungary: climatic changes, astronimical forcing and eustatic fluctuations in the Central Paratethys. Palaeogeography, Palaeoclimatology, Palaeoecology 216, 73–97.

Kamaruzzaman B.Y., Ong, M.C., 2008. Recent Sedimentation Rate and Sediment Ages Determination of Kemaman-Chukai Mangrove Forest, Terengganu, Malaysia. American Journal of Agricultural and Biological Sciences 3, 522–525.

Klaus, W., 1987. Einführung in die Paläobotanik, Band I. Franz Deuticke Verlagsgesellschaft, Vienna.

Koeppen, W., 1936. Das geographische System der Klimate. In: Koeppen, W., Geiger, R. (Eds), Handbuch der Klimatologie. Bebrüder Bornträger, Berlin, pp. 1–44.

Kovar-Eder. J., Meller, B., Zetter, R., 1998. Comparative investigations on the basal fossiliferous layers at the opencast mine Oberndorf (Köflach-Voitsberg lignite deposits, Styria, Austria; Early Miocene). Review of Palaeobotany and Palynology 101, 125–145.

Kovar-Eder, J., Kvaček, Z., Martinetto, E., Roiron, P., 2006. Late Miocene to Early Pliocene vegetation of southern Europe (7–4 Ma) as reflected in the megafossil plant record. Palaeogeography, Palaeoclimatology, Palaeoecology 238, 321–339.

Kvaček, Z., Sakala, J., 1999. Twig with attached leaves, fruits and seeds of Decodon (Lythraceae) from the Lower Miocene of northern Bohemia, and implications for the identification of detached leaves and seeds. Review of Palaeobotany and Palynology 107, 201–222.

Kvaček, Z., 2003. The Flora and Vegetation of the Karpatian. In: Brzobohatý, R. Cicha, I., Kovác, M., Rögl, F. (Eds.), The Karpatian - a Lower Miocene Stage of the Central Paratethys. Masaryk University, Brno, pp. 347–351.

Latal, C., Piller, W.E., Harzhauser, M., 2005. Small-scaled environmental changes: indications from stable isotopes of gastropods (Early Miocene, Korneuburg Basin, Austria). International Journal of Earth Sciences 95, 95–106.

Li, Z., Saito, Y., Matsumoto, E., Wang, Y., Haruyama, S., Hori, K., Doanh, L.Q., 2006. Palynological record of climate change during the last deglaciation from the Song Hong (Red River) delta, Vietnam. Palaeogeography, Palaeoclimatology, Palaeoecology 235, 406–430.

Lirer, F., Harzhauser, M., Pelosi, N., Piller, W.E., Schmid, H.P., Sprovieri, M., 2009. Astronomically forced teleconnection between Paratethyan and Mediterrean sediments during the Middle and Late Miocene. Palaeogeography, Palaeoclimatology, Palaeoecology 275, 1–13.

Lynch, J.C., Meriwether, J.R., McKee, B.A., Vera-Herrera F., Twinlley, R.R., 1989. Recent accretion in mangrove ecosystems based on ^{137}Cs and ^{210}Pb. Estuaries 4, 284–299.

Mai, D.H., 1964. Die Mastixioideen-Floren im Tertiär der Oberlausitz. Paläontologische Abhandlungen B, 2, 1–192.

Márton, E., 2008. Palaeomagnetism and paleogeography. In: Rasser, M. and Harzhauser, M. (Eds.), Palaeogene and Neogene. In.: McCann, T. (Ed.), The Geology of Central

Europe, Volume 2: Mesozoic and Cenozoic. Geological Society, London, pp. 1033–1035.

Mandic, O., Harzhauser, M., Roetzel, R., Tibuleac, P., 2008. Benthic mass-mortality events on a Middle Miocene incised-valley tidal-flat (North Alpine Foredeep Basin). Facies 54, 343–359.

Mandic, O., Harzhauser, M., Schlaf, J., Piller, W.E., Schuster, F., Wielandt-Schuster, U., Nebelsick, J.H., Kroh, A., Rögl, F., Bassant, P., 2004. Palaeoenvironmental Reconstruction of an Epicontinental Flooding - Burdigalian (Early Miocene) of the Mut Basin (Southern Turkey). Courier Forschungsinstitut Senckenberg 248, 57–92.

Martini, E., 1971. Standard Tertiary and Quaternary calcareous nannoplankton zonation. In: Farinacci, A. (Ed.), Proceedings of the II. Planktonic Conference. Tecnoscienza, Roma, pp.739–785.

Meller, B., 1998. Karpo-Taphocoenosen aus dem Karpat des Korneuburger Beckens (Unter-Miozän; Niederösterreich) – ein Beitrag zur Vegetationsrekonstruktion. Beiträge zur Paläontologie 23, 85–121.

Meller, B., Kovar-Eder, J., Zetter, R., 1999. Lower Miocene diaspore-, leaf- and palynomorph-assemblage from the base of the lignite-bearing sequence in the opencast mine Oberdorf N Voitsberg (Styria, Austira) as indication of a “Younger Mastixioid” vegetation. Palaeontographica Abt. B 252, 123–178.

Mosbrugger, V., Utescher, T., 1997. The Coexistence Approach – A new method for quantitative reconstructions of Teriary terrestrial paleoclimate data using plant fossils. Palaeogeoraphy, Palaeoclimatology, Palaeoecology 134, 61–86.

Müller, M.J., 1996. Handbuch ausgewählter Klimastationen der Erde. Forschungsstelle Bodenerosion Universität Trier, Mertesdorf (Ruwertal).

Patchineelam, S.R., Smoak, J.M., 1999. Sediment Accumulation Rates Along the Inner Eastern Brazilian Continental Shelf. Geo-Marine Letters 19, 196–201.

Peel, M.C., Finlayson, B.L., McMahon, T.A., 2007. Updated world map of the Köppen-Geiger climate classification. Hydrology and Earth System Science Discussions 4, 439–473.

Piller, W.E., Harzhauser, M., Mandic, O., 2007. Miocene Central Paratethys stratigraphy – current status and future directions. Stratigraphy 4, 151–168.

Planderová, E., 1990. Miocene microflora of Slovak Central Paratethys and its biostratigraphical significance. Dionýz Štúr Institute of Geology, Bratislava.

Rögl, F., 1998. Palaeogeographic considerations for Mediterranean and Paratethys Seaways (Oligocene to Miocene). Annalen des Naturhistorischen Museums in Wien 99, 279–310.

Scholger, R., 1998. Magnetostratigraphic and palaeomagnetic analysis from the Early Miocene (Karpatian) deposits Teiritzberg and Obergänserndorf (Korneuburg Basin, Lower Austria). Beiträge zur Paläontologie 23, 25–26.

Smoak, J. M., Patchineelam, S.R., 1999. Sediment Mixing and Accumulation in a Mangrove Ecosystem: Evidence From ^{210}Pb, ^{234}Th and ^{7}Be. Mangroves and Salt Marshes 3, 17–27.

Sovis, W., Schmid, B., 1998. Das Karpat des Korneuburger Beckens, Teil 1. Beiträge zur Paläontologie 23, 1–413.

Sovis, W., Schmid, B., 2002. Das Karpat des Korneuburger Beckens, Teil 2. . Beiträge zur Paläontologie 27, 1–467.

Turon, J., 1994. Le palynoplancton dans l'environment de l'Atlantique nord-oriental Évolution climatique et hydrologique depuis le dernier maximum glaciaire. Docorat ès sciences thesis, Université Bordeaux I, Mémoire de l'Institut de Géologie du Bassin d'Aquitaine.

Utescher, T., Mosbrugger, V., Ashraf, A.R., 2000. Terrestrial Climate Evolution in Northwest Germany over the last 25 Million years. Palaios 15, 430–449.

Utescher, T., Ivanov, D., Harzhauser, M., Bozukov, V., Ashraf, A.R., Rolf, C., Urbat, M., Mosbrugger, V., 2009. Cyclic climate and vegetation change in the late Miocene of Western Bulgaria. Palaeogeography, Palaeoclimatology, Palaeoecology 272, 99–114.

Van Santen, P., Augustinus, P.G.E.F., Janssen-Stelder, B.M., Quartel, S., Tri, N.H., 2007. Journal of Asian Earth Sciences 29, 566–575.

Wessely, G., 1998. Geologie des Korneuburger Beckens. Beiträge zur Paläontologie 23, 9–23.

Wilen, B.O., Tiner, R.W., 1993. Wetlands of the United States. In: Whigham, D.F., Dykyjová, D., Hejný, S. (Eds.), Handbook of vegetation science, Wetlands of the world I: Inventory, ecology and management., Kluwer Academic Publishers, Dordrecht, Bosten, London, pp. 129–194.

Willard, D.A., Weimer, L.M., Riegel, W.L., 2001. Pollen assemblage as paleoenvironment proxies in the Florida Everglades. Review of Palaeobotany and Palynology 113, 213–253.

Vershinin A., 2007. Book Living Black Sea. Kogorta Publishers, Krasnodar- Moscow.

Zonneveld, K.A.F., 1995. Palaeoclimatic and palaeo-ecological changes during the last deglaciation in the Eastern Mediterranean – implications for dinoflagellates ecology. Review of Palaeobotany and Palynology 84, 221–253.

Zuschin, M., Harzhauser, M., Mandic, O., 2004. Palaeoecology and taphonomy of a single parautochthonous Paratethyan tidal flat deposit (Karpatian, Lower Miocene - Kleinebersdorf, Lower Austria). Courier Forschungsinstitut Senckenberg 246, 153–168.

Chapter 3

Precipitation driven decadal scale decline and recovery of wetlands of Lake Pannon during the Tortonian

Andrea K. Kern[a*], Mathias Harzhauser[a], Ali Soliman[b], Werner E. Piller[b], Martin Gross[c]

[a] Natural History Museum Vienna, Geological-Paleontological Department, Burgring 7, 1010 Vienna, Austria.

[b] Institute of Earth Sciences, Graz University, Heinrichstrasse 26, 8010 Graz, Austria.

[c] Abteilung für Geologie & Paläontologie, Universalmuseum Joanneum, Weinzöttlstraße 16, 8045 Graz, Austria.

[*] Corresponding author. Fax: 0043-1-52177-459; E-mail address: andrea.kern@nhm-wien.ac.at

Abstract

High resolution pollen and dinoflagellate analyses were performed on a continuous 98-cm-long core from Tortonian deposits of Lake Pannon in the Styrian Basin in Austria. The sample distance of 1-cm corresponds to a resolution of roughly one decade, allowing insights into environmental and climatic changes over a millennium of Late Miocene time. Shifts in lake level, surface water productivity on a decadal- to centennial-scale can be explained by variations of rainfall during the Tortonian climatic optimum. Related to negative fine scale shifts of mean annual precipitation, shoreline vegetation belts reacted in an immediate replacement of Poaceae by Cyperaceae as dominant grasses in the marshes fringing the lake. In contrast to such near-synchronous ecosystem-responses to precipitation, a delayed lake level rise of 4–6 decades is evident in the hydrological budget of Lake Pannon. This transgression, caused by a precipitation increase up to >1200 mm/yr, resulted in a complete dieback of marshes. Simultaneously, "open-water" dinoflagellates, such as *Impagidinium*, took over in the brackish lagoon and fresh water dinoflagellates disappeared. As soon as the rainfall switched back to moderate levels of ~1100–1200 mm/yr, the rise of the lake level slowed down, the marsh plants could keep up again and the former vegetation belts became re-established.

Thus, mean annual precipitation, more than temperature, was the main driving force for high-frequency fluctuations in the Tortonian wetlands and surface water conditions of Lake Pannon. Such high resolution studies focusing on Tortonian decadal to centennial climate change will be crucial to test climate models which try to compare the Tortonian models with predictions for future climate change.

Keywords: High resolution analysis, pollen, Tortonian, palaeoclimate, palaeoenvironment, plant-climate-interaction.

3.1. Introduction

The Early Tortonian is characterized by a short global warming phase with humid conditions in Europe (e.g. Bruch et al., 2006; Bruch et al., 2007; Utescher et al., 2009; Pound et al., 2010; Utescher et al., 2011), also referred to as “washhouse climate” by Böhme et al. (2008). Simultaneously, Atlantic deep water temperatures did rise about 3°C during the Early Tortonian (Lear et al., 2003). Therefore, the Tortonian is a major target for climate models calculating future climate change. Tortonian models (e.g.: François et al., 2006; Steppuhn, et al., 2006) are then sometimes compared with proxy data to test their fit (Micheels et al., 2007; Steppuhn et al., 2007). Nevertheless, there exists surprisingly little information on the variability of Tortonian climate on a decadal to centennial scale. An opportunity to study such a high resolution archive is the deposits of Lake Pannon, which covered the Pannonian basins complex during the Late Miocene (Magyar et al., 1999a; Harzhauser and Mandic, 2008; Lirer et al., 2009; Vasiliev et al., 2010). The Tortonian vegetation surrounding the lake is documented from numerous localities. Leaf floras, fruits, seeds and pollen have been extensively described (e.g. Draxler et al., 1994; Hably and Kovar-Eder, 1996; Kovar-Eder et al., 1995; Kovar-Eder et al., 2002; Meller and Hofmann, 2004; Kovar-Eder and Hably, 2006; Erdei et al., 2007; Harzhauser et al., 2008). Generally, most of these studies dealt with the alpha diversity of a locality without referring to short shifts in local and regional vegetation. Moreover, these data allow a rough estimate of climatic parameters and indicate large-scale temporal shifts in climate during the Late Miocene in this area (Bruch et al., 2006). Aside from a pioneer study on a 37-cm-long core, covering a major transgression of Lake Pannon (Harzhauser et al., 2008), no study tried to elucidate local changes in vegetation on a decadal or centennial scale so far. To enlarge our understanding of short-termed climate variability in the Late Miocene, we performed a high-resolution study on a 98-cm-long core from the Styrian Basin. The study focuses on dinoflagellates and pollen to reconstruct vegetation dynamics around the lake in context of surface water ecology. A suitable locality for such detailed analyses is Mataschen in the eastern Styrian Basin. First paleobotanical analysis on the c. 30-m-thick section showed a change in vegetation from a swampy environment with azonal leave-floras to a more diverse assemblage at the top indicating a zonal subtropical evergreen broad leaf forest (Meller and Hofmann, 2004; Kover-Eder and Hably, 2006). These authors interpreted a warm climate for the Late Miocene with a mean annual temperature of 15°–19°. Our aim is to detect vegetation dynamics and surface water productivity on a decadal scale over a very short time span of roughly one millennium. This will allow to describe and to quantify the bandwidth of rapid climate change of early Late Miocene time.

3.2. Geological Setting

Several cores were taken from the Lias Austria GmbH clay pit at Mataschen (15°57'16''E/46°54'15''N), about 5 km SW of Fehring in the district Feldbach (Styria, SE of Austria). Mataschen is located in the Eastern Styrian Basin, which is the westernmost part of the Pannonian Basin (Fig. 3.1). The basin comprises up to 4,000 m of Neogene sediments ranging from the Lower Miocene to the Pliocene (Kollmann, 1965). The clay pit comprises c. 30 m of pelitic to psammitic deposits. The studied core was taken from the lower pelitic interval of the section belonging to the Feldbach Formation (Gross, 2004). This formation comprises lowermost Pannonian sediments, which were deposited when Lake Pannon was in its early phase and the lake level was still low. The water body was restricted to rather narrow basins with a large number of islands (Magyar et al., 1999a; 1999b). The base is formed by a more than 1.5 m think sandy unit. It is overlain by a 5-m-thick unit of clay and silt, with numerous fossils in the base. Vertebrate fossils, such as turtles, beavers and hamsters (Gross, 1994; 2004; Daxner-Höck, 2004), appear in this part, as well as leaves, seeds, pollen and in-situ tree trunks up to 4 m in height (Gross, 2004; Kovar-Eder, 2004;

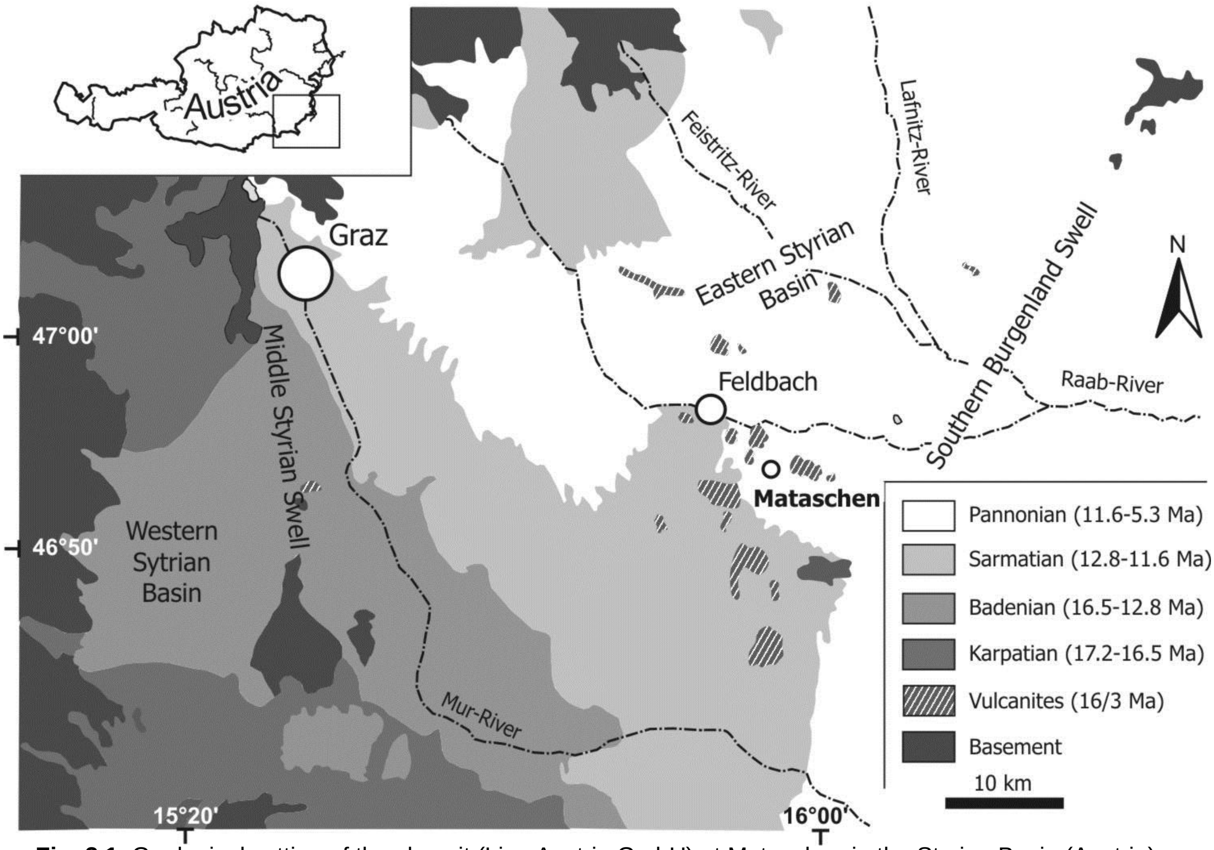

Fig. 3.1. Geological setting of the clay pit (Lias Austria GmbH) at Mataschen in the Styrian Basin (Austria) (after Gross, 2004; Gross et al., 2011).

Meller and Hofmann, 2004). The tree trunks belong to the Taxodioideae, and might represent *Glyptostrobus* in respect to the frequent occurrence of seeds and leaves of this genus (Gross, 2004; Gross et al., 2011). Above follows a coquina with shells of the bivalve *Mytilopsis neumayri* (Harzhauser, 2004) and scattered *Mytilopsis ornithopsi*s, lymnocardiids and fish remains. The analyzed cores comprise solely dark silty clay to clayey silt. No coquinas are intercalated, but debris of lymnocardiid bivalves is frequent in the upper part. Only very little indication of bioturbation is observed.

3.2.1. Stratigraphy, dating and age model

The pelitic interval of the Mataschen section belongs to the Lower Pannonian Feldbach Formation (*Mytilopsis ornithopsis* zone; Gross, 2003, 2004a; Harzhauser, 2004; = Pannonian B sensu Papp, 1951). This indicates an Early Tortonian age (early Late Miocene), which correlates to the early Pannonian in regional stratigraphy.

Based on an integrated approach combining palaeomagnetics, seismic data and mammal biostratigraphy, Gross et al. (2011) correlated the section to the short Chron C5r.2r-1n (11.308–11.263 Ma). This reduces the maximum time range of the section to about 45 kyr and suggest an average sedimentation rate of >0.7 mm/yr (maximal ~1.4 mm/yr) (Gross et al., in press). These values area also comparable to other estimations for Lake Pannon (Harzhauser et al., 2008; Lirer et al., 2009) and lacustrine-deltaic sequences in the Dacian Basin (Vasiliev et al., 2004). Thus, the studied cores of 98 cm represent between between 700–1400 years (7–14 yr/sample). As a completely constant sedimentation rate is unlikely in such a marginal setting we consider the average resolution to range around one decade.

3.3. Material and methods

98 samples were selected from two successive cores with a diameter of 100 mm, which were taken by a percussion drill. These cores were cut with a sample distance of 5 mm, but only every second sample was investigated for this study, resulting in a 1-cm sample resolution. Preparation of the palynological samples followed the steps of Green (2001) and Wood et al. (1996). Each sample was dried, weighed and one *Lycopodium clavatum* tablet was added to calculate the absolute number of pollen and dinoflagellate cysts. Then they were treated with cold HCl (34%) to remove all carbonate. After washing with distilled water, the samples were treated with HF (48%) and cold HCl to fully remove all silicates and colloids. The residue was ultrasonicated (c. 15–30 seconds) and colored with Safranine O., before it was sieved at 15 µm with a nylon sieve. Two glass slides were prepared from each sample using glycerin jelly and sealed with nail polish. In each sample, at least the first c. 250 dinoflagellate cysts and 200 pollen grains (excluding *Pinus*) were identified, respectively.

Although artificial staining was applied, some palynomorphs (less than 25 µm) still have a very pale yellow/brown color. Among the dinoflagellates, one palynomorph characterized by a surface covered by small spines could not be differenced further in the light microscope. Therefore, during routine counting, these palynomorphs were grouped as “small spiny palynomorphs” (SSP). Scanning electron microscopy revealed that SSP comprise mostly *Protoperidinium* sp. sensu Londeix et al., 2009, ?*Algidasphaeridium minutum* var. *cezare* sensu de Vernal et al., 1989 and the acritarch genus *Nannobarbophora*.
The software PAST (Hammer et al., 2001) was used to calculate cluster analyses. The data used for these analyses were transformed using the arcsin-root method (Linder and Berchtold, 1976; Zuschin and Hohenegger, 1998). These clusters are only based on sample similarity and do not reflect pollen-zones as typical in Tilia graphs (Grimm, 2004). Statistical analyses were used to characterize clusters; abbreviations mentioned in the text are µ for mean value and ó for standard deviation, which are calculated based on the percentage data. The pollen diagram was created by Tilia and Tilia-Graph (Grimm, 2004). The climatic reconstructions were achieved with the Coexistence Approach (Mosbrugger and Utescher, 1997), which is based on the presence or absence of pollen taxa. For each plant taxon, the most appropriate nearest living relative is determined to get reliable climatic data. This information provides a climatic interval, in which the nearest living relative is able to survive and reproduce. Taxa, which are today only limited to retreat areas, such as *Cathaya* or *Sciadopitys*, were excluded from the climatic analysis, because their recent distribution might not reflect their Miocene habitat requirements. Additionally, taxa were not considered, if their living environment is probably far away and/or in different altitude. They are only present in the studied assemblage because their pollen grains are suggested to be suitable for far-distance transport (e.g. *Picea*, *Tsuga*, *Ephedra* or *Keteleeria*) (Hopkins, 1950; Traverse and Ginsburg, 1966; Heusser and Balsam, 1977). All remaining taxa were analyzed to define an interval, in which all the nearest living relatives could “co-exist”. This is called the Coexistence interval and is presented here as the climatic interval, in which the fossil taxa are most likely to have existed. This method helps to objectify the data, while the interpretation of the abundances (as given in the Tilia-Graph) depends more on the personal opinion and experience of the worker.
The studied material is stored at the Natural History Museum Vienna.

3.4. Results

3.4.1. Dinoflagellates – composition and patterns

Taphonomy: The dark grey-green clay to silt and the considerable amount of iron-sulfides document low oxygen conditions. Organic material was protected from oxidation by fast burial. Therefore, selective preservation due to aerobic degradation is unlikely (see Zonneveld et al., 2008 for discussion). The concentration of dinoflagellates and acritarchs per gram sediment fluctuates strongly between ~5,000 and ~30,000. Values between 10,000 and 20,000 are typical on average in the lower part of the core whilst the upper part displays three phases of elevated values of 15,000–25,000 on average (samples 56–63, 71–80, 83–91) separated by shorter intervals of low dinoflagellate concentration. The statistical grouping of samples according to the composition as described below does not correlate at all with the pollen concentration values. This is taken as further proof that selective preservation does not obscure the overall patterns.

Composition: A rather low diversity of about 21 dinoflagellate taxa has been encountered (Table 3.1). Typical are Paratethyan endemic morphotypes of the *Spiniferites/Achomosphaera*-group spp. and *Impagidinium* spp. In addition, the assemblage is characterized by the occurrence of *Pyxidinopsis psilata*, *Polykrikos kofoidii/schwartzii*, *Protoperidinium* sp., *Mendicodinium* sp., ?*Algidasphaeridium minutum* var. *cezare* and the acritarch genus *Nannobarbophora* (*N. gedlii, Nannobarbophora* sp. 1 and *Nannobarbophora* sp. 2). The heterotrophic taxa, *Selenopemphix nephroides* s.l. and *Selenopemphix* sp.1 and "small round brown cysts" (RBC) are frequent in all samples as well. Other taxa as *Lejeunecysta* spp., *Nematosphaeropsis* sp., and *Batiacasphaera sphaerica* are rare.
The predominating *Spiniferites/Achomosphaera*-group and the small spiny palynomorphs (SSP) show a more or less opposing trend. Roughly parallel trends are documented for *Impagidinium* spp. and *Selenopemphix nephroides*. Similarly, *Spiniferites bentorii pannonicus* and *Spiniferites b. budajenoensis* display nearly parallel trends coinciding with *Selenopemphix* sp.1 with some offset. The core reveals 8 prominent peaks in the peridinioid-gonyaulacoid ratio (P/G ratio), which represents a rough estimate between heterotroph and autotroph dinoflagellates (samples 10, 15, 22, 34, 45, 60, 76 and 89). The ratio is mainly caused by the opposing trend between the SSP and the *Spiniferites/Achomosphaera*-group. These peaks seem to appear in more or less regular periodicities of 11–16 samples after sample 22. Aside from these marked fluctuations, the dinoflagellate record suggests several distinct phases:
The lower part of the core (samples 1–20) is characterized by moderate fluctuations in the RBC, SSP and *Spiniferites/Achomosphaera*-group records. Above follows a rather stable interval up to sample 48, in which none of the dominant groups shows major fluctuations. This interval coincides also with regular occurrences of *Polykrikos kofoidii/schwartzii* cysts and the main phase of *Pyxidinopsis psilata*. The following interval to sample 55 displays a sudden drop in *Spiniferites b. pannonicus, S. b. budajenoensis* and the SSP record, followed by a drop in *Selenopemphix* sp.1 with a 3-sample-delay. This low is compensated by a peak

of *Impagidinium* spp. and *Selenopemphix nephroides*. The pattern is reversed in the following interval up to sample 60. The *Impagidinium* peak decreases together with *S. nephroides*. Up to sample 76, the fluctuations of most groups, aside from the SSP, are moderate. Then, *Selenopemphix* sp.1 displays a slight peak, which is succeeded soon after by *S. b. pannonicus* and *S. b. budajenoensis* up to sample 80. The top of the core is characterized by the gradual increase of *Impagidinium* spp., RBC and *Selenopemphix nephroides* and a general decrease of the SSP.

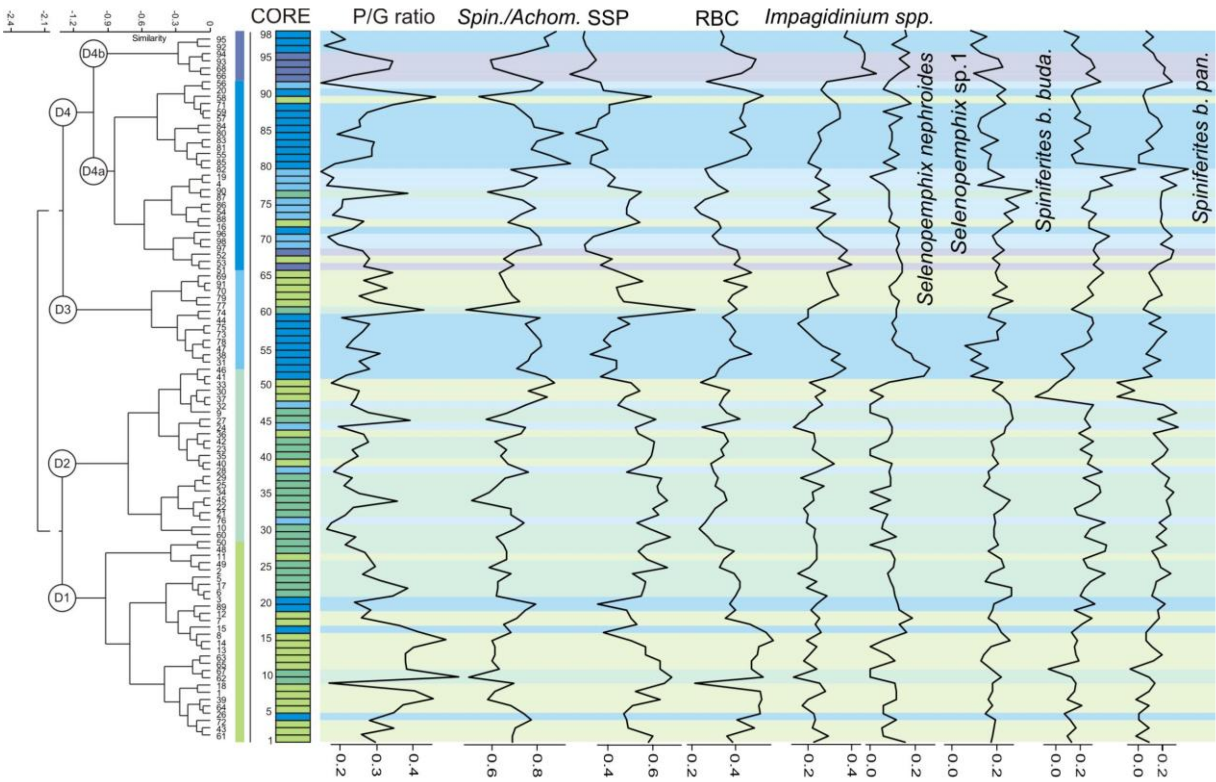

Fig. 3.2. Dinoflagellates: cluster analysis (Ward's method) based on the arcsin-root method transformed percentages (see Table 3.1 for taxa included). The most significant clusters are labeled D1–D4 (a/b) and colors are assigned to the clusters. This color code was applied to the samples according to their cluster-affiliation along the core. Arcsin-root transformed percentage-based dinoflagellates diagrams for the most important constituents are presented on the right.

Statistics: To achieve a more objective grouping of the data set, a cluster analysis (Ward's Method) was performed. This revealed a grouping of the samples according to their similarity into 4 clusters (D1–D4) and 2 sub-clusters (D4a and D4b). The four significant clusters have been transposed into a color code in Fig. 3.2 for a better visualization of the distribution within the core. Cluster D1 unites the most balanced samples (n= 28). *Spiniferites/Achomosphaera* dominate (μ=39.1%, ó=7.2) followed by SSP (μ=25.8%, ó=5.2) and RBC (μ=17.1%, ó=6.1) whilst *Impagidinium* spp. are rare (μ=6.5%, ó=2.2). All other groups remain below 5%. Cluster D2 (n=24) is similar to D1 but differs in a slight decrease of *Spiniferites/Achomosphaera* (μ=34.0%, ó=5.7) and RBC (μ=12.1%, ó=4.3) and an increase of SSP (μ=32.9%, ó=5.9). *Impagidinium* remains low (μ=4.8%, ó=1.5). The samples which form clusters D1 and D2 are mainly found in the lower half of the core and in the interval 60–65. Scattered samples of these clusters in the upper part of the core coincide with peaks in the P/G ratio.

Samples of clusters D3–D4 dominate the upper half of the core and are generally characterized by lower SSP values and higher *Spiniferites/Achomosphaera* values when compared to D1 and D2. Cluster D3 (n=13) bears only a mean of 17.9% (ó=5.4) of SSP and 7.6% (ó=1.8) RBC but 48.1% (ó=4.2) of *Spiniferites/Achomosphaera*. Simultaneously, *Spiniferites bentorii budajenoensis* increases to 8.7% (ó=3.6) whilst *Impagidinium* remains at a low level of 6.8% (ó=2.6). Samples of cluster D4a (n=27) dominate the intervals 51–59 and 80–90 and are marked by very low amounts of SSP (µ=14.1%, ó=4.3) and higher contributions by RBC (µ=15.0%; ó=4.0). *Spiniferites/Achomosphaera* attain the highest values (µ=51.2%, ó=6.2) and *Impagidinium* remains at values of 7.9% (ó=3.4). All other groups contribute less than 4% each to the assemblages. Cluster D4b comprises only few samples (n=6), encompassing interval 92–95 and samples 66 and 68, but is outstanding in its high amount of *Impagidinium* (µ=18.2%, ó=3.6) and the lowest amounts of SSP (µ=9.6%, ó=2.7). RBC values (µ=17.5%, ó=3.2) and *Spiniferites/Achomosphaera* (µ=38.7%, ó=5.5) are comparable to D1.

3.4.2. Pollen and spores

Taphonomy: The pollen preservation does not vary much within these 98 samples although the total number of pollen preserved per gram sediment differs between approximately 4,500 and 22,000. The highest pollen density occurs in the upper part of the section. The number of pollen-taxa within one sample ranges from 22 to 40. The most diverse samples are situated between sample 39 and 48 (30 to 40 taxa) followed by a diversity-low between samples 49 to 62 containing only 23 to 28 different plants. This does not correlate with the pollen-per-gram calculation indicating that the pattern is not based solely on taphonomic processes.

Composition: 71 plant taxa have been detected in all samples (Table 3.1). The most abundant taxon is *Pinus*, which usually ranges between 20–30% except for 4 peaks with more than 40% (samples 42, 47, 48, 62). Therefore, *Pinus* was not excluded from the whole assemblage for further calculations and interpretations. The next most frequent taxa are *Cathaya* and Taxodioideae, with a significantly high contribution between samples 16 to 44 (Fig. 3.3). Of the remaining gymnosperms, only *Picea* attains more than 10%, while *Abies* does hardly exceed 5%. Similar to *Abies*, *Sciadopitys* is present in almost all samples, whilst *Keteleeria*, *Ephedra*, *Ginkgo*, *Cedrus* and Cupressaceae (excluding Taxodioideae) are only sporadically found in low numbers.

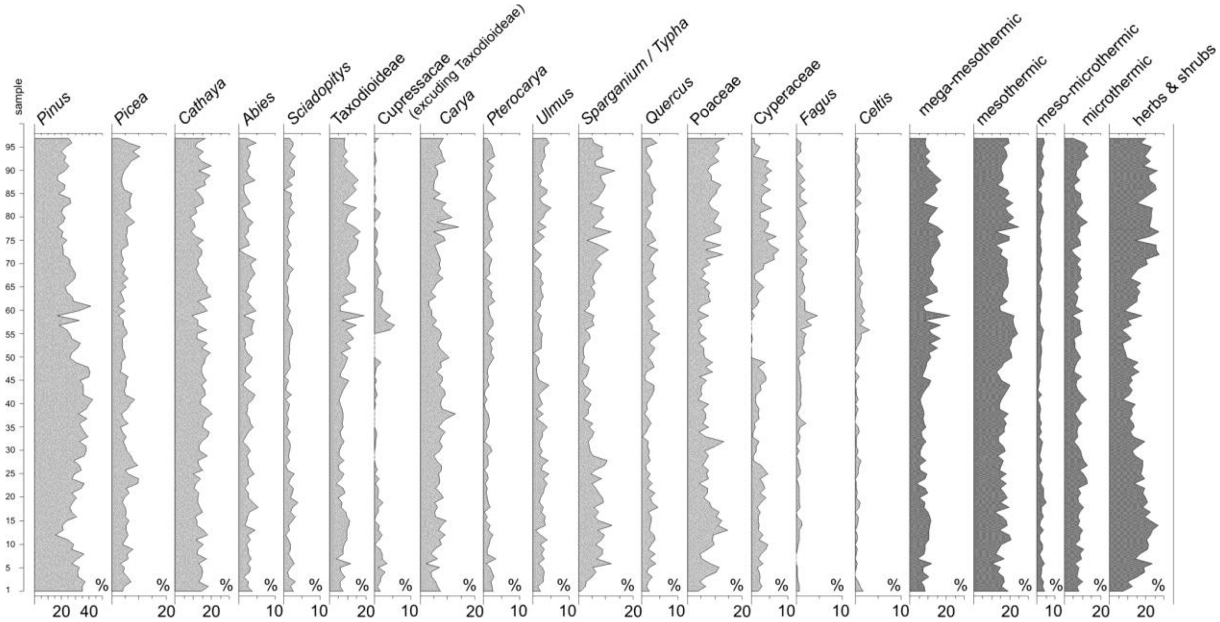

Fig. 3.3. Pollen-diagram, created after Grimm (2004), of the most important taxa and pollen groups according to their suggested ecological requirements after Jiménez-Moreno (2006) and Jimémez-Moreno and Suc (2007):
1. Megathermic-mesothermic elements ("thermophile" taxa): Araliaceae, Arecaceae, Engelhardia Euphorbiaceae, Hamameliaceae, Mastixiaceae, Myrica, Reevesia, Rutaceae, Platycarya, Symplocos, Sapotaceae, Taxodioideae. **2. Mesothermic elements** (warm temperate climate): Acer, Alnus, Betula, Buxaceae, Carpinus, Carya, Castanea-Castanopis-type, Celtis, Fagus, Fagaceae, Fraxinus, Ginkgo, Hedera, Ilex, Juglans, Liquidambar, Lonicera, Nyssa, Pterocarya, Quercus, Rhus, Salix, Tilia, Ulmus, Vitaceae, Zelkova. **3. Meso-microthermic** (cold temperate climate or elevated areas): Cedrus, Sciadopitys, Tsuga. **4. Microthermic** (mountainous areas): Abies, Picea. 5. Herbs and shrubs: Artemisia, Asteraceae, Caryophyllaceae, Chenopodiaceae, Cyperaceae, Ephedra, Ericaceae, Malvaceae, Myriophyllum, Nympheaceae, Plumbaginaceae, Poaceae, Pontamogetaceae, Sparganium/Typha, Trapaceae.

Among the angiosperms, Poaceae and *Sparganium*/*Typha* attain 4–14% and 2–13%, respectively (Fig. 3.3). These taxa along with Cyperaceae (up to 7.8%) show a clear increase up to sample 30, decrease thereafter, and increase again from sample 64 to the top. Only one angiosperm taxon, *Carya*, attains more than 15% while *Quercus*, *Ulmus*, *Fagus* and *Celtis* are less frequent. Gymnosperms dominate most samples compared with the angiosperms. Their amount reaches up to 76% at sample 42, but then decrease to the top, where many samples display a contribution by angiosperms of more than 40%.
The amount of spores is very low in all samples (< 3%) and varies only on a small scale. Only a few taxa could be identified on genus level including *Osmunda*, *Lycopodium* and different taxa of Pteridaceae, Polypodiaceae and Schizaeaceae. These were excluded from statistic analysis.
The pollen-taxa were grouped according to their suggested climate and ecological requirements following Jiménez-Moreno (2006) and Jiménez-Moreno and Suc (2007) (Fig. 3.3) in megathermic-mesothermic elements ("thermophilous" taxa), mesothermic elements (warm temperate climate), meso-microthermic (cold temperate climate or elevated areas), microthermic (mountainous areas) and herbs and shrubs. Afterwards these groups were adjusted to include all significant plants present in this assemblage.

The whole assemblage is comparable with those described in previous studies of Draxler et al. (1994) and Meller and Hofmann (2004). The exact position of those samples, however, is not indicated and therefore we refrain from integrating additional information from their SEM investigations.

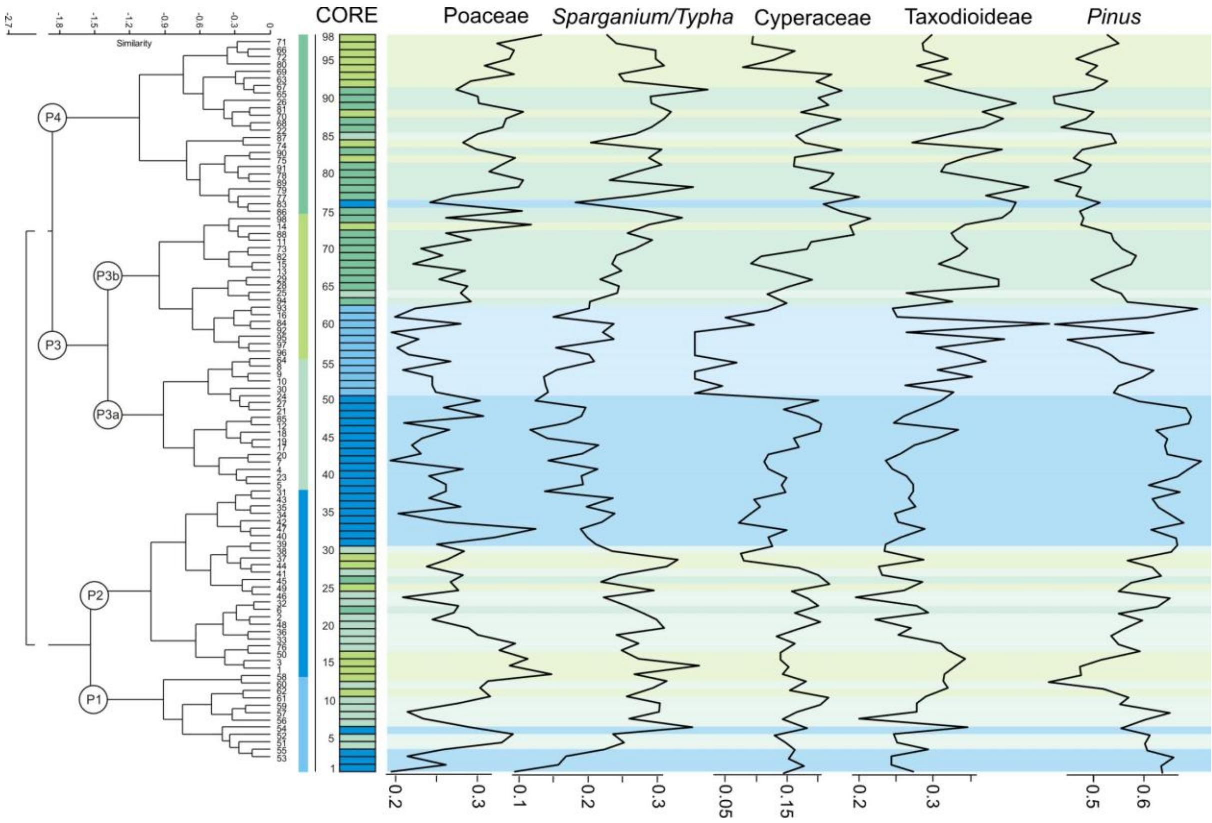

Fig. 3.4. Pollen data: cluster analysis (Ward's method) based on the arcsin-root method transformed percentages (see Table 3.1 for taxa included). The most significant clusters are labeled P1–P4 and colors are assigned to the clusters. This color code was applied to the samples according to their cluster-affiliation along the core. arcsin-root method transformed percentage-based pollen diagrams for the most important constituents of the pollen-assemblages are presented on the right.

Statistics: A cluster analysis (Ward's Method) was performed based on all pollen taxa to define differences in the palyno-assemblages. This resulted in four main clusters (P1 to P4) with 2 subclusters (P3a and P3b) (Fig. 3.4):

Cluster P1 unifies samples from the middle part of the core (samples 51 to 62) characterized by a high contribution of Taxodioideae (µ=10.4%, ó=4.0), Cupressaceae (µ=1.7%, ó=2.0), *Nyssa* (µ=0.9%, ó=0.5) and mesothermic trees, such as *Celtis* (µ=1.2%, ó=0.8), *Liquidambar* (µ=0.6%, ó=0.4), *Quercus* (µ=2.7%, ó=1.0) and *Fagus* (µ=2.0%, ó=1.1).

The second cluster P2 comprises a large group of samples from sample 31 to 50, a smaller group in the base (samples 1–3, 6) and one single sample at the top (76). This group is characterized by the frequent occurrence of *Pinus* (µ=36.0%, ó=3.8) and *Cathaya* (µ=15.8 %, ó=1.8), which is caused by the disappearance of many other taxa. Consequently, the main part of this cluster coincides with the lowest taxa concentration (Table 3.2). The decrease of

Sparganium/Typha and Poaceae as well as a break down of Cyperaceae shortly at sample 31 is most significant.

Cluster P3 is separated into subclusters P3a and P3b, which are dominating the lower third of the core. P3a comprises samples 4, 5, 7–10, 12, 17–21, 23 and 24, 27, 30, 64 and 85, while P3b-samples are represented by samples 11, 13–16, 25, 28–29, 73, 82, 84, 88 and 92–98. In both assemblages a high abundance of herbs and shrubs is typical. P3a's strongest element is *Sparganium/Typha* (µ=7.1 %, ó=1.9), but also Poaceae (µ=7.8%, ó=2.0) and Cyperaceae (µ=2.6% ó=1.0) are important constituents of the plant community. Nevertheless, *Pinus* is strongly present (µ=30.6%, ó=4.0). Cluster P3b is even more influenced by herbs and shrubs (µ=21.3%, ó=2.6), notably due to the presence of *Sparganium/Typha* (µ=7.9%, ó=4.0) and Poaceae (µ=10.4%, ó=2.4). Additionally, the appearance of Taxodioideae is important (µ=9.0%, ó=1.9).

Samples of cluster P4 are located mostly in the upper half of the section (samples 63, 65–72, 74–75, 77–81, 83, 86–87, 89–91) and two single occurrences in the lower part (sample 22 and 26). The assemblage is similar to cluster P3, due to the high amount of herbs and shrubs pollen (µ=20.4%, ó=4.4). Additionally to *Sparganium/Typha* (µ=7.6%, ó=2.3) and Poaceae (µ=8.4% ó=2.1), Cyperaceae show their widest distribution (µ=4.0%, ó=1.8). Further, the high amount of Taxodioideae (µ=12.2%, ó=2.6), and the increasing number of *Nyssa* (µ=0.4% ó=0.3) are present.

3.5. Discussion

3.5.1. Palaeoclimate

The climatic reconstruction was performed by using the Coexistence Approach (CA) of Mosbrugger and Utescher (1997). In each sample, the ecological requirements of 11 to 25 pollen taxa were compared with those of their supposed nearest living relatives to create a "coexistence interval" in which all modern relatives could co-exist. This method, applied on all 43 climatic relevant taxa, suggests a mean annual temperature (MAT) of 17.2–20.5°C, a coldest month temperature (CMT) of 9.6–13.3°C and a warmest month temperature (WMT) of 24.7–27.9°C (Table 3.2). Mean annual precipitation (MAP) ranged within 1187–1520 mm, showing a seasonality with a dry month (MPdry) of 18–24 mm and a wet month (MPwet) of 178–236 mm. The rainy season was most likely in the warmer period of the year as the warmest month precipitation (MPwarm), ranges around 118–141 mm (Table 3.2). To reduce the white-noise-signal, we used a 5-point-average in the paleoclimate estimates in Fig. 3.5 illustrating rather stable climatic conditions during deposition of the core's sediment.

Within the short interval represented by the samples of the core, the only parameter significantly changing is the MAP. From a high in the first samples, it decreases to 1100 mm (around samples 8–23) before it step-wisely reaches the lowest values of less than 1000 mm during samples 38 to 44 (Fig. 3.5). This is caused by a sudden lack of mesothermic elements such as *Engelhardia*, *Rhus* and *Reevesia* (Table 3.1). Afterwards follows a significant increase of mean annual precipitation up to almost 1200 mm within the next 5 samples representing a maximum of 70 years. Several samples indicate even higher values than 1200 mm during the following interval until the MAP drops again above sample 66. For the rest of the core-section, rainfall is oscillating around 1150 mm per year. Small scale, in-phase-shifts are also observed in the CMT and the MPdry estimates (Fig. 3.5).

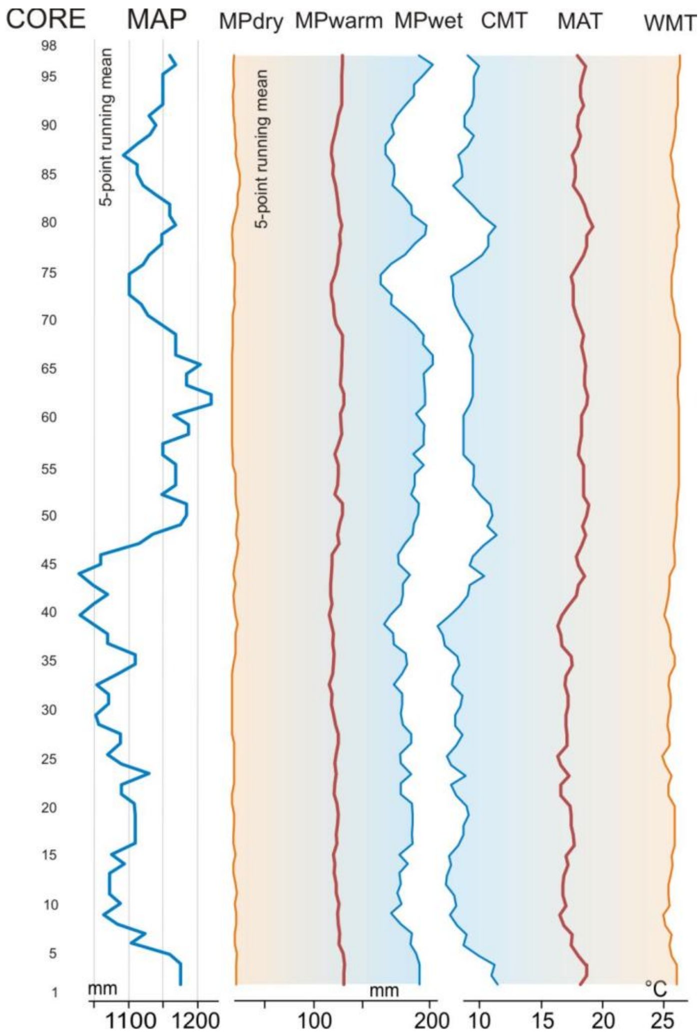

Fig. 3.5. Climate estimates based on the 5-point-running mean values calculated by the Coexistence Approach. Abbreviations refer to MAT (mean annual temperature), CMT (coldest month temperature), WMT (warmest month temperature), MAP (mean annual precipitation), MPwet (precipitation of the wettest month), MPdry (precipitation of the driest month), MPwarm (precipitation of the warmest month).

Comparing these climatic data with the updated climatic classification of Koeppen and Geiger (Koeppen, 1936; Peel et al., 2007) a Cwa climate at the transition to a Cfa climate is indicated. Only if the most extreme CA precipitation estimates for the wettest and driest months are considered, the data range within the Cfa climate boundaries. This would point to no or only very weak seasonality comparable to modern regions in East Asia, southeast North America or east South America (Utescher et al., 2009). Cwa climates reflect a stronger influence of a dry summer period like today in northern India, south-eastern Asia (south Nepal, Myanmar, northern Thailand) to east China, and in central south Africa (east Angola, Zambia, north Zimbabwe, north Mozambique) (Peel et al., 2007). This interpretation suggests a slightly warmer climatic situation in comparison to other coeval Central European localities (Bruch et al., 2007). Especially the coldest month temperature of 10° or above (Fig.

3.5; Table 3.2), which is also well represented in the abundance of thermophilic and/or evergreen taxa (mega-and mesothermic up to 20%) (Fig. 3.3) and the occurrence of rare elements (Mastixiaceae, *Engelhardia*, *Platycarya*) during the Late Miocene, is surprising, which lead to discussion about a position of the embayment in a climatically favored refuge (Kover-Eder and Hably, 2006).

3.5.2. Lake ecology and dynamics

The interpretation of the dinoflagellate assemblages in Lake Pannon is complex. Most taxa have roots in marine ancestors, which became adapted to brackish water conditions of Lake Pannon with the onset of the Late Miocene. Therefore, a straightforward comparison with congeneric open marine taxa is difficult. A more promising source for comparison are the marine-derived assemblages from the Black Sea, the Marmara Sea, the Caspian Sea, the Aral Sea and some adjacent lakes as described in numerous papers (e.g. Kouli et al., 2001; Mudie et al., 2001; 2002; 2007; Marret et al., 2004; 2007; 2009; Sorrel et al., 2006; Londeix et al., 2009; Leroy and Albay, 2010).

All samples are characterized by high terrestrial influx represented by phytoclasts and sporomorphs suggesting a near-shore depositional environment. This interpretation is also obvious based on the paleogeographic situation and sedimentological features (Gross et al., 2008). The data are thus documenting the development in an embayment of Lake Pannon during approximately one millennium. Color-code transposed cluster analysis suggests a division into a lower half of the core, rich in heterotrophs (clusters D1–D2) and an autotroph-dominated upper part (clusters D3–D4) (Fig. 3.2). The reason for the heterotroph peak is dubious. Increased diatom production is discussed by Bujak (1984) and Matsuoka (1999) as reason for the takeover by heterotrophs is unlikely as no diatoms are recorded from the Mataschen core. Matsuoka (1987) attributed the dominance of heterotrophic taxa to terrestrially originated nutrients which are transported by rivers to the area of deposition. Head et al. (2004) also concluded that the abundance of partially degraded woody tissues is an evidence for river input. Aside from high nutrient loads, this input might coincide with turbidity and reduced light penetration of surface waters due to a high fraction of suspended sediment and/or phytoplankton blooms. This in turn would impede growth of light-depending autotrophic dinoflagellates (Dale, 2001). To test this hypothesis several samples have been selected to count the amount of phytoclasts (at 10 *Lycopodium clavatium* spores). Indeed, samples with high P/G ratio are characterized by a dominance of large wood fragments while samples of low P/G ratio contain fewer and relatively smaller phytoclasts. These samples are also marked by the most prominent contribution of *Polykrikos* spp., which is a good indicator for high nutrient loads in modern coastal environments (Matsuoka et al., 2009). In modern Adriatic Sea environments increased RBC levels (as in cluster D1) are linked to high winter primary production (Zonneveld et al., 2009). Elevated nutrient levels and low salinity fit also to the constant contribution of various morphotypes of *Spiniferites bentorii* (Pospelova et al., 2002). Thus, a very shallow, freshwater influenced lagoon or embayment of Lake Pannon is indicated by the samples in the lower half of the core and interval 60–65.

Clusters D3–D4 bear the highest amounts of *Spiniferites/Achomosphaera* as well as the lowest values of heterotrophs (Fig. 3.2). A correlation of *Spiniferites*-domination and sea-level rise was documented by Morzadec-Kerfourn (2005) in estuaries of NW Europe. The decrease of heterotrophs in favor of autotrophs is also a hint to lowered nutrition loads (see above; Dale, 2009). Several species of *Spiniferites*, including *S. bentorii*, and *S. bulloides* have been documented to be indicative for stratified water bodies in marine settings (Marret and Scourse, 2003). The occurrence of *Polykrikos schwartzii/kofoidii* may suggest stratified water conditions as well (Marret and Scourse, 2003). Therefore, in the upper part of the Mataschen core, the rapid increase by *Spiniferites/Achomosphaera* and the reduction of heterotrophs is interpreted herein as transgressions of Lake Pannon waters coinciding with a reduction of fresh water influx. The occurrence of scattered samples of clusters D3–D4a in the lower half of the core indicates repeated phases of reduced nutrient/sediment loads, which allowed neritic taxa to dominate the embayment. Stratification of the water column might have been established as well.

Cluster D4b is characterized by the high contribution of *Impagidinium* spp. (Fig. 3.2). Extant *Impagidinium* species are usually found in open marine settings, indicate oligotrophic surface waters and prefer salinities above 32 psu (Rochon et al., 1999; Marret and Zonneveld, 2003). In Lake Pannon, however, the genus appeared in nearshore areas as well and had to cope with salinities far below 20 psu (Harzhauser et al., 2008). Similarly, the extant *Impagidinium caspienense* is recorded from low salinity waters of the Caspian Sea and the Aral Sea (Marret et al., 2004; Sorrel et al., 2006). In the Mataschen core, a first increase of *Impagidinium* spp. occurs between samples 51–55. Two further phases with high values of *Impagidinium* spp. occur at samples 66, 68 and 92–95, which are also grouping in cluster 5 (Fig. 3.2). This pattern is roughly paralleled by *Selenopemphix nephroides* and lowered amounts of heterotrophs. The increase in *Impagidinium* might thus reflect major transgressions of Lake Pannon and phases of increasing oligotrophy due to decreasing input of nutrients. A similar scenario from Lake Pannon was described by Harzhauser et al. (2008) when rapid transgressive pulses of the lake coincided with *Impagidinium* peaks. Sorrel et al. (2006), too, linked the sudden increase of *Impagidinium* in Holocene cores of the Aral Sea with a rising sea level. In the modern Adriatic Sea, however, water depth is not the main factor for the occurrence of *Impagidinium*-dominated assemblages (Zonneveld et al., 2009). Instead, these assemblages are rather linked to areas with well oxygenated bottom water and poor stratification. Samples of cluster 4b might thus indicate a reduced stratification of the lake in the embayment compared to samples of clusters 3 and 4.

Lake surface water salinity: The decrease of *Polykrikos* cysts in the upper half of the core fits to a scenario with lowered freshwater influx coinciding with the takeover by Lake Pannon waters as indicated by the *Impagidinium* increase. Simultaneously, a decrease in nutrient input can be expected which fits to the decrease of *Polykrikos* occurrences (Matsuoka et al., 2009). This scenario is also supported by the rare occurrence of *Pyxidinopsis psilata*. This is a brackish water species and can tolerate salinities between 3–7 psu in the modern Baltic Sea (Dale, 1996; Leroy et al., 2007). Its scarceness in the modern Caspian Sea is thus explained by Marret et al. (2004) with the comparatively higher salinity of 12–13 psu. An optimum zone for *P. psilata* between 7–12 psu was also proposed by Marret et al. (2007) for Holocene occurrences in the Black Sea. The occurrence pattern of this species in the Mataschen core would thus point to low salinities between 7–12 psu during the deposition of the lower half of the core and a takeover by saline Lake Pannon waters of >13 psu thereafter. The absence of the acritarch *Cymatiosphaera* spp. in the upper part of the core supports this interpretation as it disappears at summer surface salinities above 18 psu in Black Sea environments (Mudie et al., 2002).
The generally lowered salinities are also indicated by the morphotypes of *Spiniferites*. Ellegaard (2000) shows, that cysts of *Spiniferites* spp. with apical boss and shortened and geminal processes are developed at low salinities in recent embayments of Denmark. In the current study, many *Spiniferites* and *Achomosphaera* morphotypes with shortened, geminal and membranaceous processes similar to those illustrated in Ellegaard (2000) have been recorded.

Peridinioid-gonyaulacoid ratio: The peaks in the P/G ratio are caused by a proportional increase of heterotrophs with a simultaneous decrease of autotrophs. The ratio of the heterotrophic protoperidinioid and autotrophic gonyaulacoid dinoflagellates is used to provide information about the productivity signal (Dale and Fjellsafi, 1994). However, the distribution of most gonyaulacoid dinoflagellates (e.g. *Spiniferites* and *Impagidinium*) is not directly related to nutrient availability (e.g. Dale, 1996; Devillers and de Vernal, 2000). Nevertheless, the takeover by heterotrophs – the heterotroph signal sensu Dale (2009) – is still interpreted as evidence for elevated nutrient availability or even eutrophication (Matsuoka, 1999; Dale, 2009). The decrease of autotrophs may be caused by shading due to high concentrations of blooming phytoplankton or turbidity by sediment load. The most likely scenario to achieve elevated nutrient levels in this embayment of Lake Pannon along the Eastern Alps is a pluvial phase. Precipitation-related eutrophication events, lasting few years or even only a single year, are thus suggested by the extraordinary peaks at samples 22, 34, 45, 60, 76, 89.

Accessory taxa: Warm climatic conditions prevailed during the deposition of the studied samples based on the dominance of *Spiniferites* spp., *Selenopemphix nephroides*, and the warm-water acritarch genus *Nannobarbophora* (Head, 2003). In marine settings, *S. nephroides* is typical for river mouth areas and may be used as indicator for fluvial influx (Holzwarth et al., 2007). Although, *S. nephroides* is not exclusively neritic but may thrive in oceanic waters as well it has an affinity to eutrophic coastal settings and zones of high productivity (Marret and Zonneveld, 2003; Susek et al., 2005; Sorrel et al., 2006; Pospelova et al., 2008; Holzwarth et al., 2010). Freshwater influx is clearly documented by sporadic occurrences of coenobia of *Pediastrum boryanum* and *P. duplex* accompanied by *Botryococcus* (Batten, 1996; Matthiessen and Brenner, 1996). The heterotrophic species *Selenopemphix nephroides* and *Selenopemphix* sp.1 display a roughly opposing trend. Each is correlated in abundance with a certain gonyaulacoid: *Selneopemphix nephroides* is positively correlated with *Impagidinium* spp. and *Selenopemphi*x sp.1 is positively correlated with *Spiniferites b. pannonicus* and *S. b. budajenoensis.* The decline of the *Spiniferites* taxa in samples 48–50 is clearly followed by a decline by *Selenopemphix* sp.1 in samples 51–54. The opposite pattern is evident for the *Selenopemphix* sp.1-peak in sample 76 which is paralleled soon after by *Spiniferites* in samples 77–79. This relation of *Impagidinium* spp. with *Selenopemphix nephroides*, which is an open marine species characteristically present in coastal environments (Marret and Zonneveld, 2003) fits to the transgressive phase. The opposing trend in *Selenopemphix* sp.1, *Spiniferites b. pannonicus* and *S. b. budajenoensis* may thus indicate that these taxa have been adapted to low salinity environments in lagoons of Lake Pannon.

3.5.3. Vegetation dynamics

The Tortonian vegetation of Mataschen has already been described in several papers (e.g. Draxler et al., 1994; Kovar-Eder, 2004; Meller and Hofmann, 2004; Kovar-Eder and Hably, 2006). Herein, we try to detect changes of vegetation on a decadal to centennial scale, rather than describing a time-averaged assemblage as done in previous studies. Based on the sedimentation rate as calculated by Gross et al. (2011), the cores studied cover a time span of less than 1,400 years. Thus, the documented trends and shifts happened within very short time in a geological context, but span a fairly long time in respect to ecological studies focusing on extant vegetation systems like swamps or marshes (e.g. Effler and Goyer, 2006; Kirwan and Temmerman, 2009).

The changing of the different vegetation types is visualized by the different plant clusters (Fig. 3.4). Cluster P1 represents samples which were deposited when swampy wetlands were fringing the lake. Taxodioideae, especially the taxa *Taxodium* in the USA (Visser and Sasser, 1995; Hoeppner et al., 2008) and *Glyptostrobus* in China (Averyanov et al., 2009), form vast swamp forests. There, the tree assemblages include representatives of *Nyssa*, *Liquidambar* and *Quercus*, followed by once-a-year-flooded vegetation and riparian wetlands mainly consisting of *Quercus*, *Liquidambar*, *Fagus*, *Carya*, and *Celtis* (Wilen and Tiner, 1993). The next plant association (cluster P3) suggests open grass vegetation close to the shore due to the lack of most tree genera (Fig. 3.4). Several genera of Poaceae, Cyperaceae and *Sparganium/Typha* are known form marsh wetlands even in brackish environments. Therefore, a marsh comparable to modern marshes of coastal Louisiana (Webb et al., 1995) or Florida (Willard et al., 2001) is indicated by the composition of the samples in cluster P3a. Based on the high amount of Taxodioideae pollen, a transition of these marshes into a Taxodioideae swamp is suggested in samples of subcluster P3b, comparable to recent swamps in SE USA (Willard et al., 2001; Hoeppner et al., 2008). P4 cluster also describes a vegetation type with a high amount of marsh grasses, but further with a wide distribution of a forested wetland with Taxodioideae and an increasing number of *Nyssa* (Fig. 3.4).
P2 describes an intermediate state of the vegetation. Due the lack of Poaceae, Cyperaceae and *Sparganium/Typha*, only *Pinus* and *Cathaya* dominate the cluster associated with other hinterland taxa. These are represented by species of the genera *Carya*, *Carpinus, Tilia, Alnus* and from the Oleaceae family.

Already the lower part of the core reveals considerable fluctuations and a marked change in pollen composition (Fig. 3.4). A high number of tree species (approximately 26 plant taxa) is present but decreases for the benefit of swamp and marsh plants (Taxodioideae, Cyperaceae, Poaceae, *Sparganium/Typha*) within less than a century. Poaceae and Cyperaceae are one of the most common representatives in halophytic and brackish environments in subtropical climates (Adam, 1990; González and Dupont, 2009) and thus are the main components of many modern brackish marshes (Tzonev et al., 2008). Generally, Poaceae are more salt tolerant than Cyperaceae (González and Dupont, 2009). Therefore, the first vegetation belt around brackish Lake Pannon was presumable formed by Poaceae, followed by Cyperaceae, probably accompanied by *Typha*. Members of this genus may dominate marshes as well [e.g. New England (Mullan Crain et al., 2004), around North America's Great Lakes (Keddy and Reznicek, 1986), Florida and Louisiana (Doren et al., 1996; Willard et al., 2001)], but are very sensitive to salt content of the water and soil. *Typha* can also be otherwise an important member of swamp vegetation (Bush, 2002).

This situation changes above sample 30, where samples of cluster P2 predominate (Fig. 3.4). Most characteristic is the breakdown of marsh grasses during several decades time. Whilst Poaceae and *Sparganium/Typha* are subordinate, the number of Cyperaceae pollen is increasing. Taxodioideae and mesothermic elements become more and more important components of the assemblages. This coincides with the lowest plant diversity in the samples and with the lowest values for the mean annual precipitation (Fig. 3.6). Such a decrease in rainfall is a plausible scenario for the marsh dieback as a wetland ecosystem is highly vulnerable to changes in water supply (Lodge, 2010). For a marsh system, the hydroperiod, which means the time of total inundation of the soil, is an important factor for its proliferation. Especially the annual rainfall has been documented in ecological studies to be a crucial factor (Lodge, 2010). As a plausible scenario for the locality of Mataschen, a shorter hydroperiod causes non-ideal conditions for the Poaceae and *Sparganium/Typha* and plants adapted to the new conditions will soon take over (Keddy and Reznicek, 1986). Cyperaceae, with their lower tolerance to brackish water and their ability to cope with drier conditions, can now dominate the marsh area.

Marshes are rapidly regenerating and adapting vegetation systems. The surrounding forest, however, is more stable and is not suspected to have changed considerably in such a multi-decadal period. Therefore, the relative increase in tree taxa within this part of the core (cluster P2; Fig. 3.4) may rather be caused by the disappearance of the marsh taxa in the samples.

Thereafter, the Cyperaceae are vanishing quickly within only a few samples, coinciding with a breakdown of other grasses at sample 50 (transition from cluster P2 to P1). This pattern seems again to be strongly linked to a short-termed climate event. Within these samples, the mean annual precipitation is rising roughly about 200–300 mm. This causes not only a change in the marsh vegetation, but more intense its dieback because due to the quick ingression of Lake Pannon. A high rate of relative sea level rise increases the depth and duration of inundation, often causing plant death (Mendelssohn and McKee, 1988; Webb et al., 1995). If the marsh’s accretion cannot catch up with the acceleration of the lake level rise it will simply drown (Kirwan and Temmerman, 2009). The ingression resulted in forested swampy conditions, indicated by the gradual increase of Taxodioideae and *Nyssa* (Lodge, 2010) during this period.

Starting with sample 63, this transgressive pulse ends and assemblages of cluster P4 appear. Taxodioideae are the dominating plants forming forested swamps comparable to recent South Florida (Willard et al., 2001; Lodge, 2010). Accordingly, Poaceae, *Sparganium/Typha* and Cyperaceae become abundant again. Such a spread of non-forested wetland vegetation can be caused by the decline of the transgressive pulse or an adaptation of the marsh plants to the lake level rise (Kirwan and Temmerman, 2009; Kolker et al., 2009).

Model experiments by Kirwan and Temmerman (2009) demonstrated, that marshes can adapt to rapid rates of sea level rise within 100 years, which is supported by field observations of Clark and Patterson (1984). Further, a comparable “slow-down-scenario” might also explain the vegetation shift observed in the P4 samples of the Mataschen core. As this trend follows on, Lake Pannon’s shores become more and more dominated by widespread marshes again. Samples of subcluster P3b appear again, being characterized by pollen assemblages of forested and non-forested wetlands. Poaceae, Cyperaceae and *Sparganium/Typha* formed the first vegetation belt of Lake Pannon again, grading into Taxodioideae swamps behind. The hinterland is covered with forests, comprising tree taxa, typically for the Late Miocene, such as *Carya*, *Pterocarya*, *Fagus*, *Celtis, Ulmus* and *Carpinus,* but with a possible high amount of evergreen trees such as *Symplocos*, *Reevesia*, Sapotaceae and Mastixiaceae.

3.6. Conclusions

The pollen and dinoflagellate records reveal a complex interplay between Tortonian climate, lake level and ecosystem response (Fig. 3.6). Within a presumed time span of only one millennium, a surprisingly rapid succession of environments is documented. Due to the high stratigraphic resolution of c. 7–14 years per sample (Gross et al., 2011), the often asynchronous responses of lake-biota and its surrounding wetlands in relation to Late Miocene small scale climatic change can be described.
A brackish, but strongly freshwater influenced, lagoon with salinities between 7–12 psu developed at the margin of Lake Pannon under a moderate mean annual precipitation of c. 1100 mm. High nutrient input favored a high surface-water productivity of dinoflagellates, which have caused repeated algae bloom events of several years. During that time, the coasts were fringed by marshes of Poaceae grading into Cyperaceae landwards. Behind the brackish marsh vegetation, a forested wetland was developed, characterized by high abundances of Taxodioideae, which became replaced by mixed evergreen and deciduous forests in the hinterland. A decrease in MAP slightly below 1000 mm is expressed in the vegetation by the take-over by dry-adapted Cyperaceae grasses within c. 200–300 years. Soon after, a rapid transgression of Lake Pannon caused a total loss of the marsh ecosystem. This is reflected by the synchronous quick and strong increase of the “open-water” dinoflagellate *Impagidinium* suggesting that the marshes could not keep up with the rising lake level and drowned within some decades. Simultaneously, salinity increased above 13 psu and the nutrient load decreased. The rise of the lake level occurred with a five sample delay after a strong increase of precipitation of c. 300 mm/yr to more than 1200 mm/yr. This implies that the hydrological budget of Lake Pannon lagged with a delay of ca. 4–6 decades,

probably caused by its very large size and depth. The strong transgressive pulse lasted ~100–130 years and then slowed down as the mean annual rainfall was decreasing. This slow-down-phase allowed the marshes to re-establish and to resist further small fluctuations of the lake level. After another ~100–200 years the vegetation system was adapted to the newly established environment and Poaceae and Cyperaceae formed the dominating shoreline vegetation again. Mean annual precipitation was thus the driving force for dieback or expansion of the marshes whereas temperature did not change significantly. Although not completely in phase with the terrestrial ecosystem, the dinoflagellate spectra clearly reflect the beginning of the ingression of Lake Pannon and document an increase in salinity. A marked regularity of blooms of heterotroph dinoflagellates is observed throughout the core with a periodicity of 11–16 samples. This might suggest some influence of solar cycles such as the Gleissberg cycle or the de Vries/Suess cycle (Braun et al., 2005). Unfortunately, the studied core is too short to apply a reliable time series analysis. In any case, dinoflagellate blooms have been quasi-periodic phenomena in coastal areas of Lake Pannon during the Early Tortonian.

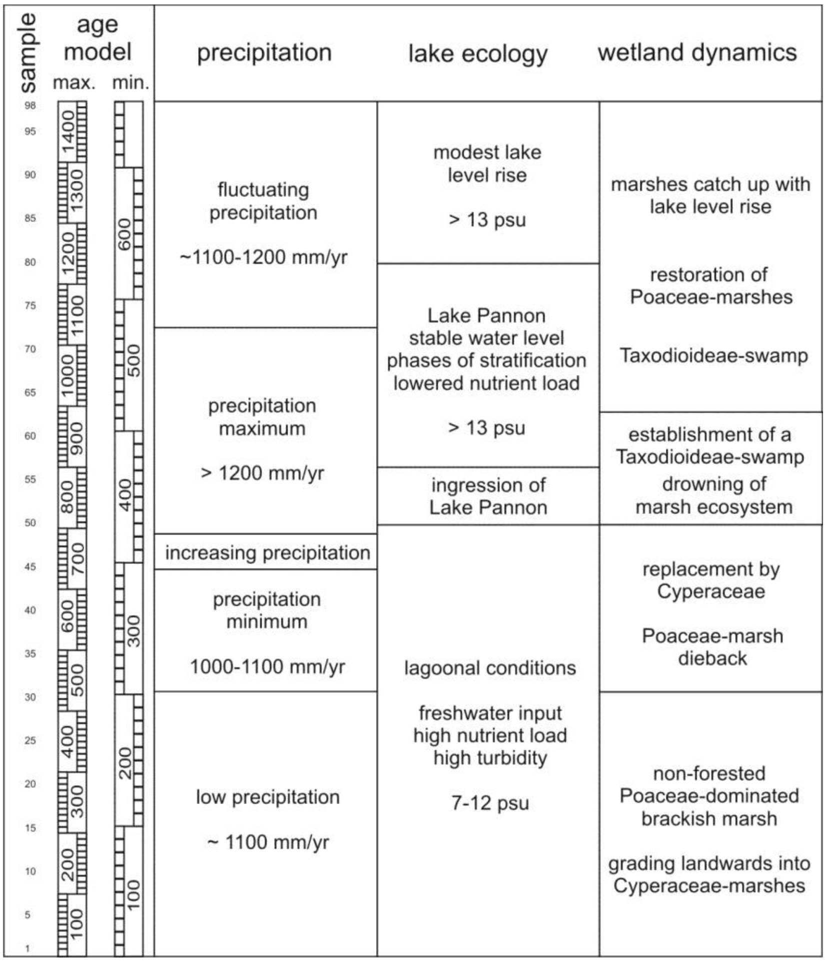

Fig. 3.6. Interpretation of the climatic parameters, lake ecology and vegetation dynamics in relation to the age model of Gross et al. (2011). Major perturbations of the vegetation belts happened within few decades whilst the restoration phases take place on a centennial scale.

These results from a Tortonian core are comparable to studies on Holocene lakes in sample density and time resolution (e.g. Hooghiemstra, 1989; Pellatt et al., 2001; Stebich et al., 2005; Tarasov et al., 2007; Jiménez-Moreno et al., 2008). Therefore, this method is capable to register climate-driven Miocene environmental dynamics on a similar high-frequency sub-Milankovitch scale. Understanding Tortonian climate as a pendant-scenario for the predicted global climate change will need much more such studies as our knowledge on pre-Quaternary high-resolution climate dynamics is still extremely poor.

Acknowledgements

The study was supported by the FWF-grants P21414-B16 (Millennial- to centennial-scale vegetation dynamics and surface water productivity during the Late Miocene in and around Lake Pannon) and P21748-N21 (Evolution and Phylogeny in Cyprideis, Ostracoda). The paper contributes to the NECLIME network.

3.7. References

Adam, P., 1990. Saltmarsh Ecology. Cambridge University Press, Cambridge, 461 p.

Averyanov, L.V., Phan, E.L., Nguyen, T.,H., Nguyen, S.K., Nguyen, T.V., Pham, T.D., 2009. Preliminary Observations of Native *Glyptostrobus pensilis* (Taxodiaceae) Stands in Vietnam. Taiwania 54, 191–212.

Batten, D.J., 1996. Palynofacies and palaeoenvironmental interpretation, In: Jansonius, J., McGregor, D.C. (Eds.), Palynology: principles and applications. American Association of Stratigraphic Palynologists Foundation 1, Dallas, 1011–1164.

Böhme, M., Ilg, A., Winklhofer, M., 2008. Late Miocene “washhouse” climate in Europe. Earth and Planetary Science Letters 275, 393–401.

Braun, H., Christl, M., Rahmstorf, S., Ganopolski, A., Mangini, A., Kubatzki, C., Roth, K., Kromer, B., 2005. Possible solar origin of the 1,470-year glacial climate cycle demonstrated in a coupled model. Nature 438, 208–211.

Bruch, A.A., Uhl, D., Mosbrugger, V., 2007. Miocene climate in Europe – Patterns and evolution. A first synthesis of NECLIME. Palaeography, Palaeoclimatology, Palaeoecology 253, 1–7.

Bruch, A.A., Utescher, T., Mosbrugger, V., Gabrielyan, I., Ivanov, D.A., 2006. Late Miocene climate in the circum-Alpine realm – a quantitative analysis of terrestrial palaeofloras. Palaeogeography, Palaeoclimatology, Palaeoecology 238, 270–280.

Bujak, J.P., 1984. Cenozoic dinoflagellate cysts and acritarchs from the Bering Sea and northern North Pacific, D.S.D.P. Leg 19. Micropaleontology 30, 180–212.

Bush, M., 2002. On the interpretation of fossil Poaceae pollen in the lowland humid neotropics. Palaeogeograohy, Palaeoclimatology, Palaeoecology 177, 5–17.

Clark, J.S., Patterson III, W.A., 1984. Pollen, ^{210}Pb and opaque spherules; an integrated approach to dating sedimentation in the intertidal environment. Journal of Sedimentary Petrology 54, 1251–1265.

Dale, B., 1996. Dinoflagellate cyst ecology: modeling and geological applications. In: Jansonius, J., McGregor, D.C. (Eds.), Palynology: Principles and Applications. American Association of Stratigraphic Palynologists Foundation 3, Dallas, 1249–1275.

Dale, B., 2001. Marine dinoflagellate cysts as indicators of eutrophication and industrial pollution: a discussion. The Science of the Total Environment 264, 235–240.

Dale, B., 2009. Eutrophication signals in the sedimentary record of dinoflagellate cysts in coastal waters. Journal of Sea Research 61, 103–113.

Dale, B., Fjellsafi, A., 1994. Dinoflagellate cysts as paleoproductivity indicators: state of the art, potential and limits. In: Zahn, R., Pedersen, T.F., Kaminski, M.A., Labeyrie, L. (Eds.), Carbon Cycling in the Glacial Ocean: Constraints on the Ocean's Role in Global Change. NATO ASI Ser. I,. 17, Springer-Verlag, Berlin pp. 521–537.

Daxner-Höck, G., 2004. Beavers and a Dwarf Hamster from Mataschen (Lower Pannonian, Styrian Basin). Joannea Geologie und Paläontologie 5, 19–33.

Draxler, I., Solti, G., Lobitzer, H., Cichocki, O., 1994. Erster Nachweis von „Alginit" (sensu Jámbor Solti, 1975) im Süsteirischen Tertiärbecken (Österreich). Jubiläumsschrift 20 Jahre Geologische Zusammenarbeit Österreich-Ungarn, Wien, Bécs, p. 19–54.

Devillers, R., de Vernal, A., 2000. Distribution of dinoflagellate cysts in surface sediments of the northern North Atlantic in relation to nutrient content and productivity in surface waters. Marine Geology 166, 103–124.

Doren, R.F., Armentano, T.V., Whiteaker, L.D., Jones, R.D., 1997. Marsh vegetation patterns and soil phosphorus gradients in the Everglades ecosystem. Aquatic Botany 56, 145–163.

Effler, R.S., Goyer, R.A., 2006. Baldcypress and water tupelo sapling response to multiple stress agents and reforestation implications for Louisiana swamps. Forest Ecology and Management 226, 330–340.

Ellegaard, M., 2000. Variations in dinoflagellate cyst morphology under conditions of changing salinity during the last 2000 years. Review of Palaeobotany and Palynology 9, 65–81.

Erdei, B., Hably, L., Kázmé, M., Utescher, T. Bruch, A.A., 2007. Neogene flora and vegetation development of the Pannonian domain in relation to palaeoclimate and palaeogeography.

François, L., Ghislain, M., Otto, D., Micheels, A., 2006. Late Miocene vegetation reconstruction with the CARAIB model. Palaeogeography, Palaeoclimatology, Palaeoecology 238, 302–320.

Gonzélez, C., Dupont, L., 2009. Tropical salt marsh succession as sea-level indicator during Heinreich events. Quaternary Science Reviews 28, 939–946.

Green, O.R., 2001. A manual of practical laboratory and field techniques in palaeobiology. Kluwer Academic Publishers, Dordrecht.

Grimm, E.C., 2004. Tilia and TG View Version 2.0.2. Illinois State Museum, Research and Collector Center.

Gross, M., 1994. Erster Nachweis der fossilen Schildkröte *Clemmydopsis turnauensis* aus dem Pannonium des Oststeirischen Tertiärbeckens (Testudines: Emydidae: Batagurinae). Mitteilungen des Naturwissenschaftlichen Vereins für Steiermark 124, 49–59.

Gross, M., 2004. Contributions to the ostracode fauna (Crustacea), paleoecology and stratigraphy of the clay pit Mataschen (Lower Pannonian, Styrian Basin, Austria). Joannea Geologie und Paläontologie 5, 49–129.

Gross M., Minati K., Danielopol D.L., Piller W.E., 2008. Environmental changes and diversification of *Cyprideis* in the Late Miocene of the Styrian Basin (Lake Pannon, Austria). Senckenbergiana lethaea 88, 161–181.

Gross, M., Piller, W.E., Scholger, R., Gitter, F., 2011. Biotic and abiotic response to palaeoenvironmental changes at Lake Pannons' western margin (Central Europe, Late Miocene). Palaeogeography, Palaeoclimatology, Palaeoecology 312, 181–193.

Hably, L., Kovar-Eder, J., 1996. A representative leaf assemblage of the Pannonian Lake from Dozmat near Szombathely (Western Hungary), Upper Pannonian, Upper Miocene. Advances in Austrian-Hungarian Joint Geological Research, Budapest, pp 69–81.

Hammer, Ø., Harper, D.A.T., Ryan, P.D., 2001. PAST; Palaeontological Statistics software package for education and data analysis. Palaeontologica Electronica 4 (1), 9 pp.

Harzhauser, M., 2004. Mollusc based Biostratigraphy of the Clay Pit Mataschen in the Styrian Basin (Pannonian). Joannea Geologie und Paläontologie 5, 149–161.

Harzhauser, M., Mandic, O., 2008. Neogene lake systems of Central and South-Eastern Europe: Faunal diversity, gradients and interrelations. Palaeogeography, Palaeoclimatology, Palaeoecology 260, 417–434.

Harzhauser, M., Kern, A., Soliman, A., Minati, K., Piller, W.E., Danielopol, D.L., Zuschin, M., 2008. Centennial- to decadal scale environmental shifts in and around Lake Pannon (Vienna Basin) related to a major Late Miocene lake level rise. Palaeogeography, Palaeoclimatology, Palaeoecology 270, 102–115.

Head, M.J., 2003. Neogene occurrences of the marine acritarch genus *Nannobarbophora* Habib and Knapp, 1982 emend., and the new species *N. gedlii*. Journal of Paleontology 77, 382–385.

Head, M.J., Riding, J.B., Eidvin, T., Chadwick, R.A., 2004. Palynological and foraminiferal biostratigraphy of (Upper Pliocene) Nordland Group mudstones at Sleipner, northern North Sea. Marine and Petroleum Geology 21, 277–297.

Heusser, L., Balsam, W.L., 1977. Pollen distribution in theNortheast Pacific Ocean.Quaternary Research 7, 45–62.

Hoeppner, S.S., Shaffer, G.P., Perkis, T.E., 2008. Through droughts and hurricanes: Tree mortality, forest structure, and biomass production on a coastal swamp targeted for restoration in the Mississippi River Deltaic Plain. Forest Ecology and Management 256, 937–948.

Holzwarth, U., Esper, O., Zonneveld, K.A.F., 2007. Distribution of organic-walled dinoflagellate cysts in shelf surface sediments of the Benguela upwelling system in relationship to environmental conditions. Marine Micropaleontology 64, 91–119.

Holzwarth, U., Esper, O., Zonneveld, K.A.F., 2010. Organic-walled dinoflagellate cysts as indicators of oceanographic conditions and terrigenous input in the NW African upwelling region. Review of Palaeobotany and Palynology 159, 35–55.

Hooghiemstra, H., 1989. Quaternary and Upper-Pliocene glaciations and forest development in the tropical Andes: evidence from a long high-resolution pollen record from the sedimentary basin of Bogotá, Colombia. Palaeogeography, Palaeoclimatology, Palaeoecology 72, 11–26.

Hopkins, J.S., 1950. Differential flotation and deposition of coniferous and deciduous tree pollen. Ecology 31, 633–641.

Jiménez-Moreno, G., 2006. Progressive substitution of a subtropical forest for a temperate one during the middle Miocene climate cooling in Central Europe according to palynological data from cores Tengelic-2 and Hidas-53 (Pannonian Basin, Hungary). Review of Palaeobotany and Palynology 142, 1–14.

Jiménez-Moreno, G., Suc, J.-P., 2007. Middle Miocene latitudinal climate gradient in Western Europe: Evidence from pollen records. Palaeogeography, Palaeoclimatology, Palaeoecology 253, 208–225.

Jiménez-Moreno, G., Fawcett, P.J., Anderson, R.S., 2008. Millennial- and centennial-scale vegetation and climate change during the late Pleistocene and Holocene from northern New Mexico (USA). Quaternary Science Reviews 27, 1142–1452.

Keddy, P.A., Reznicek, A.A., 1986. Great Lakes vegetation dynamics: The role of fluctuating water levels and buried seeds. Journal of Great Lakes Restoration 12, 25–36.

Kirwan, M., Temmerman, S., 2009. Coastal marsh response to historical and future sea-level acceleration. Quaternary Science Reviews 28, 1801–1808.

Koeppen, W., 1936. Das geographische System der Klimate. In: Koeppen, W., Geiger, R. (Eds.), Handbuch der Klimatologie. Bebrüder Bornträger, Berlin, pp. 1–44.

Kolker, A.S., Goodbred, S.L., Hameed, S., Cochran, J.K., 2009. High-resolution records of the response of coastal wetland systems to long-term and short-term sea-level variability. Estuarine, Coastal and Shelf Science 84, 493–508.

Kollmann, K., 1965. Jungtertiär im Steirischen Becken. Mitteilungen der Geologischen Gesellschaft in Wien 57, 479–632.

Kovar-Eder, J., 2004. The Upper Miocene Flora of Mataschen near Fehring, Styria – Leaf-assemblages. Joannea Geologie und Paläontologie 5, 163–176.

Kovar-Eder, J., Hably, L., 2006. The flora of Mataschen – a unique plant assemblage from the late Miocene of eastern Styria (Austria). Acta Palaeobotanica 46, 157–233.

Kovar-Eder, J., Hably, L., Derek, T., 1995. Neuhaus/Klausenbach – eine miozäne (pannone) Pflanzenfundstelle aus dem südlichen Burgenland. Jahrbuch der Geologischen Bundesanstalt 138, 321–347.

Kovar-Eder, J., Schwarz, J., Wójcicki, J., 2002. The predominantly aquatic flora from Pellendorf, Lower Austria, Late Miocene, Pannonian – a systematic study. Acta Palaeobotanica 42, 125–151.

Kouli, K., Brinkhuis, H., Dale, B., 2001. *Spiniferites cruciformis*. A fresh water dinoflagellate cyst? Review of Palaeobotany and Palynology 113, 273–286.

Leroy, S.A.G., Albay, M., 2010. Palynomorphs of brackish and marine species in cores from the freshwater Lake Sapanca, NW Turkey. Review of Palaeobotany and Palynology 160, 181–188.

Leroy, S.A.G., Marret, F. Gibert, E., Chalié, F., Reyss, J.-L., Arpe, K., 2007. River inflow and salinity changes in the Caspian Sea during the last 5500 years. Quaternary Science Reviews 26, 3359–3383.

Lear, C.H., Rosenthal, Y., Wright, J.D., 2003. The closing of a seaway: ocean water masses and global climate change. Earth and Planetary Science Letters 210, 425–436.

Linder, A., Berchtold, W., 1976. Statistische Auswertung von Prozentzahlen. 1–230, Birkhäuser, Basel.

Lirer, F., Harzhauser, M., Pelosi, N., Piller, W.E., Schmid, H.P., Sprovieri, M., 2009. Astronomically forced teleconnection between Paratethyan and Mediterranean sediments during the Middle and Late Miocene. Palaeogeography, Palaeoclimatology, Palaeoecology 275, 1–13.

Lodge, T.E., 2010.The Everglades Handbook – Understanding the Ecosystem. Taylor and Francis Group, Boca Raton.

Londeix, L., Herreyre, Y., Turon, J.-L., Fletcher, W., 2009. Last Glacial to Holocene hydrology of the Marmara Sea inferred from a dinoflagellate cyst record. Review of Palaeobotany and Palynology 158, 52–71.

Magyar, I., Geary, D.H., Müller, P., 1999a. Paleogeographic evolution of the Late Miocene Lake Pannon in Central Europe. Palaeogeography, Palaeoclimatology, Palaeoecology 147, 151–167.

Magyar, I., Geary, D.H., Sütö-Szentai, M., Lantos, M., Müller, P., 1999b. Integrated biostratigraphic, magnetostratigraphic and chronostratigraphic correlation of the Late Miocene Lake Pannon deposits. Acta Geologica Hungarica 45, 5–31.

Marret, F., Scourse, J., 2003. Control of modern dinoflagellate cyst distribution in the Irish and Celtic seas by seasonal stratification dynamics. Marine Micropaleontology 47, 101–116.

Marret, F., Zonneveld, K.A.F., 2003. Atlas of modern organic-walled dinoflagellate cyst distribution. Review of Palaeobotany and Palynology 125, 1–200.

Marret, F., Leroy, S., Chalie, F., Gasse, F., 2004. New organic-walled dinoflagellate cysts from recent sediments of Central Asian seas. Review of Palaeobotany and Palynology 129, 1–20.

Marret F., Mudie P.J., Aksu A., Hiscott, R.N., 2007. Holocene dinocyst record of a two-step transformation of the Neoeuxinian brackish water lake into the Black Sea. Quaternary International 197, 72–86.

Marret, F., Mudie, P.J., Aksu, A.E., Hiscott, R.N., 2009. A Holocene dinocyst record of a two-step transformation of the Neoeuxinian brackish water lake into the Black Sea. Quaternary International 197, 72–86.

Matsuoka, K., 1987. Organic-walled dinoflagellate cysts from surface sediments of Akkeshi Bay and Lake Saroma, North Japan. Bulletin of the Faculty of Liberal Arts, Nagasaki University, Natural Science 28, 35–123.

Matsuoka, K., 1999. Eutrophication process recorded in dinoflagellate cyst assemblages—a case of Yokohama Port, Tokyo Bay, Japan. The Science of the Total Environment 231, 17–35.

Matsuoka, K., Kawami, H., Nagai, S., Mitsunori, I., Takayama, H., 2009. Re-examination of cyst-motile relationships of *Polykrikos kofoidii* Chatton and *Polykrikos schwartzii* Bütschli (Gymnodiniales, Dinophyceae). Review of Palaeobotany and Palynology 154, 79–90.

Matthiessen, J., Brenner, W., 1996. Dinoflagellate cyst ecostratigraphy of Pliocene-Pleistocene sediments from the Yermak Plateau (Arctic Ocean, Hole 911A). Proceedings of the ODP, Scientific Results 151, 243–253.

Meller, B., Hofmann, C.-C., 2004. Paleoecology of Diospore- and Palynomorph assemblages from Late Miocene lake sediments (Mataschen near Fehring, East Styria, Austria). Joannea Geologie und Paläontologie 5, 177–217.

Mendelssohn, I.A., McKee, K.L., 1988. *Spartina alterniflora* die back in Louisiana: Time-course investigation of soil waterlogging effects. Journal of Ecology 76, 509–521.

Micheels, A., Bruch, A.A., Uhl, D., Utescher, T., Mosbrugger, V., 2007. A Late Miocene climate model simulation with ECHAM4/ML and its quantitative validation with terrestrial proxy data. Palaeogeography, Palaeoclimatology, Palaeoecology 253, 251–270.

Morzadec-Kerfourn, M.T., 2005. Dinoflagellate cysts and the paleoenvironment of Late-Pliocene Early-Pleistocene deposits of Brittany, Northwest France. Quaternary Science Reviews 16, 883–898.

Mosbrugger, V., Utescher, T., 1997. The coexistence approach – a method for quantitative reconstructions of Tertiary terrestrial palaeoclimate data using plant fossils. Palaeogeography, Palaeoclimatology, Palaeoecology 134, 61–86.

Mudie, P.J., Aksu, A.E., Yasar, D., 2001. Late Quaternary dinoflagellate cysts from the Black, Marmara and Aegean seas: variations in assemblages, morphology and paleosalinity. Marine Micropaleontology 43, 155–178.

Mudie, P.J., Rochon, A., Aksu, A.E., Gillespie, H., 2002. Dinoflagellate cysts, freshwater algae and fungal spores as salinity indicators in Late Quaternary cores from Marmara and Black seas. Marine Geology 190, 203–231.

Mudie, P.J., Marret, F., Aksu, A.E., Hiscott, R.N., Gillespie, H., 2007. Palynological evidence for climatic change, anthropogenic activity and outflow of Black Sea water during the late Pleistocene and Holocene: Centennial- to decadal-scale records from the Black and Marmara Seas. Quaternary International 167–168, 73–90.

Mullan Crain, C., Silliman, B.R., Bertness, S.L., Bertness, M.D., 2004. Physical and biotic divers of plant distribution across estuarine salinity gradients. Ecology 85, 2539–2549.

Papp, A., 1951. Das Pannon des Wiener Beckens. Mitteilungen der Geologischen Gesellschaft in Wien 39–41, 99–193.

Peel, M.C., Finlayson, B.L., McMahon, T.A., 2007. Updated world map of the Köppen-Geiger climate classification. Hydrology and Earth System Science Discussions 4, 439–473.

Pellatt, M.G., Hebda, R.J., Mathewes, R.W., 2001. High-resolution Holocene vegetation history and climate from Hole 1034B, ODP Leg 169S, Saanich Inlet, Canada. Marine Geology 147, 211–226.

Pospelova, V., Chmura, G.L., Boothman, W.S., Latimer, J.S., 2002. Dinoflagellate cyst records and human disturbance in two neighboring estuaries, New Bedford Harbor and Apponagansett Bay, Massachusetts (USA). The Science of the Total Environment 298, 81–102.

Pospelova, V., de Vernal, A., Pedersen, T.F., 2008. Distribution of dinoflagellate cysts in surface sediments from the northeastern Pacific Ocean (43–25°N) in relation to sea-surface temperature, salinity, productivity and coastal upwelling. Marine Micropaleontology 68, 21–48.

Pound, M.J., Haywood, A.M., Salzmann, U., Riding, J.B., Lunt, D.J., Hunter, S.J., 2011. A Tortonian (Late Miocene, 11.6–7.25 Ma) global vegetation reconstruction. Palaeogeography, Palaeoclimatology, Palaeoecology 300, 29–45.

Rochon, A., de Vernal, A., Turon, J.-L., Matthiessen, J., Head, M.J., 1999. Distribution of recent dinoflagellate cysts in surface sediments from the North Atlantic Ocean and adjacent seas in relation to sea-surface parameters. American Association of Stratigraphic Palynologists, Contributions Series 35, 1–150.

Sorrel, P., Popescu, S.-M., Head, M.J., Suc, J.P., Klotz, S., Oberhänsli, H., 2006. Hydrographic development of the Aral Sea during the last 2000 years based on a quantitative analysis of dinoflagellate cysts. Palaeogeography, Palaeoclimatology, Palaeoecology 234, 304–327.

Stebich, M., Brüchmann, C., Kulbe, T., Negendank, J.F.W., 2005. Vegetation history, human impact and climate change during the last 700 years recorded in annually laminated sediments of Lac Pavin, France. Review of Palaeobotany and Palynology 133, 115–133.

Steppuhn, A., Micheels, A., Geiger, G., Mosbrugger, V., 2006. Reconstructing the Late Miocene climate and oceanic heat flux using the AGCM ECHAM4 coupled to a mixed-layer ocean model with adjusted flux correction. Palaeogeography, Palaeoclimatology, Palaeoecology 238, 399–423

Steppuhn, A., Micheels, A., Bruch, A.A., Uhl, D., Utescher, T., Mosbrugger, V., 2007. The sensitivity of ECHAM4/ML to a double CO2 scenario for the Late Miocene and the comparison to terrestrial proxy data. Global and Planetary Change 57, 189–212.

Susek, E., Zonneveld, K.A.F., Fischer, G., Versteegh, G.J.M., Willems, H., 2005. Organic-walled dinoflagellate cyst production in relation to upwelling intensity and lithogenic influx in the Cape Blanc region (off north-west Africa). Phycological Research 53, 97–112.

Tarasov, P., Bezrukova, E., Karabanov, E., Nakagawa, T., Wagner, M., Kulagina, N., Letunova, P., Abzaeva, A., Granoszewski, W., Riedel, F., 2007. Vegetation and climate dynamics during the Holocene and Eemian interglacials derived from Lake Baikal pollen records. Palaeogeography, Palaeoclimatology, Palaeoecology 252, 440–457.

Traverse, A., Ginsburg, R.N., 1966. Palynology of the surface sedimentation of Great Bahamas Bank, as related to water movements and sedimentation. Marine Geology 4, 417–459.

Tzonev, R., Lysenko, T., Gussev, C., Zhelev, P., 2008. The halophytic vegetation in south-east Bulgaria and along the Black Sea coast. Hacquetia 7, 95–121.

Utescher, T., Mosbrugger, V., Ivanov, D., Dilcher, D.L., 2009. Present-day climate equivalents of European Cenozoic climates. Earth and Planetary Science Letters 284, 544–552.

Utescher, T., Bruch, A.A., Micheels, A., Mosbrugger, V., Popova, S., 2011. Cenozoic climate gradients in Eurasia - a palaeo-perspective on future climate change? Palaeogeography, Palaeoclimatology, Palaeoecology 304, 351–358.

Vasiliev, I., Krijgsman, W., Langereis, C.G., Panaiotu, C.E., Matenco, L., Bertotti, G., 2004. Towards an astrochronological framework for the eastern Paratethys Mio-Pliocene sedimentary sequences of the Focsani basin (Romania). Earth and Planetary Science Letters 227, 231–247.

Vasiliev, I., de Leeuw, A., Filipescu, S., Krijgsman, W., Kuiper, K., Stoica, M., Briceag, A., 2010. The age of the Sarmatian-Pannonian transition in the Transylvanian Basin (Central Paratethys), Palaeogeography, Palaeoclimatology, Palaeoecology 297, 54–69.

Visser, J.M., Sasser, C.E., 1995. Changes in tree species composition, structure and growth in a bald cypress-water tupelo swamp forest, 1980–1990. Forest Ecology and Management 72, 119–129.

Webb, E.C., Mendelssohn, I.A., Wilsey, B.J., 1995. Causes for vegetation dieback in a Louisiana salt marsh: A bioassay approach. Aquatic Botany 51, 281–289.

Wilen, B.O., Tiner, R.W., 1993. Wetlands of the United States. In: Whigham, D.F., Dykyjová, D., Hejný, S. (Eds.), Handbook of vegetation science, Wetlands of the world I: Inventory, ecology and management. Kluwer Academic Publishers, Dordrecht, Bosten, London, pp. 129–194.

Willard, D.A., Weimer, L.M., Riegel, W.L., 2001. Pollen assemblages as paleoenvironmental proxies in the Florida Everglades. Review of Palaeobotany and Palynology 113, 213–235.

Wood, G.D., Gabriel, A.M., Lawson, J.C., 1996. Palynological techniques - processing and microscopy. In: Jansonius, J., McGregor, D.C. (Eds.), Palynology: Principles and Applications, Vol. 1., American Association of Stratigraphic Palynologists Foundation, Dallas, pp. 29–50.

Zonneveld, K.A.F., Versteegh, G., Kodrans-Nsiah, M., 2008. Preservation and organic chemistry of Late Cenozoic organic-walled dinoflagellate cysts: A review. Marine Micropaleontology 68, 179–197.

Zonneveld, K.A.F., Chen, L., Möbius, J., Mahmoud, M.S., 2009. Environmental significance of dinoflagellate cysts from the proximal part of the Po-river discharge plume (off southern Italy, Eastern Mediterranean). Journal of Sea Research 62, 189–213.

Zuschin, M., Hohenegger, J., 1998. Subtropical Coral-reef associated sedimentary facies characterized by mollusks (Northern Bay od Safaga, Red Sea, Egypt). Facies 38, 229–254.

<u>**Chapter 4**</u>

Strong evidence for the influence of solar cycles on a Late Miocene lake system revealed by biotic and abiotic proxies

A.K. Kern [a*], M. Harzhauser[a], W.E. Piller[b], O. Mandic[a], A. Soliman[b,c]

[a] Natural History Museum Vienna, Geological-Paleontological Department, Burgring 7, 1010 Vienna, Austria.

[b] Institute of Earth Sciences, Graz University, Heinrichstrasse 26, 8010 Graz, Austria.

[c] Tanta University, Faculty of Sciences, Geology Department, Tanta 31527, Egypt.

[*] Corresponding author at: Natural History Museum Vienna, Geological-Paleontological Department, Burgring 7, 1010 Vienna, Austria. Tel: +43 1 52177 250, fax: +43 1 52177 459

E-mail addresses: andrea.kern@nhm-wien.ac.at (A.K. Kern), mathias.harzhauser@nhm-wien.ac.at (M. Harzhauser), oleg.mandic@nhm-wien.ac.at (O. Mandic), werner.piller@uni-graz.at (W.E. Piller), ali.soliman@uni-graz.at (A. Soliman).

Abstract

The Late Miocene paleogeography of central Europe and its climatic history are well studied with a resolution of c. 10^6 years. Small-scale climatic variations are yet unresolved. Observing past climatic change of short periods, however, would encourage the understanding of the modern climatic system. Therefore, past climate archives require a resolution on a decadal to millennial scale.

To detect such a short-term evolution, a continuous 6-m-core of the Paleo-Lake Pannon was analyzed in 1-cm-sample distance to provide information as precise and regular as possible. Measurements of the natural gamma radiation and magnetic susceptibility combined with the total abundance of ostracod shells were used as proxies to estimate millennial- to centennial scale environmental changes during the mid-Tortonian warm period.

Patterns emerged, but no indisputable age model can be provided for the core, due to the lack of paleomagnetic reversals and the lack of minerals suitable for absolute dating. Therefore, herein we propose another method to determine a hypothetic time frame for these deposits.

Based on statistical processes, including Lomb-Scargle and REDFIT periodograms along with Wavelet spectra, several distinct cyclicities could be detected. Calculations considering established off-shore sedimentation rates of the Tortonian Vienna Basin revealed patterns resembling Holocene solar-cycle-records well. The comparison of filtered data of Miocene and Holocene records displays highly similar patterns and comparable modulations. A best-fit adjustment of sedimentation rate results in signals which fit to the lower and upper

Gleissberg cycle, the de Vries cycle, the unnamed 500-year- and 1000-year-cycles, as well as the Hallstatt cycle. Each of these cycles has a distinct and unique expression in the investigated environmental proxies, reflecting a complex forcing-system. Hence, a single-proxy-analysis, as often performed on Holocene records, should be considered cautiously as it might fail to capture the full range of solar cycles.

Keywords: Miocene, solar cycles, Lake Pannon, magnetic susceptibility, natural gamma radiation, Ostracoda

4.1. Introduction

Understanding climate-driving mechanisms is a crucial topic in many current research projects from various scientific fields due to the high impact on all life on Earth. Studying recent climate systems is essential to recognize modern climatic patterns; though, future predictions require insights into past climatic evolution.

Unfortunately, historic reports of climatic parameters are scarce. Western scientists started recording temperature and precipitation since 1850 (Versteegh, 2005). This time span, however, covers mainly that part of history where climate was already highly influenced by humans (Tiwari and Ramesh, 2007). Furthermore, direct measurements of sun's emitted energy dates back only to the first satellite documentation from the year 1978 (e.g. Versteegh, 2005; Tiwari and Ramesh, 2007; Lockwood, 2009; Grey et al., 2010). Thus, both observations are too short to allow unequivocal conclusions on natural climate behavior. Despite this problematic issue, the combination of direct measurements of solar energy by satellites as well as weather stations around the globe, verified the positive correlation of sun and climate (Beer et al., 2000; Versteegh, 2005). Temperature and precipitation patterns are influenced by energy sent off by the sun, reaching the earth's atmosphere as so-called cosmic rays. Though the first impression, this pattern is inconstant. Regular changes could be linked to the sun's movement (Charvátova, 2000; Versteegh, 2005) and phenomena such as solar eruptions or the quasi-periodic in- and decrease of sunspots.

Sunspots, appearing as dark spots on the sun's surface, were recorded already by ancient Chinese astronomers (Hoyt and Schatten, 1998). More intensive studies were possible due to the invention of first telescopes culminating finally in the direct observation and measurements by satellites (Eddy, 1976; Hoyt and Schatten, 1998). An iterative process in respect to the amount of visible sunspots was observed for the first time by Schwabe (1844), who reported a steady in- and decrease within a 11-year cyclicity (= Schwabe cylce or sunspot-cycle). Although sunspots cause a local decrease in emitted energy, the surrounding surface of the sun releases energy in a higher degree. Accordingly, a higher number of sunspots leads to more solar power hitting the Earth's atmosphere. Satellite measurements revealed these variations to account for 0.1% of the oscillation of solar irradiance within 11 years (Lean et al., 1995). Longer cycles may modulate the intensity of the shorter ones, causing extreme climatic events. Phases of almost completely lacking sunspots are discussed to correlate with the cool historical periods, such as the Spörer Minimum (1460–1550), the Dalton Minimum (1790–1830) and the Maunder Minimum (1645–1715) (Eddy, 1976; Lean and Beer, 1995; Versteegh, 2005 and therein). Thus, the longest phase of dearth on sunspots during the late 17th century, also called the Maunder Minimum or the Little Ice Age, is discussed to be severely influenced by solar forcing (Eddy, 1976; Robock, 1979; Mörner, 2010)

The Gleissberg cycle is one of the slightly longer solar cycles, probably modulating the Schwabe cycle (Wolf, 1862; Gleissberg, 1939). Firstly assumed to have a duration of 88-years, Orgurtsov et al. (2002) detected a characteristic split into a low-frequency band signal of 50–80 years and a high-frequency signal between 90 and 140 years.

Except for the Gleissberg cycle, direct satellite measurements display neither enough data nor time to proof the existence of other cycles. Therefore, proxy data are necessary to postulate and test such longer periodicities. The best established method is the analysis of time series of atmospheric radioactive isotopes such as ^{14}C (e.g. Stuiver and Braziunas, 1989; Damon and Sonett, 1991; Peristykh and Damon, 2003; Solanki et al., 2004) and ^{10}Be (Beer et al., 1990; Wagner et al., 2001; Usoskin et al., 2003; Solanki et al., 2004) in combination with the total solar irradiance (TSI; e.g. Bard et al., 2000). Their production-rate in the atmosphere is directly linked to the amount of incoming cosmic rays, and thus allows a direct reconstruction of solar intensity (Tiwari and Ramesh, 2007).

Consequently, a ~208 year-cyclicity, named de Vries or Suess cycle (Damon and Sonett, 1991; Stuiver and Brazinas, 1993; Wagner et al., 2005), is documented in various Holocene records (e.g. Schimmelmann et al., 2003; Raspopov et al., 2008; Incarbona et al., 2008, Tarrico et al., 2009; Di Rita, 2011). It might as well be present from historical sunspot observations (Ma and Vaquero, 2009). Its influence on several climatic parameters has been discussed by Raspopov et al. (2007), who document a non-linear response of the climate system in various geographic regions.

Longer time-period sun cycles display frequencies of ~500 to 550 years (Stuiver et al., 1995; Chapman and Shackleton, 2000), ~1000 years (Stuiver et al., 1995; Chapman and Shackleton, 2000; Debret et al., 2007) and ~2400 years (Hallstatt cycle) (Damon and Sonett, 1991; Carvátová, 2000; Nederbragt and Thurow, 2005). Although these cycles appear in many studies their impact on climate is poorly resolved. A climate-link to wind stress and humidity/aridity is suggested only for the Hallstatt cycle (Nederbragt and Thurow, 2005). No

direct nexus is published for the other cycles, but highly expected since they all depend on solar activity.
Most studies on solar cycles are confined to Pleistocene and Holocene records due to limits set by the radioactive isotopes (Bard and Frank, 2006). A further problem is the availability of solid age-models with an appropriate high time-resolution. Therefore, studies outside the '^{14}C-range' usually concentrate on annually preserved records such as lake varves (Milana and Lopez, 1998; Raspopov et al., 2008; Lenz et al., 2010).
Nearly all the studies, however, center on a single proxy, which may represent only individual feedback patterns to solar activity. Therefore, we try to achieve a more detailed and complex picture by analyzing three independent but coeval 600-data-point-sets comprising natural gamma radiation, magnetic susceptibility and the total amount of ostracods. The target is a 6-m-long core with Upper Miocene lake sediments of ancient Lake Pannon in the Vienna Basin (Austria).

4.2. Geological setting

Lake Pannon (Fig. 4.1) covered the Pannonian Basin complex in central and south-eastern Europe during the Miocene and Pliocene. It formed at c. 11.6 Ma when the marine Paratethys Sea retreated to the east. The remaining lake was a brackish and slightly alkaline lacustrine system (Magyar et al., 1999; Harzhauser et al., 2004; Piller et al., 2007; Harzhauser and Mandic, 2008). Lake Pannon experienced its maximum extension of c. 290,000 km² during the Tortonian between 10.5 and 10.0 Ma.
In the Vienna Basin, this phase is recorded by the Bzenec Formation, which crops out at the opencast pit Hennersdorf (Fig. 4.1), situated app. 10 km south of the center of Vienna. It currently exposes roughly 14 meters of blue-grey clays and silts with several mollusc coquinas and scattered plant debris. Information about the lithology and biostratigraphy of the Hennersdorf section was already published in more detail by Harzhauser and Mandic (2004) and Harzhauser et al. (2008). The mollusc fauna represents assemblages of the regional middle Pannonian stage, corresponding to the middle Tortonian (Magyar et al., 1999). Magnetostratigraphy allowed a correlation with the long normal chron C5n (Magyar et al., 1999). Correlation with astronomically tuned well-logs in the Vienna Basin suggests an absolute age of 10.5–10.4 Ma for the section (Harzhauser et al., 2004; Lirer et al., 2009).
In 2009, a 15-m-long core was drilled in the clay pit of which the lower 6 m could be drilled without core break. The core comprises grey-green silty clay with occasionally occurring plant debris and mollusc coquinas; bioturbation is rare. The lower 6 m are rather homogenous; a slight fining upward trend occurs in the lower part indicated by a gradual shift from clayey silt (samples 1540 to 1230) to silty clay (sample 1231 to 979). Upsection follows

again silty clay (sample 980 to 940). The upper part of the core, which is not analyzed herein, displays a coarsening upward trend with increasing amounts of silt and few fine sand layers in the uppermost part (Fig. 4.2a).

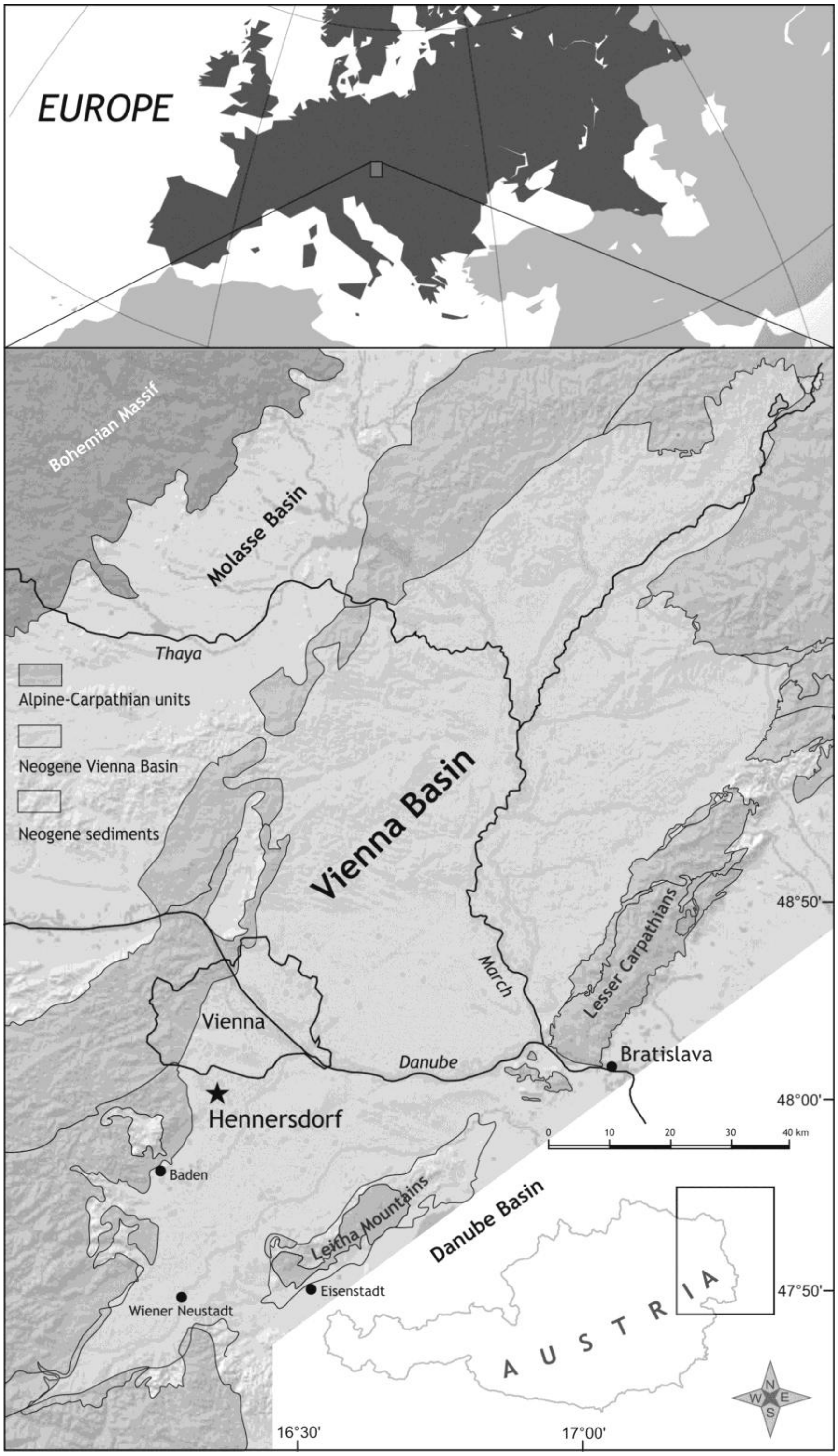

Fig. 4.1. Geological map of the Vienna Basin showing the position of the investigated core at Hennersdorf inside the Vienna Basin (modified after Harzhauser et al., 2004).

4.3. Methods

4.3.1. Sampling

The herein analyzed 6-m-core with a diameter of 15 cm was drilled at the clay pit of Hennersdorf (N48°05’52.6’’ E016°21’15.8’’). We focus on the samples from core-depth 1540 cm (named sample 1540) up to 941. This results in a total of 600 continuous and equal-spaced data points. All parts of the core were marked with a 1-cm-scale on the outside, before they were divided into two halves. One of these is kept for future studies in the Natural History Museum Vienna.

First, lithology and macroscopic fossil content such as mollusc debris and plant fossils were evaluated for each sample-cm. By the same strict sample distance, 600 measurements were taken for natural gamma radiation and magnetic susceptibility. Natural gamma radiation was measured with a hand held “Compact Gamma Surveyor” (Scintillation Gamma Radiometer) and the magnetic susceptibility was measured with an “SM-20” magnetic susceptibility meter with a sensitivity of 10^{-6} SI units (GF Instruments, Brno, Czech Republic). Afterwards the core was cut into 1-cm-thick slices for micropaleontological investigation. Each of these samples was dried, weighed and further treated with H_2O_2 and sieved with 125, 250 and 500 µm mesh-size sieves. The total number of ostracod valves was evaluated for all 600 samples (articulated specimens were counted as 1). These data were then standardized for a sample weight of 100 gram (Table 4.1). The mollusc debris was counted at a range scale from 0 to 3 (0= no shells; 1= rare debris or single shells; 2= loose coquina; 3= dense coquina) (Fig. 4.2b).

4.3.2. Data analysis

Each of the 600 data was first transferred into percentages, before an arcsin-root-transformation was applied to ensure a higher comparability within the different proxy data for further statistical processing (Linda and Berchtold, 1976; Zuschin and Hohenegger, 1998). The software PAST (Hammer et al., 2001) was used to remove trends in all data curves and to produce a 3-point-smoothing for clearer presentation (Fig. 4.2c, 4.2d, 4.2e). PAST was used to perform spectral analysis including REDFIT (Schulz and Mudelsee, 2002) and wavelet analysis. REDFIT is a Fortran 90 program, which allows overcoming the common problem in paleontology of unevenly spaced time series by fitting a first-order autoregressive process. Though sample distance is strictly consistent, due to lithologically unnoticeable changes in sedimentation rate small imbalances within the sample distances might occur. Monte-Carlo method is applied to test a bias-corrected spectrum. The frequency values of the Lomb-Scargle and REDFIT periodograms were than transferred into depth-domain to indicate the statistically relevant cycles in centimeters. Additionally, wavelet analysis was performed to detect potential non-stationary periodicities. The same methods were applied to the ^{14}C based Holocene record of solar activity of Solanki et al. (2004). Periodicities indicated by the Lomb-Scargle and REDFIT periodograms were used as target for a Gaussian bandpass filter with the AnalySeries program (Paillard et al., 1996). This is a frequency-selective filtering procedure, which removes unwanted frequency components from the time series. The bandpass filtering was applied to all three data-sets and is state-of-the-art in modern cyclostratigraphy (Weedon, 2003).

4.4. Results

4.4.1. Natural Gamma Radiation (GR)

The GR-record fluctuates between 16 and 52 cps over the whole investigated core-section and displays a high frequency oscillation (Fig. 4.2c). The record may be divided into three parts, although variations along the section appear not as significant as between certain

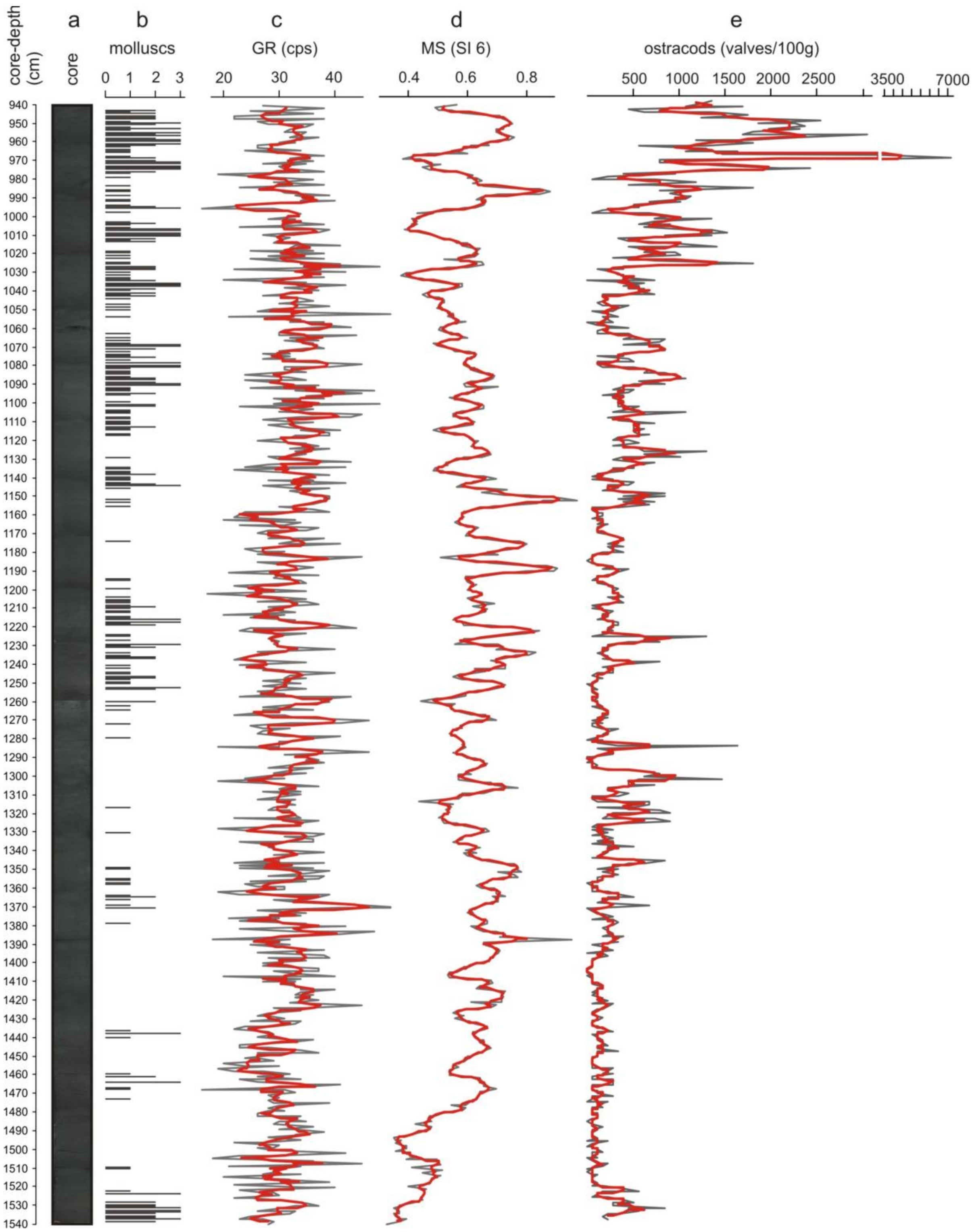

Fig. 4.2. Illustration of the raw data (600 data points for each proxy; core depth in cm corresponds to sample numbers 1540 to 940). The core picture (a) shows the rather homogenous sedimentology; mollusc abundance (b) is indicated on a semi-quantitative scale (0= no shells; 1= rare debris or single shells; 2= loose coquina; 3= dense shell bed); note that the coquinas are autochthonous (Harzhauser and Mandic, 2004). Natural gamma radiation (GR) is given in cps (c), magnetic susceptibility (MS) in Si-units (d) and the total abundance of ostracods is calculated for 100 g sediment (e). Grey lines are raw data, red lines represent the 3-point running mean.

samples. The first one reaches from sample 1540 to 1370 and comprises a rapid succession of serrated, often sharply cut, peaks. Around sample 1370 a strong peak in values occurs, marking the onset of an interval with a moderately serrated motif of comparatively low values without trend. This second part is terminated around sample 1052 with another strong positive peak. Above follow gradually decreasing values with several strongly negative peaks arranged between comparatively higher values (Fig. 4.2c). To gain more insight in this high-frequently changing record, a spectral analysis was performed on the 3-point-running-mean data set (Fig. 4.3a). This displays three strong frequencies which pass the 95% confidence interval. The most prominent cycles have wavelengths of 116.9 and 37.7 cm (Fig. 4.3a). An additional bundle of peaks in the spectral analysis suggests very prominent cycles between 8.8 and 15.2 cm (Fig. 4.3a), supporting the intuitive interpretation. Comparable cycles are indicated by the REDFIT analysis, which points to cycles with periodicities of 6.4, 8.8 and 12.8 cm, passing the 99% confidence interval (Fig. 4.3b). These results are supported by the wavelet analysis, which visualizes an especially intense signal with periodicities of 6.4–8.8 cm and around 12.6–15.4 cm. (Fig. 4.4g). The two longer periodicities at 116.9 and 37.7 cm are very distinct as well in the wavelet analysis.

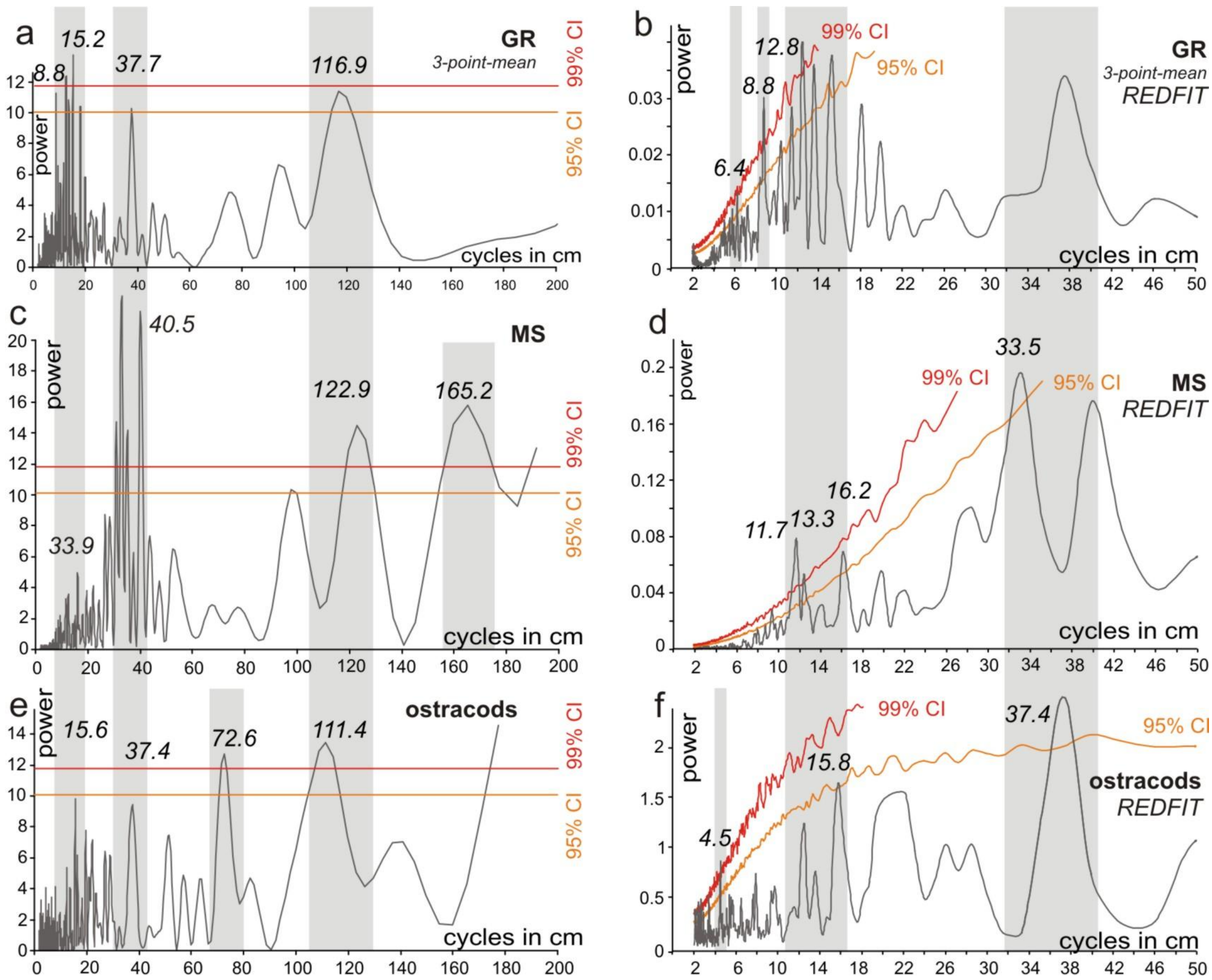

Fig. 4.3. Lomb-Scargle (left; a, c, e) and REDFIT (right; b, d, f) periodograms display repetitive periodicities in each of the three proxy-data-sets. Longer frequencies are better revealed in the power spectra, whilst short cyclicities are better supported in the REDFIT-analysis. Frequencies of 37.4 to 40.5 cm, 111.4 to 122.9 cm are evident in all proxies, while others appear only in one or two.

Filtering these data to the long periodicity, centered at 116.9 cm, shows constant amplitudes throughout the section except for a slight decline in the uppermost part (Fig. 4.4e). Applying a Gaussian filter centered at 37.7 cm, shows low but constantly increasing amplitudes in the lower part (Fig. 4.4f). The middle part displays high amplitudes and an excellent fit with the raw data. In the upper core interval the signal becomes weaker again. This pattern fits well to the wavelet analysis which suggests the strongest expression of this cycle in the middle core interval. A filter at 15.2 cm (from 12.7 to 19.0 cm) reveals the best fit with the raw data with the highest amplitudes between samples 1400 and 1330 (Fig. 4.4d). The signal intensity is weakening afterwards but displays phases of increasing amplitudes at core intervals 1290–1220, 1170–1145, 1105–1075 and 1000–950 at the top. Further, data centered at 8.8 cm (from 7.5 to 10.7 cm) reveal a similar shape in the lower and upper half of the section, with two strong and weak phases being topped by a dominating one (Fig. 4.4c). The shortest of all filtered curves centered at 6.4 cm (from 5.7–7.3 cm) is constantly in- and decreasing without phases of strong manifestation (Fig. 4.4b). Again, these phases correlate to strong signals in the wavelet analysis.

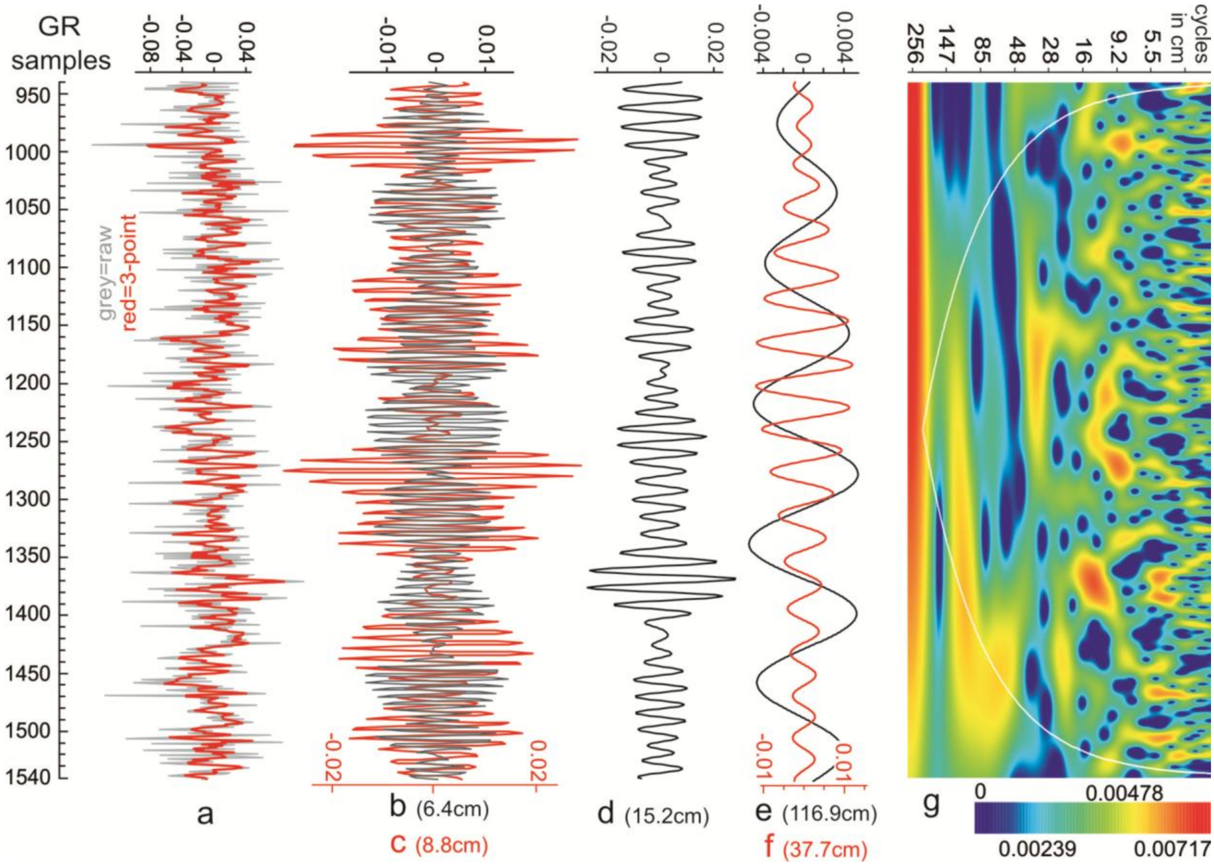

Fig. 4.4. Natural gamma radiation: a: original data (root/arcsin-transformed and detrended) were filtered according to the dominant periods revealed by the periodograms in Fig. 4.3. Gaussian filter were applied centering at b: 6.4 cm (range from 5.7–7.3 cm), c: 8.8 cm (7.5–10.7 cm), d: 15.2 cm (12.7–19.0 cm), e: 37.7 cm (32.9–44.1 cm) and f: 116.9 cm (104.8–132.2 cm); g: wavelet analyses clearly show the presence of these periodicities including the high frequency signals and also document the high-frequency modulation of the various signals.

4.4.2. Magnetic Susceptibility (MS)

The MS record (Fig. 4.2d) is strongly fluctuating with values ranging from 0.3–0.9 SI units. The raw data and the 3-point-running-mean graph already suggest a fairly regular pattern between high and low MS values. High-frequency oscillations, as in the GR record, are missing. The record shows a serrated motif with overall increasing values up to sample 1388. Above follows a serrated interval up to sample 1152 without significant trend. The upper core interval is characterized by overall decreasing values, which are arranged in rapidly fluctuating values up to sample 1030 and a decreasing frequency above.

The serration is also expressed in a very significant signal in the spectral analysis, indicating a strong periodicity at 33.9 cm and at 40.5 cm (Fig. 4.3c). This interval is also evident in the autocorrelation of the data. A third peak, passing the 95% confidence interval, occurs at 122.9 cm next to a fourth at 165.2 cm. The REDFIT analysis supports the peak at 33.5 cm and suggests two further high-frequency cycles at 11.7–13.3 cm, passing the 99%

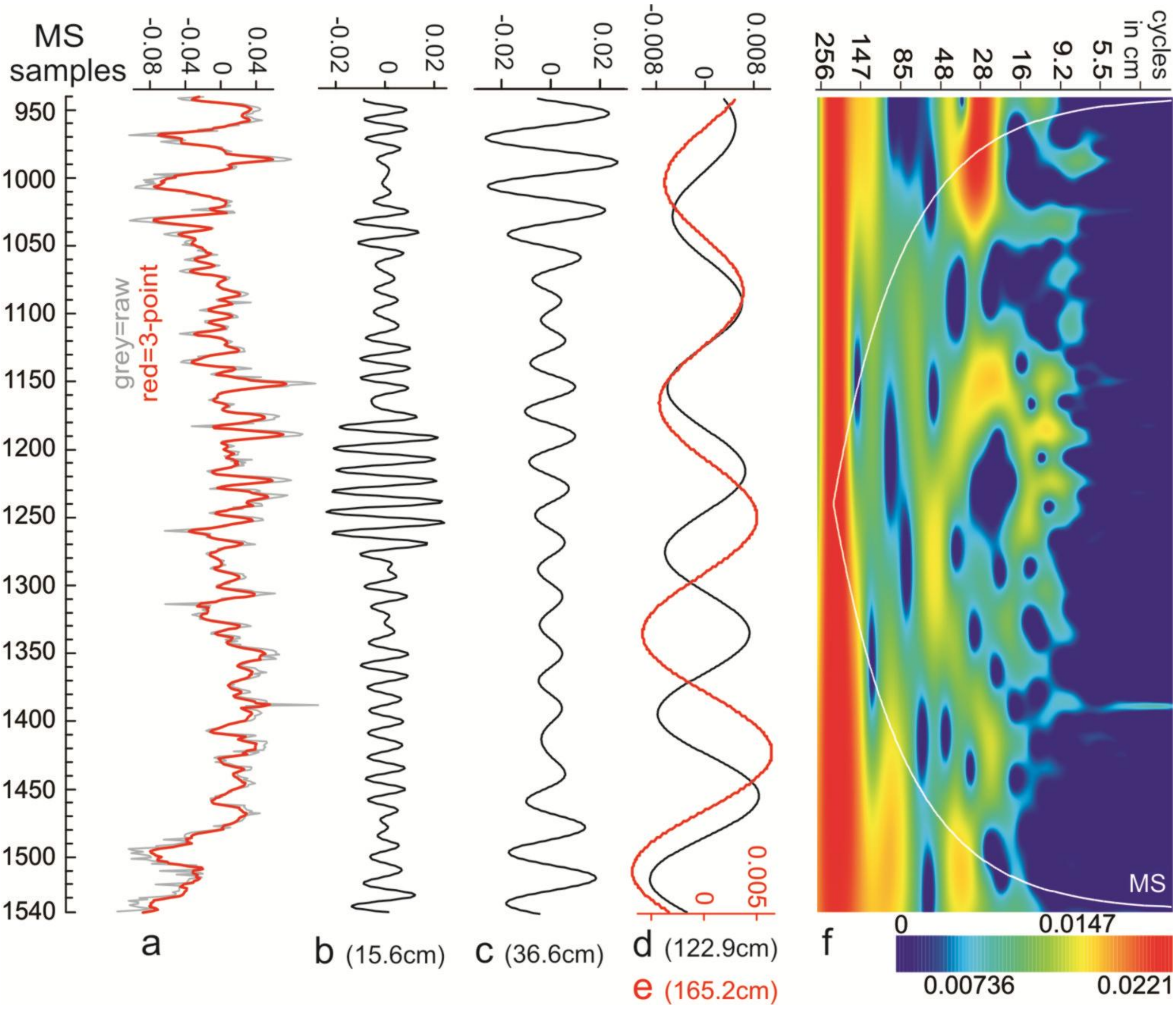

Fig. 4.5. Magnetic susceptibility: a: original data (root/arcsin-transformed and detrended) were filtered according to the dominant periods revealed by the periodograms in Fig. 4.3. Gaussian filter were applied centering at b: 15.6 cm (range from 13.0–19.6 cm), c: 36.6 cm (32.1–42.6 cm), d: 122.9 cm (109.6–139.9 cm) and e: 165.2 cm (152.6–180.1 cm); f: the wavelet analyses clearly show the presence of the low frequency periodicities. High frequency signals around 15.6 cm are strongest in the middle part of the core, whilst higher frequency signals as seen in the gamma radiation data are completely missing.

confidence interval, and a second weaker one at 16.2 cm (Fig. 4.4d). These cycles are clearly visible in the wavelet analysis (Fig. 4.5f), which documents their presence in the interval 1260–1130 cm. The wavelet illustrates clearly the lack of shorter cycles, which differs from the other two proxies.

Filtering the data according to the peaks in the Lomb-Scargle periodograms shows a continuously decreasing signal at 165.2 cm (152.6–180.1 cm) (Fig. 4.5e) and a steady signal at 122.9 cm (109.6–139.9 cm) (Fig. 4.5d). The Gaussian filter at 36.6 cm reveals strongest signals in the lower part of the core up to sample 1450 and in the top between samples 1050 and 950 (Fig. 4.5c). The high frequency filter at 15.6 centered documents highest amplitudes in the middle between samples 1270 to 1180 (Fig. 4.5b).

4.4.3. Ostracods

The samples yield mainly rich ostracod assemblages of usually disarticulated specimens. The total abundance is fluctuating drastically, ranging from only 3 shells up to 7247 per 100 gram sediment, but usually stays distinctly below 1000 specimens (Fig. 4.2e).

Except for a first small peak with about 500 to 800 valves up to sample 1524, the lower part of the core shows very low abundances up to sample 1407. A slow increase in ostracods persists upwards to sample 1278 with two peaks of up to 1600 valves. Moderate values of 200–300 valves characterize the following interval up to sample 1160 being interrupted by two single peaks with more than 700 specimens. Above, abundances are oscillating at higher levels around few hundred specimens up to peaks with 1300 specimens. At sample 1030 low values occurs again, before the numbers of shells are significantly increasing but still strongly fluctuating. The highest abundances occur in the top part of the core including several samples with extraordinary high numbers (977 to 951 cm) (Fig. 4.2e).

The Lomb-Scargle periodogram reveals only two significant signals with periodicities of 72.6 and 111.4 cm (Fig. 4.3e). Small-scale frequencies are indicated by peaks at 15.6 and 37.4 cm, but do not reach the 95% confidence interval. Both peaks, however, are much more significant in the REDFIT spectrum which verifies cycles with periodicities of 15.8 and 37.4 cm (Fig. 4.3f). This method suggests the presence of an even shorter cycle with a periodicity of 4.5 cm, passing even the 99% interval-boundary.

These high-frequency cycles are also indicated in the wavelet analysis (Fig. 4.6g), which documents their presence especially in the intervals 1540–1270 and 1080–940 while they are insignificant in the interval between. The long 111.4-cm-signal is very noticeable and continuous (Fig. 4.6g). In contrast, the 37.4-cm-signal is most prominent in the lower half of the core and the 15.8-cm-signal is best expressed in the middle of the record (Fig. 4.6g).

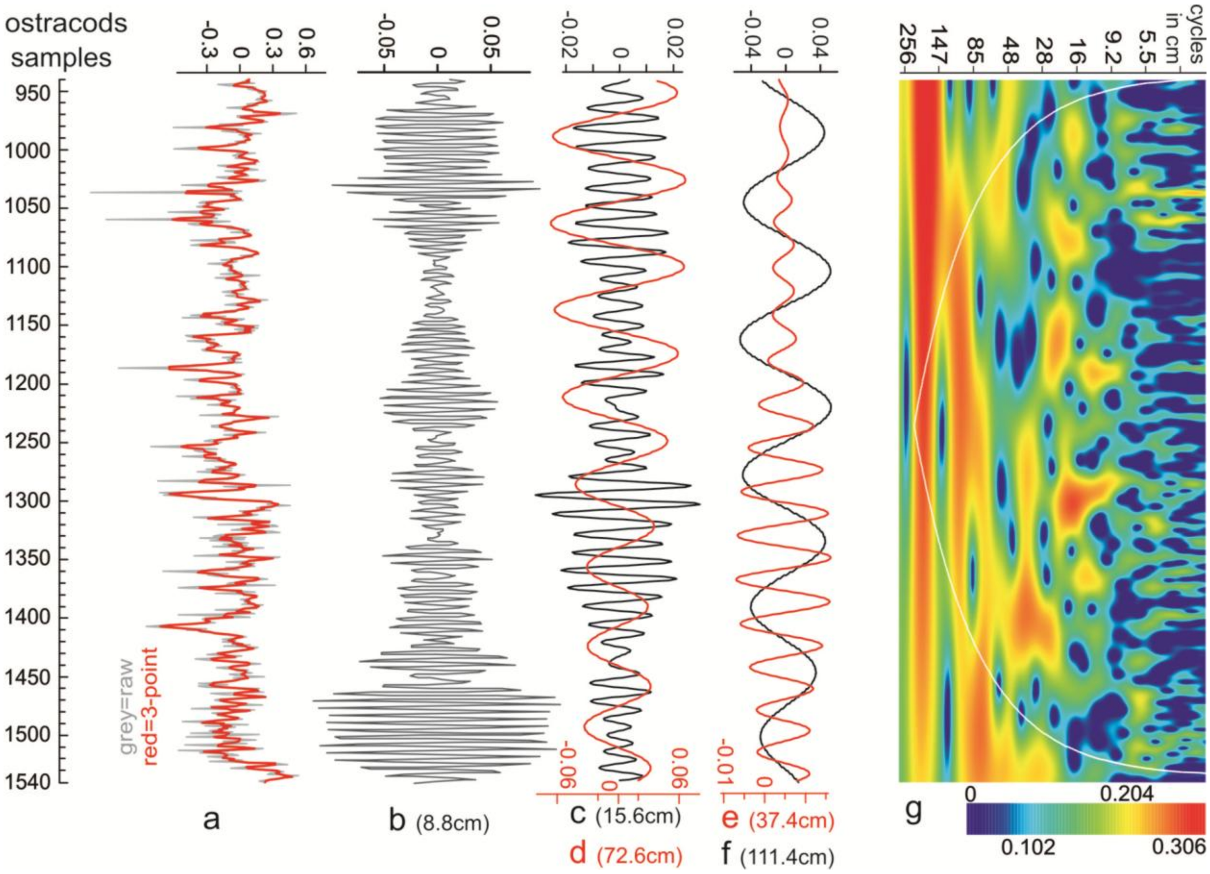

Fig. 4.6. Total abundance of ostracods per 100 g sediment: a: original data (root/arcsin-transformed and detrended) were filtered according to the dominant periods revealed by the periodograms in Fig. 4.3. Gaussian filter were applied centering at b: 8.8 cm (range from 7.5–10.7 cm), c: 15.6 cm (13.0–19.6 cm), d: 72.6 cm (63.4–85.0 cm), e: 37.4 cm (32.7–53.7 cm) and f: 111.4 cm (100.3–125.2 cm); g: these periodicities are also evident in the wavelet analyses showing the strong modulation of the 15.6 cm and 34.4 cm periodicities.

Filtering these data centered at 111.4 cm, documents the continuous expression of that long-period cycle throughout the section, which only a slight increase towards the top (Fig. 4.6f). Similar behavior, but with an more intense rise of intensity, was visible by the filtered data centered at 72.6 cm (Fig. 4.6d). The filtered 37.4-cm-cycle increases in amplitude and is very prominent in the lower half of the core, but becomes weakly expressed in the upper part of the core from sample 1150 onwards (Fig. 4.6e). Also the shortest of the filtered cycles centered at 15.6 cm is strongly variable (Fig. 4.6c). Starting with a weak signal up to approximately sample 1440, the amplitude increases significantly up to sample 1290. Afterwards it becomes very weakly expressed and rises again in the upper part of the core from sample 1070 onwards. The small-scale signal centered at 8.8 cm (7.5–10.7 cm) displays a very strong influence in the lower part of the core (Fig. 4.6b), followed by a rapid decrease and a mainly weak significance up to sample 1040, where another peak occurs. No significant strong phase follows further upwards.

4.4.4. Similarities and dissimilarities in the proxy records

All three proxies reveal different patterns and rhythms. Only two of the cycles are present in all records: the most prominent one has a periodicity of c. 116 cm and the second one centers around 37 cm (Fig. 4.3a, 4.3c, 4.3e). Moreover, all three records are characterized by a series of high-frequency cycles ranging between 8.8 and 16 cm. Unique periodicities are the strong 165-cm-cycle in the MS record (Fig. 4.3c) and the 72.6 cm cycle in the ostracod record (Fig. 4.3e). The filtered data, too, suggest that the three proxies responded differently to the various cycles. Hence, the maximum amplitudes in the ~37-cm-cycle appear in the MS record (Fig 4.5c) during phases of a weak expression of that cycle in the other proxies (Fig. 4f, 6d). These display maxima during weaker phases of the MS record. Similar relations occur in the filtered high-frequency records of the ~15.6-cm-cycle (Fig. 4.4d, 4.5b, 4.6c). Additionally, the GR and ostracod data reveal a small-scale signal around 8.8 cm, documenting a higher degree of small-scale forcing (4.4c, 4.6b).

4.5. Discussion

The reason for the described differences in the patterns may probably be proxy-inherent. The total amount of ostracods is suggested to reflect favorable lake-bottom conditions. An earlier study on the ostracods from the Hennersdorf section (Fig. 4.1) has documented severe oxygenation crises leading to reduced numbers of ostracods (Harzhauser et al., 2008). According to that paper, the assemblages are dominated by five taxa (*Cyprideis*, *Hemicytheria, Lineocypris/Caspionella*, *Amplocypris, Loxochoncha*) which occur in rather constant ratios despite the strongly fluctuating numbers of individuals. The rapid decline of ostracod abundance is therefore explained by unfavorable conditions due to poor bottom water oxygenation. Further, lowered nutrient supply might also be responsible for low counts. The GR signal, in contrast, is not solely depending on lake-bottom conditions. Generally, it is interpreted as an expression of the presence of detectable radioactive isotopes emitted by Potassium-, Uranium- and Thorium-bearing minerals (Blum et al., 1997), which are mainly transported into the lake by rivers or wind. Similarly, the MS signal is mainly a function of detrital input of carrier minerals such as magnetite and pyrrhotite (Stockhausen and Thouveny, 1999; Ellwood et al., 2000). A clear correlation between high MS values and increased precipitation in Holocene lake sediments in India was explained by Warrier and Shankar (2009) by an increased input of pedogenic magnetic particles and by intensification of chemical weathering. A relation between high water levels, humid climate and high MS signatures was also documented for Lake Hunlun in Mongolia (Hu et al., 1999) and Lake Chalco in Mexico (Lozano-García and Ortega-Guerrero, 1994). Contrary to this, Lake Mosoko in Tanzania displays lowest MS values during lake level highs and wet conditions, when heavy minerals are stored in the littoral area (Garcin et al., 2006). This seemingly simple relation between transport and MS signal, however, is strongly challenged by the formation of authigenic ferromagnetic sedimentary greigite. This ironsulfide is frequently found in Miocene sediments of Lake Pannon and related water bodies (Babinszki et al., 2007; Vasiliev et al., 2010) and formed through a series of microbially mediated reactions (Roberts et al., 2011). Hence, the measured MS-log may reflect a mixture of input of carrier minerals and authigenic modification in the lake sediment.

In addition to these factors, causing different response patterns in the studied proxies, there may be a time lag present as well. The ostracod record is expected to reflect the rise and fall of populations in a very high temporal resolution without recognizable temporal bias. Similarly, the GR record is suggested to reflect more or less coeval changes in environmental conditions. The MS signal, in contrast, may be altered by diagenetic processes and the bacteria induced formation of greigite may have occurred below the sediment/water interface resulting in a time lag. These processes might also be responsible for the absence of the high-frequency cycles in the MS signal, whereas these cycles were unaffected in the total ostracod abundance and GR records.

4.5.1. From depth to time domain – a hypothesis

There is no possibility to reconstruct an accurate absolute age-model for the herein studied core. Any transformation of the data from depth into time domain remains hypothetical. Yet knowing its stratigraphic position, we are able to link it to sediment accumulation rates in the Vienna Basin. Hence, astronomically tuned middle Tortonian drilled basinal successions of Lake Pannon indicate average sedimentation rates of c. 0.65 mm/yr (=15.4 yr/cm) (Lirer et al., 2009).

Slightly higher sedimentation rates have to be expected for the core as the drill site was closer to the shore than the above mentioned basinal drillings and within the influence of a delta system in about 4–6 km distance (Harzhauser et al., 2008). As the 6-m-long core is too short to capture the smallest Milankovitch cycles, the highly significant cycles might represent sub-Milankovitch cycles represented by solar cycles most likely.

To test this hypothesis we used the proven sedimentation rate of Lirer et al. (2009) of 0.65 mm/yr for a time domain transformation of the detected cyclicities. Those result in periodicities of ~570 yr for the dominant 37-cm-cycle and ~240 yr for the 15.6-cm-cycle. Other cycles detected (72.6 cm; ~115 cm; 165.2 cm), would represent ~1120, ~1800, and ~2540 years. These values, except for the 1800-yr-cycle, are very close to the periodicities of Holocene solar cycles (e.g. Beer et al., 1990; Stuiver and Braziunas, 1993; Solanki al., 2004; Yin et al., 2007). Based on this hypothesis we performed a best-fit adjustment of the sedimentation rate. Only a slightly increased sedimentation rate up to 0.73 mm/yr (=13.7

yr/cm), results in periodicities of 205.5–213.7, 501.4–516.5, 994.6 and 2271 years (taking the average values of 15–15.6, 33.6–37.7, 72.6, 165.2 cm, respectively), which is in full agreement with the several postulated periodicities of Holocene solar cycles compared to Solanki et al. (2004). Moreover, a strong cycle appears with a periodicity of roughly 1600 years (1526–1684 years or 111.4–122.9 cm). This cycle cannot be attributed to any known solar cycle but agrees well with the enigmatic ~1500-cycle (Bond et al., 2001). Recently, this cycle is interpreted to be a feedback mechanism to internal oceanic processes or the modulation of other solar cycles (Bard and Frank, 2006; Debret et al., 2007). Debret et al. (2009) further discussed the differences in the expressed intensity in the whole Atlantic by comparing records derived from proxies. Although present within a time variation of 1400 to 1600-yeears, no common trigger mechanism could be determined. Nevertheless, in Holocene records it is well documented from not only from marine records, but from far distant continental areas, e.g. in Canada (Campbell et al., 1998), Arabia (Parker et al., 2006) and Weber et al. (2010), who discovered a ~1500-yr-cycle even in Upper Miocene and therefore pre-glacial lake deposits of northern Greece. Still, no indication for solar origin of the 1500-year-cylce could be found (Debret et al., 2007; 2009).

4.5.2. Holocene solar cycles

Applying the-best-fit sedimentation rate of 0.73 mm/yr to the time domain transformation of the core, results in a total of 8220 years of Miocene time reflected in the core. This allows a comparison with the Holocene records, where many studies already deal with the existence of solar cycles and their influence on Earth’s climate. The longest continuous record of solar activity based on radioactive isotopes documents almost 12,000 years of solar activity (Solanki et al., 2004). This huge data set is based on a comparison between ^{10}Be and ^{14}C from tree rings and is available at http://www.ncdc.noaa.gov/paleo/recons.html. Periods and quasi-periods of solar activity were previously detected in these data also by Yin et al. (2007), who also performed a wavelet analysis.

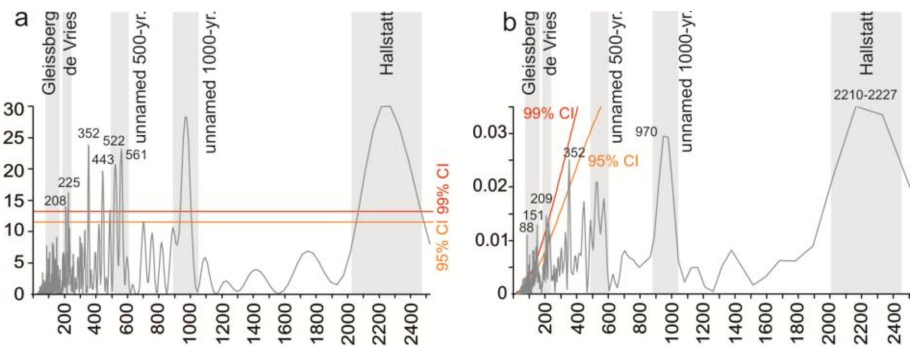

Fig. 4.7. Lomb-Scargle (a) and REDFIT (b) periodograms performed on the Holocene sunspot numbers from Solanki et al. (2004). The results of the power spectrum is comparable to results of Yin et al. (2007) and detects all known solar cycles from the de Vries cycle onwards. The REDFIT analysis, however, is able to detect also the lower and upper Gleissberg cycles. Similarly to the Miocene record, the sample resolution excludes an expression of the 11-years-Schwabe cycle.

To achieve a better understanding of these solar patterns, we utilized the Solanki-et-al.-data as well and processed them with the same methods as our Miocene records. Besides creating a power spectrum and wavelet analysis similar to Yin et al. (2007), we applied the REDFIT method and filtered the data according to the dominant periodicities to visualize the shifts in amplitude of the various solar cycles through time (Fig. 4.7 and 4.8).

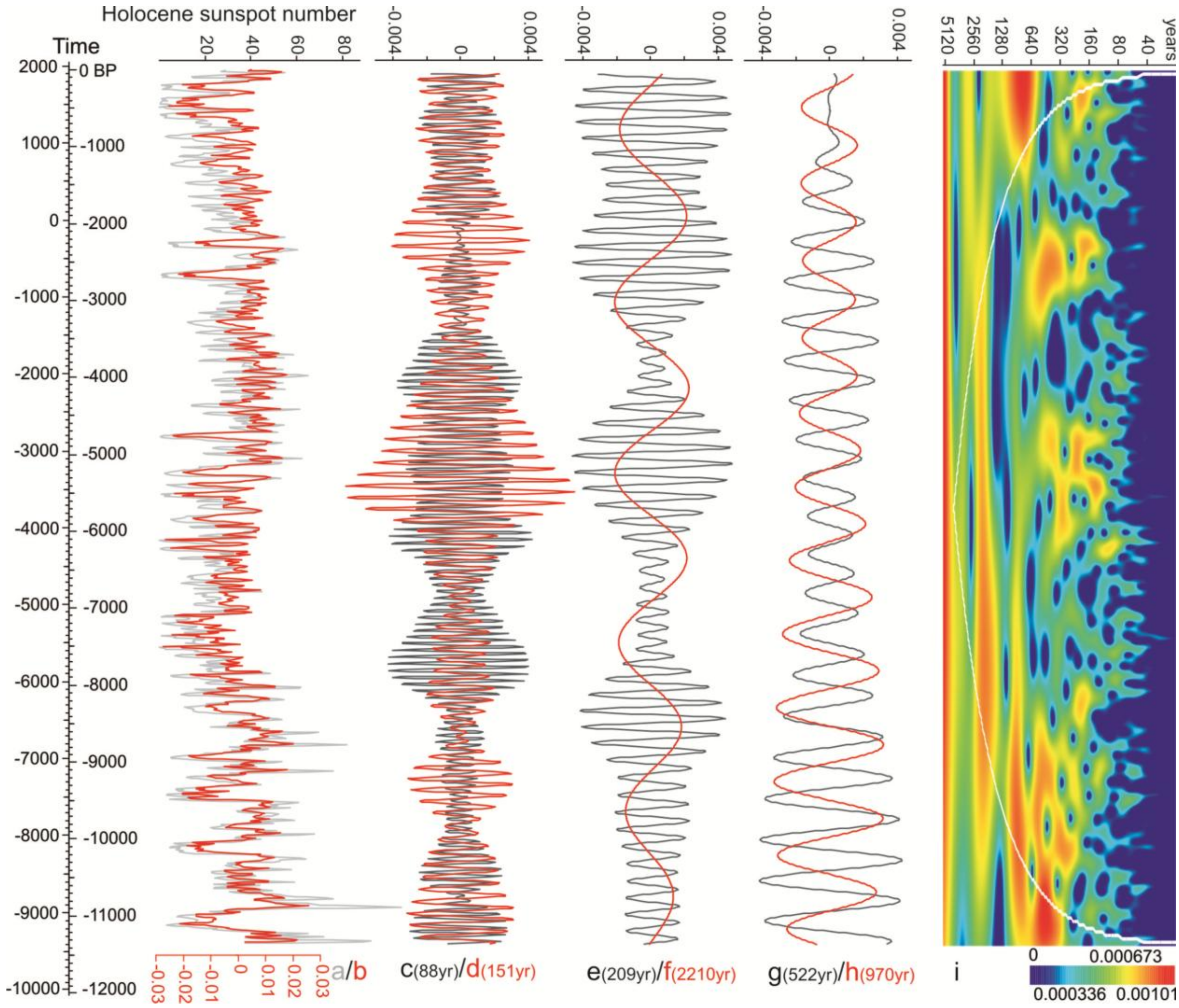

Fig. 4.8. Holocene solar activity (Solanki et al., 2004): a: calculated sunspot numbers and b: the root/arcsin-transformed and detrended data. Gaussian filters have been applied to the data according to the dominant periods revealed by the periodograms in Fig. 4.7. These filters are centered at c: 88 years (range from 79 to 98 yrs), d: 151 years (135.2–171.0 yrs), e: 209 years (192.2–229.0 yrs), f: 2210 years (1976.3–2512.6 yrs), g: 522 years (480.1–571.8 yrs) and at h: 970 years (874.1–1089.3 yrs).
The strong modulation of the signals is also evident in the wavelet analysis (i).

Our analysis is in good agreement with the results of Yin et al. (2007). Both approaches indicate the de Vries cycle with periodicities of 225- and an unnamed 352-yr-cycle (Fig. 4.7a and 4.7b). In addition to the peak at 225 years, our analysis shows an additional peak at 208 years suggesting slight shifts in the duration of the individual de Vries cycles (Fig. 4.7a). Peaks at 443 (441 in Yin et al., 2007), 522 and 561 years are also analogous to Yin et al. (2007). All these signals could be summarized to a quasi-500-year-cyclicity (Fig. 4.7a). Filtered data illustrate the constant existence of periodicity, which can in consequence of the multiple peaks only be interpreted due to a strong variation in the length of each cycle (Fig.

4.8g). The next significant peak occurs at 970 years, indicating the unnamed 1000-yr-cycle. Finally, the Lomb-Scargle periodogram shows a strong peak at 2210 to 2227 years, which represents the Hallstatt cycle (Fig. 4.7a). The Gleissberg cycle does not appear in the spectral analysis but is expressed by two very significant peaks above the 99% confidence interval at 88 and 151 years in the REDFIT analysis (Fig. 4.7b). This fact may be explained due to the presence of too much noise in the huge data set, which gets removed using the REDFIT spectrum (Schulz and Mudelsee, 2002). This solar cycle displays a wide frequency band and temporal variation in power with a lower Gleissberg band of 50–80 years and an upper Gleissberg band of 90–140 years fitting excellently to the two-fold signal in the REDFIT spectrum (Ogursov et al., 2002; Ma, 2009). The REDFIT analysis documents also the presence of a very prominent quasi-210-yr-periodicity of the de Vries cycle (Fig. 4.7b). Considering the wavelet spectrum, it is obvious, that the very high-frequency solar cycles (less than 60 years of duration) are indicated with a reduced intensity or are missing (Fig. 4.8i), which corresponds to the wavelet analysis of Yin et al. (2007). This may most likely be caused by the presence of noise due to the irregularities in the solar cyclicities. Still visible is the lower Gleissberg cycle, which is displayed with its highest intensity from 5500 to 12,000 years (Fig. 4.8i). The upper Gleissberg is well expressed, by a strongest phase between 2500 and 8000 years.

An important fact is the absence of any 1500-year-cycle (Fig. 4.7). This is a strong proof, that this periodicity is no solar cycle as suggested by Bond et al. (2001) but might result from other feed-back mechanisms (e.g. Braun et al., 2005; Versteegh, 2005; Bard and Frank, 2006; Xapsos and Burke, 2009).

The filtered data demonstrate a considerable modulation of the different solar cycles (Fig. 4.8c to 4.8h). The 1000-year-cycle shows a constant decrease in amplitude during the Holocene (Fig. 4.8h). The filtered quasi-500-yr-component has a comparable trend (Fig. 4.8g); its amplitude decreased strongly resulting in a moderate minimum around 5000–3500 B.C., then increased slightly again and becomes insignificant during the last 1000 years. In contrast, the expression of the 2210-yr Hallstatt cycle increases throughout the Holocene (Fig. 4.8f). The filtered 209-yr- component, representing the de Vries cycle, shows a much more complex pattern (Fig. 4.8e). It strongly alternates between high and low amplitude phases, but is overall steadily strengthening. Two major break-downs occurred around 5700–4500 B.C. and 2200–1500 B.C. The lower and upper Gleissberg cycles are also highly oscillating and display no phase-relation (Fig. 4.8c). The 151-yr-component develops a phase of extraordinary high amplitudes from about 4000–2500 B.C. and a second weaker phase from 700 B.C. to 200 A.D. (Fig. 4.8d), roughly coinciding with maxima in the de Vries cycle. The 88-yr-component, in contrast, tends to develop maxima in phases of low amplitude of the de Vries cyclicity.

4.5.3. Solar cycles in Miocene and Holocene times – a comparison

The close resemblance of the Lomb-Scargle periodograms of the Miocene records and the Holocene ones (Fig. 4.9) is strongly supporting our interpretation of the detected cycles as expression of variations in solar activity. The appearance of the 1500-yr-cycle as an “Earth-system-immanent cycle” is the major difference between both diagrams. This observation is of substantial importance as this cycle is also known from a Late Miocene lake in Greece (Weber et al., 2010) as well as it was indicated previously for Lake Pannon (Paulissen and Luthi, 2011).

As shown by the filtered Holocene solar activity data (Fig. 4.8a), the various cycles are strongly modulated through time. Especially the de Vries cycle appears as succession of high and low amplitude phases. The wavelet analyses show an unsteady expression of the centennial-scaled solar cycles. A strikingly similar pattern arises from the filtered MS data of Lake Pannon. The time transformed data reveal comparable durations of high-amplitude and low-amplitude phases and a near identical modulation of the signal. This coincidence in patterns may be taken as further support for our hypothesis, that the proxies may reflect the imprint of solar cycles.

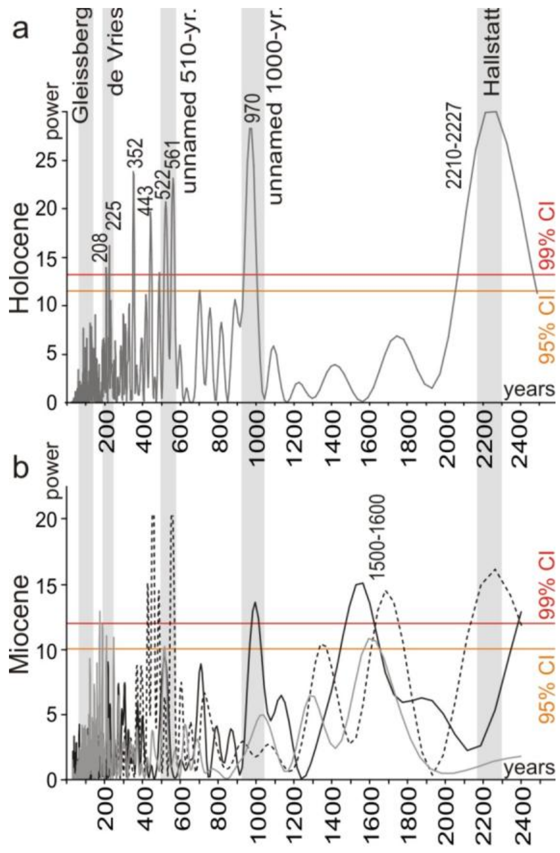

Fig. 4.9. A comparison of the Lomb-Scargle periodogram of the Holocene sunspot activity with time-converted periodograms of the Miocene proxy data. The overall similarity of the patterns is striking. Moreover, the appearance of the non-solar ~1500-yr-cycle in the Miocene data sets is obvious.
GR: gray line, MS: dashed line, ostracodes: black line.

Summarizing these facts of individual imprints of various solar cycles is significantly different, it points towards an uncertainty of single proxy records. This may complicate the creation of a “master-target-curve”. High amplitudes of certain solar-cycles in the isotope-based Solanki et al. (2004) data will not necessarily appear with the same pattern in sedimentary features. Therefore, the possibility of a non-uniform response of different environmental proxies within the same geographic area to a common external trigger should be considered in analysis of Holocene data as well.

4.5.4. Ecological interpretation

The ecological impact of solar forcing is still enigmatic. Solar energy dispersion varies globally, thus, its influence on climate has to be studied on a regional scale. Climate observations around the earth are able to detect a solar effect, but are increasingly obliterated by anthropogenic interference (Gray et al., 2010). Versteegh (2005) discussed a link between the position of the Intertropical Convergence Zone (ITCZ) and solar activity, but concluded that global data are needed to test this hypothesis.

Especially, sea- and lake-levels are sensitive to variations in solar activity (Yousef, 2006; Bruckman and Ramaos, 2009). Cosmic rays influence climatic patterns due to their influence on cloud formation (Friis-Christensen and Svensmark, 1997). The total cloud cover is an often neglected but important factor for local climate since it is in correlation with the Earth's surface temperature as well as snow/rainfall. These in turn, determine how much water is introduced into the lake-system and how much is removed due to evaporation (Friis-Christiansen and Svensmark, 1997; Grey et al., 2010). Because of their smaller water body, lakes are more sensitive to small climatic changes. Several lakes seem to reflect even the shortest known solar cycle, the 11-year Schwabe cycle (Yousef, 2006). The impact of the solar cycles on the various lakes, however, is not uniform and each lake system has to be considered separately. Similarly, the impact of the de Vries cycle depends on geographic region. This solar cycle may be expressed, e.g., by exceptional flooding events or by phases of increased aridity, pointing to a very complex sun-climate-feedback-mechanism with strong regional character (Raspopov et al., 2008). Nevertheless, significant solar-cycle-related changes in lake ecology and lake level have been variously documented for Holocene records (Vos et al., 1997; Yousef, 2006; Di Rita, 2011). Therefore, an influence of solar forcing on the environments surrounding the Miocene Lake Pannon and its hydrology is equally presumable.

The statistic analyses of the three different proxy data clearly document repetitive shifts with periodicities of c. 10–15, 37–40, 72.6, 110–120 and 165 cm (Fig. 4.3). Based on our age-model the dominant of these cycles have periods of c. 209, 510, 995, 1600 and 2300 years (Fig. 4.7b). The intensity and modulation of these various cycles for each of the proxies is individually varying. This is explained by the fact that all three proxies are linked to different environmental factors. The GR record suggests small scaled, high-frequency oscillations of the lake level which are mainly forced by the de Vries cycle. Additionally, an impression by the upper and lower Gleissberg cycles is indicated by the REDFIT analysis (Fig. 4.3b). The overall GR pattern indicates a slight transgressive tendency up to sample 1370, a rather stable phase thereafter, terminated by another transgressive pulse around sample 1052. Afterwards the decreasing values suggest a slight shallowing. This interpretation is well supported by the increasing amount of silt and the increasing amount of shell hash and coquinas. The transgressive phases, in contrast, are reflected by low settlement by molluscs (Fig. 4.2b).

The ostracod record follows this overall deepening trend but differ significantly in details. This indicates that a much more complex ecological response, instead of a simple lake-level fluctuation, is reflected by the bottom-dwelling ostracods. The de Vries cycle explains only small parts of their record; in contrast, a decadal scaled cycle close to the lower Gleissberg signal and a 500-yr-cycle dominate in the REDFIT analysis. Especially the strong dominance of the Gleissberg cycle, which coincides with the weak expression of other cycles, between the base and sample 1450, is reflected by regular small-scale variations of the lake-bottom conditions.

The 500-yr-cycle is also the dominant factor in the MS signal, pointing to a causal relation between MS signal and lake-bottom-water oxygenetation. It is strongly expressed in the lower and the top part of the core and has a moderately strong signal in the middle part.

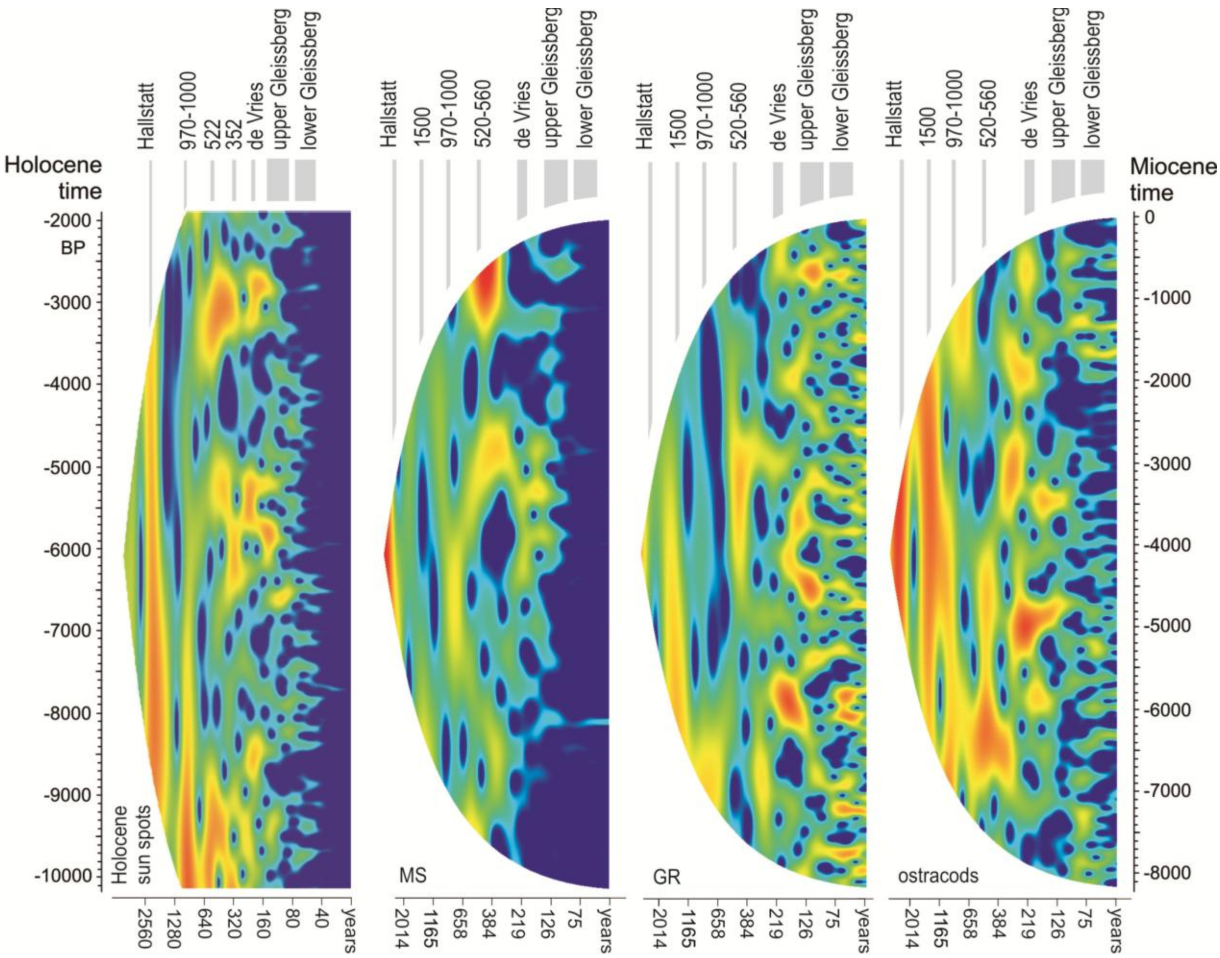

Fig. 4.10. Comparison of time-transformed wavelet spectra of the Miocene records with an equivalent time span of the Holocene sunspot record from Solanki et al. (2004). The shorter cycles are more intensly revealed in the gamma radiation and ostracod data. Each solar cycle is marked: Lower Gleissberg (50–80 yrs), Upper Gleissberg (90–140 yrs), de Vries/Suess (~208 yrs), 500 to 500 year cycle and 1000-yr-cycle, Hallstatt (~2300 yrs) next to the additionlal 352-year-cylce in the Holocene record and the 1500-year-cycle in the Miocene data sets.

Phases which reflect a significant impact of the de Vries cycle coincide with a low expression or decrease of other cyclicities. Information on higher frequencies appears to have been lost due to post-sedimentary processes such as bacteria-induced greigite formation.
All three Miocene (GR, MS, ostracods) and the Holocene records document that a low expression of the various solar cycles is reflected by low fluctuations in the environmental proxies suggesting comparatively stable – though not necessarily favorable – conditions (Fig. 4.10). Moreover, we document that the various solar cycles are reflected not uniformly by different paleoenvironments and proxies. Finally, the modulation of the cycles in the filtered data is fully comparable with that of Holocene records suggesting that the Miocene system of Lake Pannon was influenced by identical variations of solar radiation.

4.6. Conclusions

The investigated continuous 6-m-core of Tortonian lake sediments clearly displays regular fluctuations and modulations within three different environmental proxies (natural gamma radiation, magnetic susceptibility, total abundance of ostracods). Lomb-Scargle and REDFIT periodograms next to wavelet spectra of all data sets reveal distinct frequencies. Only few of these are deciphered in all proxy data sets at the same power, while some occur only in two or one proxies.
Converting these frequencies into a time-domain based on previously published sedimentation rates for Lake Pannon in the Vienna Basin, resulted in cyclicities, which agree well with known solar cycles deduced from Holocene sunspot records (Fig. 4.10). Accepting this as a hypothesis of the observed cycles represent solar cycles, a best-fit adjustment of the sedimentation rate revealed a full fit to the proposed solar cycles. This in turn might be a method to estimate hypothetical sedimentation rates in sedimentary sections for which no age control can be established.
Hence, the Late Miocene lake system seems to reflect the influences of c. 80, 120, 208, 500, 1000, 1500 and 2300 year cyclicities, corresponding to the lower and upper Gleissberg, the de Vries/Suess, the unnamed 500-year, 1000-year and the Hallstatt cycles (Fig. 4.10). After filtering the data according to the dominant frequencies, the cycles turn out to be strongly modulated, comprising phases of high amplitudes alternating with phases of low amplitudes. To test the solar-forcing-hypothesis, the data are compared with those from the Holocene isotope data of Solanki et al. (2004). The filtered Miocene data correspond strikingly with those of the Holocene records, but a significant difference is the presence of a 350-cycle in the Holocene and the appearance of a 1500-year-periodicity in all three fossil records. As the latter one, know as “Earth-system-immanent-cycle”, appears independent of solar-

forcing. Its previous connection to ice-sheet dynamics seems more unlikely due to its presence in the pre-glacial Miocene record.
All proxies reflect the influence of the de Vries, the 500-year-cycle and the above mentioned 1500-year-cycle. Of these, the 500-year-cycle seems to have played a dominant role in the lake system.
The magnetic susceptibility shows further the impact of the long Hallstatt cycle, but tends to resolve short-term variations, such as the Gleissberg cycle (Fig. 4.10). This problem could be associated to the bacterial activity in the bottom-sediments of Lake Pannon leading to the formation of greigite, which consequently destroyed any original high-frequency signal. The two short Gleissberg cycles are present only in the gamma radiation and ostracod records. Beyond that, it is impossible to detect shorter cycles such as the Schwabe cycle, as one sample roughly corresponds to one decade of Miocene time.
Thus, each proxy responds in a different intensity to certain cycles. While the MS signal seems to be partly overprinted by bacterial activity, the gamma record is supposed to document input by wind or fluvial systems. It is the most sensitive proxy and largely unaffected by post-sedimentary processes. Therefore this proxy is able to capture very high-frequency oscillations. In contrast, the establishment of hostile bottom conditions leading to low ostracod abundance may be linked to periodically increased lake stratification. Although the latter two processes might be linked, no clear phase relation is evident in the data aside from the 500-year-cycle.
The integrated analysis of different environmental proxies reflects a very complex process of how solar forcing influences climate and environment. The mechanism behind is still enigmatic and even poorly understood during the Holocene. Consequently, a single-proxy analysis, as frequently done in Holocene records, will probably fail to detect the full range of cycles. Still, these observations document the pervasive and persistent influence of changes in solar activity on Earth's climate and regional climate variability even in non-glacial periods.

Acknowledgements
This study is supported by the FWF grant P21414-B16. Further, we want to thank Anton Englert, Anton Fürst, Franz Topka, Andy Leggat and Lisa Schmidinger for core preparation, sample processing and counting of the ostracods.

4.7. References

Babinszki, E., Márton, E., Márton, P., Kiss, L.F., 2007. Widespread occurrence of greigite in the sediments of Lake Pannon: Implication for environment and magnetostratigraphiy. Palaeogeogr. Palaeoclimatol. Palaeoecol. 252, 626–636.

Bard, E., Frank, M., 2006. Climate change and solar variability: What's new under the sun? Earth Planet. Sci. Lett. 248, 1–14.

Bard, E., G. Raisbeck, F. Yiou, and J. Jouzel. 2000. Solar irradiance during the last 1200 years based on cosmogenic nuclides. TELLUS B 52 (3), 985–992.

Beer, J., Mende, W., Stellmacher, R., 2000. The role of the sun in climate forcing. Quat. Sci. Rev. 19, 403–415.

Beer, J., Blinov, A., Bonani, G., Finkel, R.C., Hofmann, H.J., Lehmann, B., Oeschger, H., Sigg, A., Schwander, J., Staffelbach, T., Stauffer, Suter, M., Wölfli, W., 1990. Use of ^{10}Be in polar ice to trace the 11-year cycle of solar activity. Nature 347, 164–166.

Blum, P., Rabaute, A., Gaudon, P., Allan, J.F. 1997. 14. Analysis of natural gamma-ray spectra obtained from sediment cores with the shipboard scintillation detector of the Ocean Drilling Program: example from leg 1561. Proceed. ODP, Sci. Res. 156, 183–195.

Bond, G., Kormer, B., Beer, J., Muscheler, R., Evans, M.N., Showers, W., Hoffmann, S., Lotti-Band, R., Hadjas, I., Bonani, G., 2001. Persistent solar influence on North Atlantic Climate during the Holocene. Science 294, 2130–2136.

Braun, H., Christl, M., Rahmstorf, S., Ganopolski, A., Mangini, A., Kubatzki, C., Roth, K., Kromer, B., 2005. Possible solar origin of the 1,470 year glacial climate cycle demonstrated in a coupled model. Nature 438, 208–211.

Bruckman, W., Ramos, E., 2009. Evidence for climate variations induced by the 11-year solar and cosmic rays cycles. Proceed. Internat. Astronom. Union 5, 446–448.

Chapman, M.R., Shackleton, N.J., 2000. Evidence of 550-year and 1000-year cyclicities in North Atlantic circulation patterns during the Holocene. The Holocene 10, 287–291.

Charcátová, I., 2000. Can origin of the 2400-year cycle of solar activity be caused by solar inertial motion? Ann. Geophys. 18, 399–405.

Damon, P.E., Sonett, C.P., 1991. Solar and terrestrial components of the atmospheric c-14 variation spectrum, in: Sonett, C.P. Giampapa, Methews, M.S. (Eds.), The sun in time. The University of Arizona, Tucson, pp. 360–388.

Debret, M., Bout-Roumazeilles, V., Grousset, F., Desmet, M., McManus, J.F., Massei, N., Sebag, D., Petit, J.-R., Copard, Y., Trentesaux, A., 2007. The origin of the 1500-year climate cycles in Holocene North-Atlantic records. Climate of the Past 3, 569–575.

Debret, M., Sebag, D., Crosta, X., Massei, N., Petit, J.-R., Chapron, E., Bout-Roumazeilles, V., 2009. Evidence from wavelet analysis for a mid-Holocene transition in global climate forcing. Quaternary Science Reviews 28, 2675–2688.

Di Rita, F., 2012. A possible solar pacemaker for Holocene fluctuations of salt-marsh in southern Italy. Quaternary International, doi:10.1016/j.quaint.2011.11.030.

Eddy, J.A., 1976. The Maunder Minimum. Science 192, 1189–1202.

Ellwood, B.B., Crick, R.E., El Hassani, A., Benoist, S.L., Young, R.H., 2000. Magnetosusceptibility event and cyclostratigraphy method applied to marine rocks: detrital input versus carbonate productivity. Geology 28, 1135–1138.

Friis-Christensen, E., Svensmark, H., 1997. What do we really know about the sun-climate connection? Adv. Space Res. 20, 913–921.

Garcin, Y., Williamson, D., Taieb, M., Vincens, A., Mathé, E.E., Majule, A., 2006. Centennial to millennial changes in maar-lake deposition during the last 45,000 years in tropical Southern Africa (Lake Masoko, Tanzania). Palaeogeogr. Palaeoclimatol. Palaeoecol. 239, 334–354.

Gleissberg, 1939. Observatory 62, 158.

Gray, L.J., Beer, J., Geller, M., Haigh, J.D., Lockwood, M., Matthes, K., Cubasch, U., Fleitmann, D., Harrison, G., Hood, L., Luterbacher, J., Meehl, G.A., Shindell, D., van Geel, B., White, W., 2010. Solar influence on Climate. Rev. Geophys. 48, RG4001.

Hammer, Ø., Harper, D.A.T., Ryan, P.D., 2001. PAST: Palaeontological Statistics Software package for education and data analysis. Palaeontol. Electron. 4 (1), 9 pp.

Harzhauser, M., Mandic, O., 2004. The muddy bottom of Lake Pannon-a challenge for dreissenid settlement (Lake Miocene; Bivalva). Palaeogeogr. Palaeoclimatol. Palaeoecol. 204, 331–352.

Harzhauser, M., Mandic, O., 2008. Neogene lake systems in Central and South-Eastern Europe: faunal diversity, gradients and interrelations. Palaeogeogr. Palaeoclimatol. Palaeoecol. 260, 417–434.

Harzhauser, M., Daxner-Höck, G., Piller, W.E., 2004. An integrated stratigraphy of the Pannonian (Late Miocene) in the Vienna Basin. Austrian Journal of Earth Science 95/96, 6–19.

Harzhauser, M., Kern, A., Soliman, A., Minati, K., Piller, W.E., Danielopol, D.L., Zuschin, M., 2008. Centennial- to decadal scale environmental shifts in and around Lake Pannon (Vienna Basin) related to a major Lake Miocene lake level rise. Palaeogeogr. Palaeoclimatol. Palaeoecol. 270, 102–115.

Hoyt, D.V., Schatten, K.H., 1998. Group sunspot numbers: A new solar activity reconstruction. Sol. Phys. 179, 189–219.

Hu, S., Wang, S., Appel, E., Ji, L., 1999. Environmental mechanism of magnetic susceptibility changes of lacustrine sediments from Lake Hulun, China. Science in China (Series D) 43, 534–540.

Incarbona, A., Ziveri, P., DiStefano. E., Lirer, F., Mortyn, G., Patti, B., Pelosi, N., Sprovieri, M., Tranchida. G., Vallefuoco, M., Albertazzi, S., Bellocci, L.G., Bonanno, A., Bonomi, S., Censi, P., Ferraro, L., Giuliani, S., Mazzola, S., Sprovieri, R., 2010. The impact of the Little Ice Age on Coccolithophores in the Central Mediterranea Sea. Climate of the Past 6, 795–805.

Lean, J., Beer, J., Bradley, R., 1995. Reconstructions of solar irradiance since 1610: Implications for climate change. Geophys. Res. Lett. 22, 3195–3198.

Lenz, O.K., Wilde, V., Riegel, W., Harms, F.-J., 2010. A 600 k.y. record of El Niño-Southern Oscillation (ENSO); Evidence for persisting teleconnections during the Middle Eocene greenhouse climate of Central Europe. Geology 38, 627 – 630.

Lirer, F., Harzhauser, M., Pelosi, N., Piller, W.E., Schmid, H.P., Sprovieri, M., 2009. Astronomically forced teleconnection between Paratethyan and Mediterranean sediments during the Middle and Late Miocene Palaeogeogr. Palaeoclimatol. Palaeoecol. 275, 1–13.

Lockwood, M., 2099. Solar Change and Climate: an update in the light of the current exceptional solar minimum. Proceedings of the Royal Society A, doi 10.1098/rspa.2009.0519.

Lozano-García, Md.S., Ortega-Guerrero, B., 1994. Palynological and magnetic susceptibility records of Lake Calco, central Mexico. Palaeogeogr. Palaeoclimatol. Palaeoecol. 109, 177–191.

Ma, L.H., 2009. Gleissberg cycle of solar activity over the last 7000 years. New Astronomy 14, 1–3.

Ma, L.H., Vaquero, J.M., 2009. Is the Suess cycle present in historical naked-eye observations of sunspots? New Astronomy 14, 307–310.

Magyar, I., Geary, D.H., Müller, P., 1999. Paleogeographic evolution of the Late Miocene Lake Pannon in Central Europe. Palaeogeogr. Palaeoclimatol. Palaeoecol. 147, 151–167.

Milana, J.P., Lopez, S., 1998. Solar cycles recorded in Carboniferous glacimarine rhythmites (Western Argentina): relationships between climate and sedimentary environment. Palaeogeogr. Palaeoclimatol. Palaeoecol. 144, 37–63.

Mörner, N.-A., 2010. Solar Minima, Earth's rotation and Little Ice Ages in the past and in the future. The North Atlantic-European case. Global and Planetary Change 72, 282–293.

Nederbragt, A.J., Thurow, J., 2005. Geographic coherence of millenial-scale climate cycles during the Holocene. Palaeogeogr. Palaeoclimatol. Palaeoecol. 221, 313–324.

Ogurtsov, M.G., Nagovitsyn, Y.A., Kocharov, G.E., Jungner, H., 2002. Long-period cycles of the sun's activity recorded in direct solar data and proxies. Sol. Phys. 211, 371–394.

Paillard, D., Labeyrie, L., Yiou, P., 1996. Macintosh program performs timeseries analysis. Trans. American Geophys. Union 77, 379.

Paulissen, W.E., Luthi, S.M., Grunert, P., Ćorić, S., Harzhauser, M., 2011. Integrated high-resolution stratigraphy of a Middle to Late Miocene sedimentary sequence in the central part of the Vienna Basin. Geologica Carpathica 62, 155–169.

Perisykh, A.-N., Damon, P.E., 2003. Persistence of the Gleissberg 88-solar cycle over the last 12,000 years: Evidence from cosmogenic isotopes. J. Geophys. Res. 108, 1003, doi:10.1029/2002JA009390.

Raspopov, O.M., Dergachev, V.A., Kuzmin, A.V., Kozyreva, O.V., Ogurtsov, M.G., Kolström, T., Lopatin, E., 2007. Regional tropospheric responses to long-term solar activity variations. Adv. Space Res. 40, 1167–1172.

Piller, W.E., Harzhauser, M., Mandic, O., 2007. Miocene Central Paratethys stratigraohy - current status and further directions. Stratigraphy 4 (2/3), 71–88.

Raspopov, O.M., Dergachev, V.A., Esper, J., Kozyreva, O.V., Frank, D., Ogursov, M., Kolström, T., Shao, X., 2008. The influence of the de Vries (~200-year) solar cycle on climate variations: Results from the Central Asian Mountains and their global link. Palaeogeogr. Palaeoclimatol. Palaeoecol. 259, 6–16.

Roberts, A.P., Chang, L., Rowan, C.J., Horng, C.-S., Florindo, F., 2011. Magnetic properties of sedimentary greigite (Fe3S4): An update. Rev. Geophys. 49, RG1002.

Robock, A., 1979. The "Little Ice Age": Northern Hemisphere average observations and model calculations. Science 206, 1402–1404.

Schimmelmann, A., Lange, C.B., Meggers, B.J., 2003. Palaeiclimatic and archaeological evidence for a ~200-yr recurrence of floods and droughts linking Calidornia, Mesoamerica and South America over the past 2000 years. The Holocene 13, 763–778.

Schulz, M., Mudelsee, M., 2002. REDFIT: estimating red-noise spectra directly from unevenly spaced paleoclimatic time series. Comput. Geosci. 28, 421–426.

Schwabe, H., 1844. Sonnen-Beobachtungen im Jahre 1843. Astronomische Nachrichten 495, 233–236.

Solanki, S.K., Usoskin, I.G., Kromber, B., Schüssler, M., Beer, J., 2004. Unusual activity of the Sun during recent decades compared to the previous 11,000 years. Nature 431, 1084–1087.

Stockhausen, H., Thouveny, N., 1999. Rock-magnetic properties of Eemian maar lake sediments from Massif Central, France: a climatic signature? Earth Planet. Sci. Lett. 173, 299–313.

Stuiver, M., Braziunas, T.F., 1989. Atmospheric 14C and century-scale solar oscillations. Nature 338, 405–408.

Stuiver, M., Braziunas, T.F., 1993. Sun, Ocean, Climate and Atmospheric $^{14}CO_2$, an evaluation of causal and spectral relationships. The Holocene 3, 289–305.

Stuiver, M., Grootes, P.M., Braziunas, T.F., 1995. The GISP2 $\delta^{18}O$ record of the past 16,500 years and the role of the sun, ocean and volcanoes. Quatern. Res. 44, 341–354.

Taricco, C., Ghil, M., Alessio, S., Vivaldo, G., 2009. Two Millenia of climate variability in the Central Mediterranean. Climate of the Past 5, 171–181.

Tiwari, M., Ramesh, R., 2007. Solar variability in the past and palaeoclimate data pertaining to the southwest monsoon. Current Science 93, 477–487.

Usoskin, I.G., Solanki, S.K., Schüssler, M., Mursula, K., Alanko, K., 2003. A millennium scale sunspot number reconstruction: evidence for an unusually active Sun since the 1940s. Phys. Rev. Lett. 91, 211101.

Vasiliev, I., de Leeuw, A., Filipescu, S., Krijgsman, W., Kuiper, K., Stoica, M., Briceag, A., 2010. The age of the Sarmatian-Pannonian transition in the Transylvanian Basin (Central Paratethys). Palaeogeogr. Palaeoclimatol. Palaeoecol. 297, 54–69.

Versteegh, G.J.M., 2005. Solar forcing of climate. 2: Evidence from the past. Space Sci. Rev. 120, 243–286.

Vos, H., Sanchez, A., Zolitschka, B., Brauer, Negendank, J.F.W., 1997. Solar activity cariations recorded in varved sediments from the crater lake of Holzmaar – a maar lake in the Westeifel volcanic firled, Germany. Surveys in Geophysics 18, 163–182.

Wagner, G., Beer, J., Masarik, J., Muscheler, R., Kubik, P.W., Mende, W., Laj, C., Raisbeck, G.M., Yiou, F., 2001. Presence of the solar de Vries cycle (~205 years) during the last ice age. Geophys. Res. Lett. 28, 303–306.

Warrier, A.K., Shankar, R., 2009. Geochemical evidence for the use of magnetic susceptibility as a paleorainfall proxy in the tropics. Chem. Geol. 265, 553–562.

Weber, M.E., Tougiannidis, N., Kleineder, M., Bertram, N., Ricken, W., Rolf, C., Reinsch, T., Antiniadis, P., 2010. Lacustrine sediments document millennial-scale climate variability in northern Greece prior to the onset of the northern hemisphere glaciation. Palaeogeogr. Palaeoclimatol. Palaeoecol. 291, 360–370.

Weedon, G., 2003. Time-Series Analysis and Cyclostratigraphy - Examining stratigraphic records of environmental cycles. Cambridge Univ. Press, Cambridge.

Wolf, R., 1862. Astronomische Mitteilungen Zürich 14.

Xapsos, M.A., Burke, E.A., 2009. Evidence of 6,000-year periodicity in reconstructed sunspot numbers. Sol. Phys. 257, 363–369.

Yin, Z.Q., Ma, L.H., Han, Y.B., Han, Y.G., 2007. Long-term variations of solar activity. Chin. Sci. Bull. 52, 2737–2741.

Yousef, S.M., 2006. 80–120 yr Long-term solar induced effects in the earth, past and predictions. Phys. Chem. Earth 31, 113–122.

Zuschin, M., Hohenegger, J., 1998. Subtropical Coral-reef associated sedimentary facies characterized by mollusks (Northern Bay of Safaga, Red Sea, Egypt). Facies 38, 229–254.

Chapter 5

High resolution analysis of Upper Miocene lake deposits suggests the influence of Gleissberg-band-solar forcing

Andrea K. Kern[1*], Mathias Harzhauser[1], Ali Soliman[2,3], Werner E. Piller[2], Oleg Mandic[1]

[1] Natural History Museum Vienna, Geological-Paleontological Department, Burgring 7, 1010 Vienna, Austria; e-mail: andrea.kern@nhm-wien.ac.at

[2] University of Graz, Institute of Earth Sciences, Heinrichstrasse 26, 8010 Graz, Austria

[3] Tanta University, Faculty of Sciences, Geology Department, Tanta 31527, Egypt.

*corresponding author

Abstract

A high-resolution multi-proxy analysis was conducted on a 1.5-m-long core of Tortonian age (~10.5 Ma; Late Miocene) from Austria (Europe). The lake sediments were studied with a 1-cm-resolution to detect all small-scale environmental variations based on palynomorphs (pollen and dinoflagellate cysts), ostracod abundance, geochemistry (carbon and sulfur) and geophysics (magnetic susceptibility and natural gamma radiation). Based on an already established age model for a longer interval of the same core, the study covers about two millennia of Late Miocene time with a resolution of ~13.7 years per sample.

No major ecological turnovers are expected in respect to this very short interval. Thus, the pollen record suggests rather stable wetland vegetation with a forested hinterland.

Shifts in the spectra can be mainly attributed to variations in transport mechanism, represented by few phases of fluvial input but mainly by changes in wind intensity and probably also wind direction. Even within this short time span, dinoflagellates document rapid changes between oligotrophic and eutrophic conditions, which are frequently coupled with lake stratification and dysoxic bottom waters. These phases prevented ostracods and molluscs from settling and fostered the activity of sulfur bacteria.

Several of the studied proxies reveal iterative patterns. To compare and detect these repetitive signals REDFIT spectra were generated and Gaussian filters were applied. Significant peaks cluster in three discrete intervals corresponding roughly to 123–114, 82–67 and 55–48 years with mean values of 115, 75 and 51 years for each group. These values range well within the expected ranges of the lower and upper Gleissberg cycles. Thus, solar forcing may have influenced the prevailing wind patterns, leading to a change in source area for the input into the lake. Moreover, the filtered data display comparable patterns and

modulations, which seem to be forced by the 1000-years and 1500-years-cycles. The 1000-years-cycle modulated especially the lake surface proxies, whilst the 1500-years-cycle is mainly reflected in hinterland proxies, indicating strong influence on transport mechanisms.

Keywords: high-resolution analysis, solar cycles, palynomorphs, Lake Pannon, Miocene.

5.1. Introduction

Reliable documentations of high frequency climate behavior, such as fluctuations in temperature or rainfall, reach back several hundred years only (Charatova, 2000; Versteegh, 2005). This is obviously too short to allow convincing interpretations of the natural variations of climatic systems. Thus, high resolution archives from the geological record may serve as additional source of information. Especially in Holocene records resolutions on decadal scales are frequently achieved. Many of these suggest repetitive climate shifts, which are strikingly similar to known variances of solar activity (e.g. Patterson et al., 2004; Versteegh, 2005; Grey et al., 2010). Typically, the 11-years Schwabe-cycle, the 22-years Hale-cycle, the 50–80-years lower Gleissberg cycle, the 90–120-years upper Gleissberg cycle, the ~210 Suess/de Vries cycle, and the 2200-2300 Hallstatt cycle along with the unnamed 500 and 1000-years cycles are discussed to have influenced the Holocene climate records (see Kern et al. 2012a for extensive discussion and references). Aside from the better understood 11-year sunspot-cycle and the 22-year Hale-cycle, the origin of other cyclic variations in sun's emitted energy is still unsolved (Versteegh, 2005). The sun's spin rate, the rotation of the sun or the strength of solar winds are discussed as explanations for longer time variations, but no studies are conclusive (Tsiropoula, 2003). Nevertheless, all of the proposed longer solar cycles have been documented globally from various geochemical and sedimentological archives (Sonett and Suess, 1984; Raspopov et al., 2004). The expression and modulation of these cycles vary strongly in their local imprint (Hoyt and Schatten, 1997; 1998) and also different responses on both hemispheres to the same cycle have been noted (Li et al., 2001; Claud et al., 2008). This documents that the detection of the signals in the geochemical and sedimentological archives is comparatively easy while their explanation is not.

Comparable studies for the Miocene are still scarce. Whereas the overall Neogene climatic history is well studied (e.g. Zachos et al., 2001; Utescher et al., 2000; 2009), small scale shifts and short periods encompassing few thousands of years are usually unresolved. During the last years, however, several high resolution studies were conducted on Late Miocene sediments of Lake Pannon (Harzhauser et al., 2008; Gross et al., 2011; Kern et al. 2012a; 2012b). All these studies were able to detect high frequency fluctuations of the paleo-environment of that lake on a decadal scale. Gross et al. (2011) and Kern et al. (2012a), by

using longer records, documented various repetitive patterns, which could be linked to known periods of solar cycles. In addition, Kern et al. (2012a) showed that different proxies, such as magnetic susceptibility, natural gamma radiation and total abundance of ostracods, reflected the different cycles in different intensity (Fig. 5.1). A causal link between these observed changes of the environmental conditions, as expressed by the proxy data and the suggested solar forcing was not discussed so far. Therefore, to elucidate the interaction between environments, climate and the presumed solar cycles, we conducted a further study, which is based on the data presented in Kern et al. (2012a) and new data on pollen, dinoflagellates, molluscs, total carbon (TC), total organic carbon (TOC), and total sulfur (TS).
These proxy-data give information on the vegetation surrounding the lake (pollen), on the surface water productivity (dinoflagellates), the lake bottom conditions and overall sediment input (ostracods, molluscs, magnetic susceptibility, natural gamma radiation, TC, TOC, TS).

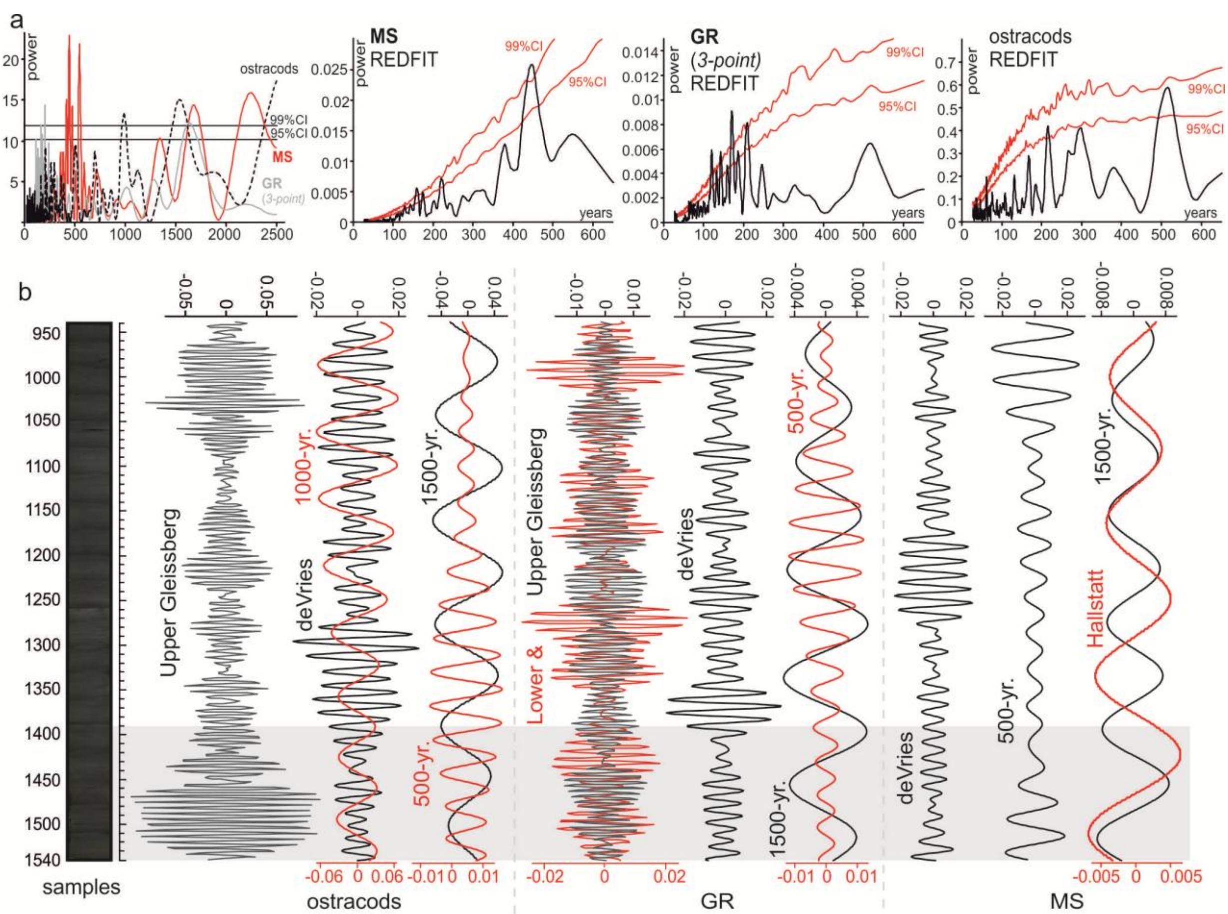

Fig. 5.1. A summary of the assumed solar cycles in the 6-m-long Hennersdorf core from Kern et al. (2012a). a: combined Lomb-Scargle periodograms of MS (magnetic susceptibility; red), GR (natural gamma radiation; gray) and the total abundance of ostracods (dashed) and REDFIT spectra. b: filtered records based on dominant frequencies as revealed by spectral analysis (modified from Kern et al. 2012a). The shaded area indicates the herein analysed interval.

5.2. Geological Setting

The Late Miocene to Pliocene Lake Pannon covered the Pannonian Basin complex (Fig. 5.2) in central and south-eastern Europe. It formed at c. 11.6 Ma when the marine Paratethys Sea retreated to the east. The remaining lake was a brackish and slightly alkaline lacustrine system (Magyar et al., 1999; Harzhauser et al., 2004; Piller et al., 2007; Harzhauser and Mandic, 2008). During the herein discussed phase at c. 10.5–10.4 Ma, Lake Pannon experienced its maximum extension (Fig. 5.2d) and deep basins with dysoxic conditions established. At that time, pelitic deposits of the Bzenec Formation were deposited in the entire Vienna Basin (Harzhauser et al., 2004).

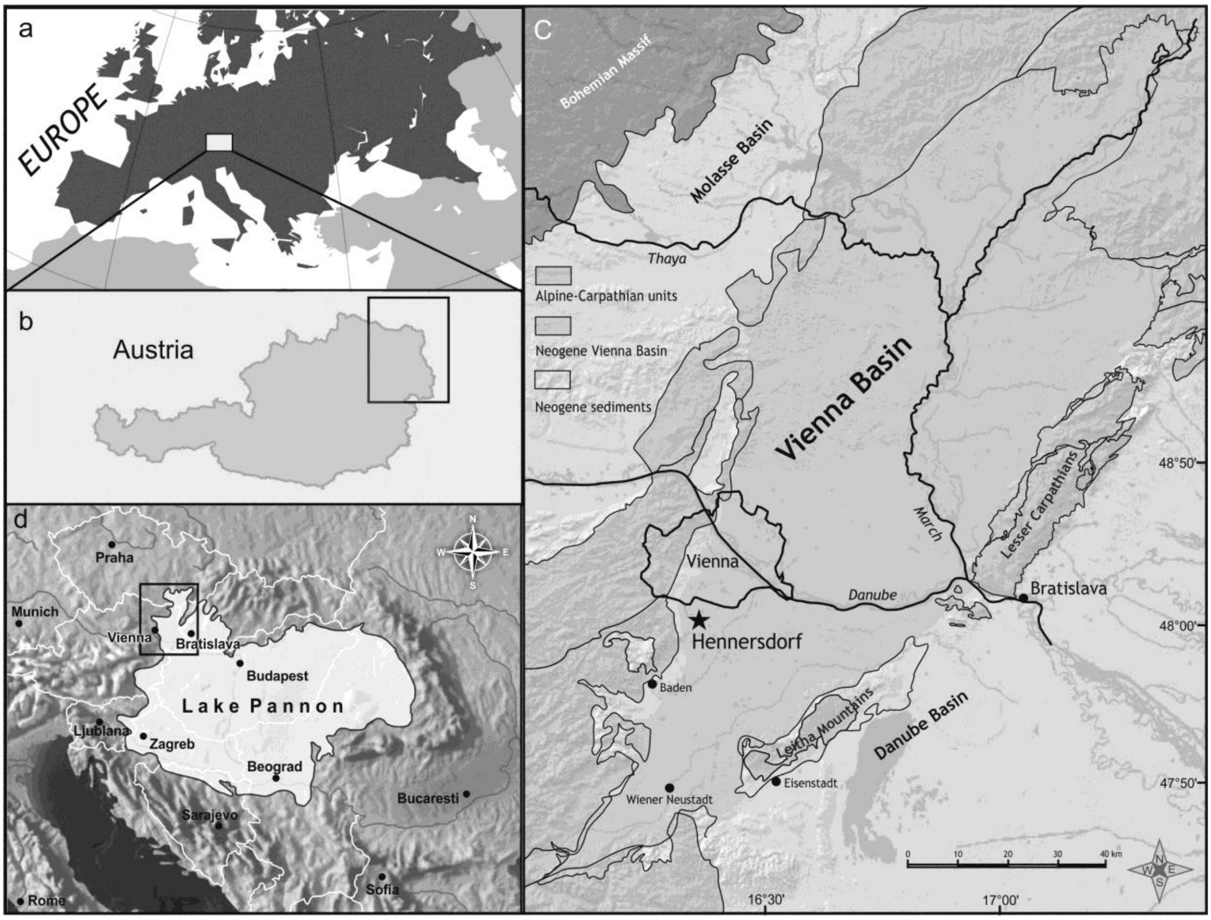

Fig. 5.2. Map showing the study area in central Europe (a) and Austria (b). The outline of the Vienna basin is presented in insert c and the drilling site is marked by an asterisk. Insert d shows the position of insert c based on a palaeographic map of Lake Pannon at ~10.5 Ma (modified from Magyar et al. 1999 and Harzhauser and Mandic 2008).

The studied core was taken at the clay pit Hennersdorf (Fig. 5.2c) app. 10 km south of the center of Vienna in the Vienna Basin (N48°05'52.6'' - E016°21'15.8''). There, more than 20 m of dark-grey to greenish clay and silt of the Bzenec Formation crop out. Its mollusc fauna is indicative for the regional middle Pannonian stage, corresponding to the middle Tortonian (Magyar et al., 1999), which is further supported by magnetostratigraphy (chron C5n, Magyar et al., 1999). The succession can be correlated with astronomically tuned well-logs in the

Vienna Basin, suggesting an absolute age of c. 10.5–10.4 Ma (Harzhauser et al., 2004; Lirer et al., 2009). A first study by Kern et al. (2012a) was conducted on a continuous 6-m-long core with homogenous sedimentology. Occasionally scattered plant debris and autochthonous mollusc coquinas were occurring while bioturbation is exceptionally rare. Kern et al. (2012a) documented a rather constant sedimentation rate ranging around 0.73 mm/yr for this part of the drilling. This corresponds to a hypothetical time resolution of 13.7 years per centimeter which represents the sample density. More detailed information on the lithology, paleontology and biostratigraphy of the Hennersdorf section was already published by Harzhauser and Mandic (2004), Harzhauser et al. (2008) and Kern et al. (2012a).

5.3. Methods

In November 2009 several consecutive cores with a diameter of 15 cm were drilled, reaching a depth of 15.4 m. The lowermost part was taken without core-break and is the most uniform part in respect to lithology. Therefore, further analyses concentrated on this deepest segment (see Kern et al. 2012a for details and sampling protocol). After cutting the core into two halves, geophysical measurements were conducted in a strict 1-cm-sample-interval including natural gamma radiation (GR) with a hand held Scintillation Gamma Radiameter and magnetic susceptibility (MS) with a “SM-20” magnetic susceptibility meter with a sensitivity of 10^{-6} SI units (GF Instruments, Brno, Czech Republic). Afterwards, the core was cut into slices, following the same 1-cm-sampling protocol, and immediately separated for the different analyses (palynology, ostracods, molluscs and geochemistry). Ostracod samples were dried, weighed and treated with H_2O_2 before sieving with 125, 250 and 500 µm mesh-size sieves. The total number of ostracod valves was evaluated first, before data were standardized for a sample weight of 100 gram (Table 5.1). For statistical analyses, these data were log-transformed. Molluscs were picked from the samples as well. As the shells were fragmented during washing, no individual numbers can be counted. Therefore, the abundance of molluscs was evaluated by using semi-quantitative categories: 0 = no fragments at all, 1 = rare fragments, 2 = frequent shell fragments, 3 = coquina layers with numerous fragments.

The geochemistry was measured by a Leco CS-300 elemental analyzer at the University of Graz, detecting total sulfur (TS), total carbon (TC) and total organic carbon (TOC, after acidification of samples to remove carbonate). The difference between TC and TOC is the total inorganic carbon content (TIC), which was used to calculate calcium carbonate equivalent percentages (c-equi = 8.34*TIC).

Preparation of the palynological samples (pollen grains, spores and dinoflagellate cysts) followed the steps of Green (2001) and Wood et al. (1996). Each sample was dried, weighed and one *Lycopodium clavatum* tablet was added to calculate the absolute number of pollen and dinoflagellate cysts. Then it was treated with cold HCl (34%) to remove all carbonate. After washing with distilled water, each sample was treated with HF (48%) and cold HCl to fully remove all silicates and colloids. The residue was ultrasonicated (c. 15–30 seconds) and colored with Safranine O., before it was sieved at 15 µm with a nylon sieve. In each sample, at least the first c. 250 dinoflagellate cysts and 200 pollen grains (excluding *Pinus*) were identified. Palynological counting was first transferred to percentages before an arcsin-root transformation was applied for further statistics (Linder and Berchtold, 1976; Zuschin and Hohenegger, 1998). For the pollen, a standard Tilia diagram was created (Grimm, 2004). To generate a paleoclimate estimate, the Coexistence Approach was used (Mosbrugger and Utescher, 1997). The method applies the natural distribution of the nearest living relatives of each taxon occurring in the fossil assemblage, and transfers these to a possible climatic interval, in which all of these Miocene plants could survive today. This climatic range is called the Coexistence Interval and resembles the most likely prevailing climatic conditions. Since far transported pollen grains as well as pollen grains of species with a recent distribution strongly influenced by human activity, may not characterize the natural distribution nor the paleo-situation, these taxa were excluded from the list before the method was applied (e.g. *Pinus*, *Abies*, *Picea*, *Cathaya* etc.). All details are summarized in Table 5.2.

To detect and describe cyclicities a combination of the software PAST (Hammer et al., 2001) for REDFIT analysis (Schulz and Mudelsee, 2002) and the software AnalySeries (Paillard et al., 1996) for filtering were used. REDFIT originally allows overcoming the common problem in paleontology of unevenly spaced time series by fitting a first-order autoregressive process. Even though sample distance is strictly consistent, due to lithologically unnoticeable slight changes in sedimentation rate, imbalances within the sampling distances might occur. Further, it allows reducing red noise by using segmentations and oversamples to fit each curve to a noise model. Monte-Carlo method is applied to test a bias-corrected spectrum. Only peaks above the 95% confidence interval in the REDFIT spectrum are considered. The age model and the sample numbering follow Kern et al. (2012a).

5.4. Results

5.4.1. Pollen

A pollen diagram was generated showing the most common plant taxa and a pollen zonation is proposed based on cluster analysis (Fig. 5.3). The diversity of the pollen assemblage is rather low, ranging from 13 to 34 taxa with a mean of 19.8 (Fig. 5.4; Table 5.1). Moreover, the diversity is decreasing from the bottom of the core (1540) to the top, but the gradient becomes less steep above sample 1490. The pollen number per gram sediment, based on

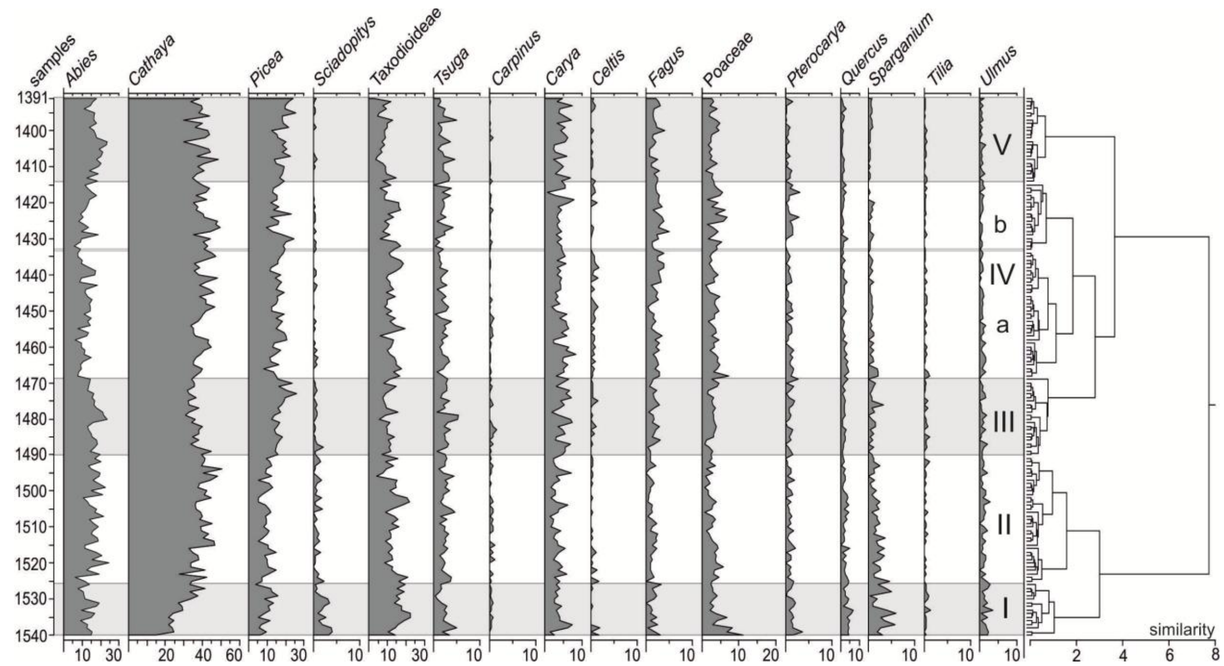

Fig. 5.3. Pollen-diagram generated with the Tilia program (Grimm, 2004) showing the most common taxa and a pollen zonation based on CONISS.

the *Lycopidum clavatum* counts, is basically high with one exceptional peak of 97,880 in sample 1500 and never falls below 12,300. The values increase moderately from bottom to sample 1500 and pass into a strongly fluctuating interval up to sample 1476. This interval shows no trend and has a mean of c. 40,700 pollen/gram. Subsequently, values drop distinctly starting from sample 1476 and display an overall decreasing trend with very low values of 14,000–16,000 pollen/gram c. up to sample 1420. Afterwards the number increases slowly again. The pollen/gram record has no correlation with the pollen diversity curve. Both lack a significant correlation with the dinoflagellates/gram record. This suggests that most of the data are not taphonomically biased, which would affect all palynomorphs.
As *Pinus* accounts up to 50% of the whole pollen spectra (Fig. 5.4), it was excluded from further analysis. The decrease in pollen diversity coincides with an increase in the number of gymnosperms (excluding *Pinus*). Starting from 60%, the values reach up to c. 90% in samples 1491 and 1405 (Fig. 5.4; Table 5.1). Among the remaining bisaccate gymnosperms, *Cathaya* is most abundant with values of almost 50% and a mean of 38.2% (Fig. 5.3; Table 5.1). *Picea* and *Abies* attain lower mean values of 14.4% and 14.6%. *Picea* displays three peaks with 25%, which slightly exceed the three *Abies* peaks. Despite the comparable values, all three Pinaceae records have different patterns (Fig. 5.3). *Cathaya* strongly increases from sample 1540 up to sample 1494 (50.6%), before it slightly drops to 31% up to sample 1472. Afterwards, the *Cathaya* record varies strongly with positive and negative peaks between 50 and 30%. *Abies* and *Picea*, in contrast, start with rather stable values and peak later at sample 1480 (21%) and 1473 (26%). *Picea* values shortly drop down to less

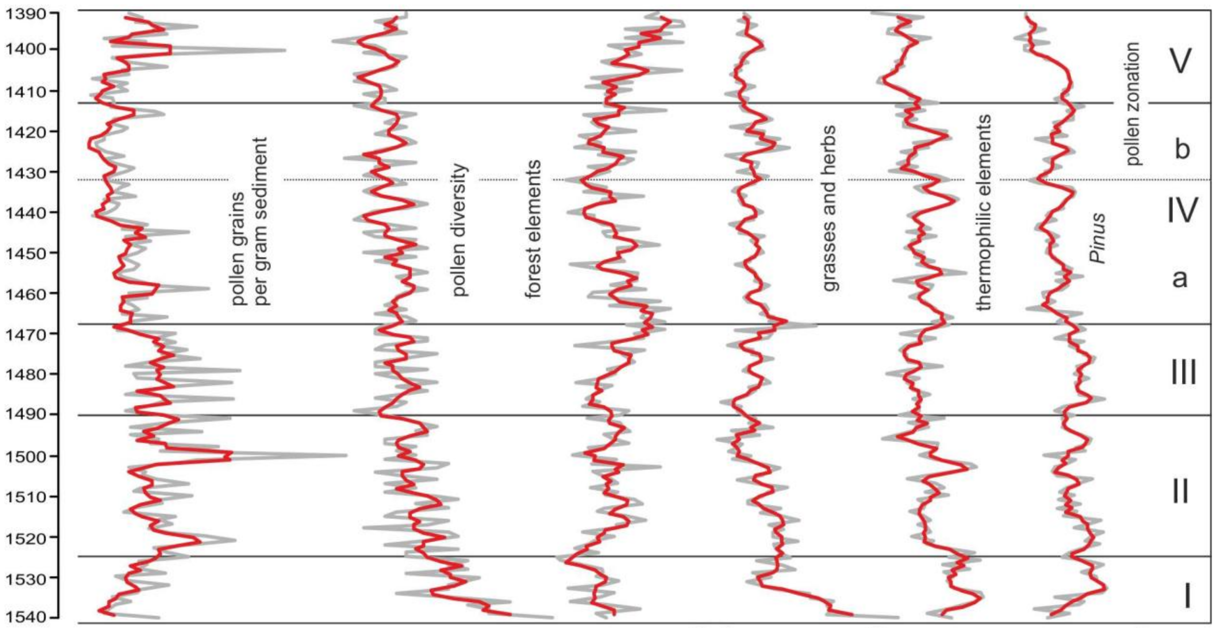

Fig. 5.4. Diagrams showing the amount of pollen per gram sediment (counts), pollen diversity (taxa), forest elements (%), gasses and herbs (%), thermophilic elements (%) and Pinus (%) in relation to the pollen zonation. Grey lines represent raw data, red lines show the 3-point-mean.

than 10%, before they increase slowly up to sample 1430 (24.4%), followed by an interval without significant trend. *Abies* decreases also down to values around 7.6%, followed by a slight increase to values between 10 and 15%, with a negative peak at sample 1432 (5.6%). A strong rise up to 18% afterwards is followed again by a short decrease down to 10%. In the top of the sequence, the abundance of *Abies* is increasing similarly to *Picea*, but displays a decreasing trend after sample 1403 (23.7%).

The rather rare angiosperms were grouped according to their ecology into hinterland forest and grasses/herbs (comparable to Jimenez-Moreno, 2006; Jimenez-Moreno and Suc, 2007; Kover-Eder et al., 2006; Table 5.1; Fig. 5.4).

The hinterland forest plants are more abundant, ranging from 5.9% to 19.3% with their highest values in the lower part (1540 to 1525) and in the middle (1469 to 1460), opposed by one negative peak at sample 1405 (5.9%). They start with a negative trend up to sample 1525; the interval up to sample 1432 is characterized by high values with two phases with several positive peaks (1503–1516, 1477–1455) and a decline afterwards up to sample 1432, which marks the turning point to overall increasing values (Fig. 5.4). Grasses/herbs start with values of almost 19% and sharply decrease to 3.9% at sample 1531. Afterwards follows a slight recovery up to sample 1528 (8.7%) and a second but less steep negative trend up to sample 1500. Rather low values without marked trend follow upsection, interrupted only at sample 1468, when grasses and herbs attain 10.8% of the spectrum (Fig. 5.4).

5.4.2. Dinoflagellate cysts

The diversity of dinoflagellate cysts is low in all samples; in total 17 different taxa were identified (Fig. 5.5; Table 5.1). The most abundant is *Spiniferites* with values up to 60%. Five different species are identified within this genus: *Spiniferites delicatus* is the most common one, frequently accounting for more than 10% of the assemblages and with a single peak topping 32% in sample 1479. All other *Spiniferites* species range below 5% with mean-values of less than 1.5% (Table 5.1). The second most frequent element is *Impagidinium* spp. with maxima of 36.7% and a mean of 20.7%. *Impagidinium sphaericum* ranges from 2–18.3% (mean 7.8%). Among the remaining taxa, especially the Protoperidinioid cysts A and Round Brown Cysts are most common with a mean of 33.7% and maxima of 18.0%, respectively. *Pyxidinopsis psilata* and *Selenopemphix sp.* are also constantly present with a mean of 2.8% and 2.2%.

Spiniferites values display a decreasing trend up to sample 1515. This is followed by a strongly fluctuating overall increase up to sample 1470 attaining a peak value of 55.7%. During the following six samples, a strong break down to 29.3% occurs. Upsection, a constant increasing trend follows peaking at sample 1443 (55.5%), followed by overall constant values around 45% until sample 1433. A short phase of low values around 35% up to sample 1428 is opposed by the highest peak at sample 1426 (60.6%). Another phase of low values up to sample 1412 is finally topped by a slight increase to values around 40% (Fig. 5.5). *Impagidinium* spp. starts with slightly increasing values, peaking at sample 1508 with 48%. At sample 1504, values crash down to 18% and drop to 15.4% in sample 1492 after a short recovery phase. Afterwards it is represented in samples constantly varying

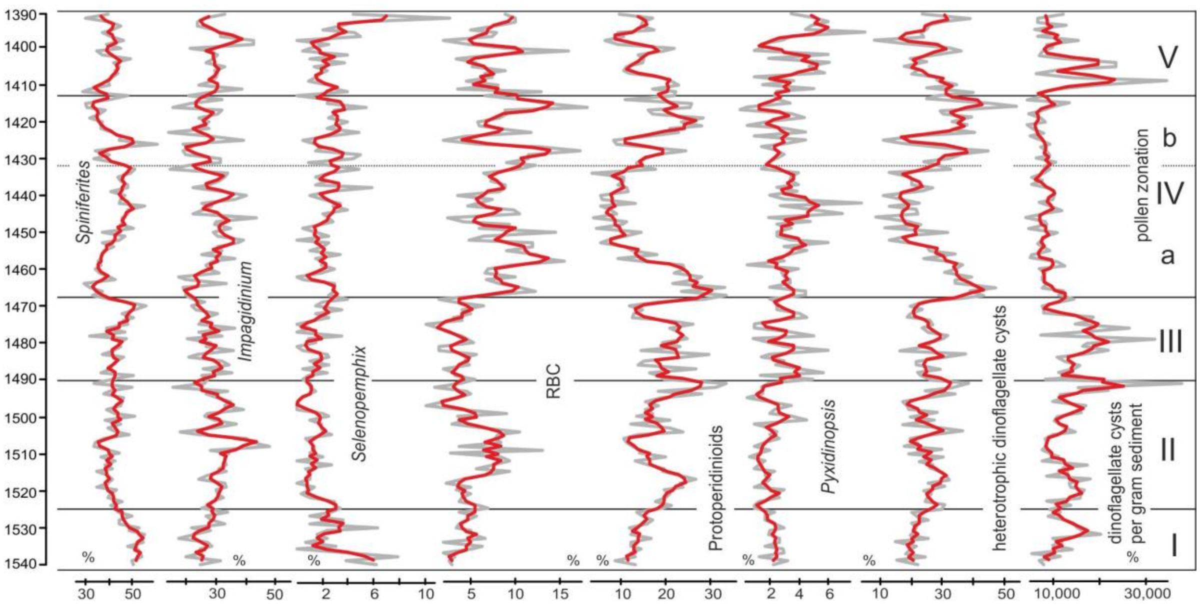

Fig.5.5. The six most important dinoflagellate cyst taxa (RBC = Round Brown Cycsts), the total heterotrophic dinoflagellates and the amount of cysts per gram sediment in relation to the pollen zonation. Grey lines represent raw data, red lines show the 3-point-mean.

between 20% to almost 40%. At sample 1462, values increase again to a peak at sample 1446 (43.3%). Upsection, another phase of strongly fluctuating values follows indicating a slight decreasing trend up to sample 1426 and an increase in abundance thereafter. A clearer trend is expressed by the Protoperidinioid cysts A (Fig. 5.5). Its values increase constantly from samples 1540 to 1517, peaking with the highest value of 26.7%. This trend is interrupted by a short break down phase to 11.6% at sample 1506, before the increasing trend is re-established peaking at sample 1491 with 33.4%. Values are decreasing inconstantly into a low phase of c. 12% from samples 1473 to 1470. This is followed by peak values of more than 30% around samples 1467 to 1465. Afterwards, the Protoperidinioid cysts A assemblage decreases considerably down to 3.4% (samples 1453–1535) and terminates with strongly fluctuating values.

5.4.3. Ostracod and mollusc abundance

We use the total amount of ostracods and the presence of autochthonous mollusc populations as rough estimates for bottom water conditions; for a discussion on the species and genera constituting the assemblage see Harzhauser and Mandic (2004) and Harzhauser et al. (2008). Within the studied core interval, the maximum abundance of ostracods/100 gram sediment is observed from sample 1540 to 1525 (Table 5.1; Fig. 5.6). Afterwards the assemblages break down nearly completely up to sample 1513, followed by a phase of strongly fluctuating values ranging from 10 to almost 300 specimens with a low phase of less than 60 ostracods between samples 1414 and 1400.

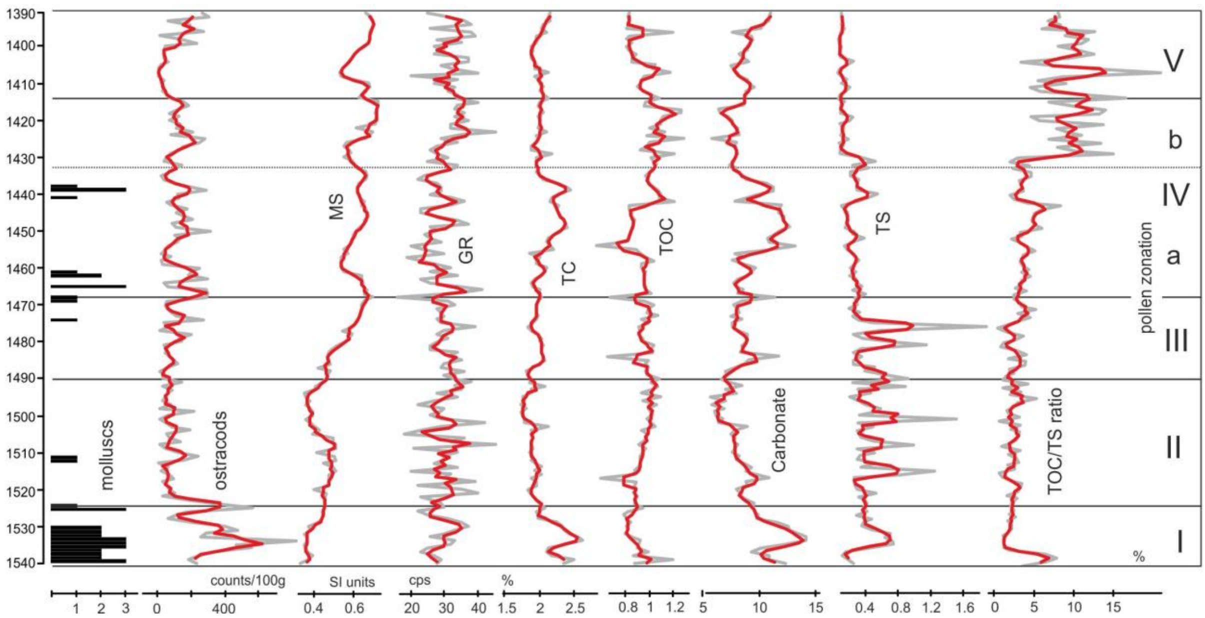

Fig. 5.6. Paleozoological, geophysical and geochemical proxies (MS = magnetic susceptibility, GR = natural gamma radiation, TC = total carbon, TOC = total organic carbon, TS = total sulfur). Grey lines represent raw data, red lines show the 3-point-mean.

5.4.4. Geochemistry

The total sulfur record (TS) displays an overall decreasing trend with higher values up to sample 1475 and depleted values thereafter (Table 5.1; Fig. 5.6). The lower part of the core up to sample 1475 has strongly fluctuating values around a mean of 0.47% with several prominent peaks of more than 0.8%. Above follows a phase with low fluctuations and a constant decline to low values around 0.2% up to sample 1443. These depleted values continue up to the top of the core, interrupted only by a short interval of slightly higher values from sample 1443 to 1430.

TC: total carbon values show variations ranging between 1.75 and 2.6% (Table 5.1; Fig. 5.6). The lower part of the core up to sample 1530 is characterized by high values with peaks of 2.5 and 2.6% in samples 1539 and 1534. Afterwards follows an interval up to sample 1457 with moderate values fluctuating around 2% with a phase of very low values around 1.7% around sample 1500 and slight increasing trend afterwards. Elevated values occur in an interval from sample 1455 to 1438 to be followed again by phase of moderately fluctuating values ranging around 2%.

TOC: the total organic carbon record is twofold: the lower part reaches from the bottom up to sample 1444 (Table 5.1; Fig. 5.6). This part is characterized by an overall mean of 0.92%, separated by moderately increasing values up to sample 1490 and a slight decrease afterwards. Four prominent negative peaks interrupt this record at samples 1517 (0.6%), 1484 (0.64%), 1468 (0.68%) and 1454 (0.56%). The upper part of the TOC record has comparatively higher values with a mean of 1.0%, starting with a strong increase in values at sample 1442.

Carbonate: the trend is roughly comparable to the TC record as the carbonate equivalent is calculated based on TC and TOC values (Table 5.1; Fig. 5.6). Comparable to the TC record, an initial phase with high values up to sample 1530 is followed by a constant decrease, which culminates in low values around sample 1500, followed by a slow but constant increasing trend with positive peaks at samples 1484 (11.7%) and 1468 (11.3%). An interval with very high values around 1% occurs up to sample 1435 ending with an abrupt decrease and a constant rise up to the top afterwards.

TOC/TS ratio: the ratio starts with an initial peak of 7.8% within the first 5 samples and remains at low levels of c. 3% up to sample 1495, when the values display a moderate increase with several peaks up to almost 5%. Around sample 1473 the values increase further, interrupted by a short phase of low values from sample 1440–1431. Afterwards, the ratio displays an overall shift towards higher values with maxima of 20% and an average of 10%.

5.4.5. Geophysics

The natural gamma radiation (GR) of the 6-m-long Hennersdorf core was already discussed by Kern et al. (2012a). The shorter herein studied part is characterized by a strongly fluctuating record (Table 5.1; Fig. 5.6) with increasing amplitudes up the interval between samples 1520 and 1500. An interval with low amplitude fluctuations reaches up to the interval around sample 1470, where strong positive and negative peaks occur. A phase of moderate fluctuations follows and stretches up to sample 1425 to pass quickly into a last interval with elevated and strongly fluctuating values.

As shown by Kern et al. (2012a) the magnetic susceptibility record (MS) lacks the high-frequency oscillations of the GR-record. The magnetic susceptibility shows a trend of increasing values towards the top of the section from 0.3 to 0.6–0.7 SI units with a low frequency fluctuation. The strongest increase of values occurs between samples 1495 and 1470. Other fluctuations are minor (Table 5.1; Fig. 5.6).

5.5. Discussion

5.5.1. General paleoclimate

32 taxa of the total assemblage are used for the Coexistence Analysis (Table 5.2). The results suggest a mean annual temperature (MAT) between 15.6 and 20.8°C with a cold season clearly above the freezing level (5–13.3°C) and a warm season range from 24.7°C to 27.9°C. The mean annual precipitation (MAP) was high, varying from a low value of 823 up to 1529 mm, displaying a clear seasonality with a wet phase of 204–236 mm and a dry phase of 9–24 mm. As the warmest month rainfall ranges from 79–172 mm, the warmer season may have coincided with the wettest one. Thus, a clear seasonality was already established at this time with a cold and a warm and presumably wetter season. Rainfall and temperature suggest a subtropical or at least warm-temperate situation compared to today (e.g. Vienna – MAT 9.8°C and MAP 660 mm; Müller, 1996). The warm temperature and especially the winter temperature above 0°C is responsible for the presence of plants, which are nowadays typical for tropical and subtropical areas, such as Arecaceae, Sapotaceae, *Engelhardia* or Taxodioidae (Denk et al., 2001; Kvaček, 2007; Kunzmann et al., 2009). These data fully correspond to previous studies from other close by localities (Bruch et al. 2004; 2006; Jimenez-Moreno et al., 2008; Harzhauser et al., 2008).

5.5.2. Vegetation reconstruction

Due the low diversity within the pollen assemblages, only a rough picture of the Late Miocene vegetation surrounding Lake Pannon can be reconstructed. The lakeshore was probably fringed by a mixture of forested and non-forested wetland vegetation. There, different Poaceae and Cyperaceae species occurred, partly associated with *Sparganium* and *Typha*. Typical trees of this zone are Taxodioideae, such as *Taxodium* or *Glyptostrobus*, along with the less frequent *Nyssa* (e.g. Willard et al., 2001; Averyanov et al., 2009; Kunzmann et al., 2009; Lodge, 2010). Due to their high frequency in the spectra and the fact that their pollen grains are usually not transported over large distances (Smirnov et al., 1996), the presence of such lakeshore-associated wetlands is most likely, although some species of Taxodioideae may grow in non-swamp vegetation as well (Thompson et al., 1999). In some distance from the lakeshore, forests dominated the landscape. This part of the vegetation comprised mainly deciduous, broad-leaved type taxa (Kovar-Eder et al., 2008), with elements such as *Carya*, *Pterocarya*, *Quercus*, *Fagus*, *Carpinus* or *Ulmus*, together with some more warm-temperate plants such as Arecaceae and rare occurrences of *Symplocos* or Sapotaceae (e.g. Jarvis and Clay-Poole, 1992; Britten and Crivelli, 1993; Wilen and Tiner, 1993; Denk et al., 2001; Kovacova et al., 2011). Gymnosperms are most abundant in the pollen samples, which can be explained by their distribution mechanisms, which favor exceptional wide transport (Hopkins, 1950; Traverse and Ginsburg, 1966; Heusser and Balsam, 1977). *Pinus* is excluded here from any environmental reconstruction as it occurs today in very different vegetation zones and altitudes. Other Pinaceae, such as *Picea* and *Abies* may indicate elevated mountainous regions, such as the close by Alps (Fauquette et al., 1999; Jimenez-Moreno et al., 2008), which were located in less than 100 kilometers distance to the position of the drilled core (Magyar et al., 1999; Harzhauser et al., 2004; Harzhauser et al., 2008). Mid-altitudinal elements are represented by *Tsuga* and *Cathaya* (Jiminez-Moreno et al., 2008; Jimenez-Moreno, 2010), although their recent distribution is not restricted to such environments. This closed vegetation may have been interrupted by some more open areas, where Poaceae have dominated and rivers, flowing into the lake, transported a high number of riparian elements into the lake (e.g. *Salix*, *Fraxinus*, *Sparganium*/*Typha*) (Chmura and Liu, 1990; Denk et al., 2001). These vegetation belts correspond fully to the Tortonian vegetation surrounding Lake Pannon as described in several previous studies (e.g. Kover-Eder et al., 2002; 2006; Harzhauser et al., 2008; Jimenez-Moreno, 2008; Kovacova et al., 2011; Kern et al., 2012b).

5.5.3. Pollen zonation

No major turnover of the general vegetation type is indicated in our record (Fig. 5.3). This is no surprise in respect to the short time span of only two millennia covered by the core. Nevertheless, the contribution of certain taxa to the spectra changes considerably along the record. Therefore, a Tiliagraph cluster analysis (Grimm, 2004) revealed significant changes of sample composition resulting in a cluster-based zonation (Fig. 5.3). Since the pollen diversity and the pollen/gram sediment counts do not show any parallels (Fig. 5.4), shifts

within the pollen percentages are presumable not only expression of a preservation bias (except for subzone IVb, see below).
Zone I (Fig. 5.3–5.4) starts with a high presence of riparian elements, which strongly decline, reaching levels below 5% after sample 1526. However, the forested wetland vegetation, represented mainly by Taxodioideae, stayed intact. This coincidence strongly points towards a decrease of fluvial input, either caused by a decrease of water supply or a migration of the river mouth. This further leads to a decrease in pollen diversity as many taxa grow in the hinterland and reach the lake only by fluvial transport.
Zone II (Fig. 5.3–5.4) reaches up to sample 1490 and coincides with a continued decline of pollen diversity. The pollen supply from the hinterland forest and from the Taxodioideae wetlands is high, causing high pollen/gram sediment values. The vegetation composition was rather uniform including a high amount of altitudinal elements, such as *Abies*, *Cathaya* and *Tsuga* as well as rare gymnosperms. Single positive outliers in the pollen/gram ratio may represent events in certain years. Considering the overall rareness of riverine elements and the fact that the most abundant pollen are distributed by wind, these events could be interpreted as several strong wind events rather than as phases of increased runoff. The extreme peaks represent the highest pollen numbers. The average values, however are higher in pollen zone III.
Within zone III (Fig. 5.3–5.4), the overall diversity and the Taxodioideae vegetation stay rather constant. Although single elements, such as *Abies* and *Cathaya* become less abundant, the number of *Picea*, *Tsuga* the amount of hinterland forest vegetation (especially *Carya* and *Fagus*) and the Poaceae are strongly increasing. This shift in composition could indicate a slight change of the source area either due to a change of the dominant wind direction or by an increase of riverine influx, which fits to several small peaks in the *Sparganium*/*Typha* counts.
Zone IV (Fig. 5.3–5.4) is subdivided into 2 subzones, ranging from sample 1468 to 1433 and 1432 to 1414. Subzone IVa is characterized by high levels of *Picea*, *Cathaya* and Poaceae, while the pollen/gram counts, the amount of *Pinus* and the contribution by forest elements drop significantly in the base of the upper subzone. Low pollen diversity, low pollen/gram values and also very low dinoflagellates/gram values coincide here. Therefore, taphonomic bias might have influenced the record in this case. Especially between samples 1440 and 1430, the lowest pollen/gram sediment values and the lowest diversity values are observed. Even robust pollen, such as *Abies* or *Tsuga*, are decreasing in numbers. Nevertheless, close-by wetland indicating Taxodioideae remain abundant, which could also point towards less wind input during this phase in addition to the taphonomic signal. This is followed by the onset of subzone IVb and an increase in diversity and pollen/gram counts. Hinterland forest

elements and all Pinaceae and Poaceae are increasing again, showing a distinct contribution by far distance pollen input.
This trend persists into the pollen zone V (Fig. 5.3–5.4; samples 1413–1391). Forest elements, *Picea* and *Abies* and the pollen/gram sediment number are still strongly increasing. Pollen diversity remains rather stable, but percentages of the hinterland forest reach the highest values, which out compete the altitudinal plants. The low but stable appearances of *Sparganium*/*Typha* may again indicate some fluvial input.
Concluding, the pollen record suggests rather stable vegetation conditions around the lake during the observed time span. Variations in the pollen spectra are therefore interpreted only as shifts of pollen supply into the lake, mainly by changing wind conditions and/or runoff.

5.5.4. Surface water conditions deduced from dinoflagellate cysts
Indicators for the lake surface water conditions are dinoflagellate cysts (Fig. 5.5). For Lake Pannon deposits, this group is often difficult to interpret, due to the marine origin of Lake Pannon and the subsequent autochthonous evolution of its biota. Many of the genera are today typically found in open marine settings. Nevertheless, some Holocene counterparts are documented from the Black Sea, the Marmara Sea, the Caspian Sea or the Aral Sea, where several species became adapted to brackish water conditions (e.g. Kouli et al., 2001; Mudie et al., 2001; 2002; 2007; 2010; Marret et al., 2004; 2007; Leroy et al., 2007; Londeix et al., 2009; Leroy and Albay, 2010). Especially, the dominance of *Spiniferites*, as obvious in all samples, is also known from the modern Marmara Sea, where it may account for more than 80% of the dinoflagellates assemblages (Londeix et al., 2009). This high amount of *Spiniferites* was documented by Harzhauser et al. (2008) to have been established in Lake Pannon shortly after a major rise of the lake level. The turning point from coastal to “offshore” conditions, marked by increasing *Impagidinium* and *Spiniferites* values is recorded at the Hennersdorf section about 40–50 cm below sample 1540. The overall constantly high values of both taxa within our samples, thus, indicate a rather stable lake levels without major shifts (Fig. 5.5).
Another significant element is *Selenopemphix*, which is commonly found in river mouth settings (Patterson et al., 2005; Holzwarth et al., 2007). Especially, *S. nephroides* has an affinity to eutrophic coastal settings and zones of high productivity (Marret and Zonneveld, 2003; Sorrel et al., 2006). The distinctive drop of *Selenopemphix* up to sample 1500 might thus indicate a decrease in freshwater influx (Fig. 5.5). This decline is partly compensated by increasing but still low values of the “open-water” taxon *Impagidinium.* In Lake Pannon, a rise of *Impagidinium* was documented to frequently coincide with deepening events (Sluijs et al., 2005; Harzhauser et al., 2008; Kern et al., 2012b). However, the rather moderate increase in the Hennersdorf core, might rather point to a weakening of river inflow and thus

comparatively more oligotrophic conditions as also preferred by *Impagidinium* (Dale, 1996; Zonneveld, 1995). At this level (Fig. 5.5), the amount of heterotrophic dinoflagellates (Round Brown Cysts (RBC) and Protoperidinioid cysts A) is decreasing, which also points to a decrease in surface water nutrients.

This situation quickly changes indicated by a strong rise of the absolute dinoflagellates/gram numbers, which culminates during pollen zone III (Fig. 5.5). During this phase, brackish, but nutrient rich, surface water conditions prevailed. *Pyxidinopsis*, a taxon well know from the modern brackish Black Sea (Leroy et al., 2007), attains stable high values. This taxon tolerates salinities between 3–7 psu in the modern Baltic Sea (Leroy et al., 2007), has its opimum from 7–12 psu and becomes rare at salinities higher than 13 psu (Marret et al., 2007).

From a peak at the border to pollen zone IVa (sample 1471) the values of Protoperidinioid cysts A strongly drop in benefit of *Impagidinium,* supporting a switch back to more oligotrophic conditions. Also the Round Brown Cysts attain their lowest abundance, pointing to a drop of surface water nutrients. Soon after, another turnover happened in pollen zone IVb, where a rise of Protoperidinioid cysts and a lagged rise of Round Brown cysts took place. Zone V starts with a second maximum of dinoflagellates abundance and the high amounts of *Selenopemphix* suggest strongly increasing riverine influence towards the top.

5.5.5. The lake bottom

5.5.5.1. Ostracods and molluscs

The ostracods of Lake Pannon have been intensively studied in numerous papers (e.g. Gross, 2004; Gross et al., 2008; 2011; Harzhauser et al., 2008; Kern et al., 2012b). A taxonomic analysis of the ostracods from core samples from Hennersdorf (Harzhauser et al. 2008) documented that the species composition of the ostracod assemblage remained roughly constant despite strong changes in the total abundance of ostracods. Poor oxygen supply on the lake bottom caused a low diversity assemblage with only five dominating taxa (*Cyprideis*, *Hemicytheria*, *Lineocypris*/*Caspionella*, *Amplocypris*, *Loxochoncha*). Bottom water oxygenation and nutrient supply strongly constrained growth and success of ostracod populations in Lake Pannon (Harzhauser et al., 2008; Gross et al., 2011; Kern et al., 2012a). The most prolific conditions for ostracod settling were established during deposition of the lower part of the core up to c. sample 1520 (Fig. 5.6). The conditions were clearly degenerating already in this interval as indicated by the negative trend which culminates in the very low abundances from sample 1520 onwards, interrupted only by short recovering phases (samples 1510–1500, 1475–1460, 1450–1440). The conditions improved again in the top (above sample 1400) with increasing amount of ostracods.

Molluscs occur as isolated shells or as discrete shell-accumulations. These represent autochthonous assemblages of dreissenid bivalves comprising only very few or even single generations (Harzhauser and Mandic, 2004). Generally, molluscs are absent from most samples, indicating hostile conditions for bivalve settlement. Only three phases of more or less continuous settlement are documented (samples 1540–1530, 1474–1461, 1441–1438) which reflect oxygenized bottom water conditions and ample food supply.

5.5.5.2. Geochemistry and geophysics

Geochemical and geophysical measurements do not simply reflect different sediment compositions as the gross-lithology is constant along the studied core.

The natural gamma radiation measurements (GR) detect the presence of radioactive isotopes emitted by Potassium-, Uranium- and Thorium-bearing minerals (Blum et al., 1997). These mainly get transported into the lake by wind or river supply (see Kern et al., 2012a for references). The magnetic susceptibility (MS) is frequently interpreted analogously, as it is determined by the presence of carrier minerals such as magnetite and pyrrhotite. Nevertheless, the simple interpretation as function of detrital input has been questioned by the frequent occurrence of greigite in Lake Pannon (Babinszk et al., 2007; Vasiliev et al., 2010). This iron-sulfide is formed under dysoxic conditions in the first centimeters below the lake bottom sediment surface by microbial reactions (Roberts et al., 2011). Thus, the detected MS signal may resemble a combined signal of input, microbial activity and bottom water conditions. Consequently, the original signal may be altered postsedimentarily and the high-frequency signals as revealed by ostracods and GR are lost (Kern et al., 2012a; Fig. 5.6). A general rise of values occurs between samples 1480 and 1470. As the input-determined GR remains at an overall similar average in that interval, the rise of the MS may possibly be affected by microbial activity within the sediment. This low-oxygen scenario fits also to the very poor ostracod assemblages.

Interpreting the geochemistry of the samples is complex since studies on comparable brackish environments are rare (e.g. Berner, 1984; Sampei et al., 1997; Reischenbacher et al., 2007; Gross et al., 2011). The main source of sulfur in lake deposits are inorganic sulfates and organic sulfur compounds (e.g. Holmer and Storkholm, 2001), which are transferred into organic sulfur mainly due to bacterial activity under oxygen depleted conditions (Goldhaber and Kaplan, 1972; Berner, 1984; Schoonen, 2004). Typically, fine grained iron-sulfide is formed in the sediment by bacteria (e.g. pyrite, greigite, etc) (Holmer and Storkholm, 2001; Egli, 2004; Pan et al., 2005), which may have been a common process in Lake Pannon (Babinszk et al., 2007; Vasiliev et al., 2010). In comparison to organic sulfur, the organic matter content in lakes is higher (Berner, 1984; Homer and Storkholm, 2001). The organic matter comprises lipids, carbohydrates, proteins and other biological components originated from the lake biota and its surroundings (Meyers, 2003). Total organic carbon (TOC) is the most common proxy to describe the amount of organic matter and as indicator of productivity (Cohen, 2003; Meyers, 2003). A covariance between TS and TOC was recorded from nearshore deposits of Lake Pannon as result of organic matter input (Gross et al., 2011). Reischenbacher et al. (2007) documented that algal blooms within a Miocene Alpine lake caused similar covariance. This covariance is missing in the Hennersdorf core, pointing to a more complex mechanism. Therefore, generally elevated sulfur values in the lower half of the core point to high bacterial activity and poor oxygenation at this level. This interpretation is supported by the near absence of benthos. Moreover, the TOC/TS ratio is frequently used as proxy for freshwater input (Berner, 1984; Sampei et al., 1997; Reischenbacher et al., 2007) as dissolved sulfate supply is strongly limited in freshwater systems compared to brackish/marine ones (Holmer and Storkholm, 2001). The even higher TOC/TS ratio above sample 1430 is also considered to reflect freshwater input. The Calcium carbonate-equivalent (c-equi) reflects the total amount of calcium carbonate in the samples and is usually interpreted to reflect autochthonous precipitation. Rantitsch et al. (2004), however, documented the influence of detrital input from the hinterland on the carbonate content. Especially along the western shores of Lake Pannon, dolomite and limestone from the Calcareous Alps constitute a major source of detrital carbonate. A second factor is the oxygenation of the lake bottom, which influences autochthonous carbonate precipitation.

In the middle part of the section (samples 1490–1465) the c-equi values are high, while ostracods are almost absent. During this phase, sulfur displays top peaks, magnetic susceptibility increases to a higher level and also the natural gamma radiation is rather high. In combination with the higher c-equi, all four proxies indicate higher input of hinterland derived particles. Another second such phase of high Calcium carbonate-equivalent values occurs between samples 1455 and 1440, again coinciding with high MS values (Fig. 5.6). A difference is the low TOC and the well-established ostracod populations suggesting a better oxygenation.

5.5.6. General trends

The ecological and environmental data of the various proxies allow a detailed interpretation of the lake record. These are discussed based on the zonation suggested by the pollen data.

Zone I (samples 1540–1526)

The high abundance of *Selenophemphix* as well as the peak of TOC/S ratio suggests strong freshwater inflow into Lake Pannon. This is supported by the presence of river-associated plants, the high pollen diversity and the high input of organic material as well as a high amount of detritic carbonate. As the overall dinoflagellates record is typical for "offshore" settings of Lake Pannon and as the core starts clearly above a major transgressive event (Harzhauser et al. 2008), a significant change of the lake level can be excluded. The rapid decline of all these proxies within zone I suggests a drop of riverine influx up to sample 1526, which defines the boundary between pollen-zones I and II. During this phase, the lake bottom waters were well oxygenated with ample nutrient supply, resulting in the establishment of large ostracod and mollusc populations. This interpretation is in agreement with the pollen data, which clearly document a gradual decrease of riverine elements (see above).

Zone II (samples 1525–1490)

The bottom water oxygenation deteriorated distinctly during zone II. Molluscs vanish completely aside from a single layer and the ostracod populations declined to very low levels and repeatedly collapsed completely. These conditions stimulated the activity of sulfur bacteria, which is expressed in increasing MS values at first and multiple peaks of sulfur. The low TOC/TS ratio indicates also low oxygen conditions and a lack of freshwater influx into the brackish lake water. Simultaneously, the surface conditions are changing. High nutrient levels in the surface waters during the initial phase of zone II, indicated by an increase of heterotrophic dinoflagellates seem to be replaced by more oligotrophic conditions in the late phase when *Impagidinium* is rising and heterotrophs are slightly decreasing. Thus, at that stage, the lake was probably stratified with a poorly oxygenized and hostile hypolimnion. Although the pollen diversity is declining, the number of pollen/gram is rising especially due to an increase of the wind-distributed hinterland forest elements and altitudinal trees such as *Abies*, *Cathaya*, *Tsuga* and *Picea*. Thus, transport by wind was probably the major source for pollen, whilst the riparian elements are nearly missing.

Zone III (samples 1489–1468)

The poorly oxygenized lake bottom conditions of zone II persisted throughout most of zone III. Although the ostracod record indicates repeated phases of habitable conditions, which result in the development short-lived populations, the TOC/TS ratio remains rather low. High ostracod abundances phases coincide with negative peaks in the otherwise high TOC level. The fluctuation appears also in the sulfur record, which has several peaks next to steeply rising magnetic susceptibility. As in zone II, the lake was probably stratified but episodically epilimnic conditions became established, which culminated in a short phase around the boundary between zones III and IV when mollusc coquinas are frequent, suggesting oxygenized lake bottom waters.

The lake surface conditions did not change much as well between zone II and III. The highest numbers of dinoflagellates/gram document prolific conditions with numerous multi-species blooms. High productivity is reflected by a high percentage of protoperidiniods, which outcompete most other heterotrophs whilst the autotrophic *Impagidinium* declines slightly. Highest numbers of pollen/gram in combination with a rapidly rising number of forest tree pollen, high amounts of altitudinal elements and *Pinus* are significant. A fast succession of peaks in the pollen/gram record suggests repeated wind events, which caused considerable pollen transport. Wind transport could also stimulate the input of hinterland derived detritic particles as indicated by the strongly rising carbonate equivalent and rather stable, elevated levels of gamma radiation.

Zone IV (samples 1467–1414)

Based on the pollen record this zone is subdivided into two sub-zones at the boundary of samples 1432/1433. This border coincides with a low in the pollen/gram ratio and is marked by a change from a higher amount of incoming wetland vegetation than hinterland or altitudinal elements. Although all these rise again towards the end of the second subzone, especially *Abies*, *Fagus*, *Pterocarya*, *Celtis* and also *Pinus* have negative peaks around sample 1433. A comparable separation of the zone is indicated by the TOC/TS record which increases slightly above the subzones boundary. Moreover, the last phase of mollusc settlement occurs slightly below the boundary.

Subzone IVa starts with a considerable peak in heterotroph dinoflagellates and low amounts of the autotrophs *Spiniferites* and *Impagidinium*. This is followed by a strong decline of heteroptrophs up the subzone boundary coincides with higher amounts of *Pyxidinopsis*, indicating lowered salinities and a switch towards more oligotrophic conditions. During this phase the ostracod assemblages experienced a phase of recovering, interrupted by repeated population collapses. The longer episodes of bottom water oxygenation (c. samples 1450–1440) might also account for the increasing sulfur recycling and very low TOC values.

The bottom water oxygenation during subzone IVa might have caused some taphonomic bias within the palynomorphs as the dinoflagellate/gram and the pollen/gram values are also very low. Below the sediment surface the dysoxic conditions prevailed, leading to constant high magnetic susceptibility values. A complete breakdown of the ostracod populations close to the subzones boundary, due to low oxygen conditions, again correlates with higher values of sulfur.

Within subzone IVb the heterotrophs take over again and *Pyxidinopsis* declines slightly; ostracods recover on a low level and TOC and GR increase. The strongest change is indicated by the TOC/TS ratio, which switches to very high values which persist into the following zone V and suggest a general shift in water chemistry towards less brackish conditions.

Zone V (samples 1413–1391)

The uppermost zone is short but appears to be twofold. The lower part is characterized by a considerable increase in dinoflagellates/gram values but declining amounts of heterotrophs. Simultaneously, the pollen/gram values slightly decrease. On the lake bottom, conditions deteriorated and ostracods display a severe crisis with the lowest abundance of the whole sequence, which coincides with declining MS values in the initial phase of zone V. Molluscs were also unable to settle the lake bottom. Therefore, this interval might correspond to a strongly stratified lake with rather oligotrophic surface water conditions with flourishing autotrophs. The slightly increasing freshwater discharge on the lake surface fostered raising levels of the oligohaline to freshwater-related *Pyxidinopsis*. The absence of noteworthy nutrient input and the lack of benthos caused relatively low amounts of organic sulfur which is thus missing for bacteria activity. Within the upper part of zone V the heterotrophs recovered and *Selenopemphix* increased strongly. On the lake bottom, ostracod populations established again and the total carbon and the carbonate content of the sediment increase. This indicates a considerable increase of nutrients coinciding with well oxygenized bottom conditions as well as high input, signalized additionally by higher GR values. These conditions might reflect the re-establishment of riverine influx in some distance, which also accounts for the possibly delayed strong increase of hinterland forest and higher altitudinal elements along rise in the abundance of marsh-associated taxa such as *Nyssa* and Taxodioideae. Correspondingly, the high TOC/TS values throughout this zone support this interpretation of decreasing salinity due to increased freshwater supply.

5.5.7. Presence of solar cycles

5.5.7.1. Periodicities

Along the longer sequence of 6 meter, Kern et al. (2012a) already demonstrated periodicities in the MS-, GR- and ostracod records, which fit to those of the lower and upper Gleissberg cycles (50–80 and 90–120 years), the deVries/Suess cycle (~210 years), the 500- and 1000-year cycles and the Hallstatt cycle (~2300 years) (Fig. 5.1). The same techniques were applied herein, but due the shorter time interval of c. 2055 years, only the Lower and Upper Gleissberg and the deVries/Suess cycles can be expected to be present. Shorter cyclicities, such as the 11-year-Schwabe-sunspot cycle or the 22-year-Hale cycle, approximate the time resolution of the sampling and thus cannot be detected (Hoyt and Schatten, 1998; Versteegh, 2005; Gray et al., 2010). Thus, in respect to the time model of 13.7 yr/cm, only a

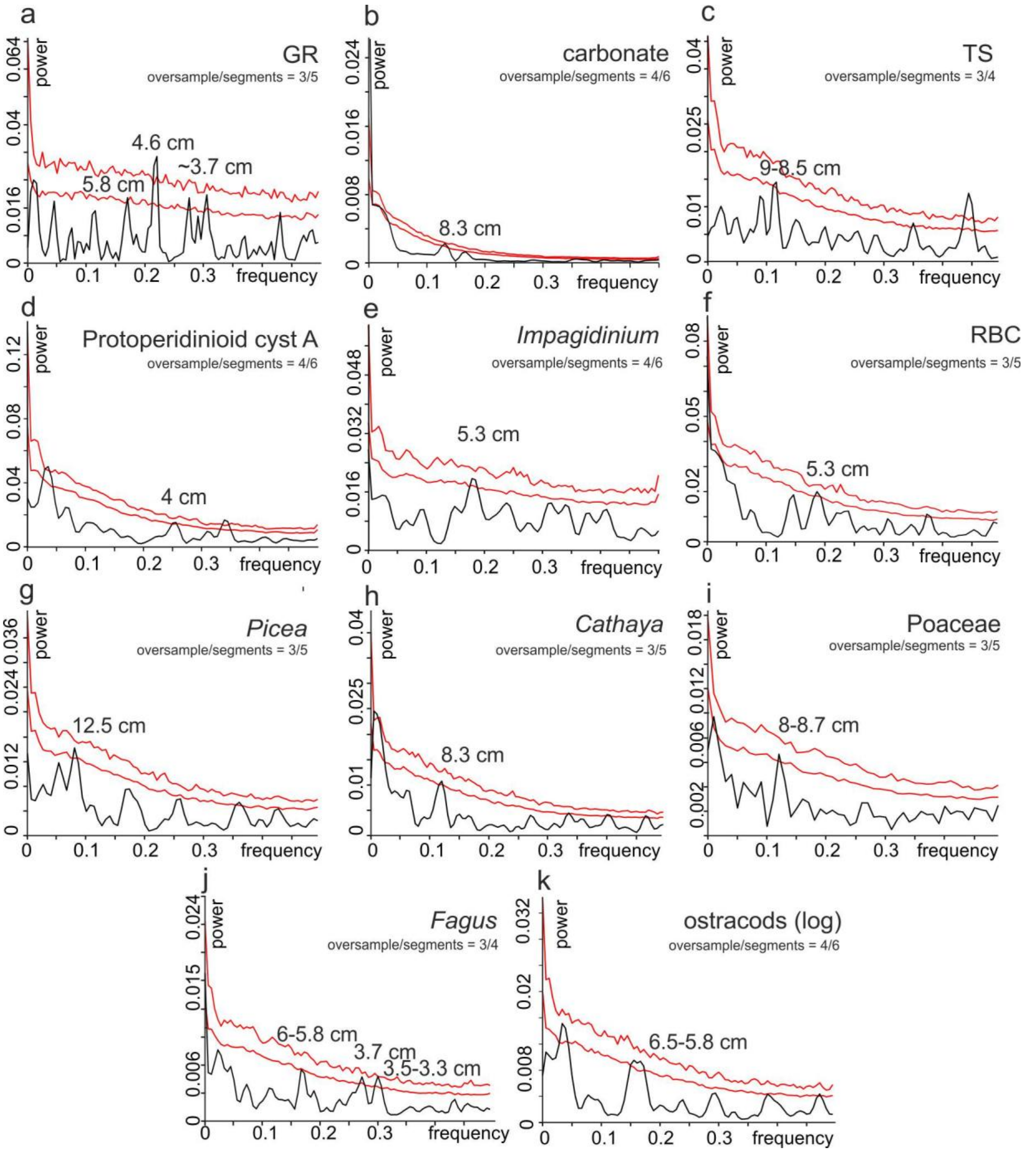

Fig. 5.7. REDFIT periodograms of 11 proxies with significant peaks passing the 95% confidence interval (lower red line; upper line represents 99% CI). GR = natural gamma radiation, TS = total sulfur, RBC = Round Brown Cysts. Frequencies are converted in cm for easier comparison.

part of the frequency spectrum can be considered. Very low frequencies (<0.05) may not show enough repetitions within the investigated sequence and high frequencies >0.3 are too close to the time resolution.

In the following we give a short overview of significant periodicities as revealed by REDFIT spectral analysis. Eleven proxies revealed signals above the 95% confidence interval: GR, carbonate, TS, Protoperidinoid cysts A, *Impagidinium*, Round Brown Cysts, *Picea*, *Cathaya*, Poaceae, *Fagus* and ostracods, (Fig. 5.7). Several others indicate peaks at comparable frequencies, but did not reach the 95% CI and are not discussed herein.

GR (Fig 5.7a): three peaks between 0.167–0.173, 0.213–0.22 and at 0.273 are detected. This corresponds to a repetitive signal of ~5.8, ~4.6 and 3.7 cm and 79.5, 67.1 and 50.7 years in time.

Carbonate (Fig. 5.7b): one peak at 0.12 almost passes the 99% CI, while a second one at 0.18 reaches the 95% CI. This represents 8.3 cm (113.7 years) and 5.6 cm (76.7 years), respectively.

TS (Fig 5.7c): one peak at 0.111–0.117 reaches above the 95% CI; this corresponds to 9–8.5 cm or 123.3–116.5 years. A second peak at 0.089 does not reach the 95% CI but might represent a split peak of the same signal.

Protoperidinoid cyst A (Fig. 5.7d): only one wide peak reaches above the 95% CI at 0.247–0.253, resulting in a cyclicity of ~4 cm or 54.8 years.

Impagidinium (Fig. 5.7e): several peaks are observed but only one at 0.183–0.189 is strong enough to pass into the 95 %CI; it corresponds to a frequency of 5.5–5.3 cm or 75.4–72.6 years.

Round Brown Cysts (Fig. 5.7f): several peaks are observed but only at 0.187 the 95% CI is passed. This means cycles of 5.3 cm or 73.3 years.

Picea (Fig. 5.7g): this pollen shows a rather weak peak at 0.08–0.087, corresponding to 12.5–11.5 cm or 171.3–157.5 years. All higher frequency signals fail to reach the 95 % CI.

Cathaya (Fig. 5.7h): within this spectrum, many high frequency signals occur, but only one at 0.12 is significant enough to pass the 95% CI value, corresponding to 8.3 cm or 114.2 years.

Poaceae (Fig. 5.7i): a clear peak at 0.115–0.125 is detected, which corresponds to 8.7–8 cm or 119.2–109.6 years.

Fagus (Fig. 5.7j): REDFIT detects several peaks within this data set; first at 0.1667–0.172 and two neighboring peaks at 0.267–0.272 and 0.29–0.3. These frequencies correspond to 6–5.8 cm, ~3.7 cm and 3.5–3.3 cm or to 82.2–79.5 years, 50.7 years and 48–45.2 years.

Although several other pollen taxa reflect also repetitive abundance patterns, these were excluded as they all represent very rare elements (e.g. *Tilia*, Arecaceae, Ericaceae, Rosaceae, etc.).

Thus, although these proxies are related to different environments and origin, they display common repetitive signals. Significant peaks cluster in three discrete intervals corresponding roughly to 123–114, 82–67 and 55–48 years with mean values of 115, 75 and 51 years for each group. These values range well within the expected ranges of the lower Gleissberg cycle with a 50–80-years period (Ogurtsov et al., 2002; de Jager et al., 2010) and the upper Gleissberg-cycle with a 90–120-years period (Wolf, 1862; Gleissberg, 1939; Ogurtsov et al., 2002). These results seem to be robust as Harzhauser et al. (2008) and Kern et al. (2012a)

detected comparable peaks within the lower and upper Gleissberg frequency band in core intervals below and above the herein studied interval.
Only the singly weak *Picea* peak of roughly 170–160 years does not fit to any known cycles. It could be either a heterodyne of the Gleissberg cycle with the ~200 year de Vries solar cycle.

5.5.7.2. Filtered records
As the REDFIT spectra detect 3 dominant frequencies, the corresponding Gaussian filters were applied to the data (Fig. 5.8). One frequency interval is represented in *Cathaya*, Poaceae, total sulfur and the carbonate content. The two pollen peaks at 0.12 (*Cathaya* and Poaceae) result in fully comparable filtered signals with low expressions in the lower half of the core (especially in zone II) and an increasingly stable and prominent signal in the upper part. This pattern is also comparable to the filtered carbonate content, which expresses lower intensities at the same levels. The forth proxy within this frequency window is sulfur. The filtered signal is roughly the opposite of the previously discussed pollen curves, with highest amplitudes in zones I and II. The next frequency window with several peaks occurs between 0.16 and 0.186. The dinoflagellates taxa *Impagidinium* (0.185) and Round Brown Cysts (0.186) show comparable filtered curves, starting with a low intensity in zone I, followed by a strong rise in zone II. Both again display a low amplitude interval in the transition from zone III to IV, which is longer in *Impagidinium*. At the top (mainly zone V), there is another decrease within the *Impagidinium* signal, which is again only weakly reflected in the Round Brown Cysts values. The ostracods (0.16) display only vague parallels with the dinoflagellates signal. Zones I and II are characterized by moderately intense amplitudes and zone III nearly lacks any significant cycles. Above, the signal becomes prominent in zone IV and fades out thereafter.
Some resemblance is also displayed by *Fagus* (0.17) with a low amplitude phase at the transition from zone II to III and comparatively stable signals below. No parallels with these signals are expressed in the filtered GR signal (0.167). It starts with insignificant cycles in zones I and II, rises strongly in zone III when all other proxies have the lowest amplitude signals, and remains prominent thereafter. The highest frequency cycles are detected in the GR record, in *Fagus* and the protoperidinioid cysts. The gamma radiation reflects two significant frequencies at 0.21 and 0.29, which both result in different patterns after filtering. The signal (filtered at 0.21) appears overall constant with a less intense signal at the transition from zone I to II and in the upper part of Subzone IVa. The higher frequency GR record (filtered at 0.29) displays very regular variations between tops and lows with low amplitude intervals around samples 1520, 1490, 1450, 1430 and 1390. *Fagus* (0.27) lacks

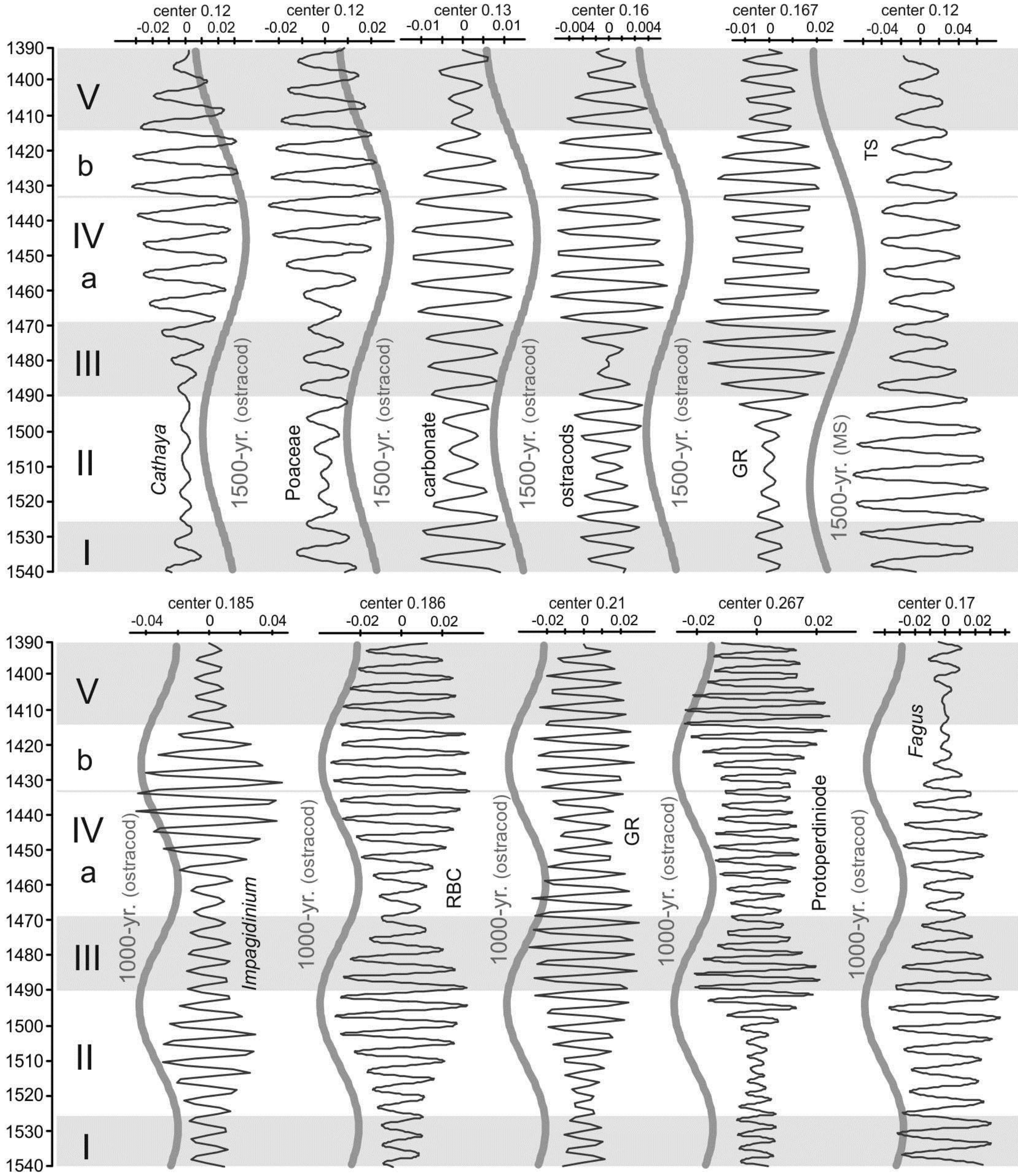

Fig. 5.8. Gaussian filter were applied to selected proxies, which revealed significant peaks in the REDFIT periodograms. The modulation is compared with 1000-year and 1500-year cycles of the identical core interval detected in the longer ostracod and MS records presented in Kern et al. (2012a) (see Fig. 5.1); GR = natural gamma radiation, TS = total sulfur, MS = magnetic susceptibility, RBC = Round Brown Cysts).

this modulation and begins with low amplitudes in zone I and the basal zone II followed by a rapid intensification in zones II and III, a steady decrease in zone IV and a more prominent signal again in zone V. The Protoperidinioid cysts (0.27), in contrast, start with low values throughout zones I and II, followed by high amplitudes in zone III. Zone IVa is characterized by moderate amplitudes followed by a high phase during zones VIb and V.

5.5.7.3. Modulation of the Gleissberg cycles

Although the data were filtered at slightly different frequencies, the resulting patterns display several similarities with comparable low and high amplitude intervals and similar turning points (Fig. 5.8). Since all these proxies are independent from each other, representing partly different paleoenvironments, this modulation suggest a common forcing mechanism. Kern et al. (2012a) showed that the quasi periodic 1000-years and 1500-years cycles are among the dominant cycles in the 6-m-long record of the Hennersdorf core. Therefore, the filtered 1000-years and 1500-years signals of the ostracod and MS record of Kern et al. (2012a) were used as target curves for the herein described shorter records. This comparison reveals that the signal modulation of a certain proxy often coincides with one of these periodicities (Fig. 5.8). Especially the *Impagidinum*, Round Brown Cysts and the GR (0.21) signals display a strong 1000-years-modulation, which is also visible in the protoperidinioids signal. The 1500-years-periodicity influences the *Cathaya*, Poaceae, carbonate contents and ostracod records and seems also to be present in the *Fagus* (0.27) and TS signals.

This grouping suggests a strong influence of the 1000-years solar cycle on lake surface dwelling dinoflagellates and might be considered as “lake cycle”. Shifts between oligotrophic versus eutrophic conditions are the most reliable explanation for this cyclicity. Fluctuating nutrient input would also fit to the similarities with the GR record.

The second group, modulated by the 1500-years-cycle, suggests a forcing of the transport mechanism from the hinterland as pollen is mostly concerned. Changing intensity of transport into the lake and/or lake bottom oxygenation would also modify the TS signal and the carbonate content. Both are clearly constraining ostracod abundance. This cycle might be referred to as “land cycle”. Fluvial transport is an unlikely mechanism to explain most parts of the record (except for the base and the very top). Therefore, these variations in transport may be best explained by changes in the wind-derived input. Indeed, wind activity could be linked directly to the amount of solar radiation and cloud cover. Clouds cause different patterns of rainfall and sunlight reaching the surface leading to unequal heating and evaporation of land and water (Svensmark and Friis-Christiansen, 1997). Thus, sun activity and cloud formation determine the wind activity especially on the continent and in particular at land/water interfaces, such as seas or large lakes like Lake Pannon. This 1500-yr cycle is an “Earth-system-immanent-cycle” and not directly linked to solar forcing (see Bond et al., 2001; Bard and Frank, 2006; Debret et al., 2007 and Kern et al., 2012a for discussion). Therefore, this obvious influence on Late Miocene environmental proxies suggests a much more complex interplay between solar forcing and Earth’s climate. The changes in wind-triggered input into the lake result in shifts in dust (detritic carbonate) and pollen transport into the lake. These shifts affect the life in the lake distinctly more than the surrounding vegetation and explain why the overall vegetation did not change significantly. Moreover, the lake surface dwelling dinoflagellates and the lake bottom dwelling ostracods will react more or less in phase with any environmental change whilst large parts of the terrestrial vegetation will react with some delay (e.g. trees and other perennial plants). Despite the minor changes in cloud cover and/or wind intensity, changes of the Early Tortonian climate were not intense enough to force changes in the vegetation during this very short period of roughly 2000 years.

5.6. Conclusion

High-frequency environmental changes in and around paleo-Lake Pannon are documented for two millennia of Late Miocene time based on terrestrial and aquatic (planktic) palynomorphs, benthic ostracods and molluscs and a set of geochemical and geophysical data. These proxies allow a comparison of coeval environmental shifts in the surroundings of the lake, including its hinterland, with surface and bottom water conditions (Fig 5.9). The overall vegetation did not change significantly during the observed interval. Similarly, the lake level was rather stable. Nevertheless, several phases can be separated based on cluster analysis of the pollen data, suggesting considerable changes in pollen transport.
During the first phase (pollen zone I) of slightly more than 200 years fluvial influx is detected by higher input of river-associated vegetation and the occurrence of freshwater-tolerant dinoflagellates. This resulted in a high TOC/TS ratio and in well oxygenated bottom water conditions as suggested by a large population of ostracods and molluscs. During the

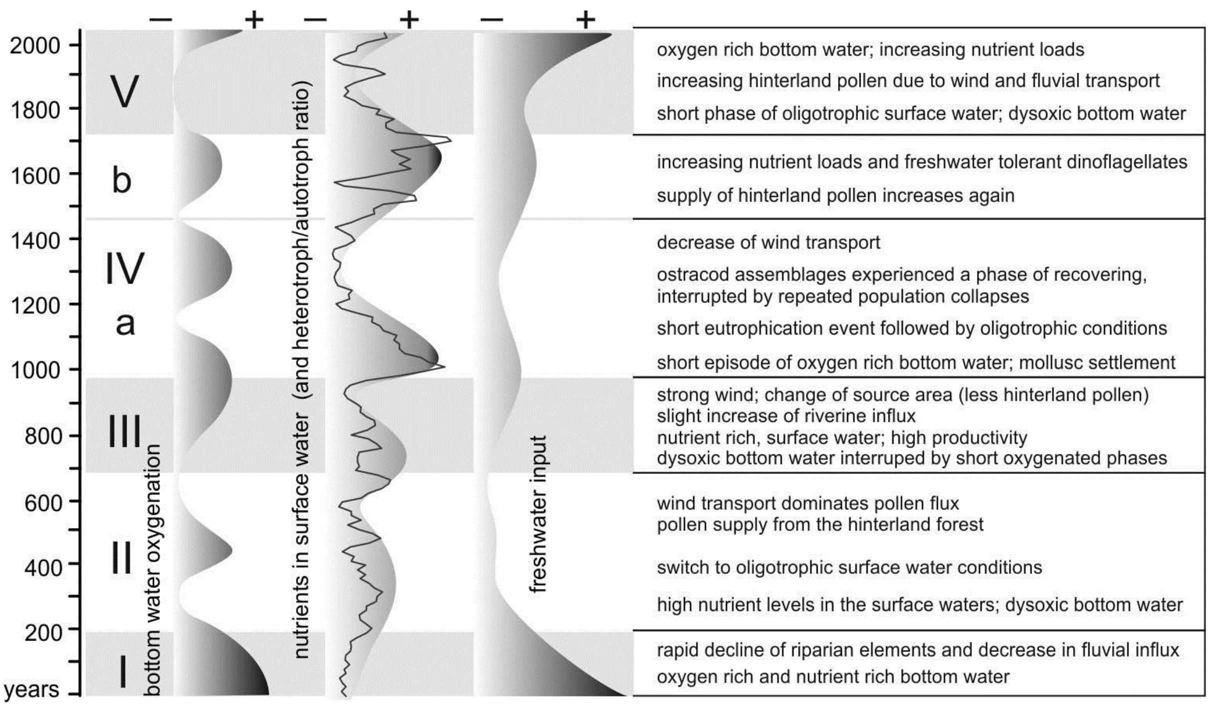

Fig. 5.9. Simplified overview of the major environmental changes as indicated by the various proxies and tentative interpretation of the bottom water oxygenation, nutrient load and freshwater input.

following ~500 years (pollen zone II), riverine influx ceased and pollen transport was mainly wind triggered as most of the pollen originate from hinterland forests and even mountainous areas (Fig. 5.4). Surface water conditions switched from eutrophic towards more oligotophic ones and dysoxic bottom waters developed. These conditions fostered the activity of sulfur bacteria in the lake sediment indicated by high sulfur values, a low TOC/S ratio and the increasing magnetic susceptibility. Extraordinary high pollen/gram sediment counts reflect several wind events which transported wind dispersed pollen into the lake. This trend is even enhanced during the following ~300 years (pollen zone III) but the decline of hinterland elements may indicate a change in the source area. The high input coincides with ample nutrient supply in the surface waters and blooms of heterotrophic dinoflagellates, while bottom waters remained poorly oxygenized. The conditions were strongly fluctuating during the following ~700 years (pollen zone IV). A short phase of epilimnic bottom conditions is followed by a succession of dysoxic phases. Although an about 150 years lasting phase of well oxygenated bottom conditions caused some taphonomic bias in the palynomorphs low amounts of dinoflagellates coincide distinctly with this oligotrophic phase. Overall, the contribution by wind transport seems to have declined and phases of high hinterland input alternate with intervals of predominant contribution from the close by wetlands. During the last phase (pollen zone V) bottom water conditions improved distinctly after a short dysoxic phase and moderate fluvial influx is re-established. Thus, our data document high-resolution analyses of Miocene multi-proxy records may reveal rapid environmental shifts with a temporal resolution which is comparable to Holocene records.

Several of these changes occur simultaneously in many proxies and display repetitive patterns. These appear in frequencies of 123–114, 82–67 and 55–48 years, which point towards the influence of the upper and lower Gleissberg cycles, corroborating results of Kern et al. (2012a), which were based on a much longer core interval. The observed changes in wind intensity and probably also direction, as revealed by the pollen spectra, might document the influence of these solar cycles on prevailing weather conditions. This could be partly explained by feedback mechanisms between solar energy and cloud formation. Moreover, both frequency bands of the Gleissberg cycle are modulated by higher order cycles such as 1000-years-cycle and the quasi-periodic Earth-system-immanent 1500-years-cycle, which are not directly linked to solar forcing. Especially, the long trend in windiness fits to the 1000-years-modulation and might explain its prevalence in hinterland proxies.

Our data suggest that high-resolution-studies of Miocene deposits are powerful tools to detect high-frequency environmental changes in a resolution, which so far is mainly realized in Holocene records.

Acknowledgement

This study is supported by the FWF grant P21414-B16. Further, we want to thank Anton Englert, Anton Fürst, Franz Topka, Andy Leggat and Lisa Schmidinger for core preparation, sample processing and counting of the ostracods. We thank Martin Gross for background information concerning geophysics and geochemistry. This paper is contributing to the NECLIME network.

5.7. References

Averyanov, L.V., Phan, E.L., Nguyen, T.,H., Nguyen, S.K., Nguyen, T.V., Pham, T.D., 2009. Preliminary Obervations of Native *Glyptostrobus pensilis* (Taxodiaceae) Stands in Vietnam. Taiwania 54 (3), 191–212.

Babinszki, E., Marton, E., Martin, P., Kiss, L.F., 2007. Widespread occurence of greigite in the sediments of Lake Pannon: Implications fo the environment and magnetostratigraphy. Palaeogeography, Palaeoclimatology, Palaeoecology 252, 626–636.

Bard, E., Frank, M., 2006. Climate change and solar variability: What's new under the sun? Earth and Planetary Science Letters 248, 1–14.

Berner, R.A., 1984. Sedimentary pyrite formation: An up-date. Geochimica, Cosmohimica Acta 48, 605–615.

Blum, P., Rabaute, A., Gaudon, P., Allan, J.F., 1997. 14. Analysis of natural gamma-ray spectra obtained from sediment cores with the shipboard scintillation detector of the Ocean Drilling Program: example from leg 1561. Proceedings of the Ocean Drilling Program, Scientific Results 156, 183–195.

Bond, G., Kormer, B., Beer, J., Muscheler, R., Evans, M.N., Showers, W., Hoffmann, S., Lotti-Band, R., Hadjas, I., Bonani, G., 2001. Persistent solar influence on North Atlantic Climate during the Holocene. Science 294, 2130–2136.

Britten, R.H., Crivelli, A.J., 1993. Wetlands of southern Europe and North Africa: Mediterranean wetlands. In: Whigham, D.F., Dykyjová, D., Hejný, S. (Eds.), Handbook of Vegetation Science, Wetlands of the World I: Inventory, Ecology and Management. Kluver Academic Publishers, Dordrecht, pp. 129–194.

Bruch, A.A., Utescher, T., Alcalde Olivares, C., Dolakova, N., Ivanov, D., Mosbrugger, V., 2004. Middle and Late Miocene spatial temperature patterns and gradients in Europe – preliminary results based on palaeobotanical climate reconstructions. Courier Forschungsinstitut Senckenberg 249, 15-27.

Bruch, A.A., Utescher, T., Mosbrugger, V., Gabrielyan, I., Ivanov, D.A., 2006. Late Miocene climate in the circum-Alpine realm – a quantitative analysis of terrestrial palaeofloras. Palaeogeography, Palaeoclimatology, Palaeoecology 238, 270–280.

Charcátová, I., 2000. Can origin of the 2400-year cycle of solar activity be caused by solar inertial motion? Annales Geophysicae 18, 399–405.

Cho, H.-J., Matsuoka, K., 2001. Distribution of dinoflagellate cysts in surface sediments from the Yellow Sea and East China Sea. Marine Micropaleontology 43, 103–123.

Chmura, G.L., Liu, K.-B., 1990. Pollen in the lower Mississippi River. Review of Palaeobotany and Palynology 64, 253–26 1.

Claud, C., Cagnazzo, C., Keckhut, P., 2008. The effect of the 11-year solar cycle on the temperature in the lower stratosphere. Journal of Atmospheric and Solar-Terrestrial Physics 70, 2031–2040.

Cohen, A.S., 2003. Paleolimnology – The History and Evolution of Lake Systems. Oxford University Press, New York.

Dale, B., 1996. Dinoflagellate cysts ecology: modelling and geological applications. In: Jansonius, J., McGregor, D.C. (Eds.), Palynology: Principles and Applications. American Association of Stratigraphic Palynologists Foundation, Dallas, pp. 1249–1276.

Debret, M., Bout-Roumazeilles, V., Grousset, F., Desmet, M., McManus, J.F., Massei, N., Sebag, D., Petit, J.-R., Copard, Y., Trentesaux, A., 2007. The origin of the 1500-year climate cycles in Holocene North-Atlantic records. Climate of the Past 3, 569–575.

De Jeager, C., Duhau, S., van Geel, 2010. Quantifying and specifying the solar influence on terrestrial surface temperature. Journal of Atmospheric and Solar-Terrestrial Physics 72, 926–937.

Denk, T., Frotzler, N., Davitashvili, N., 2001. Vegetational patterns and distribution of relict taxa in humid temperatue forests and wetlands of Georgia (Transcaucasia). Biological Journal of the Linnean Society 72, 287–332.

Egli, R., 2004. Characterization of individual rock magnetic components by analysis of remanence cures. 3. Bacterial magnetite and natural processes in lakes. Physics and Chemistry of the Earth 29, 869–884.

Ellegaard, M., 2000. Variations in dinoflagellate cyst morphology under conditions of changing salinity during the last 2000 years. Review of Palaeobotany and Palynology 9, 65–81.

Fauquette, S., Clauzon, G., Suc, J.-P., 1999. A new approach for paleoaltitude estimates based on pollen records: example of the Mercantour Massif (southeastern France) at the earliest Pliocene. Earth Planetary Science Letters 170, 35–47.

Gleissberg, 1939. Observatory 62, 158.

Godhe, A., Norén F., Kuylenstierna, M., Ekberg, C., Karlson, B., 2001. Relationship between planktonic dinoflagellate abundance, cyst recovered in sediment traps and environmental factors in Gullmar Fjord, Sweden. Journal of Plankton Research 23, 923–938.

Goldhaber, M.B., Kaplan, I.R., 1974. The sulfur cycle. In: Goldberg, E.D., (Ed.), The Sea, Vol. 5, John Wiley Sons, London, pp. 569–655.

Gray, L.J., Beer, J., Gellar, M., Haigh, J.D., Lockwood, M.,Matthes, K., Cubasch, U., Fleitmann, D., Harrison, G., Hood, L., Lutenbacker, J., Meehl, G.A., Shindell, D., van Geel, B., White, W., 2010. Solar influence on climate. Review of Geophysica 48, RG4001.

Green, O.R., 2001. A manual of practical laboratory and field techniques in palaeobiology. Kluwer Academic Publishers, Dordrecht.

Grimm, E.C., 2004. Tilia and TG View Version 2.0.2. Illinois State Museum, Research and Collector Center.

Gross, M., 2004. Zur Ostracodenfauna (Crustacea), Paläoökologie und Stratigrafie der Tongrube Mataschen (Unter-Pannonium, Steirisches Becken, Österreich). Joannea Geologie und Paläontologie 5, 49–129.

Gross M., Minati K., Danielopol, D.L., Piller, W.E., 2008. Environmental changes and diversification of Cyprideis in the Late Miocene of the Styrian Basin (Lake Pannon, Austria). Senckenbergiana lethaea 88, 161–181.

Gross, M., Piller, W.E., Scholger, R., Gitter, F., 2011. Biotic and abiotic response to palaeoenvironmental changes at Lake Pannon's western margin (Central Europe, Lake Miocene). Palaeogeography, Palaeoclimatology, Palaeoecology 312, 181–193.

Guiry, M.D., Guiry, G.M., 2012. AlgaeBase. World-wide electronic publication, National University of Ireland, Galway. http://www.algaebase.org; searched on 17 April 2012.

Hammer, Ø., Harper, D.A.T., Ryan, P.D., 2001. PAST: Palaeontological Statistics Software package for education and data analysis. Palaeontologica Electronica 4 (1), 9 pp.

Harzhauser, M., Mandic, O., 2004. The muddy bottom of Lake Pannon-a challenge for dreissenid settlement (Lake Miocene; Bivalva). Palaeogeography, Palaeoclimatology, Palaeoecology 204, 331–352.

Harzhauser, M., Mandic, O., 2004. The muddy bottom of Lake Pannon. Palaeogeography, Palaeoclimatology, Palaeoecology 204, 331–352.

Harzhauser, M., Mandic, O., 2008. Neogene lake systems in Central and South-Eastern Europe: faunal diversity, gradients and interrelations. Palaeogeography, Palaeoclimatology, Palaeoecology 260, 417–434.

Harzhauser, M., Daxner-Höck, G., Piller, W.E., 2004. An integrated stratigraphy of the Pannonian (Late Miocene) in the Vienna Basin. Austrian Journal of Earth Sciences 95/96, 6–19.

Harzhauser, M., Kern, A., Soliman, A., Minati, K., Piller, W.E., Danielopol, D.L., Zuschin, M., 2008. Centennial- to decadal scale environmental shifts in and around Lake Pannon (Vienna Basin) related to a major Lake Miocene lake level rise. Palaeogeography, Palaeoclimatology, Palaeoecology 270, 102–115.

Heusser , L., Balsam, W.L., 1977. Pollen distribution in the Northeast Pacific Ocean. Quaternary Research 7, 45–62.

Holmer, M., Storkholm, P., 2001. Sulphate reduction and sulphur cycling in lake sediments: a review. Freshwater Biology 46, 431–451.

Hopkins, J.S., 1950. Differential floating and deposition of conifers and deciduous tree pollen. Ecology 31, 633–641.

Hoyt, D.V., Schatten, K.H., 1997. The role of the sun in climate change. Oxford University Press, Oxford, U.K. 279 p.

Hoyt, D.V., Schatten, K.H., 1998. Group sunspot numbers: A new solar activity reconstruction. Solar Physics 179, 189–219.

Holzwarth, U., Esper, O., Zonneveld, K., 2007. Distribution of organic-walled dinoflagellate cysts in shelf surface sediments of the Benguela upwelling system in relationship to environmental conditions. Marine Micropaleontology 64, 91–119.

Holzwarth, U., Esper, O., Zonneveld, K.A.F., 2010. Organic-walled dinoflagellate cysts as indicators of oceanographic conditions and terrigenous input in the NW African upwelling region. Review of Palaeobotany and Palynology 159, 35–55.

Jarvis, D.I., Clay-Poole, S.T., 1992. A comparison of modern pollen rain and vegetation in southwestern Sichuan Province, China. Review of Palaeobotany and Palynology 75, 239–258.

Jiménez-Moreno, G., 2006. Progressive substitution of a subtropical forest for a temperate one during the middle Miocene climate cooling in Central Europe according to palynological data from cores Tengelic-2 and Hidas-53 (Pannonian Basin, Hungary). Review of Palaeobotany and Palynology, 142, 1–14.

Jimenez-Moreno, G., 2010. *Cathaya*: a gymnosperm most likely indicating a mid-altitude coniferous forest during the Neogene in the European area. 8th European Palaeobotany – Palynology Conference, Budapest, Hungary, 126.

Jimenez-Moreno, G., Suc, J.-P., 2007. Middle Miocene latitudinal climate gradient in Western Europe: Evidence from pollen records. Palaeogeography, Palaeoclimatology, Palaeoecology 253, 208–225.

Jimenez-Moreno, G., Fauquette, S., Suc, J.-P., 2008. Vegetation, climate and paleoaltitudinal reconstructions of eastern alpine mountain ranges during the Miocene based on pollen records from Austria, Central Europe. Journal of Biogeogralhy 35, 1638–1649.

Kern, A.K., Harzhauser, M., Piller, W.E., Mandic, O., Soliman, A., 2012a. Strong evidence for the influence of solar cycles on a Late Miocene Lake system revealed by biotic and abiotic proxies. Palaeogeography, Palaeoclimatology, Palaeoecology 329–330, 124–136.

Kern, A.K., Harzhauser, M., Soliman, A., Piller, W.E., Gross, M., 2012b. Precipitation driven decadal scale decline and recovery of wetlands of Lake Pannon during the Tortonian. Palaeogeography, Palaeoclimatology, Palaeoecology 317–318, 1–12.

Kouli, K., Brinkhuis, H., Dale, B., 2001. *Spiniferites cruciformis*. A fresh water dinoflagellate cyst? Review of Palaeobotany and Palynology 113, 273–286.

Kovar-Eder, J., Schwarz, J., Wojcicki, J.J., 2002. The predominantly aquatic flora from Pellendorf, Lower Austria, late Miocene, Pannonian – a systematic study. Acta Palaeobotanica 42, 125–151.

Kovar-Eder, J., Kvaček, Z., Martinetto, E., Roiron, P., 2006. Late Miocene to Early Pliocene vegetation of southern Europe (7–4 Ma) as reflected in the megafossil plant record. Palaeogeography, Palaeoclimatology, Palaeoecology 238, 321 – 339.

Kovar-Eder, J., Jechorek, H., Kvaček, Z., Parashiv, V., 2008. The integrated plant record to reconstruct Neogene zonal vegetation in Europe. Palaios 23, 97–111.

Kunzmann, L., Kvaček, Z., Mai, D.H., Walther, H., 2009. The genus Taxodium (Cupressaceae) in Palaeogene and Neogene of Central Europe. Review of Palaeobotany and Palynology 153, 153–183.

Kvaček, Z., 2007. Do extant nearest relatives of thermophile European Cenozoic plant elements reliably reflect climatic signal? Palaeogeography, Palaeoclimatology, Palaeoecology 253, 32–40.

Leroy, S.A.G., Albay, M., 2010. Palynomorphs of brackish and marine species in cores from the freshwater Lake Sapanca, NW Turkey. Review of Palaeobotany and Palynology 160, 181–188.

Leroy, S.A.G., Marret, F., Gibert, E.,Chalie, F:, Reyss, J.-L., Arpe, K., 2007. River inflow and salinity changes in the Caspian Sea during the last 5500 years. Quaternary Science Reviews 26, 3359 – 3383.

Li, K.J., Yun, H.S., Gu, X.G., 2001. Hemispheric variation in solar activity. The Astrophysical Journal 554, L115–L117.

Linder, A., Berchtold, W., 1976. Statistische Auswertung von Prozentzahlen. 1–230, Birkhäuser, Basel.

Lirer, F., Harzhauser, M., Pelosi, N., Piller, W.E., Schmid, H.P., Sprovieri, M., 2009. Astronomically forced teleconnection between Paratethyan and Mediterranean sediments during the Middle and Late Miocene. Palaeogeography, Palaeoclimatology, Palaeoecology 275, 1–13.

Lodge, T.E., 2010.The Everglades Handbook – Understanding the Ecosystem. Taylor and Francis Group, Boca Raton.

Londeix, L., Herreyre, Y., Turon, J.-L., Fletcher, W., 2009. Last Glacial to Holocene hydrology of the Marmara Sea inferred from a dinoflagellate cyst record. Review of Palaeobotany and Palynology 158, 52–71.

Magyar, I., Geary, D.H., Müller, P., 1999. Integrated Paleogeographic evolution of the Late Miocene Lake Pannnon in Central Europe. Palaeogeography, Palaeoclimatology, Palaeoecology 147, 151–167.

Marret, F., Zonneveld, K.A.F., 2003. Atlas of modern organic-walled dinoflagellate cyst distributions. Review of Palaeobotany and Palynology 125, 1–200.

Marret, F., Leroy, S., Chalie, F., Gasse, F., 2004. New organic-walled dinoflagellate cysts from recent sediments of Central Asian seas. Review of Palaebotany and Palynology 129, 1–20.

Marret F., Mudie P.J., Aksu A., Hiscott R.N., 2007. Holocene dinocyst record of a two-step transformation of the Neoeuxinian brackish water lake into the Black Sea. Quaternary International 197, 72–86.

Matthiessen, J., 1995. Distribution pattern of dinoflagellate cysts and other organic-walled microfossils in recent Norwegian-Greenland Sea sediments. Marine Micropaleontology 24, 307–334.

Meyers, P.A., 2003. Applications of organic geochemistry to paleolimnological reconstructions: a summary of examples from the Laurentian Great Lakes. Organic Geochemistry 34, 261–289.

Mosbrugger, V., Utescher, T., 1997. The coexistence approach – a method for quantitative reconstructions of Tertiary terrestrial palaeoclimate data using plant fossils. Palaeogeography, Palaeoclimatology, Palaeoecology 134, 61–86.

Mudie, P.J., 1992. Circum-arctig Quaternary and Neogene marine palynofloras: palaeoecology and statistical analysis. In: Head, M.J. and Wrenn, J.H., (Eds), Neogene and Quaternary dinoflagellate cysts and acritarchs. American Association of Stratigraphical Palynologists Foundation, College Station, TX, pp. 327–390.

Mudie, P.J., Aksu, A.E., Yasar, D., 2001. Late Quaternary dinoflagellate cysts from the Black, Marmara and Aegean seas: variations in assemblages, morphology and paleosalinity. Marine Micropaleontology 43, 155–178.

Mudie, P.J., Rochon, A., Aksu, A.E., Gillespie, H., 2002. Dinoflagellate cysts, freshwater algae and fungal spores as salinity indicators in Late Quaternary cores from Marmara and Black seas. Marine Geology 190, 203–231.

Mudie, P.J., Marret, F., Aksu, A.E., Hiscott, R.N., Gillespie, H., 2007. Palynological evidence for climatic change, anthropogenic activity and outflow of Black Sea water during the late Pleistocene and Holocene: Centennial- to decadal-scale records from the Black and Marmara Seas. Quaternary International 167–168, 73-90.

Müller, M.J., 1996. Handbuch ausgewählter Klimastationen der Erde. Forschungsstelle Bodenerosion Universität Trier, Mertesdorf (Ruwertal).

Ogurtsov, M.G., Nagovitsyn, Y.A., Kocharov, G.E., Jungner, H., 2002. Long-period cycles of the sun’s activity recorded in direct solar data and proxies. Solar Physics 211, 371–394.

Patterson, R.T., Prokoph, A., Kumar, A., Chang, A.S., Roe, H.M., 2005. Late Holocene variability in pelagic fish scales and dinoflagellate cysts along the west coast of Vancouver Island, NE Pacific Ocean. Marine Micropaleontology 55, 183–204.

Paillard, D., Labeyrie, L., Yiou, P., 1996. Macintosh program performs timeseries analysis. Transaction American Geophysical Union 77, 379.

Patterson, R.T., Prokoph, A., Chang, A., 2004. Late Holocene sedimentary response to solar and cosmic ray activity influenced climate variability in the NE Pacific. Sedimentary Geology 172, 67–84.

Pan, Y., Deng, C., Liu, Q., Petersen, N., Zhu, R., 2004. Biomineralization and magnetism of bacterial magnetosomes. Chinese Science Bulletin 49, 2563–2568.

Piller, W.E., Harzhauser, M., Mandic, O., 2007. Miocene Central Paratethys stratigraphy - current status and further directions. Stratigraphy 4 (2/3), 71–88.

Rantitsch, G., Müller, N., Ebner, F., 2004. Geochemical and mineralogical investigations of Pannonian Sediments on the clay put Mataschen (Styrian Basin, Austria). Joannea Geologie und Paläontologie 5, 219–230.

Reischenbacher, D., Fifelj, H., Sachsenhofer, R.F., Jelen, B., Ćorić, S., Gross, M., Reichenbacher, B., 2007. Early Badenian paleoenvironment in the Lavanttal Basin (Mühldorf Formation, Austria): Evidence from geochemistry and paleontology. Austrian Journal of Earth Sciences 100, 202–229.

Roberts, A.P., Chang, L., Rowan, C.J., Horng, C.-S., Florindo, F., 2011. Magnetic properties of sedimentary greigite (Fe3S4): An update. Review of Geophysics 49, RG1002.

Sampei, Y., Matsumoto, E., Kamei, T., Tokuoka, T., 1997. Sulfur and organic carbon relationship in sediments from coastal brackish lakes in the Shimane peninsula district, southwest Japan. Geochemical Journal 31, 245–262.

Schoonen, M.A.A., 2004. Mechanism of sedimentary pyrite formation. In: Amend, J.P., Edwards, K.J., Lyons, T., (Eds.). Sulfur Biogeochemistry: Past and Present. The Geological Society of America Special Papers 379, pp. 117 – 134, Boulder, CO.

Schulz, M., Mudelsee, M., 2002. REDFIT: estimating red-noise spectra directly from unevenly spaced paleoclimatic time series. Computers & Geosciences 28, 421–426.

Sluijs, A., Pross, J., Brinkhuis, H., 2005. From greenhouse to icehouse; organic-walled dinoflagellate cysts as paleoenvironmental indicators in the Paleogene. Earth-Science Reviews 68, 281–315.

Smirnov, A., Chmura, G.L., Lapointe, M.F., 1996. Spartial distribution of suspended pollen in the Mississippi River as an example of pollen transport in alluvial channels. Review of Palaeobotany and Palynology 92, 69–81.

Solanki, S.K., Usoskin, I.G., Kromber, B., Schüssler, M., Beer, J., 2004. Unusual activity of the Sun during recent decades compared to the previous 11,000 years. Nature 431, 1084–1087.

Sonett, C.P., Suess, H.E., 1984. Correlation of bristlecone pine ring widths and atmospheric ^{14}C variations: a climate-Sun relation. Nature 307, 141–143.

Sorrel, P., Popescu, S.-M., Head, M.J., Suc, J.P., Klotz, S., Oberhänsli, H., 2006. Hydrographic development of the Aral Sea during the last 2000 years based on a quantitative analysis of dinoflagellates cysts. Palaeogeography, Palaeoclimatology, Palaeoecology 234, 304–327.

Svensmark, H., Friis-Christensen, E., 1997. What do we really know about the sun-climate connection? Advances in Space Research 20, 913–921.

Thompson, R.S:, Anderson, K.H., Bartlein, P.J., 1999. Atlas of relations between climatic parameters and distributions of important trees and shrubs in North America. US Geological Survey Professional Paper 1650-A.

Traverse, A., Ginsburg, R.N., 1966. Palynology of the surface sedimentstation of Great Bahamas Bank, as related to water movements and sedimentation. Marine Geology 4, 417–459.

Tsiropoula, G., 2003. Signatures of solar activity variability in meteorological parameters. Journal of Atmospheric and Solar-Terrestrial Physics 65, 469–482.

Utescher, T., Mosbrugger, V:, Ashraf, A.R., 2000. Terrestrial climate evolution in Northwest Germany over the last 25 Million years. Palaios 15, 430–449.

Utescher, T., Ivanov, D., Harzhauser, M., Bozukov, V., Ashraf, A.R., Rolf, C., Urbat, M., Mosbrugger, V., 2009. Cyclic climate and vegetation change in the late Miocene of Western Bulgaria. Palaeogeography, Palaeoclimatology, Paleoecology 272 (1-2), 99–114.

Vasiliev, I., de Leeuw, A., Filipescu, S., Krijgsman, W., Kuiper, K., Stoica, M., Briceag, A., 2010. The age of the Sarmatioan-Pannonian transition in the Transylvanian Basin (Central Paratethys). Palaeogeography, Palaeoclimatology, Palaeoecology 297, 54–69.

Versteegh, G.J.M., 2005. Solar forcing of climate. 2: Evidence from the past. Space Science Reviews 120, 243–286.

Wilen, B.O., Tiner, R.W., 1993. Wetlands of the United States. In: Whigham, D.F., Dykyjová, D., Hejný, S. (Eds.), Handbook of Vegetation Science, Wetlands of the World I: Inventory, Ecology and Management. Kluwer Academic Publishers, Dordrecht, pp. 129–194.

Willard, D.A., Weimer, L.M., Riegel, W.L., 2001. Pollen assemblages as paleoenvironmental proxies in the Florida Everglades. Review of Palaeobotany and Palynology 113, 213–235.

Wolf, R., 1862. Astronomische Mitteilungen Zürich 14.

Wood, G.D., Gabriel, A.M., Lawson, J.C., 1996. Palynological techniques - processing and microscopy. In: Jansonius, J., McGregor, D.C. (Eds.), Palynology: Principles and Applications, Vol. 1., American Association of Stratigraphic Palynologists Foundation, Dallas, pp. 29–50.

Zachos, J., Pagani, M., Sloan, L., Thomas, E., Billups, K., 2001. Trends, Rhythms, and Aberrations in Global Climate 65 Ma to Present. Science 292, 686-693.

Zonneveld, K.A.F, 1995. Palaeoclimatic and palaeo-ecological changes during the last deglaciation in the Eastern Mediterranean – implications for dinoflagellate ecology. Review of Palaeobotany and Palynology 84, 221–253.

Zonneveld, K.A.F., Chen, L., Möbius, J., Mahmoudc, M.S., 2009. Environmental significance of dinoflagellate cysts from the proximal part of the Po-river discharge plume (off southern Italy, Eastern Mediterranean). Journal of Sea Research 62, 189–213.

Zuschin, M., Hohenegger, J., 1998. Subtropical Coral-reef associated sedimentary facies characterized by mollusks (Northern Bay of Safaga, Red Sea, Egypt). Facies 38, 229–254.

Chapter 6

Millennial- to centennial-scale vegetation dynamics in relation to other environmental proxies during the Miocene in and around the Paratethys Sea and Lake Pannon – a synopsis

The herein presented studies document multi-proxy high-resolution analyses as a powerful tool to resolve paleo-environmental changes on millennial, centennial and even decadal scale. Time resolution is the most difficult factor for such approaches beyond the ^{14}C range since it requires either a previously well constrained system or annually preserved sediments, such as varves. Even well dated and astronomically tuned sites cannot ignore problems of dating as the errors in absolute dating exceeds that of the herein aimed resolution many times and even astronomical tuning is limited to a millennial scale as well.
The herein proposed methodology relies on a best fit scenario in which detected cyclicities in the geological record (if present in several proxies with distinct frequency ratios) are compared with known sub-Milankovitch cycles with similar frequency ratios. Ideally, such patterns should reflect the relation between the lower and upper Gleissberg cycles (~50–80 and ~90–140 years), the de Vries/Suess cycle (~200–210 years), the ~500-years-cycle, the ~1000-years-cycle and the Hallsatt-cycle (~2400 years) and others. The presence of such a repetitive frequency pattern in the geological archive is a solid argument to suggest solar forcing and to estimate sedimentation rate on this account. Therefore, this is the first study specifically discussing the potential of Miocene sediments to reflect the presence of solar cycles in non-varved sediments.
Each of the investigated localities represents slightly different depositional conditions (estuarine, lagoonal lacustrine, offshore lacustrine) as well as different climate scenarios (Mid-Miocene Climatic Optimum, Early Tortonian warm phase and Tortonian transition) Nevertheless, all localities showed the clear presence of sub-millennial-scale environmental shifts in vegetation, surface water productivity, bottom water conditions, salinity and sediment input. These are linked to small-scaled climate change such as changing precipitation and/or wind regime in the lake settings and additionally to the influence by precession-driven sea-level change in the marine key study. For none of the examples, temperature was recognized as driving factor, as this seems to be a more stable parameter on these short temporal scales.

6.1. Short-term environmental changes

The Miocene climate history of Europe is already well outlined (e.g. Rögl, 1998; Kvaček et al., 2006; Utescher et al., 2006; Bruch et al., 2007). Thus, the aim of the herein summarized thesis was to document the significance of small-scale environmental changes within this already established large-scale frame.

The Late Burdigalian Stetten section in the Korneuburg Basin (Chapter 2) portrays a paleo-estuary (Harzhauser et al., 2002). Such a depositional setting represents a sensitive transitional system depending on the predominance of either the incoming riverine freshwater or the Paratethyan sea water. The 20-cm-sample-density within a 21-m-long sequence, corresponding to ~21,000 years of one precession cycle, results in a temporal resolution of roughly 1000 years per sample. This millennial scale resolution – still high compared to common pre-Pleistocene analyses – allows detecting step-wise shifts in the vegetation, such as the change from a salt-water dominated marsh to a freshwater influenced forested wetland (Chapter 2). Higher frequency fluctuations could not be resolved and therefore no sub-Milankovitch forcing can be identified. Nevertheless, the millennial-scale resolution contributes to understanding of Miocene costal wetland vegetation, where already a slight increase in salinity may act as an obstacle for many plants, limiting the assemblage to few specialists (Adam, 1990; Willard et al., 2001). Moreover, despite a clear sedimentological cyclicity, which is related to the 21-kyr-precession forcing, the climate data suggest rather stable conditions. This might point to the capacity of the subtropical vegetation to buffer the precessional-related climate signal. The presence of the precessional cyclicity in the sea-level signal might be explained by the fact that the Central Paratethys was just an appendix of the Western Tethys Ocean and that therefore, the mechanisms forcing the hydrological budget of the huge Western Tethys Ocean are not necessarily visible in its northern embayment on a regional scale.

A pendant to this Early Miocene wetland vegetation is represented by the Late Miocene wetland setting of Mataschen (Chapter 3). Although not directly connected to a sea, this vegetation is under influence of brackish water of Lake Pannon. The proximity of the section to the shore is expressed by very high contributions of the surrounding marsh vegetation in the pollen assemblages. In this sensitive setting, even small environmental changes were detected, showing that climate change and lake level are the driving forces for shifts in the regional vegetation. First, a drop of the mean annual precipitation caused a shorter inundation period of the marshes reflected immediately in a turn-over in the dominating grass families. Second, a rise of the mean annual precipitation of about 200–300 mm seems to have caused a lake level rise with a delay of c. 5 decades. The transgression resulted in a flooding of the marshes and allowed “open-water” dinoflagellates to dominate the lake surface waters. Additionally, the dinoflagellate cysts show repetitive switches from heterotrophic to autotrophic assemblages, indicating iterative eutrophication events and nutrient flux with a frequency of roughly 100–200 years.

Unlike Mataschen, the Hennersdorf core represents a lake setting in several kilometers distance from the shoreline (Harzhauser et al., 2008). For the vegetation reconstruction, this results in an overrepresentation of wind-spread and/or thick-walled, transport-resistant pollen grains. Consequently, the paleo-assemblages are less diverse (Hopkins, 1950; Heusser and Balsam, 1977) and taphonomic factors, such as wind and river inflow have to be strongly considered when interpreting pollen-based vegetation dynamics. This initial condition limited the Hennersdorf assemblage mainly to hinterland forest elements and some lower altitude taxa, while the more sensitive marsh vegetation is underrepresented and accounts for only 5–10% of the spectra (Chapter 5). Exceptions are caused by increased runoff. During phases of predominant wind transport, differences in the pollen spectra seem to reflect mainly shifts in the prevailing wind patterns, suggested by changes of the source area. Thus, although these parts reflect changes in the environment and/or climate, they do not necessarily mirror variations within the vegetation. A more complete picture of the system can be reconstructed if additional proxies are added with identical sample resolution (ostracods, geophysics and geochemistry). These allow detecting changes of bottom water oxygenation on a decadal scale. A complex regime is expected as periods of high/low ostracod occurrences and phases of higher sediment input are not correlated with the magnetic susceptibility record. The ostracod record and the sediment input are expected to reflect ecological shifts by a very high temporal resolution without recognizable temporal bias. The magnetic susceptibility signal, in contrast, may be altered by sulfur bacteria activity below the sediment/water interface resulting in a time lag. These processes might also be responsible for the absence of the high-frequency cycles in the magnetic susceptibility signal, whereas these cycles were unaffected in the remaining proxies. The dinoflagellates suggest fluctuating nutrient availability in the surface waters. These changes, however, have a lower frequency and are less regular as at Mataschen. The lagoonal-coastal setting of Matschen was obviously much more sensitive to high frequency environmental changes compared to the buffered open lake setting of Hennersdorf.

Hence, the paleogeographic setting is a key factor for selecting a sample location for successful high-resolution environmental reconstructions. Not only preservation alone is important but the depositional conditions and processes of sediment supply determine the potential to detect such processes even on a decadal level. On the other hand, the sensitive coastal settings may be prone to capture also rare and exceptional climatic events whilst the buffered “offshore” situation might reflect the general trends more reliably. In any case, Lake Pannon was clearly never a completely stable and uniform environment although the rather homogenous pelitic sedimentation does not reflect the dynamics on first sight.

6.2. Consideration of paleoclimatic estimates

This thesis comprises studies on different time slices. The first one treats samples of late Burdigalian age (~16.5 Ma), when a subtropical climate became established with the onset of the Mid-Miocene Climatic Optimum as the warmest phase of the Neogene (e.g. Zachos et al., 2001; Utescher et al., 2000; Jimenéz-Moreno et al., 2005; Bruch et al., 2007). The other studies considered Tortonian floras. Although the Tortonian succeeds the Mid-Miocene Climatic Optimum, it is characterized by a global warm phase with humid conditions in Europe (Böhme et al., 2008; Bruch et al., 2011). As a consequence, Atlantic deep water temperatures about 3°C higher than today prevailed during the early Tortonian (Lear et al., 2003). Therefore, this Late Miocene stage is a major target for climate models calculating future climate change. In ideal cases, climate models (François et al., 2006) are tested with proxy data to demonstrate their significance (Micheels et al., 2007). Nevertheless, surprisingly little information on the variability of Tortonian climate on a decadal to centennial scale does exist. Similarly, little data are available concerning seasonality; although the expressions of a long dry phase or frost during the cold months determine plant distribution much more than the mean annual temperature or the mean annual precipitation (Woodward and Williams, 1987; Inouye, 2001). Exceptions are water-associated habitats like marshes (Lodge, 2010) as presented in Chapter 3.

In contrast to many other climatic reconstruction methods, the Coexistence Approach is able to detect such climatic pattern by referring to collected climatic data of recent plants (Mosbrugger and Utescher, 1997). So far, however, this method is mainly used to compare large scale geographic areas or long time intervals (Bruch et al., 2006; 2007; 2011), but not in high-resolution studies.

When calculating short-term climatic evolution, some additional aspect should be considered. The Coexistence Approach displays palaeoclimate as intervals, which widths depending on the climatic significance of (few) particular taxa (Mosbrugger and Utescher, 1997). Thus, a moderately to low diverse assemblage leads to a larger Coexistence Interval, which may be problematic if only the mean values of the interval is considered. Likewise, the “offshore” Hennersdorf record is less suitable for analysis than the “coastal” Matschen record. Further, only presence and absence data are considered. In palynology, where plant determination is often limited to generic level, this may result in uniform intervals in localities of different ages. Comparing the late Early Miocene (Stetten; Chapter 2) and the early Late Miocene (Mataschen; Chapter 3), this leads to almost identical climatic data since both localities contain several identical plant taxa, but in different amounts. Although the Mataschen flora is known for its high percentages of evergreen trees (Meller and Hoffmann, 2004; Kovar-Eder and Hably, 2006) and was discussed as a refuge area during the Late Miocene, the total rate

of all subtropical elements remains higher in the Early Miocene assemblage suggesting an overall warmer climate consequently. On the other hand, these data may also indicate an underestimation of the warm climate conditions of earliest Tortonian by other reconstructions. Another problematic aspect of using the Coexistence Approach occurred by describing climatic changes on less than millennial scale. It is difficult to reveal vegetation dynamics with a sample resolution of roughly one decade by presence/absence data only. The climatically significant elements often class among the rare elements, especially in the offshore settings of Lake Pannon. The absence of such an element in a single sample along the core would result in a different Coexistence Interval for the sample even if this element occurs in the surrounding samples. Despite non-forested vegetation is known to respond quickly to alternations in the environment (Chapter 3), trees and several perennial plants within naturally balanced vegetation lack this capacity and may be expected to display a delayed response. Thus, the absence of a taxon in a sample during very short intervals may usually be explained by taphonomic bias and its overall pollen scarcity in the total plant community. Nevertheless, this plant is probably still present and therefore might be an important taxon for paleo-climate estimate of the studied section. If such climate indicating elements are repetitively missing, this allows at least conclusions on iteratively occurring processes which influence fossilization potential and/or transport mechanisms.
In the Coexistence Analysis, however, this would result in unrealistic severe and quick changes in estimated climatic boundaries. To overcome this problem, one solution may be creating running mean values to decipher trends (Chapter 3).
Despite all these problematic issues, the Coexistence Approach is still by far the most reliable way to calculate temperature from a pollen assemblage. In particular, it provides absolute climatic data, which can additionally be compared with recent localities around the globe (e.g. Utescher et al., 2009).

6.3. Presence of sub-Milankovitch cycles in the Late Miocene

The cause of the cyclic signals in geological archives remains enigmatic. All herein studied localities exhibit repetitive signals on different levels and frequencies but only the long Hennersdorf core was sufficient to document statistically significant cycles (Chapter 4 and 5). A prerequisite for their analysis is a high sample number, which allows detecting the supposed cycles at least 3–4 times within the record. Further, the cycle duration shall comprise multiple times of the time resolution to avoid a signal representing simply provided by the age model. At Mataschen (Chapter 3), several elements showed peaks in the spectral analysis, but none crossed the border of the 95% confidence interval. Especially the ratio of autotrophic and heterotrophic dinoflagellate cysts reflects repetitive turnovers of the assemblages. As the used age model offers a wide range of 7–14 years per sample (Gross et al., 2011), these cyclic events could not be identified as any distinct solar cycle. But the calculated frequencies would fit either to the upper Gleissberg cycle (90–140 years; Orgutsov et al., 2007) or to the deVries/Suess cycle (~200 years) (Damon and Sonett, 1991; Stuiver and Brazinas, 1993). Therefore, the studies on the 6-m-long Hennersdorf core were conducted particularly to test the hypothesis that observed cycles are related to solar forcing. Based on the calculated sedimentation rate, the data on natural gamma radiation, magnetic susceptibility, total abundance of ostracods and molluscs cover about 8200 years of Late Miocene time. Thus, the record is long enough to detect and discuss most known solar cycles except for the shortest ones, which are too close at sample resolution. Indeed, the presence of solar forcing is certain and the lower and upper Gleissberg cycle, the deVries/Suess cycle, the 500-years and 1000-years-cycle and the Hallstatt cycle can be detected, though none of the proxies alone does reflect all. In addition, a non-sun-related 1500-years-cycle is significant. Some peaks of one proxy, though present, remain below the 95% confidence interval but are very distinct in others. Additionally, even those cycles which are significant in all proxies (e.g. the deVries cycle) display different modulations for each proxy. The synchronicity of turning points in the modulations of the filtered curves of largely independent proxies was striking, supporting the assumption of a common trigger. Therefore, this modulation was investigated in more detail for the 150-sample by additional palynological record and geochemistry of the Hennersdorf core (Chapter 5), which reveals a distinct imprint of the lower and upper Gleissberg cycles. The expression of these cycles is coupled with the 1000-years and 1500-years-cycles. The 1000-years-cycle modulated especially the lake surface proxies, while the 1500-years-cycle is mainly reflected in hinterland proxies, indicating strong influence on transport mechanisms. The repetitive changes in the palynological spectra can be interpreted as variations in the wind pattern, leading to different amounts of sediment and pollen input. Although the alternation of prevailing wind directions fits to the explanation of solar influence (Svensmark and Friis-Christensen, 1997) the question to which degree longer solar cycles determine climatic conditions remains unsolved.

Despite the precise environmental data for the land, surface water and bottom water conditions, no straightforward interpretation of solar influence on ecosystems can be presented. Furthermore, it remains difficult to decipher the effect of each solar cycle in particular, whereas a modulating effect and heterodynes between various solar cycles are evident (Chapter 5). This complex situation, however, is comparable to the short solar forcing modulation known from the last millennium (e.g. Grey et al., 2010). These data suggest treating studies based on one single proxy with caution, as this may not be able to detect all possible solar cycles.

An important outcome is the very prominent presence of the 1500-year-cycle. Considering all known sub-Milankovitch cyclicities, this 1500-year-cycle remains un-resolved so far as it has no direct link to solar activity (e.g. Solanki et al., 2004). Nevertheless, its presence in all proxies (Chapter 4) as well as its modulating force on small-scale solar cycles (Chapter 5) documents it as a strong factor for environmental evolution.

6.4. Conclusion

While astronomical tuning fostered time resolutions in geological records down to Milankovitch cycles (10^4–10^6 yr), few studies exist that try to resolve the resolution beyond those scales in pre-Quaternary records. This, however, will be crucial to achieve a deeper understanding of Earth's climate system in the past and make serious predictions for the future. Here I present first key studies to explore the strength of high resolution studies in Neogene coastal marine and lacustrine settings. Sub-Milankovitch cycles can be detected in these geological archives to a high degree of probability – although direct evidence is missing so far. The resolution ranges from millennia down to decadal-scale cycles such as the Gleissberg solar cycle. Since all known solar cycles have a quasi-periodic pace, peaks in spectral analyses of geological records will always scatter within a certain bandwidth rather than be presented by single peaks. Thus, large data series are necessary to detect statistically significant frequencies in REDFIT and Lomb-Scargle periodograms. These can be obtained quickly and at low costs by using geophysical data on magnetic susceptibility and/or natural gamma radiation, whereas sample preparation and analysis for palynology is incomparably more time consuming and labor-intensive. Therefore, geophysical data should provide the basis for statistic analysis to reveal the potential presence of any cyclicity before biotic data are evaluated in a second step. These, however, are then the prerequisite to understand the influence of the Sun's activity on the Earth's environments. Important patterns of climate fluctuations, which influenced the Miocene environments, are completely overlooked so far. Thus, intense efforts to build up a global high-resolution climate archive will be urgently needed to herald a new age of time-resolution in pre-Quaternary records, focusing on 10–10^3 scales.

Chapter 7

References and supplementary material

7.1 References collection from Chapter 1 and 6

Adam, P., 1990. Saltmarsh Ecology. Cambridge University Press, Cambridge, 461 p.

Agustí, J., Cabrera, L., Garcés, M., Llenas, M., 1999. Mamman turnover and global climatic change in the late Miocene terrestrial record of the Vallès Penedès (NE Spain). In: Agustí, J., Rook, L., Andrews, P. (Eds.) Hominoid evolution and climate change in Europe, Volume 1: The evolution of Neogene terrestrial ecosystem in Europe. Cambridge University Press, Cambridge 397–412.

Alley, R.B., 2000. Ice-core evidence of abrupt climate changes. Proceedings of the National Academy of Science USA 97, 1331–1334.

An, Z., Kutzbach, J.E., Prell, W.L., Porter, S.C., 2001. Evolution of Asian monsoons and phased uplift of the Himalaya-Tibet plateau sine late Miocene times. Nature 411, 62–66.

Babcock, H. W., 1961. The Topology of the Sun's Magnetic Field and the 22-year Cycle. Astrophysical Journal 133, 572.

Baldi, T., 1980. The early history of the Paratethys. (Bulletin of the Hungarian Geological Society 110, 456–472.

Beer, J., Andree, H., Oeschger, H., Stauffer, B., Balzer, R., Bonani, G., Stoller, M., Suter, M., Wölfli, W., Finkel, R.C., 1983. Temporal Be-10 variations in Ice. Radiocarbon 25, 269–278.

Beer, J., Blinov, A., Bonani, G., Finkel, R.C., Hofmann, H.J., Lehmann, B., Oeschger, H., Sigg, A., Schwander, J., Staffelbach, T., Stauffer, B., Suter, M., Wölfli, W., 1990. Use of ^{10}Be in polar ice to trace the 11-year cycle of solar activity. Nature 347, 164–166.

Beer, J., Mende, W., Stellmacher, R. 2000. The role of the sun in climate forcing. Quaternary Science Reviews. Bruch, A.A., Utescher,T., Mosbrugger, V., Gabrielyan, I., Ivanov, D.I., 2006. Late Miocene climate in the circum-Alpine realm – a quantitative analysis of terrestrial palaeofloras. Palaeogeography, Palaeoclimatology, Palaeoecology 238, 270–280.

Benevolenskaya, E.E., 1998. A Model of the Double Magnetic Cycle of the Sun. The Astrophysical Journal 509, L49–L52, doi:10.1086/311755.

Birks, H. J. B., Birks, H. H., 1980. Quaternary Palaeoecology. Edward Arnold, London, pp. 289.

Böhme, M., 2003. Miocene Climatic Optimum: evidence from Lower Vertebrates of Central Europe. Palaeogeography, Palaeoclimatology, Palaeoecology 195, 389–401.

Böhme, M., Bruch, A.A., Selmeier, A., 2007. The reconstruction of Early and Middle Miocene climate and vegetation of Southern Germany as determined from the fossil wood flora. Palaeogeography, Palaeoclimatology, Palaeoecology 253, 91–114.

Böhme, M., Ilg, A., Winklhofer, M., 2008. Late Miocene "washhouse" climate in Europe. Earth and Planetary Science Letters 275, 393–401.

Böhme, M., Ilg, A., Ossig, A., Küchenhoff, H., 2006. A new method to estimate paleoprecipitation using fossil amphibians and reptiles and the Middle and Late Miocene precipitation gradients in Europe. Geology 34, 425–428.

Bonan, G.B., Pollard, D., Thomson, S.I., 1992. Effects of boreal forest vegetation on global climate. Nature 359, 716–718.

Bond, G.C., Lotti, R., 1995. Iceberg Discharges into the North Atlantic on millennial time scales during the Last Glaciation. Science 267, 1005–1010.

Bond, G.C., Showers, W., Cheseby, M., Lotti, R., Almansi, P., deMenocal, P., Priore, P., Cullen, H., Hadjdas, I., Bonani, G., 1997. A pervasive millennial-scale cycle in North Atlantic Holocene and Glacial climates. Science 278, 1257–1266.

Brandano, M., Brilli, M, Corda, L., Lustrino, M., 2010. Miocene C-isotope signature from the central Apennine successions (Italy): Monterey vs. regional controlling factors. Terra Nova 22, 125–130.

Bray, R. J., Loughhead, R. E., 1965. Sunspots. Wiley, New York, pp. 261.

Bruch, A.A., Uhl, D., Mosbrugger, V., 2007. Miocene climate in Europe - patterns and evolution. Palaeogeography, Palaeoclimatology, Palaeoecology 253, 1–7.

Bruch, A.A., Utescher, T., Alcade Olivares, C., Dolakova, N., Mosbrugger, V., 2004. Middle and Late Miocene spartial temperature pattern and gradients in Central Europe – preliminary results based on paleobotanical climate reconstructions. Courier Forschungsinstiture Senkenberg 249, 15–27.

Bruch, A.A., Utescher, T., Mosbrugger, V., Gabrielyan, I., Ivanov, D.A., 2006. Late Miocene climate in the circum-Alpine realm - a quantitative analysis of terrestrial palaeofloras. Palaeogeography, Palaeoclimatology, Palaeoecology 238, 270–280.

Bruch, A.A., Utescher, T., Mosbrugger, V. and NECLIME members, 2011. Precipitation patterns in the Miocene of Central Europe and the development of continentality. Palaeogeography, Palaeoclimatology, Palaeoecology 304, 202–211.

Chapman, M.R., Shackleton, N.J., 2000. Evidence of 550-year and 1000-year cyclicities in North Atlantic circulation patterns during the Holocene. The Holocene 10, 287–291.

Charatova, I. 2000. Can origin of the 2400-year cycle of solar activity be caused by solar inertial motion? Annuales Geohysicae 18, 399–405.

Cubasch, U., Zorita, E., Kaspar, F., Gonzalez-Rouco, J.F., von Storch, H., Prömmel, K., 2006. Simulation of the role of solar and orbital forcing on climate. Advances in Space Research 37, 1629–1634.

Damon, P.E., Sonett, C.P., 1991. Solar and terrestrial components of the atmospheric ^{14}C variations spectrum. In: Sonett, C.P., Giampapa, M.S., Matthews, M.S. (Eds.) The Sun in Time. University of Arizona, Tuscon, 360–388.

Dansgaard, W., 1985. Greenland ice core studies. Palaeogeography, Palaeoclimatology, Palaeoecology 50, 185–189.

Dansgaard, W., Johnsen, S.J. Moller, J., Langway, C.C. Jr., 1969. One thousand centuries of climatic record from Camp Century on the Greenland ice sheet. Science 166, 377–381.

de Boer, P.L. and Smith, D.G. 2009 (eds). Orbital Forcing and Cyclic Sequences. IAS Special Publication 19, 1–576.

De Noblet, N.I., Prentice, I.C., Joussaume,S., Texier, D., Botta, A., Haxeltine, A., 1996. Possible role of atmosphere-biosphere interactions in triggering the last glaciations. Geophysical Research Letters 23, 3191–3194.

Debret, M., Bout-Roumazeilles, V., Grousset, F., Desmet, M., McManus, J.F., Massei, N., Sebag, D., Petit, J.-R., Copard, Y., Trentesaux, A., 2007. The origin of the 1500-year climate cycles in Holocene North-Atlantic records. Climate of the Past 3, 569–575.

Debret, M., Bout-Roumazeilles, V., Grousset, F., Desmet, M., McManus, J.F., Massei, N., Sebag, D., Petit, J.-R., Copard, Y., Trentesaux, A., 2007. The origin of the 1500-year climate cycles in Holocene North-Atlantic records. Climate of the Past 3, 569–575.

Debret, M., Sebag, D., Crosta, X., Massei, N., Petit, J.-R., Chapron, E., Bout.Roumazeilles, V., 2009. Evidence from wavelet for a mid-Holocene transition in global climate forcing. Quaternary Science Reviews 28, 2675–2688.

Di Rita, F., 2011. A possible solar pacemaker for Holocene fluctuations of a salt-marsh in southern Italy. Quaternary International. doi: 10.1016/j.quaint.2011.11.030

Eddy, J.A., 1976. The Maunder Minima. Science 192, 1189–1202.

Eronen, J.T. 2006. Eurasian Neogene large herbivorous mammals and climate. Acta Zoologica Fennica 216, 1–72.

Fairbridge, R.W., Sanders, J.E., 1987. The Sun's orbit, A.D. 750–2050: basis for new perspectives on planetary dynamics and Earth–Moon linkage. In: Rampino, M.R., Sanders, J.E., Newman, W.S., Koenigsson, L.K. (Eds.), Climate, History, Periodicity, and Predictability. Nostrand Reinhold, New York, pp. 446– 471.

Flato, G.M., Boer, G.J., 2001. Warming asymmetry in climate change simulations. Geophysical Research Letters 28, 195–198.

Fortelius, M., Eronen, J.T., Jernvall, J., Liu, L., Pushkina, D., Rinne, J., Tesakov, A., Vislobokova, I., Zhang, Z., Zhou, L., 2002. Fossil Mammals Resolve Regional Patterns of Eurasian Climate Change During 20 Million Years. Evolutionary Ecology Research 4, 1005–1016.

Fortelius, M., Eronen, J.T., Liu, L., Pushkina, D., Tesakov, A., Vislobokova, I.A., Zhang, Z., 2006. Late Miocene and Pliocene large land mammals and climatic changes in Eurasia. Palaeogeography, Palaeoclimatology, Palaeoecology 238, 219–227.

François, L., Ghislain, M., Otto, D., Micheels, A., 2006. Late Miocene vegetation reconstruction with the CARAIB model. Palaeogeography, Palaeoclimatology, Palaeoecology 238, 302–320.

Friis-Christiansen, E., Svensmark, H., 1997. What do we really know about the sun-climate connection? Advances in Space Research 20, 913–921.

Givulescu, R., 1957. Flora pliocena de la Cornitel. Bibliotheca Gelogica Palaeontologica 3, 1–130.

Gleissberg, 1939. Observatory 62, 158.

Gleissberg, W., 1965. The eighty-year cycle in auroral frequency numbers. Journal of the British Astronomical Association 75, 227.

González, C., Dupont, L., 2010. Tropical vegetation evidence for rapid sea level changes associated with Heinrich Events. IOP Conference Series: Earth and Environmental Science 9, 012003, 1–8.

Gordon, A.H., 1992. Interhemispherics constants of mean global temperature anomalies. International Journal of Climatology 12, 1–9.

Gray, L.J., Beer, J., Geller, M., Haigh, J.D., Lockwood, M., Matthes, K., Cubasch, U., Fleitmann, D., Harrison, G., Hood, L., Luterbacher, J., Meehl, G.A., Shindell, D., van Geel,B., White, W., 2010. Solar influences on climate. Reviews of Geophysics 48, RG4001, 1–53.

Grootes, P.M., Stuiver, M., White, J.W.C., Johnsen, S.J. and Jouzel, J., 1993. Comparison of oxygen isotope records from the GISP2 and GRIP Greenland ice cores. Nature 366, 552–554.

Gross M., Minati K., Danielopol D.L., Piller W.E., 2008. Environmental changes and diversification of Cyprideis in the Late Miocene of the Styrian Basin (Lake Pannon, Austria). Senckenbergiana lethaea 88, 161–181.

Gross, M., Piller, W.E., Scholger, R., Gitter, F., 2011. Biotic and abiotic response to palaeoenvironmental changes at Lake Pannon’s western margin (Central Europe, Lake Miocene). Palaeogeography, Palaeoclimatology, Palaeoecology 312, 181–193

Guiot, J., 1994. Statistical analysis of biospherical variability. In: Duplessey,J.-C., Spyridakis, M.-T. (eds.), Long-term climate variations. NATO ASI Series 22, 277–298.

Guo, Z.T., Ruddiman, W.F., Hao, Q.Z., Wu, H.B., Quao, Y.S., Zhu, R.X., Peng, S.Z., Wei,J.J., 2002. Onset of the Asian desertification by 22 Myr ago interfered from loess deposits in China. Nature 416, 159–163.

Hagenberg, T.K., Bond, G., deMenocal, P., 1994. Milankovitch band forcing of sub-Milankovitch climate variability during the Pleistocene. Paleooceanography 9, 545–558.

Hale, G. E., Ellerman, F., Nicholson, S. B., Joy, A. H., 1919. The Magnetic Polarity of Sun-Spots. Astrophysical Journal 49, 153.

Harrison, T.M., Yin, A., 2004. Timing and processes of Himalayan and Tibet uplift. Himalayan Journal of Sciences 2, 152–153.

Harzhauser, M., Mandic, O., 2004. The muddy bottom of Lake Pannon – a challenge for dressenid settlement (Late Miocene; Bivalva). Palaeogeography, Palaeoclimatology, Palaeoecology 204, 331–352.

Harzhauser, M., Piller, W.E., 2007, Benchmark data of a changing sea. – Palaeogeography, Palaeobiogeography and Events in the Central Paratethys during the Miocene. Palaeogeography, Palaeoclimatology, Palaeoecology 253, 8–31.

Harzhauser, M., Böhme, M., Mandic, O., Hofmann, Ch.-Ch., 2002. The Karpatian (Late Burdigalian) of the Korneuburg Basin – A Palaeoecological and Biostratigraphical Synthesis. Beiträge zur Paläontologie 27, 441–456.

Harzhauser, M., Piller, W.E., Müllegger, S., Grunert, P., Micheels, A. 2010. Changing seasonality patterns in Central Europe from Miocene Climate Optimum to Miocene Climate Transition deduced from the *Crassostrea* isotope archive. Global and Planetary Change 76, 77–84.

Harzhauser, M., Daxner-Höck, G., Piller, W.E., 2004. An integrated stratigraphy of the Pannonian (Late Miocene) in the Vienna Basin. Austrian Journal of Earth Science 95/96.

Harzhauser, M., Kern, A., Soliman, S., Minati, K., Piller, W.E., Danielopol, D.L., Zuschin, M., 2008. Centennial- to decadal scale environmental shifts in and around Lake Pannon. Palaeogeography, Palaeoclimatology, Palaeoecology 270, 102–115.

Hays, J.D., Imbrie, J., Shackleton, N.J., 1976. Variations in the Earth’s Orbit: Pacemaker of the Ice Ages. Science 194, 1121–1132.

Heinrich, H., 1988. Origin and consequences of cyclic ice rafting in the Northeast Atlantic Ocean during the past 130,000 years. Quaternary Research 29, 142–152.

Hemming, S.R., 2004. Heinrich events: massive late Pleistocene detritus layers of the North Atlantic and their global climate imprint. Reviews of Geophysics 42, RG1005, doi:10.1029/2003RG000128.

Heusser, L., Balsam,W.L., 1977. Pollen distribution in theNortheast Pacific Ocean.Quaternary Research 7, 45–62.

Hinnov, L.A., Schulz, M., Yiou, P., 2002. Interhemispheric space-time attributes of the Dansgaard-Oeschger oscillations between 100 and 0 ka. Quaternary Science Reviews 21, 1213–1228.

Hoffmann, W.A., Jackson, R.B., 2000. Vegetation-climate feedback in the conversion of tropical savanna and grassland. Journal of Climate 13, 1593–1602.

Hofmann, C.-C., Zetter, R., 2005. Reconstruction of different wetland plant habitats of the Pannonian Basin System (Neogene, Eastern Austria). Palaios 20, 266–279.

Hopkins, J.S., 1950. Differential flotation and deposition of coniferous and deciduous tree pollen. Ecology 31, 633–641.

Houghton, J.T., Callander, B.A., Varney, S.K., 1992 (Eds). Climate Change: The supplementary report to the IPCC 1991 Scientific Assessment, Cambridge University Press, Cambridge, UK.

Houghton, J.T., Meira Filho, L.G., Callender, B.A., Harris, N., Kattenberg, A., Maskell, K., 1995 (Eds.). The science of climate change. Cambridge University Press, Cambridge, UK.

Hoyt, D.V., Schatten, K.H., 1998. Group sunspot numbers. A new solar activity reconstruction. Solar Physics 179, 189–219.

Inouye, D.W., 2001. The ecoloy and evolutionary significance of frost in the context of climate change. Ecology Letters 3, 457–463.

Jakubcová, I., Pick, M., 1987. Correlation between solar motion, earthquake and other geophysical phenomena. Annales Geophysicae 5B, 135–141.

Jiménez-Moreno, G., Anderson, R.S., Fawcett, P.J., 2007. Orbital- and millennial-scale vegetation and climate changes of the past 225 ka from Bear Lake, Utah-Idaho (USA). Quaternary Science Reviews 26, 1713–1724.

Jiménez-Moreno, G., Fawcett, P.J., Anderson, R.S., 2008. Millennial- to centennial-scale vegetation and climate change during the late Pleistocene and Holocene from northern New Mexico (USA). Quaternary Science Reviews 27, 1442–1452.

Jiménez-Moreno, G., Rodríguez-Tovar, F.I., Pardo-Igúzquiza, E., Fauquette, S., Suc J.P., Müller, P., 2005. High-resolution palynological analysis in the late early-middle Miocene core from the Pannonian Basin, Hungary: climatic changes, astronimical forcing and eustatic fluctuations in the Central Paratethys. Palaeogeography, Palaeoclimatology, Palaeoecology 216, 73–97.

Jones, P.D., Parker, D.E., Osborn, T.J., Briffa, K.R., 2011. Global and hemispheric temperature anomalies – land and marine instrumental records. In: Trends, A Compendium of data on Global Change. Carbon Dioxide Information Analysis Center, Oak Ridge National Laboratory, U.S. Department of Energy, Oak Ridge, Tennessee, U.S.A., doi: 10.3334/CDIAC/cli.002

Jose, P.D., 1965. Sun's motion and sunspots. Astronomical Journal 70, 193–200.

Klaus, W., 1987. Einführung in die Paläobotanik: Grundlagen - Kohlebildung - Arbeitsmethoden einschließlich Palynologie. Deuticke, Vienna, Austria, pp. 314.

Kloosterboer-van Hoeve, Steenbrink, J., Visscher, H., Brinkhuis, H., 2006. Millennial-scale climatic cycles in the Early Pliocene pollen record of Ptolemais, northern Greece. Palaeogeography, Palaeoclimatology, Palaeoecology 229, 321–334.

Kollmann, K., 1965. Jungtertiär im Steirischen Becken. Mitteilungen der Geologischen Gesellschaft in Wien 57, 479–632.

Komitov, B., Kaftan, V. 2004. The sunspot activity in the last two millenia on the basis of indirect and instrumental Indexes: time series models and their extrapolations for the 21st Century. Proceedings of the International Astronomical Union 2004, 113–114.

Korpás-Hódi, M., 1983. Palaeoecology and biostratigraphy of the Pannonian Mollusca fauna in the northern foreland of the Transdanubian Central Range. Annales Hungarici Geologici Instituti 66, 1–163.

Kosi, W., Sachsenhofer, R.F., Schreilechener, M., 2003. High resolution sequence stratigraphy of upper Sarmatian and Pannonian units in the Styrian Basin, Austria. Österreichische Akademie der Wissenschaften, Schriftenreihe der Erdwissenschaftlichen Kommissionen 16, 63–86.

Kováč, M., Barath, I., Harzhauser, M., Hlavaty, I., Hudackova, N., 2004. Miocene depositional systems and sequence stratigraphy of the Vienna Basin. Courier Forschungsinstitut Senckenberg 246, 187–212.

Kovar-Eder, J., Hably, L., 2006. The flora of Mataschen – a unique plant assemblage from the late Miocene of eastern Styria (Austria). Acta Palaeobotanica 46, 157–233.

Kovar-Eder, J. & Kvaček, Z. 2007. The integrated plant record (IPR) to reconstruct Neogene vegetation: the IPR-vegetation analysis. Acta Palaeobotanica, 47 (2), 391–418.

Kovar-Eder, J., Kvaček, Martinetto, E., Roiron, P., 2006. Late Miocene to Early Pliocene vegetation of southern Europe (7–4 Ma) as reflected in the megafossil plant record. Palaeogeography, Palaeoclimatology, Palaeoecology 238, 321 – 339.

Kovar-Eder, J., Jechorek, H., Kvaček, Z., Parashiv, V., 2008. The integrated plant record to reconstruct Neogene zonal vegetation in Europe. Palaios 23, 97–111.

Kvaček, Z., 2007. Do extant nearest relatives of thermophile European Tertiary elements reliably reflect climatic signal? Palaeogeography, Palaeoclimatology, Palaeoecology 253, 32–40.

Kvaček, Z., Kovač, M., Kovar-Eder, J., Doláková, N., Jechorek, H., Parashiv, V., Kovačova, M., Sliva, L., 2006. Miocene evolution of landscape and vegetation in the Central Paratethys. Geologica Carpathica 57, 295–310.

Laskar, J., Joutel, F., Boudin, F., 1993. Orbital, precessional, and insolation quantities fro the Earth from -20 Myr to +10 Myr. Astronomy and Astrophysics 270. 522–533.

Laskar, J., Fienga, A., Gastineau, M., Manche, H., 2011. La2010: A new orbital solution for the long term motion of the Earth. Astronomy & Astrophysics, 532, id.A89.

Lear, C.H., Rosenthal, Y., Wright, J.D., 2003. The closing of a seaway: ocean water masses and global climate change. Earth and Planetary Science Letters 210, 425–436.

Lenz, O.K., Wilde, V., Riegler, W., Harms, F.-J., 2010. A 600 k.y. record of El Niño-Southern Oscillation (ENSO): Evidence for persisting teleconnections during the Middle Eocene greenhouse climate of Central Europe. Geology, 627–630.

Lewis**,** A.R., Marchant, D.R., Ashworth, A.C., Hemming, S.R., Machlus, M.L., 2007. Major middle Miocene global climate change: Evidence from East Antarctica and the Transantarctic Mountains: Geological Society of America Bulletin 119, 1449–1461.

Li, K.J., Yun, H.S., Gu, X.M., 2010. Hemispheric variations in solar activity. The Astronomical Journal 554, 115–117.

Linzer, H.-G., Decker, K., Peresson, H., Dellmour, R., Frisch, W., 2002. Balancing lateral orogenic float of the Eastern Alps. Tectonophysics 354, 211-237.

Lirer, F., Harzhauser, M., Pelosi, N., Piller, W.E., Schmid, H.P., Sprovieri, M., 2009. Astronomically forced teleconnection between Paratethyan and Mediterranean sediments during the Middle and Late Miocene Palaeogeography, Palaeoclimatology, Palaeoecology 275, 1–13.

Liu, L., Eronen, J.T., Fortelius, M., 2009. Significant mid-latitude aridity in the middle Miocene of East Asia. Palaeogeography, Palaeoclimatology, Palaeoecology 279, 201–206.

Lodge, T.E., 2010.The Everglades Handbook – Understanding the Ecosystem. Taylor and Francis Group, Boca Raton.

MacFadden, B.J., 2005. Terrestrial mammalian herbivore response to declining levels of atmospheric CO_2 during the Cenozoic: Evidence from North American fossil horses (Family Equidae). In: Ehlinger, J.R., Cerling, T.E:, Dearing, M.D., (Eds.) A history of atmospheric CO_2 and its effect on plants, animals and the ecosystem. Ecological studies 177, 273–292.

Magyar, I., Geary, D.H., Müller, P., 1999. Paleogeographic evolution of the Late Miocene Lake Pannon in Central Europe. Palaeogeography, Palaeoclimatology, Palaeoecology 147, 151–167.

Mai, D.H., 1964. Die Mastixiodeen-Floren im Tertiär der Oberlausitz. Paläontologische Abhandlungen B (Berlin) 2, 1, 1–192.

Marsh, N., Svensmark, H., 2003. Galactic cosmic ray and El Niño Southern Oscillation trends in International satellite cloud climatology project D2 low-cloud properties. Journal of Geophysical Research 108 (D6)4195, doi: 10.1029/2001JD001264.

Marsh, N., Svensmark, H., 2004. Comment in “Solar influences on cosmic ray and cloud formation: A reassessment” by Bomin Sun and Raymond S. Bradley, Journal of Geophysical Research 109, D14205, doi: 10.1029/2003JD004063.

McCarthy, B.C., Small, C.J., Rubino, D.L., 2001. Composition, structure and dynamics of Dysart Woods, in old-growth mixed mesophytic forest of southeastern Ohio. Forest Ecology and Management 140, 193–213.

Meehl, G.A., Stocker, T.F., Collins, W.D., Friedlingstein, P., Gaye, A.T., Gregory, J.M., Kitoh, A, Knutti, R., Murphy, J.M., Noda, A., Raper, S.C.B., Watterson, I.G., Weaver, A.J., Zhao, Z.-C., 2007. Global climate projections. In: Solomon, S., Qin, D., Manning, M., Chen, Z., Marquis, M., Averyt, K.B., Tignor, M., Miller, H.L., (Eds.), Climate Change 2007: the physical basis: Contributions of Working Group I to the Forth Assessment Report of the Intergovernmental Panel on Climate Change. Cambridge University Press, Cambridge.

Meller, B., Hofmann, C.-C., 2004. Paleoecology of Diospore- and Palynomorph assemblages from Late Miocene lake sediments (Mataschen near Fehring, East Styria, Austria). Joannea Geologie und Paläontologie 5, 177–217.

Micheels, A., Bruch, A.A., Uhl, D., Utescher, T., Mosbrugger, V., 2007. A Late Miocene climate model simulation with ECHAM4/ML and its quantitative validation with terrestrial proxy data. Palaeogeography, Palaeoclimatology, Palaeoecology 253, 251–270.

Micheels, A., Burch, A.A., Mosbrugger, V., 2009. Miocene climate modeling sensitivity experiments for different CO_2 consentrations. Palaeontologica Electronica 12.2.5A. 20p.

Milankovitch, M., 1930. Mathematische Klimalehre und Astronomische Theorie der Klimaschwankungen. Handbuch der Klimatologie Band 1, Teil A, Borntrager Berlin.

Milankovitch, M., 1941. Kanon der Erdbestrahlung und seine Anwendung auf das Eiszeitproblem. Belgrade: Zavod Udžbenike I Nastavna Sredstva.

Molnar, P., 2005. Mio-Pliocene growth of the Tibetan Plateau and Evolution of the East Asian Climate. Palaeontologica Electronica 8, 1–23.

Moran, K., Backman, J., Brinkhuis, H., Clemens, S.C., Cronin, T., Dickens, G.R., Eynaud, F., Gattacceca, J., Jakobsson, M., Hordan, R.W., Kaminski, M., King, J., Koc, N., Krylov, A., Martinez, N., Matthiessen, J., McInroy, D., Moore,T.C., Onodera, J., O’Regan, M., Pälike, H., Rea, B., Rio, D., Sakamoto, T., Smith, D.C., Stein, R., St John, K., Suto, I., Suzuki, N., Takahashi, K., Watanabe, M., Yamamoto, M., Farrell, J., Frank, M., Kubik, P., Jokat, W., Kristoffersem, Y., 2006. The Cenozoic palaeoenvironment of the Arctic Ocean, Nature 441, 601–605.

Mosbrugger, V., Utescher, T., 1997. The coexistence approach - a method for quantitative reconstructions of Tertiary terrestrial palaeoclimate data using plant fossils. Paleogeography, Palaeoclimatology, Palaeoecology 134, 61–86.

Mosbrugger, V., Utescher, T., Dilcher, D., 2005. Cenozoic continental climatic evolution of Central Europe. Proceedings of the National Academy of Sciences 102 (42), 14964–14969.

Müller, P., Geary, D.H., Magyar, I., 1999. The endemic molluscs of the Late Miocene Lake Pannon: their origin, evolution, and family taxonomy. Lethaia 32, 47–60.

Muñoz, A., Ojedaa, J., Sánchez-Valverde, B., 2002. Sunspot-like and ENSO/NAO-like periodicities in lacustrine laminated sediments of the Pliocene Villarroya Basin (La Rioja, Spain). Journal of Paleolimnology 27, 453–463.

Nederbragt, A.J., Thurow, J., 2005. Geographic coherence of millennial-scale climate cycles during the Holocene. Palaeogeography, Palaeoclimatology, Palaeoecology 221, 313–324.

Neff, U., Burns, S.J., Mangini, A., Mudelsee, M.,Fleitmann, D.,Matter, A., 2001. Strong coherence between solar variability and the monsoon in the Oman between 9 and 6 kyr ago. Nature 411, 290–293.

Neubauer, F., Genser, J., 1990. Achitektur und Kinematik der östlichen Zentralalpen – eine Übersicht. Mitteilungen des Naturwissenschaftlichen Vereins für Steiermark 120, 203–219.

Niggemann, S., Mangini, A., Mudelsee, M., Richter, D.K., Wurth, G., 2003. Sub-Milankovitch climate cycles in Holocene stalagmites from Sauerland, Germany. Earth and Planetary Science Letters 216, 539–547.

Nordemann, D.J.R., Rogozo, N.R., de Faria, H.H., 2005. Solar activity and El Niño signals observed in Brazil and Chile tree ring records. Advances in Space Research 35, 891–896.

Ogurtsov, M.G., Nagovitsyn, Y.A., Kocharov, G.E., Jungner, H., 2002. Long-period cycles of the sun’s activity recorded in direct solar data and proxies. Solar Physics 211, 371–394.

Pagani, M., Freeman, K.H., Arthur, M.A., 1999. Late Miocene Atmospheric CO_2 Concentrations and the Expansion of C_4 Grasses. Science 285, 5429, 876–879.

Papp, A., 1951. Das Pannon des Wiener Beckens. Mitteilungen der Geologischen Gesellschaft in Wien 39–41, 99–193.

Paulissen, W.E., Luthi, S.M., 2011. High-frequency cyclicity in a Miocene sequence of the Vienna Basin established from high—resolution logs and robust chronostratigraohic tuning. Palaeogeography, Palaeoclimatology, Palaeoecology 307, 313–323.

Paulissen, E. Luthi, S.M., Grunert, P. Ćorić, S., Harzhauser, M., 2011. Integrated high-resolution stratigraphy of a Middle to Late Miocene sedimentary sequence in the central part of the Vienna Basin. Geologica Carpathica 62, 155-169.

Peristykh, A.N., Damon, P.E., 2003. Persistence of the Gleissberg 88-year solar cycle over the last ~12,000 years: Evidence from cosmogenic isotopes. Journal of Geophysical Research 108, NO. A1, 1003, doi: 10.1029/2002JA009390.

Perry, C.A., Hsu, K.J., 2000. Geophysical, archaeological, and historical evidence support a solar-output model for climate change. Proceedings of the National Academy of Sciences 97, 12433–12438.

Piller, W.E., Harzhauser, M., Mandic, O., 2007. Miocene Central Paratethys stratigraphy - current status and future directions. Stratigraphy 4, 151–168.

Popov, S.V., Rögl, F., Rozanov, A.Y., Steininger, F.F., Shcherba, I.G., Kováč, M., 2004. Lithological-Paleogeographic maps of Paratethys. 10 Maps Late Eocene to Pliocene: Courier Forschungsinstitut Senckenberg 250, 1– 46.

Pound, M.J., Haywood, A.M., Salzmann, U., Riding, J.B., Lunt, D.J.,Hunter, S.J., 2011. A Tortonian (Late Miocene, 11.61–7.25 Ma) global vegetation reconstruction. Palaeogeography, Palaeoclimatology, Palaeoecology 300, 29–45.

Raspopov, O.M., Dergachev, V.A., Esper, J., Kozyreva, O.V., Frank, D., Ogursov, M., Kolström, T., Shao, X., 2008. The influence of the de Vries (~200-year) solar cycle on climate variations: Results from the Central Asian Mountains and their global link. Palaeogeography, Palaeoclimatology, Palaeoecology 259, 6–16.

Raspopov, O.M., Dergachew, V.A., Kolström, T., 2004. Periodicity of climate conditions and solar variability derived from dendrochronological and other palaeoclimatic data in high latitudes. Palaeogeography, Palaeoclimatology, Palaeoecology 209, 127–139.

Ratschbacher, L., Frisch, W., Linzer, H.-G., Merle, O., 1991. Lateral extrusion in the Eastern Alps 1. Structural Analysis. Tectonics 10, 257–271.

Rigoz, N.R., da Silva, H.E., Nordemann, D.J.R., Echer, E., de Souza Echer, M.P., Prestes, A., 2008. The Medieval and Modern Maximum solar activity imprints in tree ring data from Chile and stable isotope records from Antarctica and Peru. Journal of Atmospheric and Solar-Terrestrial Physics 70, 1012–1024.

Robock, A., 1979. The “Little Ice Age”: Northern hemisphere average observations and model calculations. Science 206, 1402–1404.

Rodrígez-Tovar, F., Pardo-Igúzquiza, E., 2003. Strong evidence of high-frequency (sub-Milankovitch) orbital forcing by amplitude modulation of Milankovitch signals. Earth and Planetary Science Letters 210, 179–189.

Rögl, F., 1998. Palaeogeographic considerations for Mediterranean and Paratethys Seaways (Oligocene to Miocene). Annalen des Naturhistorischen Museums Wien 99 A, 279–310.

Rögl, F., 1999. Mediterranen and Paratethys. Facts and hypotheses of an Oligocene to Miocene paleogeography (short overview) Geologica Carphatica 50, 339–349.

Royden, L. H.; Horvath, F. The Pannonian System. A study in basin evolution. American Association of Petrolium Geology Memoirs 45, 333 - 346.

Rusu, A., 1988. Oligocene events in Transylvania (Romania) and the first separation of Paratethys. Dari Seama, Inst. Geo. Geofiz. 72–73, 207–223.

Sachsenhofer, R. F., 1996. The Neogene Styrian Basin: An overview. Mitteilungen der Gesellschaft der Bergbaustudenten Österreichs 41, 19–32.

Sanchez-Goni, M.F., Cacho I., Turon, J.L., Guiot, J., Sierro, F.J., Peypouquet, J.P., Grimalt, J., Shackleton, N.J., 2002. Synchronicity between marine and terrestrial responses to millennial scale climatic variability during the last glacial period in the Mediterranean region. Climate Dynamics 19, 95–105.

Schimmelmann, A., Lange, C.B., Meggers, B.J., 2003. Palaeoclimatic and archaeological evidence for a ~200-yr recurrence of floods and droughts linking California, Mesoamerica and South America over the past 2000 years. The Holocene 13, 763–778.

Schwabe, H., 1844. Sonnen-Beobachtungen im Jahre 1843. Astronomische Nachrichten 495, 233–236.

Shevenell, A.E., Kennett, J.P., Lea, D.W., 2004. Middle Miocene Southern Ocean cooling and Antarctic cryosphere expansion: Science 305, 1766–1770.

Solanki, S.K., Usoskin, I.G., Kromber, B., Schüssler, M., Beer, J., 2004. Unusual activity of the Sun during recent decades compared to the previous 11,000 years. Nature 431, 1084–1087.

Sonett, C.P., Finney, S.A., 1990. The spectrum of radiocarbon. Philosophical Transactions of the Royal Society London, series A 330, 413–426.

Sonett, C.P., Suess, H.E., 1984. Correlation of bristlecone pine ring widths with atmospheric ^{14}C variations: a climate-sun relation. Nature 307, 141–143.

Sovis, W., Schmid, B., 1998. Das Karpat des Korneuburger Beckens, Teil 1. Beiträge zur Paläontologie 23, 1–413.

Sovis, W., Schmid, B., 2002. Das Karpat des Korneuburger Beckens, Teil 2. Beiträge zur Paläontologie 27, 1–467.

Spicer, R.,A., Harris, N.B.W., Widdowson, M., Herman, A.B., Guo, S., Valdes, P.J., Wolfe, J.A., Kelley, S.P., 2003. Constant elevation of Southern Tibet over the past 1 million years. Nature 412, 622–624.

Steininger, F.F., Berggren, W.A., Kent, D.V., Bernor, R.L., Sen, S., Agusti, J., 1996. Circum-Mediterranean Neogene (Miocene and Pliocene) marine-continental chronologic correlations of European mammal units. In: Bernor, R.L., Fahlbusch, V., Mittmann, H.-W. (Eds.), The Evolution of Western Eurasian Neogene Mammal Faunas. Columbia University Press, New York, pp. 7–46.

Steppuhn, A., Micheels, A., Bruch, A.A., Uhl., D., Utescher, T., Mosbrugger, V., 2007. The sensitivity of ECHAM4/ML to a double CO_2 scenario for the Late Miocene and the comparison to terrestrial proxy data. Global and Planetary Change 57, 189–212.

Stuchlik, L., Ivanov, D, Palamarev, E., 1999. Middle and Late floristic changes in the northern and southern parts of the Central Paratethys. Acta Palaeobotanica, Suppl. 2, 391–397.

Stuiver, M., Braziunas, T.F., 1993. Sun, Ocean, Climate and Atmospheric $^{14}CO_2$, an evaluation of causal and spectral relationships. The Holocene 3, 289–305.

Stuiver, M., Grootes, P.M., Braziunas, T.F., 1995. The GISP2 $\delta^{18}O$ record of the past 16,500 years and the role of the sun, ocean and volcanoes. Quaternary Research 44, 341–354.

Suess, H.E., 1980. The radiocarbon in tree rings f the last 8000 years, Radiocarbon 22, 200–209.

Sun, J., Zhang, Z. 2008. Palynological evidence for the Mid-Miocene Climatic Optimum recorded in Cenozoic sediments of the Tian Shan Range, northwestern China. Global and Planetary Change 64, 53–68.

Sun, X., Wang, P., 2005. How old is the Asian monsoon system? – Palaeobotanical records from China. Palaeogeography, Palaeoclimatology, Palaeoecology 222, 181–222.

Süto-Szentai, M., 1991. Szervesvázú mikroplankton zónák Magyarország pannóniai rétegösszletében. Újabb adatok a zonációról és a dinoflagelláták evolúciójáról. Öslénytani Vitak (Disscuss. Palaeontol.) 36–37, 157–200.

Svensmark, H., Friis-Christensen, E., 1997. What do we really know about the sun-climate connection? Advances in Space Research 20, 913–921.

Taricco, C., Ghil, M., Alessio, S., Vivaldo, G., 2009. Two millennia of climate variability in the Central Mediterranean. Climate of the Past 5, 171–181.

Tripple, B.J., Pagani, M., 2007. The early origins of terrestrial C_4 photosynthesis. Annual Review of Earth and Planetary Science 35, 435–461.

Tsiropoula, G., 2003. Signatures of solar activity variability in meteorological parameters. Journal of Atmospheric and Solar-Terrestrial Physics 65, 469–482.

Uhl, D., 2006. Fossil plants as palaeoenvironmental proxies – some remarks on selected approaches. Acta Palaeobotanica 46, 87–100.

Uhl, D., Bruch, A.A., Traiser, Ch., Klotz, S., 2006. Palaeoclimate estimates for the Middle Miocene Schrotzburg flora (S-Germany) – A multi-method approach. International Journal of Earth Sciences 95, 1071–1085.

Utescher, T., Mosbrugger, V., Ashraf, A.R., 2000. Terrestrial climate evolution in Northwest Germany over the last 25 Million years. Palaios 15, 430–449.

Utescher, T., Mosbrugger, V., Ivanov, D., Dilcher, D.L., 2009. Present-day climatic equivalents of European Cenozoic climates. Earth and Planetary Science Letters 284, 544–552.

Versteegh, G.J., 2005. Solar forcing of climate. 2: Evidence from the past. Space Science Reviews 120, 243–286.

von Rad, U., Schaaf, M., Michels, K.H., Schulz, H., Berger, W.H., Sirocko, F., 1997. A 5000-yr record of climate change in varved sediments from the oxygen minimum zone off Pakistan, Northeastern Arabian Sea. Quaternary Research 51, 39–53.

Vos, H., Sanchez, A., Zolitschka, B., Brauer, A., Negendank, J.F.W., 1997. Solar activity variations recorded in varved sediments from the Crater Lake of Holzmaar – a maar lake in the Westeifel volcanic field, Germany. Surveys in Geophysics 18, 163–182.

Wagner, G., Beer, G.J., Masarik, J., Muscheler, R., Kubik, P.W., Mende, W., Laj, C., Raisbeck, G.M., Yiou, F., 2001. Presence of the Solar de Vries Cycle (~205 years) during the Last Ice Age. Geophysical Research Letters 2, 303–306, doi:10.1029/2000GL006116.

Wang, X., Zhang, Q.-B., 2011. Evidence of solar signals in tree rings of Smith fir from Sygera Mountains in southeast Tibet. Journal of Atmospheric and Solar-Terrestrial Physics 73, 1959–1966.

Wessely, G., 1988. Structure and development of the Vienna basin in Austria. - In: L. Royden and F. Horváth (eds.). The Pannonian Basin. A study in basin evolution. American Association of Petroleum Geologists, Memoir 45, 333-346.

Wessely, G., 1998. Geologie des Korneuburger Beckens. Beiträge zur Paläontologie 23, 9–23.

Wiermann, S. Gubatz, 1992. Pollen wall and sporopollenin. International Review of Cytology - a Survey of Cell Biology 140, 35–72.

Willard, D.A., Weimer, L.M., Riegel, W.L., 2001. Pollen assemblage as paleoenvironment proxies in the Florida Everglades. Review of Paleobotany and Palynology 113, 213–253.

Willson, R.C., Gulkis, S., Janssen, M., Hudson, H. S., Chapman, G.A., 1981. Observations of Solar Irradiance Variability. Science 211, 700–702.

Wolf, R., 1862. Astronomische Mitteilungen Zürich 14.

Wolfe, J.A., 1979. Temperature parameters of humid and mesic forest of Eastern Asia and relation to forests of other regions of the Northern Hemisphere and Australasia. U.S. Geological Survey professional paper 1106, 1–37.

Woodward, F.I., Williams, B.G., 1987. Climate and plant distribution at global and local scales. Plant Ecology 69, 1–3, 189–197.

Yin, Z.Q., Ma, L.H., Han, Y.B., Han, Y.G., 2007. Long-term variations of solar activity. Chinese Science Bulletin 52, 2737–2741.

Zachos, J.C., Stott, L.D., Lohmann, K.C., 1994. Evolution of early Cenozoic marine temperatures. Paleoceanography 9, 353–387.

Zachos, J., Pagani, M., Sloan, L., Thomas, E., Billips, K., 2001. Trends, rhythms, and aberrations in global climate 65 Ma to present. Science 5517, 686–693.

Zetter, R., 1989. Methodik und Bedeutung einer routinemäßig kombinierten lichtmikroskopischen und rasterelektronenmikroskopischen Untersuchung fossiler Mikrofloren. Courier Forschungsinstitut Senkenberg 109, 41–50.

Zetter, R., Ferguson, D.K., 2001. Trapaceae pollen in the Cenozoic. Acta Palaeobotanica 41, 321–339.

7.2. Supplementary material <u>Chapter 2</u>

7.2.1. Pollen countings **(Table 2.1)**

The table shows the counted results of all samples (SPK-C1 -2 to SPK-C1 21) for all determined pollen taxa. Additionally, percentage data of angiosperms opposed to gymnosperms and the percentages of gymnosperms, angiosperms, spores and dinoflagellates are shown.

SPK-C1 samples	percentages of determinded pollen-taxa	*Pinus*	*Picea*	*Cathaya*	*Abies*	*Ephedra*	Taxodiaceae	*Sciadopitys*	*Carya*	*Pterocarya*	*Alnus*	*Engelhardia*	*Platycarya*	*Quercus*	*Celtis*	*Ulmus*
-2		9.09	4.55	2.27	2.27	0.00	25.00	0.00	13.64	4.55	13.64	2.27	0.00	2.27	4.55	2.27
-1.6		11.32	0.00	11.32	0.00	0.00	3.77	0.00	20.75	16.98	7.55	5.66	0.00	3.77	0.00	1.89
-1		32.00	4.57	18.86	4.00	0.00	1.14	0.00	5.71	6.86	12.57	1.14	0.00	1.71	0.57	0.00
-0.6		5.56	4.17	8.33	0.00	0.00	5.56	1.39	18.06	16.67	11.11	1.39	1.39	2.78	1.39	4.17
0		14.93	2.99	9.70	0.75	0.00	5.22	0.00	8.21	12.69	19.40	2.24	1.49	2.99	0.00	1.49
1		14.71	5.88	20.59	2.94	2.94	11.76	0.00	11.76	8.82	5.88	0.00	0.00	2.94	0.00	2.94
2		29.17	8.33	20.83	0.00	0.00	8.33	0.00	12.50	0.00	4.17	0.00	0.00	4.17	0.00	0.00
3		0.00	6.25	6.25	6.25	0.00	12.50	0.00	6.25	0.00	0.00	6.25	0.00	6.25	6.25	0.00
4		0.00	0.00	20.00	0.00	0.00	10.00	0.00	30.00	10.00	0.00	10.00	0.00	0.00	0.00	0.00
5		7.59	1.90	4.43	1.27	0.00	34.18	0.00	8.86	2.53	17.72	6.96	2.53	3.80	0.00	1.90
6		5.47	3.48	5.97	2.49	0.00	8.96	0.00	17.41	7.96	6.97	12.94	1.00	4.48	0.00	1.49
7		5.64	5.02	9.09	5.33	0.31	10.34	0.00	11.91	9.40	8.78	7.52	4.70	3.76	0.31	1.57
8		7.32	5.81	9.34	4.55	0.25	12.63	0.25	12.12	10.61	4.80	7.58	3.79	2.78	0.25	1.52
9		7.30	7.73	7.73	5.58	0.00	11.16	0.00	11.59	9.44	5.15	9.44	2.15	2.15	0.00	1.72
10		7.14	5.56	9.13	3.17	0.00	6.35	0.79	10.32	8.73	8.33	6.35	2.78	3.17	0.40	0.40
11		5.02	3.34	12.04	6.69	0.33	8.70	0.00	9.03	6.69	7.02	9.03	2.34	2.34	1.00	1.00
12		7.51	8.87	7.51	9.90	0.34	5.46	0.00	8.53	3.75	2.39	12.29	2.73	1.37	1.02	1.71
15		4.12	7.22	2.06	11.00	0.00	6.87	0.00	8.25	3.44	2.75	17.87	1.72	4.12	0.69	1.03
16		13.28	11.72	8.20	12.11	0.00	7.42	0.39	16.02	3.91	1.95	3.91	0.00	1.95	0.78	0.78
17		13.57	9.44	11.21	15.34	0.00	6.78	0.00	11.80	4.72	0.88	4.72	0.29	2.06	0.59	0.88
18		4.82	6.14	7.46	17.11	0.00	4.82	0.44	11.40	3.95	0.44	8.33	1.32	2.63	0.44	0.88
19		7.25	9.92	3.82	18.32	0.00	8.78	0.38	12.60	2.67	0.76	9.16	0.76	1.53	0.38	0.38
20		10.15	14.03	8.36	22.39	0.00	8.36	1.19	13.73	1.19	1.19	3.88	0.60	1.49	0.30	0.60
21		6.93	12.54	7.26	3.30	0.00	13.53	0.33	8.91	6.60	2.64	5.28	0.99	2.97	0.33	1.65

SPK-C1 samples	*Zelkova*	*Lonicera*	*Betula*	Tiliaceae	Lythraceae	Oleaceae	Arecaceae	*Symplocos*	Poaceae	*Fagus*	*Castanea*	*Carpinus*	*Liquidambar*	Amaranthaceae	Chenopodiaceae	*Artemisia*	Mastixiaceae	Sapotaceae
-2	0.00	0.00	0.00	0.00	0.00	0.00	2.27	0.00	4.55	0.00	2.27	0.00	0.00	0.00	0.00	0.00	0.00	0.00
-1.6	1.89	0.00	0.00	0.00	1.89	1.89	0.00	0.00	5.66	0.00	0.00	0.00	1.89	0.00	0.00	0.00	0.00	0.00
-1	0.00	1.14	0.00	6.86	0.57	0.57	0.00	0.00	0.00	0.00	0.00	0.00	0.00	0.00	0.00	0.00	0.00	0.00
-0.6	0.00	0.00	1.39	6.94	4.17	0.00	0.00	0.00	0.00	0.00	0.00	0.00	0.00	0.00	0.00	0.00	0.00	0.00
0	0.00	0.75	0.75	5.97	0.75	0.00	0.75	1.49	2.99	0.00	0.00	0.00	0.75	0.00	0.75	0.00	0.00	0.00
1	0.00	0.00	0.00	2.94	0.00	0.00	0.00	2.94	2.94	0.00	0.00	0.00	0.00	0.00	0.00	0.00	0.00	0.00
2	0.00	0.00	0.00	0.00	0.00	0.00	0.00	4.17	4.17	0.00	0.00	0.00	0.00	0.00	0.00	4.17	0.00	0.00
3	0.00	0.00	0.00	0.00	0.00	0.00	6.25	0.00	25.00	0.00	0.00	0.00	0.00	0.00	0.00	0.00	0.00	0.00
4	0.00	0.00	0.00	0.00	0.00	0.00	0.00	10.00	10.00	0.00	0.00	0.00	0.00	0.00	0.00	0.00	0.00	0.00
5	0.63	0.63	0.00	0.63	2.53	0.00	1.27	0.63	0.00	0.00	0.00	0.00	0.00	0.00	0.00	0.00	0.00	0.00
6	0.50	1.99	0.00	1.00	1.49	3.48	1.00	1.49	1.00	0.00	1.00	0.00	0.50	0.00	1.49	0.00	0.00	0.00
7	0.31	0.63	0.00	0.31	2.51	1.57	0.00	1.88	0.31	0.31	1.57	0.00	0.00	0.00	0.63	0.00	0.00	1.57
8	0.00	0.51	0.25	0.76	3.03	3.54	0.25	0.25	1.26	0.76	0.25	0.25	0.76	0.25	0.00	0.00	0.51	0.51
9	0.00	0.00	0.43	0.86	3.43	6.01	0.00	0.00	1.29	0.43	0.43	0.86	0.00	0.00	0.43	0.00	0.86	0.00
10	0.00	1.19	0.00	0.40	3.17	5.56	1.19	0.00	3.17	0.79	0.00	0.79	0.00	0.00	1.59	0.40	0.00	0.40
11	0.67	0.33	0.67	0.33	2.01	7.02	1.00	0.00	3.34	1.00	0.67	0.00	0.00	0.00	2.01	0.00	0.00	0.00
12	0.34	0.00	0.68	0.68	2.73	6.83	0.34	0.34	1.37	2.05	0.00	0.34	0.68	0.00	3.75	0.68	0.34	0.00
15	0.69	0.34	0.00	0.34	1.72	7.22	0.69	0.34	3.44	2.41	1.37	0.00	0.00	0.00	3.44	0.34	0.34	0.00
16	0.00	0.39	0.78	0.39	0.78	1.56	0.00	0.00	5.47	0.00	0.00	0.39	0.78	0.00	0.78	0.00	1.17	0.00
17	0.29	0.00	0.29	0.29	0.88	1.77	0.59	0.88	2.06	1.77	0.00	0.29	0.00	0.00	1.77	0.00	0.29	0.00
18	0.44	0.44	0.44	0.88	1.32	7.02	0.44	0.44	3.51	0.00	0.88	0.00	0.44	0.88	4.39	0.00	0.00	0.00
19	0.38	0.00	0.76	0.00	1.91	6.11	0.00	0.00	2.67	0.76	0.76	0.00	0.38	0.00	2.67	0.00	0.00	0.38
20	0.00	0.00	0.30	0.00	0.60	2.09	0.30	0.00	1.49	0.90	0.00	0.90	0.00	0.00	1.79	0.00	0.60	0.00
21	0.33	0.00	0.00	0.33	3.63	4.29	1.32	0.33	4.95	2.97	0.00	0.99	0.00	0.00	0.33	0.00	0.00	0.00

SPK-C1 samples	*Nyssa*	*Sparganium*	*Ilex*	*Myrica*	Loranthaceae	Euphorbiaceae	Ericaceae	Rutaceae	Rubiaceae	Elegnaceae	Araliaceae	Vitaceae	Fagaceae	Apiaceae	Cyperaceae	*Salix*	*Fraxinus*	Asteraceae	*Tricolporopollenites wackersdorfensis*
-2	0.00	0.00	0.00	0.00	0.00	0.00	0.00	0.00	0.00	0.00	0.00	0.00	0.00	0.00	0.00	0.00	4.55	0.00	0.00
-1.6	0.00	0.00	0.00	1.89	1.89	0.00	0.00	0.00	0.00	0.00	0.00	0.00	0.00	0.00	0.00	0.00	0.00	0.00	0.00
-1	0.00	1.14	0.00	0.00	0.00	0.00	0.57	0.00	0.00	0.00	0.00	0.00	0.00	0.00	0.00	0.00	0.00	0.00	0.00
-0.6	0.00	2.78	0.00	0.00	1.39	0.00	0.00	0.00	0.00	0.00	0.00	0.00	0.00	0.00	0.00	1.39	0.00	0.00	0.00
0	0.75	0.00	0.00	0.00	0.75	0.00	0.00	0.00	0.00	0.00	0.00	0.00	0.00	0.00	0.00	0.75	0.00	0.75	0.00
1	0.00	0.00	0.00	0.00	0.00	0.00	0.00	0.00	0.00	0.00	0.00	0.00	0.00	0.00	0.00	0.00	0.00	0.00	0.00
2	0.00	0.00	0.00	0.00	0.00	0.00	0.00	0.00	0.00	0.00	0.00	0.00	0.00	0.00	0.00	0.00	0.00	0.00	0.00
3	0.00	0.00	0.00	0.00	0.00	0.00	0.00	6.25	0.00	0.00	0.00	0.00	0.00	0.00	6.25	0.00	0.00	0.00	0.00
4	0.00	0.00	0.00	0.00	0.00	0.00	0.00	0.00	0.00	0.00	0.00	0.00	0.00	0.00	0.00	0.00	0.00	0.00	0.00
5	0.00	0.00	0.00	0.00	0.00	0.00	0.00	0.00	0.00	0.00	0.00	0.00	0.00	0.00	0.00	0.00	0.00	0.00	0.00
6	0.00	0.00	1.49	0.00	0.50	0.00	0.00	0.50	0.00	0.00	0.00	0.00	0.50	0.00	0.00	1.49	1.99	0.00	0.00
7	0.00	0.31	0.63	0.00	0.00	0.31	0.00	0.94	0.94	0.00	0.00	0.00	0.00	0.00	0.00	0.00	1.57	0.00	0.00
8	0.00	2.02	0.00	0.00	0.00	0.00	0.00	0.00	0.00	0.00	0.00	0.00	0.00	0.00	0.00	0.25	1.01	0.00	0.00
9	0.00	1.29	0.00	0.00	0.00	0.00	1.72	0.43	0.00	0.00	0.00	0.00	0.00	0.00	0.00	0.00	0.43	0.00	0.00
10	0.40	4.76	0.00	0.00	0.00	0.00	0.00	0.79	0.00	0.00	0.00	0.00	0.00	0.00	0.00	0.40	2.38	0.00	0.00
11	1.67	0.33	0.33	0.00	0.00	0.00	0.00	0.33	0.00	0.00	0.00	0.00	0.00	0.00	0.00	0.67	1.34	0.00	0.00
12	1.02	0.00	0.00	0.00	0.00	0.00	0.34	0.34	0.00	0.00	0.00	0.00	0.00	0.00	0.00	0.00	1.71	0.00	0.34
15	1.03	1.72	0.00	0.00	0.00	0.00	0.69	0.69	0.00	0.69	0.00	0.00	0.00	0.00	0.00	0.00	1.03	0.00	0.00
16	0.00	1.17	0.39	0.00	0.00	0.00	0.00	0.78	0.00	0.00	0.00	0.00	0.00	0.00	0.00	0.78	0.78	0.00	0.00
17	0.00	2.06	0.00	0.00	0.29	0.00	0.00	0.00	0.00	0.29	0.29	0.29	0.00	0.00	0.29	1.77	0.29	0.00	0.00
18	0.00	3.07	0.44	0.00	0.00	0.00	0.00	0.00	0.00	0.00	0.00	0.00	0.00	0.00	0.00	1.32	1.75	0.00	0.00
19	0.76	1.53	0.00	0.00	0.00	0.00	0.38	0.38	0.00	0.00	0.00	0.00	0.00	0.00	0.76	1.15	0.76	0.00	0.00
20	0.00	1.49	0.00	0.00	0.00	0.00	0.00	0.00	0.00	0.00	0.00	0.00	0.00	0.30	0.00	0.60	0.00	0.00	0.00
21	0.00	3.63	0.33	0.00	0.00	0.33	0.00	0.00	0.00	0.00	0.66	0.00	0.00	0.00	0.00	0.33	0.00	0.00	1.32

SPK-C1 samples	total pollen-taxa	percentages of determined gymnosperms	determined angiosperms	precentages of spores, pollen, dinoflagellates and algae: gymnosperms	angiosperms	spores	dinoflagellates	green algae
-2	16	43	57	15.14	42.16	41.62	1.08	0.00
-1.6	16	43	57	15.14	42.16	41.62	1.08	0.00
-1	17	26	74	22.53	51.10	23.63	2.75	0.00
-0.6	19	26	74	22.53	51.10	23.63	2.75	0.00
0	25	61	39	50.75	30.45	16.92	1.88	0.00
1	13	25	75	27.56	49.33	15.11	8.00	0.00
2	10	34	66	35.70	46.45	16.99	0.86	0.00
3	12	59	41	36.67	35.56	24.44	3.33	0.00
4	7	67	33	35.75	31.84	26.26	6.15	0.00
5	18	31	69	11.08	45.12	42.22	1.58	0.00
6	29	30	70	16.08	29.37	21.68	32.87	0.00
7	29	49	51	28.72	54.05	16.89	0.34	0.00
8	33	26	74	25.14	50.47	18.95	5.44	0.00
9	25	36	64	40.61	37.33	8.60	5.09	8.37
10	30	40	60	32.74	50.53	8.30	5.10	3.32
11	32	39	61	30.39	49.41	10.87	8.49	0.85
12	34	32	68	21.23	48.11	12.74	13.21	4.72
15	33	31	69	15.23	26.40	2.88	25.05	30.45
16	29	53	47	31.42	18.93	2.92	45.02	1.71
17	34	56	44	30.10	22.62	4.00	40.99	2.30
18	32	41	59	26.07	27.94	3.21	33.82	8.96
19	31	48	52	22.58	25.49	5.59	34.46	11.87
20	27	64	36	33.63	17.22	4.73	41.71	2.69
21	31	44	56	27.65	39.23	7.97	22.54	2.62

7.2.2. Coexistence Approach climatic data **(Appendix 1)**

The appendix lists all by the Coexistence Approach reconstructed climatic intervals for each sample including the number of taxa contributing to create this data and the taxa, which were excluded. Abbreviations: CMT: Coldest month temperature, WMT: warmest month temperature, MAT: mean annual temperature, MAP: mean annual precipitation, MPwet, MPdry MPwarm: precipitation of the wettest, driest and warmest month.

Temperature data is given in °C, precipitation in mm per year/per month.

Coexistence approach data

all samples	MAT	15,7	20,8	CMT	9,6	13,3	WMT	24,7	27,9	MAP	823	1372	MPwet	204	236	MPdry	9	24	MPwarm	79	172
	number of analysed taxa:				36			excluded taxa:		*Catahya, Sciadopitys*											
SPK-C1 -2.0	MAT	15,6	23,9	CMT	5,0	16,4	WMT	24,7	28,1	MAP	823	1520	MPwet	204	245	MPdry	8	24	MPwarm	79	180
	number of analysed taxa:				14			excluded taxa:		*Picea, Catahya*											
SPK-C1 -1.6	MAT	15,6	21,9	CMT	5,0	13,6	WMT	24,7	28,1	MAP	823	1520	MPwet	204	245	MPdry	8	59	MPwarm	79	180
	number of analysed taxa:				13			excluded taxa:		*Cathaya*											
SPK-C1 -1.0	MAT	15,6	20,8	CMT	5,0	13,3	WMT	24,7	28,1	MAP	823	1372	MPwet	204	236	MPdry	9	24	MPwarm	79	180
	number of analysed taxa:				13			excluded taxa:		*Cathaya*											
SPK-C1 -0.6	MAT	15,6	20,8	CMT	5,0	13,3	WMT	24,7	28,1	MAP	823	1520	MPwet	204	236	MPdry	9	24	MPwarm	82	172
	number of analysed taxa:				16			excluded taxa:		*Cathaya, Sciadopitys*											
SPK-C1 0.0	MAT	15,6	20,8	CMT	5,0	13,3	WMT	24,7	27,9	MAP	823	1520	MPwet	204	236	MPdry	9	37	MPwarm	79	172
	number of analysed taxa:				19			excluded taxa:		*Catahya*											
SPK-C1 1.0	MAT	13,6	20,8	CMT	1,8	13,3	WMT	23,6	28,1	MAP	505	1520	MPwet	109	236	MPdry	9	64	MPwarm	45	180
	number of analysed taxa:				10			excluded taxa:		*Ephedra, Catahya*											
SPK-C1 2.0	MAT	13,6	25,0	CMT	1,8	19,8	WMT	23,6	28,3	MAP	505	1520	MPwet	109	245	MPdry	8	67	MPwarm	45	180
	number of analysed taxa:				5			excluded taxa:		*Picea, Catahya*											
SPK-C1 3.0	MAT	15,6	23,9	CMT	5,0	19,4	WMT	24,7	28,1	MAP	823	1520	MPwet	204	245	MPdry	8	24	MPwarm	79	180
	number of analysed taxa:				8			excluded taxa:		*Picea, Catahya*											
SPK-C1 4.0	MAT	15,6	23,9	CMT	5,0	16,4	WMT	24,7	29,5	MAP	823	1520	MPwet	204	245	MPdry	8	59	MPwarm	79	208
	number of analysed taxa:				6			excluded taxa:		*Catahya*											
SPK-C1 5.0	MAT	15,6	20,8	CMT	5,0	13,3	WMT	24,7	28,1	MAP	823	1520	MPwet	204	236	MPdry	9	37	MPwarm	79	180
	number of analysed taxa:				15			excluded taxa:		*Catahya*											
SPK-C1 6.0	MAT	15,6	20,8	CMT	5,0	13,3	WMT	24,7	28,1	MAP	823	1372	MPwet	204	236	MPdry	9	37	MPwarm	79	180
	number of analysed taxa:				22			excluded taxa:		*Catahya*											
SPK-C1 7.0	MAT	15,6	20,8	CMT	5,0	13,3	WMT	24,7	28,1	MAP	823	1372	MPwet	204	236	MPdry	9	24	MPwarm	79	180
	number of analysed taxa:				25			excluded taxa:		*Catahya*											
SPK-C1 8.0	MAT	15,7	20,8	CMT	9,6	13,3	WMT	24,7	28,1	MAP	823	1372	MPwet	204	236	MPdry	9	24	MPwarm	79	172
	number of analysed taxa:				26			excluded taxa:		*Catahya, Sciadopitys*											

SPK-C1 9.0	MAT	15,7	20,8	CMT	9,6	13,3	WMT	24,7	28,1	MAP	823	1372	MPwet	204	236	MPdry	9	37	MPwarm	79	172
	number of analysed taxa:				21			excluded taxa:		*Catahya*											
SPK-C1 10.0	MAT	15,6	20,8	CMT	5,0	13,3	WMT	24,7	27,9	MAP	823	1372	MPwet	204	236	MPdry	9	24	MPwarm	79	180
	number of analysed taxa:				22			excluded taxa:		*Catahya, Sciadopitys*											
SPK-C1 11.0	MAT	15,6	20,8	CMT	5,0	13,3	WMT	24,7	27,9	MAP	823	1372	MPwet	204	236	MPdry	9	24	MPwarm	79	172
	number of analysed taxa:				24			excluded taxa:		*Ephedra, Catahya*											
SPK-C1 12.0	MAT	15,7	20,8	CMT	9,6	13,3	WMT	24,7	27,9	MAP	823	1372	MPwet	204	236	MPdry	9	24	MPwarm	79	180
	number of analysed taxa:				25			excluded taxa:		*Ephedra, Catahya*											
SPK-C1 13.0	MAT	0,0	0,0	CMT	0,0	0,0	WMT	0,0	0,0	MAP	0	0	MPwet	0	0	MPdry	0	0	MPwarm	0	0
	number of analysed taxa:				0			excluded taxa:		none											
SPK-C1 14.0	MAT	0,0	0,0	CMT	0,0	0,0	WMT	0,0	0,0	MAP	0	0	MPwet	0	0	MPdry	0	0	MPwarm	0	0
	number of analysed taxa:				0			excluded taxa:		none											
SPK-C1 15.0	MAT	15,7	20,8	CMT	9,6	13,3	WMT	24,7	27,9	MAP	823	1372	MPwet	204	236	MPdry	9	24	MPwarm	79	180
	number of analysed taxa:				25			excluded taxa:		*Catahya*											
SPK-C1 16.0	MAT	15,7	20,8	CMT	9,6	13,3	WMT	24,7	28,1	MAP	823	1372	MPwet	204	236	MPdry	9	24	MPwarm	79	172
	number of analysed taxa:				21			excluded taxa:		*Catahya, Sciadopitys*											
SPK-C1 17.0	MAT	15,7	20,8	CMT	9,6	13,3	WMT	24,7	28,1	MAP	823	1372	MPwet	204	236	MPdry	9	24	MPwarm	79	172
	number of analysed taxa:				28			excluded taxa:		*Catahya*											
SPK-C1 18.0	MAT	15,6	20,8	CMT	5,0	13,3	WMT	24,7	28,1	MAP	823	1372	MPwet	204	236	MPdry	9	24	MPwarm	79	172
	number of analysed taxa:				24			excluded taxa:		*Catahya, Sciadopitys*											
SPK-C1 19.0	MAT	15,6	21,9	CMT	5,0	13,6	WMT	24,7	27,9	MAP	823	1372	MPwet	204	245	MPdry	9	24	MPwarm	79	172
	number of analysed taxa:				22			excluded taxa:		*Picea, Catahya, Sciadopitys*											
SPK-C1 20.0	MAT	15,7	23,1	CMT	9,6	16,4	WMT	24,7	28,1	MAP	823	1372	MPwet	204	245	MPdry	8	24	MPwarm	79	172
	number of analysed taxa:				19			excluded taxa:		*Catahya, Sciadopitys*											
SPK-C1 21.0	MAT	15,6	20,8	CMT	5,0	13,3	WMT	24,7	28,1	MAP	823	1372	MPwet	204	236	MPdry	9	24	MPwarm	79	180
	number of analysed taxa:				24			excluded taxa:		*Picea, Catahya, Sciadopitys*											

7.3. Supplementary material <u>Chapter 3</u>

7.3.1. Pollen and dinoflagellate cyst countings **(Table 3.1)**

Data sheet with a list of selected dinoflagellates and pollen taxa in percentages (occurring with more than 1 percent at least in one sample) used for statistical analysis.

sample	total taxa	determined pollen /gramm	total pollen/gramm	*Abies*	*Cathaya*	*Cedrus*	Cupressacae	*Ephedra*	*Ginkgo*	*Keteleeria*	*Picea*	*Pinus*	*Sciadopitys*	Taxodiaceae	*Tsuga*	*Acer*	Alangiaceae	*Alnus*
98	26	4817.8	7814.6	2.1	17.0	0.0	0.9	0.0	0.0	0.0	3.0	25.3	1.5	8.6	2.1	0.0	0.3	0.6
97	22	15618.6	22343.8	4.8	11.9	0.0	0.0	0.0	0.0	0.0	6.5	27.2	2.5	7.9	1.7	0.0	0.0	0.0
96	27	6953.6	9891.0	2.3	11.2	0.0	0.0	0.0	0.0	0.0	10.6	23.6	2.3	8.0	0.9	0.0	0.0	0.3
95	26	6489.6	9559.3	3.2	15.9	0.0	0.0	0.0	0.0	0.0	7.9	20.0	1.6	9.8	0.6	0.0	0.3	0.0
94	25	3476.5	5094.7	3.0	12.6	0.0	0.3	0.0	0.0	0.0	10.2	23.4	3.0	7.5	0.6	0.0	0.0	0.0
93	23	3810.3	5389.5	2.4	14.7	0.0	0.5	0.0	0.0	0.5	7.2	21.7	2.1	10.2	0.3	0.0	0.0	0.0
92	26	5280.9	8021.2	3.0	19.7	0.0	0.0	0.0	0.0	0.5	5.9	25.1	1.6	8.1	0.3	0.3	0.8	0.0
91	26	5937.8	8393.5	2.2	13.3	0.0	0.0	0.0	0.3	0.0	4.6	22.8	2.8	10.5	0.6	0.0	0.0	0.0
90	27	4165.9	6071.8	2.6	19.3	0.0	0.0	0.0	0.3	1.3	3.9	16.7	2.9	13.1	0.7	0.0	0.0	0.0
89	29	6599.2	9716.6	4.6	16.3	0.0	0.3	0.0	0.0	0.3	3.7	16.9	0.9	16.0	0.9	0.0	0.6	0.0
88	24	10903.3	14822.2	1.4	16.8	0.0	0.0	0.0	0.0	0.3	4.1	22.9	2.3	12.8	0.3	0.0	0.0	0.0
87	27	6484.4	8556.1	1.3	11.2	0.3	0.0	0.0	0.0	0.3	4.8	21.7	0.0	14.7	0.3	0.3	0.0	0.0
86	28	4801.1	6961.6	1.8	13.2	0.0	0.0	0.3	0.0	0.0	7.4	17.6	2.1	12.9	0.6	0.0	0.0	0.0
85	28	9013.9	11736.6	2.3	15.2	0.0	0.6	0.0	0.0	0.3	6.7	25.8	1.8	10.0	0.6	0.3	0.0	0.0
84	23	4819.5	6662.7	3.1	15.7	0.0	0.0	0.0	0.0	0.6	6.9	26.6	2.2	7.2	0.0	0.0	0.3	0.0
83	24	6194.3	8225.6	1.0	11.0	0.0	0.0	0.0	0.0	0.3	7.1	21.1	1.6	14.6	1.3	0.3	0.0	0.0
82	29	4087.2	5585.4	1.6	12.2	0.0	1.6	0.0	0.0	0.0	4.8	19.6	2.9	11.3	0.6	0.0	0.0	0.0
81	28	4574.3	6393.6	2.3	8.5	0.0	0.9	0.0	0.0	1.1	6.5	22.4	1.4	9.7	1.1	0.0	0.0	0.0
80	32	10999.5	15713.6	4.0	10.2	0.0	0.0	0.0	0.0	0.6	8.7	21.4	1.2	9.3	0.9	0.0	0.0	0.0
79	23	6371.9	8236.9	2.8	10.8	0.0	0.0	0.0	0.0	0.3	5.9	16.7	1.0	13.6	0.3	0.0	0.0	0.0
78	26	12075.2	16062.6	2.8	8.7	0.0	0.6	0.0	0.0	0.3	5.6	20.9	1.6	17.1	0.6	0.0	0.0	0.0
77	30	9607.0	13392.4	1.8	11.6	0.0	0.6	0.0	0.0	0.9	5.4	20.0	0.9	13.1	0.3	0.0	0.3	0.0
76	25	6415.2	9372.3	2.5	15.9	0.0	0.5	0.0	0.0	0.3	5.8	23.9	1.3	15.9	0.5	0.0	0.0	0.0
75	27	6680.2	9696.4	3.0	11.8	0.0	0.0	0.0	0.6	0.9	6.1	20.6	2.1	15.5	0.0	0.0	0.0	0.0
74	24	12704.7	19388.9	0.0	14.6	0.0	0.7	0.0	0.0	0.0	3.7	21.3	1.1	14.6	1.1	0.0	0.0	0.4
73	24	8375.8	12307.9	2.3	14.8	0.0	0.6	0.0	0.0	0.0	3.5	20.9	1.6	11.3	0.3	0.0	0.0	0.0
72	26	5890.1	7831.4	4.8	12.7	0.3	0.0	0.0	0.0	0.6	4.2	25.9	1.1	10.1	0.3	0.0	0.0	0.0
71	28	6172.2	8777.1	3.2	13.2	0.0	0.8	0.0	0.0	0.3	3.5	26.3	1.1	10.5	0.8	0.3	0.0	0.0
70	27	3200.4	4974.2	3.8	11.4	0.0	1.2	0.0	0.0	0.9	5.0	27.9	2.6	11.4	0.6	0.0	0.0	0.3
69	27	7922.5	12545.8	4.5	12.5	0.0	1.7	0.0	0.0	0.0	4.2	30.3	1.4	10.8	0.6	0.0	0.3	0.0
68	31	2584.1	3809.9	3.5	14.0	0.0	0.8	0.0	0.0	1.3	6.2	29.4	1.3	9.2	0.8	0.0	0.3	0.3
67	31	6406.1	9653.3	2.8	15.7	0.0	1.1	0.0	0.0	0.6	4.1	26.2	0.6	11.0	0.3	0.0	0.3	0.3
66	32	3410.2	4811.6	2.7	17.8	0.0	0.5	0.0	0.0	0.3	5.5	22.5	1.1	14.2	0.8	0.0	0.0	0.3
65	29	3181.6	4550.2	2.0	17.0	0.0	2.2	0.0	0.0	0.8	3.4	24.3	1.1	14.2	1.1	0.0	0.3	0.0
64	25	3196.1	4322.6	3.6	19.9	0.0	1.9	0.0	0.0	1.4	4.1	27.6	1.4	6.8	1.4	0.0	0.0	0.0
63	30	5836.8	7619.3	2.4	12.4	0.0	2.2	0.0	0.0	0.3	4.6	28.6	1.4	10.3	0.8	0.0	0.5	0.0
62	31	6364.9	9118.5	3.5	15.6	0.0	1.4	0.0	0.0	0.7	2.1	41.8	0.9	5.9	0.2	0.0	0.0	0.0
61	37	5263.0	7420.2	4.9	18.0	0.0	2.5	0.0	0.0	0.5	5.2	32.3	1.7	6.2	0.2	0.0	0.5	0.0
60	40	9178.9	13008.1	1.5	9.5	0.0	4.3	0.3	0.3	0.0	2.8	16.9	1.2	19.3	0.0	0.0	0.3	0.0
59	34	3921.1	6482.2	4.3	12.4	0.0	2.8	0.3	0.0	1.0	4.3	33.4	1.0	6.8	0.5	0.3	0.0	0.3
58	36	5870.4	9352.2	3.8	12.8	0.0	5.5	0.0	0.0	0.0	4.5	18.6	1.7	14.8	0.3	0.0	0.0	0.7
57	30	3864.5	6160.7	3.5	17.1	0.0	4.1	0.0	0.0	1.4	5.5	23.8	2.3	9.0	1.4	0.0	0.0	0.6
56	30	4114.4	6594.0	4.0	12.3	0.0	0.0	0.0	0.0	1.0	5.6	25.8	2.3	11.3	0.7	0.3	0.0	0.0

sample	total taxa	determined pollen/gramm	total pollen/gramm	*Abies*	*Cathaya*	*Cedrus*	Cupressacae	*Ephedra*	*Ginkgo*	*Keteleeria*	*Picea*	*Pinus*	*Sciadopitys*	Taxodiaceae	*Tsuga*	*Acer*	Alangiaceae	*Alnus*
55	36	6250.6	10206.6	1.4	12.2	0.0	0.0	0.0	0.2	1.6	4.1	27.5	1.8	13.1	0.7	0.5	0.0	0.2
54	36	5184.4	8079.6	1.9	17.7	0.0	0.0	0.0	0.2	1.1	4.1	33.5	1.5	9.1	0.6	0.0	0.2	0.9
53	31	5338.4	8382.6	1.7	14.7	0.3	0.0	0.0	0.0	1.2	4.1	31.4	1.7	11.9	0.7	0.5	0.0	0.7
52	36	5443.5	8811.8	2.5	19.3	0.0	0.0	0.2	0.6	2.3	4.8	27.2	1.5	6.7	1.0	0.2	0.0	0.6
51	37	5341.2	7639.9	3.8	17.0	0.0	0.0	0.0	0.2	2.4	5.1	26.2	1.3	10.3	0.9	0.2	0.2	0.2
50	24	4853.4	6791.9	3.3	16.2	0.0	1.8	0.0	0.0	0.0	3.6	30.6	1.5	9.3	0.6	0.0	0.0	0.0
49	25	4604.8	6241.1	2.0	14.7	0.0	0.5	0.0	0.0	0.0	3.8	39.6	1.8	8.1	0.0	0.0	0.3	0.5
48	28	5265.2	7675.6	2.0	14.8	0.0	0.3	0.0	0.0	0.3	3.3	40.7	1.0	6.6	0.5	0.0	0.0	0.0
47	25	8105.1	12241.7	3.6	15.8	0.0	0.0	0.0	0.0	0.8	6.0	40.2	0.3	6.0	0.5	0.0	0.0	0.3
46	24	5665.5	8385.0	1.9	17.1	0.0	0.5	0.0	0.0	0.0	5.3	33.9	1.3	10.7	0.0	0.0	0.0	0.8
45	27	6449.4	9546.6	1.1	14.7	0.0	0.0	0.0	0.3	0.0	5.4	36.2	0.8	9.0	0.3	0.0	0.0	0.6
44	25	4927.6	7238.3	2.8	16.4	0.0	0.3	0.3	0.0	0.0	4.8	35.6	0.6	7.3	0.0	0.0	0.0	0.0
43	25	6159.9	9635.6	4.5	16.8	0.0	0.8	0.0	0.0	0.0	5.0	36.0	2.0	6.4	0.3	0.0	0.0	0.6
42	28	5094.5	7749.2	3.7	14.1	0.0	0.0	0.2	0.2	0.5	8.7	42.7	0.5	5.5	0.0	0.2	0.0	0.2
41	25	6619.6	9910.9	2.5	14.0	0.0	0.3	0.0	0.0	0.0	6.7	39.9	1.4	5.9	0.0	0.0	0.0	0.6
40	25	5888.6	8076.8	2.5	17.8	0.0	0.0	0.0	0.3	0.0	5.7	38.0	1.4	6.8	0.8	0.0	0.0	0.0
39	23	7133.5	10330.5	2.2	20.4	0.0	0.0	0.0	0.0	0.0	3.6	32.5	0.8	7.3	0.6	0.0	0.3	0.0
38	24	6912.9	9811.8	3.0	16.7	0.0	0.0	0.0	0.0	0.5	4.3	38.4	1.3	7.3	0.3	0.0	0.0	0.3
37	24	4576.4	7031.0	3.3	15.5	0.0	0.0	0.0	0.0	0.3	6.1	33.3	0.9	7.0	1.5	0.0	0.3	0.0
36	32	6631.6	9947.4	4.1	15.4	0.0	0.0	0.0	0.0	0.8	3.3	34.3	0.8	7.4	0.8	0.0	0.0	0.0
35	27	6716.0	10122.8	2.7	18.7	0.7	0.5	0.0	0.0	0.2	4.1	36.7	1.7	6.1	0.2	0.0	0.0	0.0
34	27	4548.8	6988.6	2.0	17.8	0.0	0.5	0.3	0.0	0.0	5.5	39.1	0.8	6.3	0.3	0.0	0.3	0.3
33	30	5456.9	9026.0	1.1	14.9	0.0	0.3	0.0	0.0	0.3	4.3	33.0	1.6	8.1	1.6	0.0	0.0	0.3
32	24	7475.0	10920.1	2.5	13.1	0.0	0.3	0.0	0.0	0.6	5.0	37.7	1.7	6.4	0.6	0.0	0.0	0.0
31	26	5160.5	7807.5	3.4	13.7	0.0	0.0	0.0	0.0	0.3	5.7	38.1	1.6	5.4	0.3	0.0	0.0	0.3
30	27	4633.2	6905.8	2.2	17.6	0.0	0.0	0.0	0.0	0.5	7.3	36.9	1.4	5.4	0.3	0.0	0.0	0.3
29	27	5441.0	9023.6	2.8	12.3	0.0	0.0	0.0	0.0	0.6	8.0	28.6	1.5	8.0	0.9	0.3	0.0	0.3
28	26	5887.4	9275.1	2.8	13.1	0.0	0.3	0.0	0.0	0.0	9.8	33.2	0.6	5.0	0.3	0.0	0.3	0.0
27	24	4360.3	6546.6	3.6	15.3	0.0	0.8	0.0	0.0	0.8	5.0	34.8	1.1	5.3	0.6	0.0	0.0	0.0
26	31	8801.1	13059.7	4.4	9.7	0.0	0.0	0.0	0.0	0.9	6.2	29.3	2.9	7.9	0.3	0.0	0.9	0.3
25	28	5643.1	8728.9	2.4	13.9	0.0	1.2	0.0	0.0	0.3	10.0	27.2	1.8	6.6	0.6	0.0	0.0	0.0
24	28	4399.5	6616.0	2.8	11.5	0.0	0.3	0.0	0.0	1.5	9.7	36.6	1.3	3.8	0.8	0.0	0.0	0.5
23	31	7331.1	11251.9	1.7	10.3	0.0	1.1	0.0	0.0	0.0	5.6	34.3	2.5	7.5	0.8	0.0	0.0	0.3
22	31	6242.4	9471.9	2.6	13.0	0.0	0.9	0.0	0.0	0.0	6.4	27.2	2.3	8.4	1.2	0.0	0.3	0.0
21	29	4946.6	7553.5	2.7	12.4	0.0	0.8	0.0	0.0	0.5	4.9	31.4	1.9	4.9	1.6	0.0	0.3	1.1
20	30	5340.8	8457.5	4.1	12.3	0.3	2.2	0.0	0.0	0.3	4.1	27.9	3.8	7.1	0.8	0.0	0.0	0.0
19	34	6588.5	9798.3	5.4	13.7	0.0	0.9	0.0	0.0	0.3	5.1	25.9	2.3	6.3	0.3	0.0	0.0	0.0
18	27	5088.2	7079.2	2.9	15.1	0.0	0.9	0.0	0.0	0.6	5.5	27.2	1.7	9.3	0.6	0.0	0.3	0.0
17	30	5191.9	7702.7	2.5	11.2	0.0	0.3	0.0	0.0	0.3	4.9	30.9	3.0	9.8	0.3	0.0	0.0	0.0
16	22	7576.1	11602.5	2.2	12.3	0.0	0.0	0.0	0.0	0.6	6.3	24.2	2.2	11.3	0.0	0.0	0.0	0.0
15	27	4886.0	7433.2	1.6	12.1	0.0	1.3	0.0	0.0	0.3	5.6	20.7	1.3	10.5	0.0	0.0	0.3	0.7
14	27	5010.8	7931.0	4.6	15.6	0.0	1.0	0.0	0.0	0.3	5.3	20.9	1.7	9.6	2.0	0.0	0.0	0.3
13	27	6115.1	9334.7	2.5	17.7	0.0	2.1	0.0	0.0	0.4	6.0	15.9	0.4	9.5	1.1	0.0	0.4	0.7

sample	total taxa	determined pollen/gramm	total pollen/gramm	*Abies*	*Cathaya*	*Cedrus*	Cupressacae	*Ephedra*	*Ginkgo*	*Keteleeria*	*Picea*	*Pinus*	*Sciadopitys*	Taxodiaceae	*Tsuga*	*Acer*	Alangiaceae	*Alnus*
12	30	4546.9	7512.3	3.2	11.6	0.0	1.2	0.0	0.0	0.6	5.2	24.6	1.2	9.9	0.3	0.0	0.3	0.0
11	23	4398.4	6657.8	2.1	15.5	0.0	0.0	0.0	0.0	0.6	4.0	28.9	1.8	8.2	1.2	0.0	0.3	0.0
10	29	4605.9	6663.3	2.6	12.4	0.0	1.4	0.0	0.0	1.2	7.8	27.4	1.7	7.5	1.2	0.0	0.6	0.3
9	27	4447.9	6713.9	2.7	11.9	0.0	2.2	0.0	0.0	1.3	5.9	36.7	1.3	7.5	0.3	0.0	0.3	0.0
8	22	4626.0	7393.7	3.4	17.4	0.0	2.0	0.0	0.0	1.1	6.3	31.9	2.0	4.0	0.6	0.0	0.3	0.0
7	23	3260.8	4488.0	2.5	12.9	0.0	3.2	0.0	0.0	0.0	3.2	27.6	2.9	11.5	1.1	0.0	0.0	0.0
6	27	3676.6	5714.8	3.3	14.4	0.0	1.1	0.0	0.0	0.3	4.6	32.9	1.9	6.0	0.5	0.0	0.0	0.0
5	30	4203.8	6617.4	3.0	15.4	0.0	2.7	0.0	0.0	0.0	4.3	31.8	1.1	6.2	1.3	0.0	0.3	0.0
4	31	4741.4	6681.7	1.4	14.7	0.0	1.7	0.0	0.0	0.0	5.8	32.3	1.2	8.4	0.6	0.0	0.0	0.9
3	30	3422.7	5168.7	2.8	12.9	0.0	1.5	0.0	0.0	0.0	7.3	37.4	3.0	5.8	0.3	0.0	0.0	0.0
2	27	4038.7	6491.7	2.5	18.1	0.0	0.6	0.0	0.0	0.0	4.6	35.0	1.8	5.8	0.9	0.0	0.3	0.0
1	32	3503.4	5402.3	3.8	14.8	0.0	1.4	0.0	0.0	1.2	4.1	35.1	2.6	7.2	1.4	0.0	0.3	0.3

sample	Araliaceae	Arecaceae	*Artemisia*	Asteraceae	*Betula*	Buxaceae	Caprifoliaceae	*Carpinus*	*Carya*	Caryophyllaceae	*Castanea/Castanopsis*-Type	*Celtis*	Chenopodiaceae	Cyperaceae	*Engelhardia*	Ericaceae	Euphorbiaceae	Fagaceae	*Fagus*
98	0.0	0.0	0.0	0.0	0.0	0.0	0.0	0.6	8.6	0.0	0.0	0.6	0.3	0.9	0.0	0.0	0.0	0.0	0.0
97	0.0	0.0	0.3	0.0	0.0	0.0	0.0	0.0	7.4	0.0	0.0	0.3	0.0	0.8	0.3	0.0	0.0	0.0	1.1
96	0.0	0.0	0.3	0.0	0.0	0.0	0.0	0.3	6.9	0.0	0.0	0.3	0.0	2.6	0.3	0.0	0.0	0.0	0.9
95	0.0	0.0	0.0	0.0	0.0	0.0	0.0	0.3	7.6	0.0	0.3	0.0	0.0	1.6	0.3	0.0	0.0	0.0	1.0
94	0.0	0.3	0.0	0.0	0.0	0.0	0.0	0.3	8.1	0.0	0.3	0.9	0.0	0.6	0.3	0.3	0.0	0.0	0.0
93	0.0	0.0	0.0	0.0	0.0	0.0	0.0	0.0	9.1	0.0	0.0	0.8	0.0	4.8	0.3	0.0	0.0	0.0	0.3
92	0.0	0.0	0.0	0.3	0.0	0.0	0.0	0.0	5.4	0.0	0.0	0.3	0.0	3.8	0.0	0.0	0.0	0.0	1.4
91	0.0	0.3	0.0	0.0	0.0	0.0	0.0	0.6	6.5	0.0	0.0	0.6	0.0	5.6	0.9	0.0	0.0	0.0	0.3
90	0.0	0.0	0.0	0.0	0.0	0.0	0.0	1.3	6.5	0.0	0.0	1.0	0.0	3.9	0.3	0.0	0.0	0.0	1.0
89	0.0	0.0	0.0	0.0	0.0	0.0	0.0	0.9	5.2	0.0	0.0	0.3	0.0	4.6	0.9	0.0	0.3	0.0	1.8
88	0.0	0.0	0.0	0.3	0.0	0.0	0.0	0.3	4.9	0.0	0.0	0.3	0.0	2.9	0.0	0.0	0.3	0.0	0.6
87	0.0	0.3	0.0	0.0	0.0	0.0	0.0	0.0	5.1	0.0	0.3	1.3	0.0	5.4	0.0	0.0	0.0	0.0	1.9
86	0.0	0.0	0.0	0.0	0.0	0.0	0.0	0.3	7.4	0.0	0.0	0.9	0.0	3.5	0.0	0.0	0.0	0.0	0.9
85	0.0	0.0	0.0	0.0	0.0	0.0	0.0	0.3	5.0	0.0	0.0	0.0	0.0	2.6	0.0	0.0	0.3	0.0	0.9
84	0.0	0.3	0.0	0.0	0.0	0.0	0.0	0.0	9.4	0.0	0.0	1.3	0.0	3.1	0.0	0.0	0.0	0.0	2.2
83	0.0	0.0	0.0	0.0	0.3	0.0	0.0	0.0	7.8	0.0	0.0	0.0	0.0	5.5	0.3	0.0	0.0	0.0	0.3
82	0.0	0.6	0.0	0.0	0.0	0.0	0.0	0.3	9.3	0.0	0.0	0.0	0.0	2.6	0.0	0.3	0.6	0.0	1.0
81	0.0	0.0	0.0	0.0	0.0	0.0	0.0	0.6	11.6	0.3	0.0	0.6	0.3	2.6	0.9	0.0	0.0	0.0	1.4
80	0.0	0.0	0.3	0.3	0.3	0.0	0.0	0.3	5.9	0.0	0.3	0.6	0.0	5.0	0.3	0.0	0.0	0.0	2.2
79	0.0	1.0	0.0	0.0	0.0	0.0	0.0	0.3	13.9	0.0	0.3	0.3	0.0	4.5	0.7	0.0	0.0	0.0	1.7
78	0.0	0.3	0.0	0.0	0.0	0.0	0.0	0.3	5.0	0.0	0.0	0.9	0.0	3.4	0.6	0.0	0.0	0.0	0.6
77	0.0	0.3	0.0	0.0	0.0	0.0	0.0	0.0	8.7	0.0	0.0	0.3	0.0	6.9	0.6	0.0	0.0	0.0	1.5
76	0.0	0.0	0.3	0.5	0.0	0.0	0.0	0.0	9.1	0.0	0.0	0.5	0.0	4.3	0.0	0.0	0.0	0.0	0.5
75	0.0	0.6	0.0	0.0	0.0	0.0	0.0	0.6	5.5	0.0	0.3	0.6	0.0	5.5	0.3	0.0	0.0	0.0	0.9
74	0.0	0.7	0.0	0.0	0.0	0.0	0.0	0.4	6.0	0.0	0.4	0.4	0.0	7.8	0.0	0.0	0.0	0.0	2.2
73	0.0	0.0	0.0	0.0	0.0	0.0	0.0	0.0	6.8	0.0	0.0	0.0	0.0	6.1	0.0	0.0	1.0	0.0	1.0
72	0.0	1.1	0.0	0.0	0.0	0.0	0.0	0.3	7.3	0.0	0.0	0.8	0.0	6.5	0.0	0.0	0.0	0.0	2.3
71	0.0	0.3	0.0	0.5	0.0	0.0	0.0	0.5	7.3	0.0	0.0	0.8	0.0	3.5	0.0	0.0	0.0	0.0	2.2
70	0.0	0.3	0.3	0.0	0.0	0.0	0.0	1.2	7.3	0.0	0.0	1.2	0.0	3.2	0.6	0.0	0.0	0.0	0.9
69	0.0	1.1	0.0	0.0	0.0	0.0	0.0	0.0	6.2	0.0	0.0	1.4	0.0	1.1	0.3	0.0	0.0	0.0	1.7
68	0.0	0.8	0.0	0.3	0.0	0.0	0.0	0.5	8.6	0.3	0.0	0.5	0.0	0.8	0.5	0.0	0.0	0.0	1.3
67	0.0	0.6	0.0	0.0	0.0	0.0	0.0	0.3	6.1	0.0	0.0	1.7	0.3	2.2	0.3	0.0	0.0	0.0	1.4
66	0.0	0.3	0.0	0.0	0.0	0.0	0.0	1.1	5.5	0.0	0.3	1.1	0.0	3.6	0.3	0.3	0.0	0.0	1.9
65	0.0	0.6	0.0	0.0	0.0	0.0	0.0	0.8	3.9	0.0	0.0	1.1	0.0	2.2	0.3	0.0	0.0	0.0	1.7
64	0.0	0.0	0.0	0.0	0.3	0.0	0.0	0.0	5.7	0.0	0.0	0.8	0.3	1.4	0.8	0.0	0.0	0.0	0.5
63	0.0	0.5	0.0	0.0	0.0	0.0	0.0	1.6	3.2	0.0	0.0	1.4	0.0	2.2	1.4	0.0	0.0	0.0	1.9
62	0.0	0.7	0.0	0.0	0.0	0.0	0.0	0.5	3.3	0.0	0.2	1.4	0.0	1.4	0.0	0.2	0.0	0.0	1.9
61	0.0	0.5	0.0	0.0	0.2	0.0	0.0	0.2	4.2	0.5	0.2	2.0	0.0	0.2	0.5	0.0	0.7	0.5	2.0
60	0.0	1.2	0.0	0.0	0.3	0.0	0.0	0.0	4.3	0.0	0.6	1.2	0.0	0.9	0.3	0.3	0.0	0.0	4.6
59	0.0	0.0	0.0	0.0	0.5	0.0	0.0	1.3	6.1	0.0	0.0	1.8	0.0	0.0	0.3	0.0	0.0	0.5	2.0
58	0.0	0.7	0.0	0.3	0.3	0.0	0.0	0.3	4.5	0.0	0.3	1.0	0.0	0.0	0.0	0.0	0.3	0.3	3.4
57	0.0	0.6	0.0	0.3	0.0	0.0	0.0	1.2	7.2	0.0	0.0	3.2	0.0	0.0	0.6	0.0	0.3	0.3	0.9
56	0.0	0.0	0.0	0.7	0.0	0.0	0.0	0.3	7.6	0.0	0.3	1.3	0.0	0.0	0.7	0.0	0.0	0.3	2.0

sample	Araliaceae	Arecaceae	*Artemisia*	Asteraceae	*Betula*	Buxaceae	Caprifoliaceae	*Carpinus*	*Carya*	Caryophyllaceae	*Castanea/Castanopsis*-Type	*Celtis*	Chenopodiaceae	Cyperaceae	*Engelhardia*	Ericaceae	Euphorbiaceae	Fagaceae	*Fagus*
55	0.0	1.4	0.0	0.2	0.2	0.0	0.0	0.7	7.4	0.0	0.0	1.1	0.0	0.5	0.7	0.0	0.5	0.0	1.6
54	0.0	0.6	0.0	0.4	0.2	0.0	0.0	0.6	6.5	0.0	0.0	0.9	0.2	0.0	0.2	0.0	0.0	0.0	1.7
53	0.0	1.2	0.0	0.0	0.0	0.0	0.0	0.5	7.1	0.0	0.0	0.2	0.0	0.0	1.2	0.0	0.3	0.0	1.3
52	0.0	0.8	0.0	0.0	0.0	0.0	0.0	1.1	8.8	0.2	0.0	0.0	0.0	0.2	0.4	0.0	1.1	0.0	1.9
51	0.0	0.2	0.0	0.0	0.5	0.2	0.2	0.9	10.5	0.0	0.0	0.7	0.4	0.0	0.2	0.0	0.5	0.0	0.4
50	0.0	0.0	0.0	0.9	0.0	0.0	0.0	0.9	7.5	0.0	0.0	0.3	0.0	3.9	0.0	0.3	0.0	0.0	0.9
49	0.0	0.0	0.0	0.0	0.0	0.0	0.0	0.3	7.6	0.0	0.0	0.0	0.0	2.0	0.0	0.0	0.0	0.0	0.5
48	0.0	0.0	0.0	0.0	0.0	0.0	0.0	0.8	6.1	0.3	0.5	0.0	0.0	3.3	0.5	0.0	0.0	0.0	0.5
47	0.0	0.0	0.0	0.0	0.0	0.0	0.0	0.0	8.0	0.3	0.0	0.8	0.0	4.1	0.0	0.0	0.0	0.0	0.8
46	0.0	0.0	0.0	0.0	0.0	0.0	0.0	1.1	8.3	0.0	0.0	0.3	0.0	4.0	0.0	0.0	0.0	0.0	0.8
45	0.0	0.3	0.0	0.0	0.0	0.0	0.0	0.8	7.1	0.3	0.0	0.0	0.0	2.5	0.0	0.0	0.0	0.0	1.1
44	0.0	0.3	0.0	0.0	0.0	0.0	0.0	0.8	8.8	0.3	0.0	0.3	0.0	2.8	0.0	0.0	0.3	0.0	1.1
43	0.0	0.0	0.0	0.0	0.0	0.0	0.0	0.3	9.2	0.0	0.0	0.3	0.0	1.4	0.6	0.0	0.0	0.0	1.1
42	0.0	0.0	0.0	0.0	0.0	0.0	0.0	0.2	7.9	0.2	0.0	0.5	0.0	1.2	0.0	0.0	0.0	0.0	0.7
41	0.0	0.3	0.0	0.0	0.0	0.0	0.0	0.3	7.3	0.0	0.0	0.0	0.3	1.4	0.0	0.0	0.0	0.0	1.1
40	0.0	0.0	0.0	0.0	0.0	0.0	0.0	0.5	8.2	0.0	0.0	0.5	0.0	2.2	0.0	0.0	0.0	0.0	0.5
39	0.0	0.0	0.0	0.0	0.0	0.0	0.0	0.6	12.9	0.0	0.0	0.3	0.0	2.0	0.0	0.0	0.0	0.0	0.3
38	0.0	0.0	0.0	0.0	0.0	0.0	0.0	0.5	9.4	0.3	0.0	0.0	0.0	2.2	0.0	0.0	0.0	0.0	0.8
37	0.0	0.6	0.0	0.3	0.0	0.0	0.0	0.3	7.9	0.0	0.0	0.0	0.0	0.9	0.0	0.0	0.0	0.0	2.1
36	0.0	0.0	0.3	0.3	0.0	0.0	0.0	0.3	6.9	0.0	0.0	0.5	0.0	1.1	0.8	0.0	0.3	0.0	0.8
35	0.0	0.0	0.0	0.2	0.0	0.0	0.0	0.7	9.2	0.5	0.5	0.7	0.0	0.7	0.0	0.0	0.0	0.0	0.5
34	0.0	0.0	0.0	0.0	0.0	0.0	0.0	0.5	7.8	0.3	0.0	0.3	0.0	0.5	0.3	0.0	0.0	0.0	0.8
33	0.0	0.0	0.0	0.0	0.0	0.0	0.0	0.8	7.0	0.0	0.0	0.3	0.0	2.2	0.0	0.0	0.3	0.0	0.5
32	0.0	0.0	0.0	0.0	0.0	0.0	0.0	1.4	8.1	0.0	0.0	0.3	0.0	1.4	0.0	0.0	0.0	0.0	0.0
31	0.0	0.0	0.0	0.0	0.0	0.0	0.0	1.3	7.0	0.0	0.0	0.5	0.0	1.6	0.0	0.0	0.0	0.0	0.5
30	0.0	0.0	0.3	0.0	0.0	0.0	0.0	0.0	4.9	0.0	0.0	0.3	0.0	0.5	0.3	0.0	0.0	0.0	0.0
29	0.0	0.0	0.0	0.0	0.3	0.0	0.0	0.0	6.2	0.0	0.0	1.2	0.0	0.6	0.3	0.0	0.0	0.0	0.3
28	0.0	0.0	0.0	0.0	0.0	0.0	0.0	0.0	7.8	0.0	0.0	0.8	0.6	2.8	0.0	0.0	0.0	0.0	0.6
27	0.0	0.0	0.0	0.0	0.0	0.0	0.0	0.0	7.8	0.0	0.0	0.6	0.0	3.9	0.0	0.3	0.0	0.0	0.8
26	0.0	0.9	0.3	0.0	0.0	0.0	0.0	0.6	6.7	0.0	0.0	0.6	0.0	4.7	0.6	0.0	0.0	0.0	0.9
25	0.0	0.6	0.0	0.0	0.0	0.0	0.0	0.3	6.9	0.3	0.0	0.0	0.0	2.4	0.9	0.0	0.0	0.0	0.0
24	0.0	0.0	0.0	0.0	0.0	0.0	0.0	0.5	7.1	0.3	0.0	0.3	0.0	3.3	0.0	0.0	0.0	0.0	0.5
23	0.0	0.0	0.0	0.3	0.0	0.0	0.0	0.3	5.8	0.6	0.3	0.3	0.0	3.9	0.0	0.3	0.0	0.0	0.6
22	0.0	0.6	0.0	0.3	0.0	0.0	0.0	0.6	7.5	0.3	0.0	0.3	0.0	2.6	0.6	0.0	0.0	0.0	0.6
21	0.0	0.0	0.0	0.0	0.0	0.0	0.0	0.0	8.6	0.3	0.0	0.3	0.0	4.1	0.0	0.0	0.3	0.0	0.5
20	0.0	0.0	0.0	0.3	0.3	0.0	0.0	0.5	5.5	0.3	0.0	1.1	0.0	2.7	0.8	0.0	0.0	0.0	0.5
19	0.0	0.0	0.0	0.3	0.0	0.0	0.0	0.3	6.6	0.0	0.0	0.9	0.0	1.7	0.3	0.3	0.0	0.0	0.9
18	0.0	0.0	0.3	0.0	0.0	0.3	0.0	0.6	5.5	0.0	0.0	0.0	0.0	2.6	0.0	0.0	0.0	0.0	0.0
17	0.0	0.0	0.0	0.0	0.0	0.0	0.0	0.3	5.7	0.0	0.0	0.5	0.0	1.9	0.5	0.3	0.0	0.0	0.3
16	0.0	0.0	0.0	0.0	0.3	0.0	0.0	0.0	9.4	0.0	0.0	0.6	0.0	1.9	0.0	0.0	0.0	0.0	0.9
15	0.0	0.0	0.0	0.0	0.0	0.0	0.0	0.0	7.9	0.3	0.0	0.3	0.3	2.3	0.3	0.0	0.0	0.0	1.3
14	0.0	0.0	0.0	0.0	0.3	0.0	0.0	0.7	6.6	0.0	0.3	0.0	0.0	2.0	0.0	0.0	0.0	0.0	0.7
13	0.0	0.0	0.0	0.0	0.0	0.0	0.0	0.4	9.2	0.4	0.0	0.4	0.0	3.2	0.7	0.0	0.0	0.0	0.7

sample	Araliaceae	Arecaceae	*Artemisia*	Asteraceae	*Betula*	Buxaceae	Caprifoliaceae	*Carpinus*	*Carya*	Caryophyllaceae	*Castanea/Castanopsis*-Type	*Celtis*	Chenopodiaceae	Cyperaceae	*Engelhardia*	Ericaceae	Euphorbiaceae	Fagaceae	*Fagus*
12	0.0	0.0	0.0	0.0	0.0	0.0	0.0	0.3	7.2	0.3	0.0	0.3	0.3	2.3	0.0	0.3	0.3	0.0	0.6
11	0.0	0.0	0.6	0.0	0.0	0.0	0.0	0.3	7.9	0.0	0.0	0.0	0.0	4.6	0.0	0.0	0.0	0.0	0.3
10	0.0	0.0	0.0	0.0	0.0	0.0	0.0	0.6	5.2	0.0	0.0	0.3	0.3	4.0	0.3	0.0	0.6	0.0	0.3
9	0.0	0.0	0.0	0.3	0.0	0.0	0.0	0.0	3.8	0.0	0.0	0.3	0.3	2.7	0.0	0.0	0.0	0.0	0.0
8	0.3	0.0	0.0	0.0	0.0	0.0	0.0	0.3	6.3	0.0	0.0	0.0	0.0	2.0	0.0	0.0	0.0	0.0	0.0
7	0.0	0.0	0.0	0.0	0.0	0.4	0.0	0.7	2.2	0.4	0.4	0.4	0.0	3.2	0.4	0.0	0.0	0.0	0.0
6	0.3	0.0	0.0	0.3	0.0	0.0	0.0	0.5	7.1	0.0	0.0	0.3	0.0	1.6	0.5	0.0	0.3	0.0	0.3
5	0.0	0.0	0.0	0.3	0.0	0.0	0.0	0.3	3.8	0.0	0.3	0.0	0.0	2.2	0.0	0.0	0.0	0.0	0.3
4	0.3	0.3	0.0	0.3	0.0	0.0	0.0	0.6	4.3	0.0	0.0	0.0	0.6	2.6	0.3	0.0	0.0	0.0	0.3
3	0.0	0.0	0.0	0.3	0.0	0.0	0.0	0.5	5.8	0.0	1.3	0.5	0.0	2.3	0.0	0.0	0.0	0.0	0.5
2	0.0	0.3	0.0	0.0	0.0	0.0	0.0	0.9	6.4	0.0	0.0	0.9	0.0	3.1	0.3	0.0	0.0	0.0	0.6
1	0.0	0.0	0.0	0.3	0.0	0.0	0.0	0.6	7.5	0.3	0.0	1.7	0.0	2.0	0.3	0.0	0.0	0.0	0.6

sample	*Fraxinus*	Hamamelidaceae	*Hederea*	*Ilex*	*Juglans*	Lamiaceae	*Liquidambar*	*Lonicera*	Lythraceae	Malvaceae	Mastixiaceae	*Myriophyllum*	*Myrica*	Nympheaceae	*Nyssa*	Oleaceae	Onagraceae	*Platycarya*	Plumbaginaceae
98	0.0	0.0	0.3	0.0	0.6	0.0	0.3	0.0	0.0	0.0	0.0	0.0	0.0	0.0	0.0	0.0	0.0	0.0	0.0
97	0.0	0.0	0.0	0.3	0.3	0.0	0.3	0.0	0.0	0.0	0.0	0.0	0.0	0.0	0.0	0.0	0.0	0.0	0.0
96	0.0	0.0	0.0	0.3	0.0	0.0	0.0	0.0	0.0	0.0	0.0	0.0	0.0	0.0	0.6	0.0	0.0	0.0	0.0
95	0.0	0.0	0.0	0.0	0.6	0.0	0.0	0.3	0.0	0.0	0.0	0.0	0.6	0.0	0.3	0.0	0.0	0.3	0.0
94	0.0	0.0	0.0	0.0	0.0	0.0	0.3	0.0	0.0	0.0	0.3	0.0	0.0	0.0	0.0	0.3	0.0	0.0	0.0
93	0.0	0.0	0.0	0.0	0.0	0.0	0.5	0.0	0.0	0.0	0.0	0.0	0.0	0.0	0.0	0.5	0.0	0.0	0.0
92	0.0	0.0	0.0	0.3	0.3	0.0	0.0	0.0	0.0	0.0	0.0	0.0	0.5	0.0	0.3	0.0	0.0	0.0	0.0
91	0.0	0.0	0.0	0.0	0.0	0.0	0.6	0.0	0.0	0.0	0.0	0.0	0.0	0.0	0.3	0.0	0.0	0.0	0.0
90	0.0	0.0	0.0	0.0	0.0	0.0	0.0	0.0	0.0	0.0	0.0	0.0	0.3	0.0	0.7	0.3	0.0	0.3	0.0
89	0.0	0.0	0.0	0.0	0.3	0.0	0.3	0.0	0.0	0.0	0.0	0.0	0.0	0.0	0.3	0.3	0.0	0.0	0.3
88	0.0	0.0	0.0	0.0	0.9	0.0	0.6	0.0	0.0	0.0	0.0	0.0	0.3	0.0	0.0	0.0	0.0	0.0	0.0
87	0.0	0.0	0.0	0.0	0.3	0.0	0.0	0.0	0.0	0.0	0.0	0.0	0.0	0.0	0.3	0.3	0.0	0.0	0.0
86	0.0	0.0	0.0	0.0	0.6	0.0	0.3	0.0	0.0	0.0	0.3	0.0	0.3	0.0	0.3	0.6	0.0	0.0	0.0
85	0.0	0.0	0.0	0.3	0.3	0.0	0.9	0.0	0.0	0.0	0.0	0.0	0.0	0.3	0.9	0.0	0.0	0.0	0.0
84	0.0	0.0	0.0	0.0	0.6	0.0	0.6	0.0	0.0	0.0	0.0	0.0	0.0	0.0	0.0	0.3	0.0	0.0	0.0
83	0.0	0.0	0.0	0.0	0.6	0.0	0.6	0.0	0.0	0.0	0.0	0.0	0.3	0.0	0.0	0.0	0.0	0.0	0.0
82	0.0	0.0	0.0	0.0	0.6	0.0	0.3	0.0	0.0	0.0	0.0	0.0	0.3	0.0	0.0	0.6	0.0	0.0	0.0
81	0.0	0.0	0.0	0.0	0.3	0.0	0.3	0.0	0.0	0.0	0.0	0.0	0.0	0.0	0.6	0.0	0.0	0.0	0.0
80	0.3	0.0	0.0	0.3	1.2	0.0	1.6	0.0	0.0	0.0	0.0	0.0	0.0	0.0	0.9	0.6	0.0	0.3	0.0
79	0.0	0.0	0.0	0.0	0.0	0.0	0.7	0.0	0.0	0.0	0.0	0.0	0.0	0.0	0.0	0.0	0.0	0.0	0.0
78	0.0	0.0	0.0	0.3	0.0	0.0	0.0	0.0	0.0	0.0	0.3	0.0	0.3	0.3	0.3	0.0	0.0	0.0	0.0
77	0.0	0.0	0.0	0.0	0.6	0.0	0.3	0.0	0.0	0.0	0.6	0.0	0.3	0.0	0.3	0.0	0.0	0.0	0.0
76	0.0	0.0	0.0	0.0	0.0	0.0	0.3	0.3	0.0	0.0	0.0	0.0	0.0	0.0	0.3	0.0	0.0	0.0	0.0
75	0.0	0.0	0.0	0.0	0.3	0.0	0.0	0.0	0.0	0.0	0.0	0.0	0.3	0.0	0.6	0.0	0.0	0.3	0.0
74	0.0	0.0	0.0	0.4	0.4	0.0	0.4	0.0	0.0	0.0	0.0	0.0	0.0	0.0	0.4	0.0	0.0	0.0	0.0
73	0.0	0.0	0.0	0.3	0.0	0.0	0.3	0.0	0.0	0.0	0.0	0.0	0.0	0.0	0.0	0.0	0.0	0.3	0.0
72	0.0	0.0	0.0	0.0	0.3	0.0	0.3	0.0	0.0	0.0	0.0	0.0	0.0	0.0	0.6	0.0	0.0	0.0	0.0
71	0.0	0.0	0.3	0.0	0.8	0.0	0.5	0.0	0.0	0.0	0.0	0.0	0.0	0.3	0.5	0.0	0.0	0.0	0.0
70	0.0	0.0	0.0	0.0	0.6	0.0	0.0	0.0	0.0	0.0	0.0	0.0	0.0	0.0	0.6	0.0	0.0	0.0	0.0
69	0.0	0.0	0.0	0.0	0.3	0.0	0.6	0.0	0.0	0.0	0.0	0.0	0.0	0.0	0.8	0.0	0.0	0.3	0.0
68	0.0	0.0	0.0	0.0	0.5	0.0	0.3	0.0	0.0	0.0	0.0	0.0	0.0	0.0	0.0	0.8	0.0	0.0	0.0
67	0.0	0.0	0.0	0.0	0.8	0.0	0.3	0.0	0.0	0.0	0.0	0.0	0.6	0.0	0.0	0.0	0.0	0.0	0.0
66	0.0	0.0	0.0	0.3	0.8	0.0	1.4	0.0	0.0	0.0	0.0	0.0	0.0	0.0	0.5	0.3	0.0	0.0	0.0
65	0.0	0.0	0.0	0.0	0.6	0.0	0.8	0.0	0.0	0.0	0.0	0.0	0.0	0.0	0.3	0.0	0.0	0.0	0.0
64	0.0	0.0	0.0	0.0	1.1	0.0	0.8	0.0	0.0	0.0	0.0	0.0	0.0	0.0	0.3	0.0	0.0	0.0	0.0
63	0.0	0.0	0.3	0.0	1.1	0.0	0.8	0.0	0.0	0.3	0.0	0.0	0.5	0.0	0.0	0.3	0.0	0.0	0.0
62	0.0	0.0	0.0	0.0	0.2	0.0	0.7	0.0	0.0	0.0	0.0	0.0	0.0	0.2	1.4	0.5	0.0	0.2	0.0
61	0.0	0.0	0.0	0.0	0.7	0.0	0.0	0.0	0.2	0.0	0.0	0.0	0.0	0.2	0.5	0.7	0.0	0.0	0.0
60	0.0	0.0	0.0	0.3	0.9	0.0	0.9	0.0	0.0	0.9	0.0	0.3	0.6	1.5	0.9	0.3	0.0	0.3	0.0
59	0.0	0.0	0.0	0.5	0.8	0.0	1.0	0.0	0.0	0.0	0.0	0.0	0.5	0.5	1.0	0.3	0.0	0.3	0.0
58	0.0	0.0	0.0	0.3	0.7	0.0	0.7	0.0	0.0	0.0	0.0	0.0	0.7	0.3	1.7	0.7	0.0	0.0	0.0
57	0.0	0.0	0.0	0.3	0.9	0.0	1.2	0.0	0.0	0.0	0.0	0.0	0.0	0.0	1.2	0.0	0.0	0.0	0.0
56	0.0	0.0	0.0	0.3	1.3	0.0	1.0	0.0	0.7	0.0	0.0	0.0	0.0	0.0	1.0	0.7	0.0	0.0	0.0

sample	*Fraxinus*	Hamamelidaceae	*Hederea*	*Ilex*	*Juglans*	Lamiaceae	*Liquidambar*	*Lonicera*	Lythraceae	Malvaceae	Mastixiaceae	*Myriophyllum*	*Myrica*	Nympheaceae	*Nyssa*	Oleaceae	Onagraceae	*Platycarya*	Plumbaginaceae
55	0.0	0.0	0.0	0.2	0.5	0.0	0.5	0.0	0.0	0.0	0.0	0.0	0.5	0.0	0.2	0.0	0.0	0.0	0.0
54	0.0	0.6	0.2	0.2	0.6	0.0	0.4	0.0	0.0	0.0	0.0	0.0	0.0	0.0	0.9	0.0	0.0	0.0	0.0
53	0.0	0.0	0.0	0.0	0.5	0.0	0.5	0.0	0.0	0.0	0.0	0.0	0.7	0.0	0.5	0.0	0.0	0.0	0.0
52	0.0	0.0	0.0	0.0	0.8	0.0	0.4	0.0	0.0	0.0	0.0	0.0	0.8	0.2	1.0	0.0	0.0	0.0	0.0
51	0.0	0.0	0.0	0.2	1.1	0.0	0.2	0.0	0.0	0.0	0.0	0.0	0.0	0.0	0.0	0.0	0.0	0.0	0.2
50	0.0	0.0	0.0	0.0	0.3	0.0	0.3	0.0	0.0	0.0	0.3	0.0	0.0	0.0	0.0	0.0	0.0	0.0	0.0
49	0.0	0.0	0.0	0.0	0.5	0.0	0.0	0.0	0.0	0.0	0.5	0.0	0.3	0.0	0.3	0.3	0.0	0.0	0.0
48	0.0	0.0	0.0	0.0	0.5	0.0	0.0	0.0	0.0	0.0	0.3	0.0	0.3	0.0	0.0	0.3	0.0	0.0	0.0
47	0.0	0.0	0.0	0.0	0.5	0.0	0.3	0.0	0.0	0.0	0.0	0.0	0.0	0.0	0.0	0.0	0.0	0.0	0.0
46	0.0	0.0	0.0	0.0	0.0	0.0	0.0	0.0	0.0	0.0	0.3	0.0	0.3	0.0	0.5	0.5	0.0	0.0	0.0
45	0.0	0.0	0.0	0.0	0.3	0.0	0.0	0.0	0.3	0.0	0.0	0.0	0.6	0.0	0.8	0.3	0.0	0.0	0.0
44	0.0	0.0	0.0	0.0	0.3	0.0	0.3	0.0	0.0	0.0	0.0	0.0	0.0	0.0	0.0	0.0	0.0	0.0	0.0
43	0.0	0.0	0.0	0.0	0.3	0.0	0.0	0.3	0.0	0.0	0.0	0.0	0.0	0.0	0.0	0.3	0.0	0.0	0.0
42	0.0	0.0	0.0	0.0	0.2	0.0	0.0	0.2	0.0	0.0	0.2	0.0	0.2	0.0	0.0	0.5	0.0	0.0	0.0
41	0.0	0.0	0.0	0.0	0.3	0.0	0.3	0.0	0.0	0.0	0.0	0.0	0.0	0.0	0.3	0.0	0.0	0.0	0.0
40	0.0	0.0	0.0	0.3	0.8	0.0	0.3	0.0	0.0	0.0	0.0	0.0	0.3	0.0	0.3	0.0	0.0	0.0	0.0
39	0.0	0.0	0.0	0.0	0.0	0.0	0.0	0.0	0.0	0.0	0.0	0.0	0.3	0.0	0.0	0.0	0.0	0.0	0.0
38	0.0	0.0	0.0	0.0	0.0	0.0	0.5	0.3	0.0	0.0	0.0	0.0	0.0	0.0	0.0	0.3	0.0	0.0	0.0
37	0.0	0.0	0.0	0.0	0.0	0.0	0.6	0.0	0.0	0.0	0.0	0.0	0.0	0.3	0.0	0.0	0.0	0.0	0.0
36	0.0	0.0	0.0	0.0	0.3	0.0	0.0	0.3	0.0	0.0	0.0	0.0	0.3	0.3	0.0	0.5	0.3	0.0	0.0
35	0.0	0.0	0.0	0.2	0.5	0.0	0.2	0.0	0.0	0.0	0.0	0.0	0.0	0.0	0.0	0.2	0.0	0.0	0.0
34	0.0	0.0	0.0	0.0	0.8	0.3	0.0	0.0	0.0	0.0	0.0	0.0	0.0	0.3	0.0	0.0	0.0	0.0	0.0
33	0.0	0.3	0.0	0.0	0.3	0.0	0.5	0.0	0.0	0.0	0.0	0.0	0.3	0.3	0.0	0.5	0.3	0.0	0.0
32	0.0	0.0	0.0	0.0	0.8	0.0	0.0	0.0	0.0	0.0	0.0	0.0	0.3	0.0	0.3	0.0	0.0	0.0	0.0
31	0.0	0.0	0.0	0.0	0.8	0.3	0.0	0.0	0.0	0.0	0.0	0.0	0.0	0.0	0.0	0.8	0.0	0.0	0.0
30	0.0	0.0	0.0	0.0	1.1	0.0	0.3	0.0	0.0	0.0	0.3	0.0	0.0	0.0	0.3	0.0	0.0	0.0	0.0
29	0.0	0.0	0.0	0.0	0.0	0.0	0.0	0.0	0.0	0.0	0.0	0.0	0.0	0.0	0.0	1.2	0.0	0.0	0.0
28	0.0	0.0	0.0	0.0	0.8	0.3	0.0	0.0	0.0	0.0	0.0	0.0	0.0	0.0	0.3	0.3	0.0	0.0	0.0
27	0.0	0.0	0.0	0.0	0.3	0.0	0.0	0.0	0.0	0.0	0.0	0.0	0.0	0.0	0.6	0.0	0.0	0.3	0.0
26	0.0	0.0	0.0	0.3	0.0	0.0	0.0	0.3	0.0	0.0	0.3	0.0	0.0	0.0	0.3	0.0	0.3	0.0	0.0
25	0.0	0.0	0.0	0.3	0.0	0.0	0.3	0.3	0.0	0.0	0.0	0.0	0.0	0.0	0.0	0.3	0.0	0.0	0.0
24	0.0	0.0	0.0	0.3	0.8	0.0	0.0	0.0	0.0	0.0	0.0	0.0	0.0	0.0	0.5	0.3	0.0	0.0	0.0
23	0.0	0.0	0.0	0.0	0.3	0.0	0.3	0.0	0.0	0.0	0.0	0.0	0.3	0.0	0.0	1.1	0.0	0.0	0.0
22	0.0	0.0	0.0	0.3	0.6	0.0	0.0	0.0	0.0	0.0	0.3	0.0	0.0	0.0	0.3	0.6	0.0	0.0	0.0
21	0.0	0.0	0.0	0.0	1.1	0.0	0.0	0.3	0.0	0.0	0.0	0.0	0.0	0.0	0.0	0.0	0.0	0.0	0.0
20	0.0	0.0	0.0	0.0	0.0	0.0	0.3	0.3	0.0	0.0	0.3	0.0	0.0	0.0	0.0	0.0	0.0	0.0	0.0
19	0.0	0.0	0.0	0.0	0.3	0.0	0.6	0.3	0.0	0.0	0.0	0.0	0.6	0.0	0.3	0.0	0.0	0.3	0.0
18	0.0	0.0	0.0	0.3	0.0	0.0	0.3	0.0	0.0	0.0	0.0	0.0	0.0	0.0	0.0	0.0	0.0	0.0	0.0
17	0.0	0.0	0.0	0.0	0.0	0.0	0.3	0.0	0.0	0.0	0.0	0.0	0.3	0.0	0.3	0.0	0.0	0.0	0.0
16	0.0	0.0	0.0	0.0	0.3	0.0	0.0	0.0	0.0	0.0	0.0	0.0	0.0	0.0	0.3	0.3	0.0	0.0	0.0
15	0.0	0.0	0.0	0.0	0.3	0.0	0.0	0.0	0.0	0.0	0.0	0.0	0.0	0.0	0.0	0.7	0.0	0.0	0.0
14	0.0	0.0	0.0	0.0	0.7	0.0	0.0	0.0	0.0	0.0	0.0	0.0	0.3	0.0	0.0	0.3	0.0	0.0	0.0
13	0.0	0.0	0.0	0.0	0.0	0.0	0.0	0.0	0.0	0.0	0.0	0.0	0.0	0.0	0.0	0.4	0.0	0.0	0.0

sample	*Fraxinus*	Hamamelidaceae	*Hederea*	*Ilex*	*Juglans*	Lamiaceae	*Liquidambar*	*Lonicera*	Lythraceae	Malvaceae	Mastixiaceae	*Myriophyllum*	*Myrica*	Nympheaceae	*Nyssa*	Oleaceae	Onagraceae	*Platycarya*	Plumbaginaceae
12	0.0	0.0	0.0	0.0	0.0	0.0	0.6	0.3	0.0	0.0	0.0	0.0	0.0	0.0	0.6	0.0	0.0	0.3	0.0
11	0.0	0.0	0.0	0.0	0.6	0.0	0.0	0.0	0.0	0.0	0.0	0.0	0.0	0.0	0.0	0.3	0.0	0.0	0.0
10	0.0	0.0	0.0	0.0	0.3	0.0	0.0	0.0	0.0	0.0	0.3	0.0	0.0	0.0	0.0	0.6	0.0	0.0	0.0
9	0.0	0.0	0.0	0.0	0.3	0.0	0.3	0.3	0.0	0.0	0.0	0.0	0.0	0.0	0.0	0.3	0.0	0.3	0.0
8	0.0	0.0	0.0	0.0	0.9	0.0	0.0	0.0	0.0	0.0	0.0	0.0	0.0	0.0	0.6	0.0	0.0	0.0	0.0
7	0.0	0.0	0.0	0.0	0.0	0.0	0.4	0.0	0.0	0.0	0.0	0.0	0.0	0.0	0.0	0.7	0.0	0.0	0.0
6	0.0	0.0	0.0	0.0	0.3	0.0	0.0	0.0	0.0	0.0	0.0	0.0	0.3	0.0	0.0	0.0	0.0	0.0	0.0
5	0.0	0.0	0.0	0.0	0.3	0.0	0.5	0.0	0.0	0.0	0.3	0.0	0.8	0.0	0.3	0.0	0.0	0.3	0.0
4	0.0	0.0	0.0	0.0	0.3	0.0	0.0	0.3	0.0	0.0	0.3	0.0	0.6	0.0	0.0	0.0	0.0	0.0	0.0
3	0.0	0.0	0.0	0.0	0.8	0.3	0.5	0.0	0.0	0.0	0.3	0.0	0.0	0.0	0.5	0.3	0.0	0.3	0.0
2	0.0	0.0	0.0	0.3	1.5	0.0	0.0	0.0	0.0	0.0	0.0	0.0	1.2	0.0	0.0	0.3	0.0	0.0	0.0
1	0.0	0.0	0.0	0.0	0.6	0.0	0.3	0.0	0.0	0.0	0.3	0.0	0.3	0.0	0.0	0.6	0.0	0.0	0.0

sample	Poaceae	Potamogetaceae	*Pterocarya*	*Quercus*	Reevesia	*Rhus*	Rosaceae	Rubiaceae	Rutaceae	*Salix*	Sapotaceae	*Sparganium/Typha*	*Symplocos*	*Tilia*	Trapaceae	*Ulmus*	Vitaceae	*Zelkova*
98	13.7	0.0	0.9	2.4	0.0	0.3	0.0	0.3	0.0	0.0	0.0	5.1	0.0	0.3	0.0	3.6	0.0	0.0
97	10.2	0.0	1.7	4.0	0.0	0.0	0.0	0.0	0.0	0.0	0.0	5.7	0.0	0.0	0.0	4.2	0.0	0.6
96	11.5	0.0	2.3	1.1	0.0	0.0	0.3	0.0	0.0	0.0	0.3	8.6	0.3	0.0	0.0	3.2	0.6	0.3
95	11.1	0.3	2.5	1.3	0.0	0.0	0.0	0.0	0.0	0.0	0.0	8.6	0.0	0.3	0.0	3.2	0.0	0.0
94	9.3	0.0	3.0	2.1	0.0	0.0	0.0	0.0	0.0	0.0	0.0	9.3	0.0	0.3	0.0	3.3	0.0	0.0
93	11.5	0.0	1.1	2.7	0.0	0.0	0.0	0.3	0.3	0.0	0.0	5.9	0.0	0.0	0.0	2.4	0.0	0.0
92	8.4	0.0	2.7	2.2	0.0	0.0	0.0	0.0	0.0	0.0	0.3	6.2	0.0	0.0	0.0	2.2	0.0	0.3
91	7.4	0.0	1.5	0.9	0.0	0.3	0.0	0.0	0.0	0.0	0.0	13.3	0.0	0.3	0.0	2.8	0.3	0.3
90	8.8	0.3	2.3	2.0	0.0	0.0	0.0	0.0	0.0	0.0	0.0	8.2	0.0	0.3	0.0	1.3	0.3	0.0
89	8.9	0.0	1.8	2.1	0.0	0.3	0.0	0.0	0.0	0.0	0.0	8.3	0.0	0.0	0.0	2.1	0.3	0.0
88	12.2	0.0	0.9	2.9	0.0	0.0	0.0	0.0	0.0	0.0	0.0	9.9	0.0	0.0	0.0	1.7	0.3	0.0
87	10.9	0.0	0.6	3.8	0.0	0.3	0.3	0.0	0.0	0.0	0.3	9.3	0.0	0.3	0.0	3.8	0.0	0.0
86	10.6	0.0	2.1	2.6	0.0	0.3	0.0	0.6	0.0	0.3	0.6	8.2	0.0	0.0	0.0	3.5	0.0	0.0
85	8.8	0.0	3.2	2.6	0.0	0.0	0.0	0.3	0.0	0.0	0.0	7.0	0.0	0.0	0.0	1.8	0.6	0.3
84	7.8	0.0	1.3	3.1	0.0	0.0	0.0	0.0	0.0	0.0	0.0	4.1	0.0	0.0	0.0	2.5	0.3	0.3
83	8.8	0.0	1.0	1.3	0.0	0.0	0.0	0.3	0.0	0.0	0.0	9.1	0.0	0.3	0.0	4.9	0.0	0.0
82	11.6	0.3	1.3	2.6	0.0	0.3	0.0	0.6	0.0	0.0	0.0	8.0	0.3	0.3	0.0	3.2	0.0	0.0
81	10.5	0.0	1.4	2.0	0.0	0.3	0.0	0.0	0.0	0.0	0.0	9.1	0.3	0.0	0.0	2.8	0.0	0.3
80	9.6	0.0	2.2	1.2	0.0	0.0	0.3	0.6	0.0	0.0	0.0	7.1	0.0	0.0	0.0	1.6	0.0	0.0
79	12.2	0.0	2.4	1.0	0.0	0.0	0.0	0.0	0.0	0.0	0.0	5.2	0.0	0.0	0.0	3.5	0.3	0.0
78	11.8	0.0	1.6	2.5	0.0	0.0	0.0	0.0	0.0	0.0	0.0	11.8	0.0	0.0	0.0	1.2	0.0	0.0
77	7.2	0.6	1.8	3.0	0.0	0.0	0.0	1.5	0.0	0.0	0.3	7.2	0.0	0.0	0.0	3.0	0.3	0.0
76	5.8	0.0	2.3	3.8	0.0	0.0	0.0	0.0	0.0	0.0	0.0	3.3	0.0	0.3	0.0	2.0	0.3	0.0
75	12.1	0.3	0.9	1.5	0.0	0.3	0.0	0.0	0.0	0.0	0.0	7.9	0.0	0.0	0.0	0.0	0.6	0.0
74	6.7	0.4	0.0	4.5	0.0	0.0	0.0	0.0	0.0	0.0	0.0	10.8	0.0	0.0	0.0	0.7	0.0	0.0
73	12.9	0.0	1.3	2.9	0.0	0.3	0.0	0.6	0.3	0.0	0.0	8.0	0.0	0.0	0.0	2.3	0.0	0.3
72	6.8	0.0	2.3	2.0	0.0	0.0	0.0	0.8	0.0	0.0	0.0	6.5	0.0	0.8	0.0	1.1	0.0	0.3
71	8.3	0.0	1.9	3.2	0.0	0.0	0.0	0.0	0.5	0.0	0.0	8.3	0.0	0.0	0.0	0.0	0.0	0.3
70	5.3	0.0	1.5	2.9	0.0	0.0	0.0	0.0	0.0	0.0	0.3	7.0	0.3	0.0	0.0	1.5	0.0	0.0
69	6.5	0.0	1.7	2.8	0.0	0.3	0.0	0.0	0.0	0.0	0.0	5.7	0.3	0.3	0.0	2.3	0.0	0.0
68	4.9	0.0	0.5	3.8	0.0	0.0	0.3	0.0	0.0	0.0	0.0	5.4	0.0	0.3	0.0	1.9	0.0	0.5
67	8.0	0.6	2.2	2.2	0.0	0.0	0.0	0.0	0.0	0.6	0.0	6.1	0.0	0.0	0.0	2.8	0.3	0.3
66	6.3	0.0	1.1	1.1	0.0	0.0	0.0	0.0	0.0	0.0	0.0	4.7	0.0	0.8	0.0	1.9	0.3	0.5
65	8.1	0.3	2.2	1.7	0.0	0.0	0.0	0.0	0.0	0.0	0.0	5.9	0.0	0.3	0.0	2.2	0.3	0.3
64	7.7	0.0	1.9	1.6	0.0	0.0	0.0	0.0	0.0	0.0	0.0	5.7	0.0	0.0	0.0	2.7	0.3	0.0
63	8.4	0.0	3.0	3.2	0.3	0.0	0.0	0.0	0.0	0.0	0.0	4.1	0.0	0.3	0.0	1.9	0.0	0.0
62	5.0	0.7	1.2	1.2	0.0	0.0	0.2	0.0	0.0	0.0	0.0	4.0	0.2	0.0	0.0	2.1	0.0	0.0
61	4.0	1.0	1.5	2.2	0.0	0.0	0.2	0.7	0.5	0.0	0.0	2.2	0.0	0.5	0.0	0.7	0.0	0.0
60	7.7	0.3	1.8	3.7	0.3	0.0	0.3	0.0	0.3	0.3	0.0	5.5	0.0	0.0	0.0	2.1	0.0	0.3
59	3.8	0.3	2.5	1.8	0.0	0.0	0.0	0.0	0.0	0.0	0.0	4.8	0.0	0.0	0.0	1.8	0.0	0.5
58	5.2	0.7	2.4	2.8	0.0	0.0	0.0	0.3	0.0	0.0	0.0	5.5	0.0	0.7	0.0	1.4	0.3	1.0
57	4.1	0.0	1.4	2.9	0.0	0.0	0.0	0.0	0.0	0.0	0.0	2.3	0.0	0.6	0.0	1.7	0.3	0.0
56	4.6	0.0	1.0	5.0	0.0	0.0	0.0	0.7	0.0	0.0	0.0	4.0	0.0	0.7	0.0	2.6	0.0	0.0

sample	Poaceae	Potamogetaceae	*Pterocarya*	*Quercus*	Reevesia	*Rhus*	Rosaceae	Rubiaceae	Rutaceae	*Salix*	Sapotaceae	*Sparganium/Typha*	*Symplocos*	*Tilia*	Trapaceae	*Ulmus*	Vitaceae	*Zelkova*
55	7.0	0.2	2.7	2.9	0.0	0.0	0.0	0.5	0.5	0.0	0.2	4.3	0.0	0.0	0.0	2.3	0.0	0.5
54	4.3	0.0	1.7	1.9	0.0	0.4	0.0	0.0	0.0	0.0	0.2	2.4	0.0	0.4	0.0	2.4	0.4	0.2
53	6.0	0.0	2.3	3.5	0.0	0.0	0.7	0.7	0.2	0.0	0.0	1.8	0.0	0.0	0.0	2.1	0.2	0.0
52	5.9	0.4	1.9	2.7	0.0	0.4	0.0	0.6	0.0	0.0	0.6	1.9	0.0	0.8	0.0	0.2	0.0	0.2
51	6.1	0.4	2.7	1.6	0.0	0.0	0.4	0.9	0.0	0.0	0.0	2.0	0.0	0.4	0.0	1.4	0.0	0.2
50	9.0	0.0	2.1	2.7	0.0	0.0	0.0	0.0	0.0	0.0	0.0	1.5	0.3	0.0	0.0	1.8	0.0	0.0
49	6.6	0.0	1.3	3.3	0.3	0.0	0.0	0.0	0.0	0.0	0.3	3.8	0.0	0.0	0.0	1.0	0.0	0.0
48	9.2	0.0	1.0	1.3	0.0	0.0	0.0	0.0	0.3	0.0	0.0	3.6	0.0	0.3	0.0	1.0	0.5	0.0
47	4.4	0.0	1.3	0.8	0.0	0.3	0.3	0.0	0.0	0.0	0.5	2.8	0.0	0.3	0.0	1.3	0.0	0.0
46	6.9	0.0	1.1	0.8	0.0	0.0	0.0	0.0	0.3	0.0	0.3	1.3	0.0	0.0	0.0	1.9	0.0	0.0
45	5.4	0.0	1.4	3.4	0.0	0.0	0.0	0.0	0.0	0.0	0.3	2.0	0.0	0.6	0.0	4.2	0.0	0.0
44	4.8	0.0	0.6	3.4	0.0	0.0	0.0	0.0	0.0	0.0	0.3	4.5	0.0	0.0	0.0	2.8	0.3	0.0
43	5.3	0.3	0.3	2.8	0.0	0.0	0.0	0.0	0.0	0.0	0.0	3.6	0.0	0.0	0.0	1.4	0.3	0.0
42	3.7	0.0	1.0	2.0	0.0	0.0	0.2	0.0	0.0	0.0	0.0	2.0	0.0	0.0	0.0	2.0	0.0	0.0
41	7.8	0.0	0.3	1.1	0.0	0.0	0.0	0.0	0.0	0.0	0.3	4.5	0.0	0.3	0.3	2.5	0.3	0.0
40	5.7	0.3	0.5	1.4	0.0	0.0	0.0	0.0	0.0	0.0	0.0	3.6	0.0	0.5	0.0	0.8	0.0	0.0
39	6.7	0.0	1.1	0.6	0.0	0.0	0.0	0.3	0.0	0.0	0.0	3.6	0.0	0.3	0.0	2.8	0.3	0.3
38	6.7	0.0	1.6	1.6	0.0	0.0	0.0	0.0	0.0	0.0	0.0	1.9	0.0	0.3	0.3	1.1	0.0	0.3
37	5.8	0.0	1.5	2.4	0.0	0.0	0.0	0.3	0.0	0.0	0.0	5.5	0.0	0.0	0.0	2.7	0.6	0.0
36	7.7	0.3	1.1	1.6	0.0	0.0	0.0	0.3	0.0	0.0	0.0	3.8	0.0	0.5	0.0	3.8	0.5	0.0
35	4.1	0.0	0.7	1.2	0.0	0.0	0.0	0.0	0.0	0.0	0.0	5.6	0.0	0.0	0.0	2.4	0.0	0.0
34	6.8	0.0	1.0	0.3	0.0	0.0	0.3	0.0	0.0	0.0	0.0	4.8	0.0	0.0	0.0	2.5	0.0	0.0
33	13.2	0.0	0.3	1.6	0.0	0.0	0.0	0.3	0.0	0.0	0.0	3.5	0.0	0.0	0.0	1.6	0.5	0.0
32	10.0	0.0	1.7	1.4	0.0	0.0	0.0	0.3	0.0	0.0	0.0	3.9	0.0	0.3	0.0	1.7	0.3	0.0
31	6.2	0.3	2.3	2.1	0.0	0.0	0.3	0.0	0.0	0.0	0.0	4.4	0.3	0.0	0.0	2.6	0.3	0.0
30	7.9	0.0	1.1	1.6	0.0	0.0	0.3	0.0	0.0	0.0	0.0	5.4	0.0	0.5	0.3	1.6	1.1	0.3
29	6.8	0.6	1.2	2.2	0.0	0.0	0.0	0.3	0.0	0.0	0.3	10.5	0.0	0.0	0.0	4.0	0.3	0.3
28	5.6	0.0	1.1	0.8	0.0	0.0	0.0	0.3	0.0	0.0	0.0	9.5	0.0	0.0	0.0	2.5	0.3	0.3
27	7.8	0.0	0.3	1.1	0.0	0.0	0.0	0.0	0.0	0.0	0.0	5.8	0.0	0.3	0.0	2.2	0.6	0.0
26	7.0	0.3	0.9	2.3	0.0	0.0	0.0	0.0	0.0	0.0	0.0	4.7	0.0	0.3	0.0	4.4	0.6	0.0
25	7.6	0.6	1.2	1.5	0.0	0.0	0.0	0.0	0.0	0.0	0.0	8.5	0.0	0.3	0.0	2.7	0.6	0.3
24	4.3	0.8	0.5	2.8	0.0	0.0	0.0	0.0	0.0	0.0	0.0	4.8	0.0	0.3	0.0	3.8	0.3	0.0
23	7.5	0.6	0.8	1.4	0.0	0.0	0.0	0.0	0.0	0.0	0.6	6.4	0.0	0.6	0.0	3.1	0.8	0.0
22	7.2	0.3	0.6	3.5	0.0	0.0	0.0	0.0	0.3	0.0	0.0	7.5	0.0	0.3	0.0	2.9	0.0	0.0
21	5.9	0.8	1.1	2.2	0.0	0.0	0.3	0.0	0.0	0.0	0.0	8.6	0.0	0.3	0.0	1.9	0.8	0.3
20	8.2	0.0	1.1	2.7	0.0	0.0	0.0	0.0	0.0	0.0	0.3	9.3	0.0	0.5	0.0	1.6	0.3	0.0
19	8.8	1.4	1.7	4.3	0.0	0.0	0.0	0.3	0.0	0.0	0.3	5.7	0.3	0.0	0.0	2.8	0.6	0.3
18	11.6	0.6	0.3	1.7	0.0	0.0	0.0	0.9	0.3	0.0	0.3	7.2	0.0	0.0	0.0	2.3	0.9	0.0
17	10.4	0.8	1.1	2.5	0.0	0.0	0.0	0.5	0.3	0.0	0.0	6.0	0.0	0.3	0.0	3.3	1.1	0.3
16	12.6	0.6	0.3	2.5	0.0	0.0	0.0	0.0	0.0	0.0	0.0	7.2	0.0	0.0	0.0	3.1	0.0	0.3
15	11.1	0.0	1.6	2.3	0.0	0.0	0.0	0.3	0.0	0.0	0.0	12.5	0.0	0.0	0.0	3.3	0.3	0.3
14	14.6	0.0	1.3	2.0	0.0	0.0	0.0	0.0	0.3	0.0	0.0	7.0	0.0	0.0	0.0	0.7	0.3	0.7
13	9.5	0.0	2.5	3.2	0.0	0.0	0.0	0.7	0.0	0.0	0.0	9.5	0.0	0.4	0.0	2.1	0.0	0.4

sample	**Poaceae**	**Potamogetaceae**	***Pterocarya***	***Quercus***	**Reevesia**	***Rhus***	**Rosaceae**	**Rubiaceae**	**Rutaceae**	***Salix***	**Sapotaceae**	***Sparganium/Typha***	***Symplocos***	***Tilia***	**Trapaceae**	***Ulmus***	**Vitaceae**	***Zelkova***
12	9.0	0.0	1.7	3.5	0.0	0.0	0.0	0.0	0.0	0.0	0.0	8.4	0.0	0.0	0.0	3.8	1.4	0.6
11	9.7	0.0	1.5	2.4	0.0	0.0	0.3	0.0	0.0	0.0	0.0	6.4	0.0	0.3	0.0	2.1	0.0	0.0
10	7.5	0.0	0.9	1.7	0.0	0.3	0.0	0.0	0.0	0.0	0.0	8.9	0.0	0.0	0.0	3.2	0.9	0.0
9	4.6	0.0	1.1	3.5	0.0	0.0	0.0	0.0	0.0	0.0	0.0	8.9	0.0	0.0	0.3	2.2	0.5	0.3
8	5.4	0.0	3.4	2.0	0.0	0.0	0.0	0.0	0.0	0.0	0.0	6.6	0.0	0.0	0.0	3.1	0.3	0.0
7	8.2	0.0	0.7	3.9	0.0	0.0	0.0	0.0	0.0	0.0	0.0	11.8	0.0	0.0	0.0	1.4	0.0	0.0
6	11.4	0.0	1.6	1.9	0.0	0.0	0.0	0.0	0.0	0.0	0.0	5.4	0.0	0.3	0.0	2.4	0.0	0.3
5	10.5	0.0	2.2	1.1	0.0	0.0	0.0	0.0	0.0	0.3	0.0	6.2	0.0	0.5	0.0	3.0	0.3	0.5
4	6.6	0.0	2.9	2.9	0.3	0.0	0.0	0.0	0.3	0.0	0.3	4.9	0.0	0.0	0.0	2.9	1.2	0.0
3	4.5	0.0	2.0	1.8	0.0	0.3	0.0	0.8	0.0	0.0	0.0	2.8	0.3	0.0	0.0	2.8	0.0	0.0
2	6.7	0.0	2.1	1.2	0.0	0.0	0.0	0.0	0.0	0.0	0.0	2.5	0.0	0.0	0.0	1.2	0.3	0.3
1	3.8	0.0	2.6	2.0	0.0	0.0	0.0	0.0	0.3	0.0	0.0	0.9	0.0	0.3	0.0	2.0	0.0	0.6

sample	*cf. Algid. minutum cezare/Cyst of Pentapharsodinium dalei*	*Batiacasphaera sphaerica*	*Impagidinium spp*	*Lejeunecysta spp.*	*Mendicodinium sp.*	*Nematosphaeropsis sp.*	*Polykrikos cysts*	*Polysphaeridium zoharyi*	*Pyxidinopsis psilata*	Rounded brown cysts	*Selenopemphix nephroides*	*Selenopemphix sp. 1*	Small Spiny palynomorph	*Spiniferites bentorii budajenoensis*	*Spiniferites bentorii pannonicus*	*Spiniferites bentorii oblongus*	*Spiniferites/Achomosphaera spp*
98	0.0	0.0	13.7	0.3	0.0	0.3	0.0	0.0	0.0	10.7	2.3	0.7	8.3	1.7	1.7	0.3	60.0
97	0.0	0.0	12.7	0.7	0.0	0.3	0.3	0.0	0.0	11.7	2.7	2.3	8.0	3.7	2.7	0.0	55.0
96	0.0	0.0	17.7	0.0	0.0	0.0	0.0	0.0	0.0	10.7	1.0	0.7	8.7	2.7	1.3	0.0	57.3
95	0.0	0.0	19.3	0.0	0.0	0.0	0.0	0.0	0.0	15.0	3.0	1.7	10.3	4.0	2.7	0.0	44.0
94	0.0	0.0	19.3	0.3	0.0	0.0	0.0	0.0	0.0	22.3	1.7	4.3	11.7	6.0	3.0	0.0	31.3
93	0.0	0.0	18.3	0.0	0.0	0.0	0.0	0.0	0.0	20.7	3.0	5.0	9.0	7.0	4.7	0.0	32.3
92	0.0	0.0	23.7	0.3	0.0	0.0	0.3	0.0	0.0	17.0	1.7	1.0	5.0	5.0	4.3	0.0	41.7
91	0.0	0.0	8.0	0.0	0.0	0.0	0.0	0.0	0.0	7.0	0.7	3.3	12.7	8.3	6.0	0.0	54.0
90	0.0	0.0	6.7	0.3	0.0	0.3	0.7	0.0	0.0	18.0	0.3	5.7	13.7	3.3	1.7	0.0	49.3
89	0.0	0.0	8.0	0.0	0.0	0.0	0.0	0.0	0.0	24.7	1.7	4.0	31.3	2.7	1.3	0.0	26.3
88	0.0	0.0	10.7	0.0	0.0	0.0	0.7	0.0	0.0	17.7	3.3	5.7	15.7	3.3	1.7	0.0	41.3
87	0.0	0.0	11.7	0.0	0.0	0.0	0.7	0.0	0.0	17.3	0.3	3.0	15.3	4.0	2.0	0.0	45.7
86	0.0	0.0	11.3	0.0	0.0	0.3	0.3	0.0	0.0	16.3	2.0	1.7	12.3	3.0	3.3	0.0	49.3
85	0.0	0.0	7.7	0.0	0.0	0.0	0.3	0.0	0.0	18.3	0.7	1.3	11.3	6.0	4.0	0.0	50.3
84	0.0	0.0	6.0	0.0	0.0	0.0	0.0	0.0	0.0	13.3	1.0	1.7	6.3	5.7	3.0	0.0	63.0
83	0.0	0.0	6.7	0.0	0.0	0.0	0.0	0.0	0.0	18.3	1.0	4.3	13.3	3.0	1.7	0.0	51.7
82	0.0	0.0	5.7	0.0	0.0	0.0	0.0	0.0	0.0	20.3	0.7	1.7	15.0	4.7	2.7	0.0	49.3
81	0.0	0.0	4.7	0.0	0.0	0.0	0.0	0.0	0.0	19.1	1.7	3.0	10.4	2.7	1.0	0.0	57.4
80	0.0	0.3	4.0	0.0	0.0	0.0	0.0	0.0	0.0	11.7	0.3	2.7	10.0	3.3	1.0	0.0	66.7
79	0.0	0.0	6.7	0.0	0.0	0.0	0.0	0.0	0.0	6.7	1.3	2.7	14.0	18.7	10.0	0.0	40.0
78	0.0	0.0	5.3	0.3	0.0	0.0	0.0	0.3	0.0	7.7	0.0	5.3	17.3	8.3	3.7	0.0	51.7
77	0.0	0.0	8.7	0.0	0.0	0.0	0.3	0.0	0.0	10.0	0.3	1.3	15.0	11.7	7.0	0.0	45.7
76	0.0	0.0	6.0	0.7	0.0	0.0	0.3	0.0	0.0	12.7	0.7	12.3	27.3	6.0	4.0	0.0	30.0
75	0.0	0.0	8.7	0.3	0.0	0.0	1.0	0.0	0.0	6.7	0.7	5.7	22.7	5.7	3.7	0.0	45.0
74	0.0	0.3	4.7	0.0	0.0	0.0	0.3	0.0	0.0	4.7	0.7	8.7	21.3	4.3	3.7	0.0	51.3
73	0.0	0.0	10.3	0.3	0.0	0.0	0.0	0.0	0.0	5.7	1.0	5.3	21.3	7.3	4.0	0.0	44.7
72	0.0	0.0	7.3	0.0	0.0	0.0	0.0	0.0	0.0	10.0	0.7	7.3	26.7	5.7	3.7	0.3	38.3
71	0.0	0.0	5.7	0.0	0.0	0.0	0.0	0.0	0.0	10.7	1.7	5.0	18.7	5.7	4.3	0.0	48.3
70	0.0	0.0	7.3	0.0	0.0	0.0	0.0	0.0	0.0	8.3	1.3	3.3	10.7	10.7	6.0	0.0	52.3
69	0.0	0.0	11.0	0.0	0.0	0.0	0.0	0.0	0.0	10.3	1.7	4.0	8.3	7.3	3.7	0.0	53.7
68	0.0	0.0	13.7	0.0	0.0	0.0	0.0	0.0	0.3	15.3	1.3	5.3	8.7	6.7	6.3	0.0	42.3
67	0.0	0.0	11.0	0.0	0.0	0.0	0.0	0.0	0.0	16.7	1.7	3.3	16.7	8.0	5.7	0.3	36.7
66	0.0	0.0	15.0	0.0	0.0	0.0	0.0	0.0	0.0	14.7	2.0	4.7	12.7	6.7	3.3	0.0	41.0
65	0.0	0.0	8.0	0.0	0.0	0.0	0.0	0.0	0.0	20.3	2.0	3.7	20.0	9.0	2.0	0.0	35.0
64	0.0	0.0	8.7	0.0	0.0	0.0	0.3	0.0	0.0	11.7	1.3	4.3	27.7	6.7	2.7	0.0	36.7
63	0.0	0.0	9.7	0.0	0.0	0.0	0.0	0.0	0.0	18.7	0.7	6.0	18.0	5.3	3.3	0.0	38.3
62	0.0	0.0	11.0	0.0	0.0	0.0	0.3	0.0	0.0	14.0	1.0	3.3	19.0	6.7	4.0	0.0	40.7
61	0.0	0.0	7.1	0.0	0.0	0.0	0.3	0.0	0.0	12.5	1.7	7.5	20.3	4.7	2.0	0.0	43.7
60	0.0	0.0	4.0	0.0	0.0	0.0	0.0	0.0	0.0	15.7	1.3	3.3	50.3	2.7	1.3	0.0	21.3
59	0.0	0.0	4.0	0.0	0.0	0.0	0.0	0.0	0.0	11.0	1.3	2.7	18.3	6.3	3.7	0.0	52.7
58	0.0	0.0	2.3	0.0	0.0	0.0	0.0	0.0	0.0	13.3	1.0	5.7	22.7	6.7	2.0	0.0	46.3
57	0.0	0.0	3.7	0.0	0.0	0.0	0.0	0.0	0.0	14.8	1.3	4.0	16.2	5.4	4.7	0.0	49.8
56	0.0	0.0	5.3	0.0	0.0	0.0	0.3	0.0	0.0	13.0	1.0	4.3	13.7	6.3	3.3	0.0	52.7

sample	***cf. Algid. minutum cezare/Cyst of Pentapharsodinium dalei***	***Batiacasphaera sphaerica***	***Impagidinium spp***	***Lejeunecysta spp.***	***Mendicodinium sp.***	***Nematosphaeropsis sp.***	***Polykrikos cysts***	***Polysphaeridium zoharyi***	***Pyxidinopsis psilata***	**Rounded brown cysts**	***Selenopemphix nephroides***	***Selenopemphix sp. 1***	**Small Spiny palynomorph**	***Spiniferites bentorii budajenoensis***	***Spiniferites bentorii pannonicus***	***Spiniferites bentorii oblongus***	***Spiniferites/Achomosphaera spp***
55	0.0	0.0	7.0	0.0	0.0	0.0	0.0	0.0	0.0	14.7	1.3	0.3	16.0	4.7	2.7	0.0	53.3
54	0.0	0.0	11.7	0.0	0.0	0.0	0.3	0.0	0.0	20.7	3.3	1.7	10.0	1.3	1.7	0.0	49.3
53	0.0	0.3	9.1	1.0	0.0	0.0	0.3	0.0	0.0	13.2	3.7	0.7	17.9	2.0	3.7	0.0	48.0
52	0.0	0.0	13.0	1.3	0.0	0.3	0.0	0.0	0.0	10.3	7.0	2.7	18.0	3.0	1.3	0.7	42.3
51	0.0	0.0	9.6	1.4	0.0	0.0	0.0	0.0	0.3	9.2	5.8	0.7	13.0	2.0	2.4	1.0	54.6
50	0.0	0.0	4.3	0.0	0.3	0.0	0.7	0.0	0.0	5.6	0.7	5.0	22.9	1.0	0.0	0.7	58.8
49	0.0	0.0	7.5	0.0	0.0	0.0	0.7	0.0	0.0	13.1	0.0	3.3	26.8	0.3	0.7	0.3	47.4
48	0.0	0.0	5.5	0.0	0.0	0.0	0.3	0.0	0.0	11.7	0.3	5.2	21.0	0.0	0.0	0.3	55.7
47	0.0	0.0	6.8	0.0	0.0	0.0	0.3	0.0	0.3	10.2	0.0	6.5	18.6	6.5	4.3	0.6	45.7
46	0.0	0.0	4.3	0.0	0.0	0.0	0.0	0.0	0.6	12.1	0.0	6.8	25.8	5.3	7.1	0.3	37.6
45	0.0	0.0	3.5	0.0	0.3	0.0	0.6	0.0	0.3	16.4	0.6	7.3	33.3	5.0	3.2	0.3	29.2
44	0.0	0.0	1.9	0.0	0.0	0.0	0.3	0.0	0.3	6.1	1.0	5.8	24.7	6.1	7.4	0.3	46.2
43	0.0	0.0	5.1	0.0	0.3	0.0	0.0	0.0	0.0	11.6	1.0	5.5	25.7	3.9	2.6	0.0	44.4
42	0.0	0.0	5.4	0.0	0.9	0.0	0.9	0.0	0.0	12.9	0.6	3.0	32.4	6.6	3.9	0.0	33.3
41	0.0	0.0	4.7	0.0	1.5	0.0	0.3	0.0	0.0	10.7	0.0	3.6	32.0	4.1	5.0	0.0	38.2
40	0.0	0.0	6.6	0.0	0.0	0.0	0.9	0.0	0.3	11.4	0.0	3.3	31.4	6.3	4.2	0.6	35.0
39	0.0	0.0	9.8	0.0	0.0	0.0	0.3	0.0	0.9	8.0	0.9	4.3	29.1	5.5	2.4	0.0	38.8
38	0.0	0.0	5.7	0.0	0.0	0.0	0.7	0.0	0.3	8.7	0.7	2.7	21.3	8.7	3.7	1.0	46.7
37	0.0	0.0	2.8	0.0	0.0	0.0	0.3	0.0	0.8	9.8	0.8	2.8	35.8	4.5	5.3	0.8	36.3
36	0.3	0.0	7.3	0.0	0.0	0.0	0.6	0.0	0.0	9.1	0.9	2.0	33.6	7.9	4.7	0.0	33.6
35	0.0	0.0	4.9	0.0	0.3	0.0	0.0	0.0	0.3	11.6	0.0	3.6	34.3	8.2	6.4	0.0	30.4
34	0.0	0.5	5.1	0.0	0.0	0.0	0.8	0.0	0.3	12.4	0.8	6.8	38.4	6.5	4.9	0.0	23.5
33	0.0	0.0	3.4	0.0	1.2	0.0	0.3	0.0	0.3	9.2	0.0	5.2	31.7	3.1	5.5	0.3	39.7
32	0.0	0.0	3.9	0.0	0.0	0.0	0.6	0.0	0.0	7.9	0.6	3.6	34.1	3.6	5.7	0.0	39.9
31	0.0	0.0	3.8	0.0	0.3	0.0	0.6	0.0	0.0	6.7	0.3	3.8	25.2	9.6	3.5	0.0	46.0
30	0.3	0.0	5.3	0.0	1.5	0.0	0.6	0.0	0.0	5.3	0.3	3.6	30.6	5.9	4.7	0.3	41.5
29	0.0	0.0	5.2	0.0	0.0	0.0	1.1	0.0	0.0	7.4	1.4	3.6	39.6	4.9	3.0	0.5	33.3
28	0.0	0.0	5.6	0.0	0.0	0.3	0.6	0.0	0.0	9.0	0.0	4.2	28.9	9.8	4.8	0.3	36.5
27	0.0	0.0	5.8	0.0	0.0	0.0	0.3	0.0	0.0	14.6	0.9	2.6	25.9	9.6	2.3	0.0	37.9
26	0.3	0.0	5.8	0.0	0.0	0.0	0.6	0.0	0.0	11.6	1.2	4.9	29.7	4.7	3.2	0.3	37.8
25	0.3	0.0	4.4	0.0	0.0	0.0	0.3	0.0	0.0	10.4	1.0	5.4	38.3	5.4	3.9	0.0	30.6
24	0.3	0.0	2.4	0.0	0.0	0.0	0.3	0.0	0.0	14.5	0.6	3.0	23.6	9.4	5.7	0.0	40.2
23	0.9	0.0	5.7	0.0	0.0	0.0	0.9	0.0	0.3	16.7	0.9	2.3	28.7	6.0	3.2	0.0	34.5
22	0.0	0.0	3.7	0.0	0.0	0.0	1.4	0.0	0.0	16.5	1.1	7.1	28.4	4.8	2.8	0.0	34.1
21	0.9	0.0	8.0	0.0	0.0	0.0	0.6	0.0	0.3	14.8	1.2	7.1	**27.2**	4.1	2.4	0.0	33.4
20	0.0	0.0	5.6	0.0	0.0	0.3	0.9	0.0	0.6	13.4	1.6	3.4	11.8	6.9	4.7	0.3	50.5
19	0.0	0.0	4.7	0.0	0.0	0.0	0.7	0.0	0.3	15.0	1.7	3.3	21.7	3.0	3.3	0.3	46.0
18	0.0	0.0	6.2	0.0	0.3	0.0	0.3	0.0	0.0	11.7	3.6	2.6	23.1	6.2	3.6	0.3	42.0
17	0.0	0.0	5.3	0.0	0.0	0.0	0.0	0.0	0.0	19.9	1.7	4.0	25.2	4.3	2.7	0.0	36.9
16	0.0	0.0	6.6	0.7	1.0	0.3	0.0	0.0	0.0	26.0	2.6	4.9	13.5	2.6	1.6	0.0	40.1
15	0.0	0.0	3.9	0.3	0.0	0.0	0.0	0.0	0.0	29.0	0.3	6.8	22.9	3.5	1.6	0.3	31.3
14	0.0	0.0	5.7	0.0	0.0	0.0	0.7	0.0	0.0	23.3	0.0	3.0	29.0	3.0	2.3	0.3	32.7
13	0.0	0.0	4.3	0.0	0.7	0.0	0.3	0.0	0.0	22.5	0.7	2.0	29.1	3.3	4.0	0.0	33.1

sample	*cf. Algid. minutum cezare/Cyst of Pentapharsodinium dalei*	*Batiacasphaera sphaerica*	*Impagidinium spp*	*Lejeunecysta spp.*	*Mendicodinium* sp.	*Nematosphaeropsis sp.*	*Polykrikos* cysts	*Polysphaeridium zoharyi*	*Pyxidinopsis psilata*	Rounded brown cysts	*Selenopemphix nephroides*	*Selenopemphix* sp. 1	Small Spiny palynomorph	*Spiniferites bentorii budajenoensis*	*Spiniferites bentorii pannonicus*	*Spiniferites bentorii oblongus*	*Spiniferites/Achomosphaera* spp
12	0.0	0.0	3.2	0.0	0.0	0.0	0.0	0.0	0.0	20.4	1.3	1.6	35.0	3.9	2.6	0.0	32.0
11	0.0	0.0	5.7	0.0	0.0	0.3	0.3	0.0	0.0	20.3	0.0	3.0	35.0	0.3	0.3	0.0	34.7
10	0.0	0.0	1.8	0.3	0.0	0.0	0.6	0.0	0.0	24.6	0.0	4.9	40.1	2.7	2.1	0.3	22.5
9	0.0	0.0	6.5	0.0	0.0	0.0	0.4	0.0	0.0	4.4	1.2	3.2	36.7	3.2	2.8	0.4	41.1
8	0.0	0.0	7.6	0.0	0.3	0.0	0.3	0.0	0.0	23.9	1.3	3.3	24.9	3.0	2.0	0.0	33.2
7	0.0	0.0	4.0	0.0	0.0	0.0	0.3	0.0	0.0	24.0	1.3	2.7	35.0	2.0	0.7	0.0	30.0
6	0.0	0.0	3.0	0.0	0.0	0.0	0.0	0.0	0.0	23.3	0.3	3.3	23.7	4.3	2.0	0.0	40.0
5	0.0	0.0	5.2	0.0	0.0	0.0	0.0	0.0	0.0	23.5	0.3	2.3	20.5	1.6	1.0	0.0	45.6
4	0.0	0.0	5.3	0.0	0.0	0.3	0.0	0.0	0.0	15.3	1.3	3.7	21.3	2.3	1.0	0.3	49.0
3	0.0	0.0	4.9	0.0	0.0	0.3	0.0	0.0	0.0	21.6	0.3	3.6	22.2	3.3	2.1	0.6	41.0
2	0.0	0.0	8.3	0.0	0.0	0.0	0.3	0.0	0.0	12.3	0.3	3.3	31.9	2.0	0.7	0.3	40.5
1	0.0	0.0	5.0	0.0	0.0	0.0	0.0	0.0	0.0	14.0	2.3	3.0	30.3	2.7	2.0	0.7	40.0

7.3.2. Coexistence Approach climatic data **(Table 3.2)**

Detailed climatic values of the Coexistence intervals is shown next to the total taxa number of taxa included in each estimate. the total number in gerneal and a list of excluded plants for each of the intervals.

sample	taxa anlaysed	MAT min (°C)	MAT max (°C)	CMT min (°C)	CMT max (°C)	WMT min (°C)	WMT max (°C)	MAP min (mm/yr)	MAP max (mm/yr)	Mpwet min (mm/m)	Mpwet max (mm/m)	Mpdry min (mm/m)	Mpdry max (mm/m)	Mpwarm min (mm/m)	Mpwarm max (mm/m)	excluded taxa
98	16	11,5	20,5	-1	13,3	23	28,1	735	1520	109	195	18	24	66	141	*Picea, Cathaya, Tsuga, Sciadopitys*
97	13	15,6	21,9	5	13,6	24,7	28,1	823	1520	204	245	8	24	79	180	*Picea, Cathaya, Tsuga, Sciadopitys*
96	16	15,6	21,9	5	13,6	24,7	27,9	823	1520	204	236	8	24	79	180	*Picea, Cathaya, Tsuga, Sciadopitys*
95	15	15,6	20,8	5	13,3	24,7	27,9	823	1520	204	236	9	37	79	180	*Picea, Cathaya, Tsuga, Sciadopitys*
94	14	15,7	20,8	9,6	13,3	24,7	28,1	823	1520	204	236	9	24	79	180	*Picea, Cathaya, Tsuga, Sciadopitys*
93	11	15,6	23,1	5	16,4	24,7	28,1	823	1520	204	245	8	24	79	180	*Picea, Cathaya, Tsuga, Sciadopitys, Keteleeria*
92	16	12,9	21,9	0,9	13,6	23,6	27,9	641	1520	106	245	8	24	66	180	*Picea, Cathaya, Tsuga, Sciadopitys, Keteleeria*
91	16	15,6	20,8	5	13,3	24,7	27,9	823	1520	109	236	18	24	79	180	*Picea, Cathaya, Tsuga, Sciadopitys*
90	15	15,6	20,8	5	13,3	24,7	27,9	823	1520	204	236	9	24	79	180	*Picea, Cathaya, Tsuga, Sciadopitys, Keteleeria*
89	17	15,6	23,1	5	16,4	24,7	28,1	823	1520	109	245	18	24	79	180	*Picea, Cathaya, Tsuga, Sciadopitys, Keteleeria*
88	13	11,5	23,1	-1	16,4	23	28,1	619	1520	109	245	8	24	45	180	*Picea, Cathaya, Tsuga, Sciadopitys, Keteleeria*
87	16	13,3	20,8	0,9	13,3	23,6	27,9	735	1520	106	195	18	24	55	180	*Picea, Cathaya, Tsuga, Keteleeria, Cedrus*
86	17	15,7	23,1	9,6	16,4	23,6	27,9	735	1520	175	195	18	24	55	180	*Picea, Cathaya, Tsuga, Sciadopitys, Ephedra*
85	16	11,5	21,9	-0,1	13,6	23	27,9	641	1520	109	245	8	43	55	180	*Picea, Cathaya, Tsuga, Sciadopitys, Keteleeria*
84	14	13,3	21,9	-0,1	13,6	23	28,1	619	1520	109	245	8	24	66	180	*Picea, Cathaya, Sciadopitys, Keteleeria*
83	14	15,6	20,8	5	13,3	24,7	28,1	823	1520	204	236	9	43	79	172	*Picea, Cathaya, Tsuga, Sciadopitys, Keteleeria*
82	17	13,6	20,8	1,8	13,3	23,6	28,1	735	1520	109	195	18	43	49	180	*Picea, Cathaya, Tsuga, Sciadopitys*
81	17	15,6	21,9	5	13,6	24,7	27,9	823	1520	109	245	18	24	79	180	*Picea, Cathaya, Tsuga, Sciadopitys, Keteleeria*
80	18	15,6	23,1	5	16,4	24,7	27,9	823	1520	204	245	8	24	79	172	*Picea, Cathaya, Tsuga, Sciadopitys, Keteleeria*
79	12	15,6	23,1	5	16,4	24,7	28,1	823	1520	204	245	8	24	79	180	*Picea, Cathaya, Tsuga, Sciadopitys, Keteleeria*
78	16	15,7	23,1	9,6	16,4	24,7	27,9	823	1520	204	245	8	24	79	180	*Picea, Cathaya, Tsuga, Sciadopitys, Keteleeria*
77	17	15,7	23,1	9,6	16,4	24,7	27,9	823	1520	204	245	8	24	79	180	*Picea, Cathaya, Tsuga, Sciadopitys, Keteleeria*
76	11	11,5	20,8	-1	13,3	23	27,9	619	1520	109	236	9	24	55	180	*Picea, Cathaya, Tsuga, Sciadopitys, Keteleeria*
75	15	15,6	23,1	5	16,4	24,7	27,9	823	1520	92	245	18	24	79	180	*Picea, Cathaya, Sciadopitys, Keteleeria*
74	14	13,3	23,1	-0,1	17	23	27,9	641	1520	109	245	8	24	55	180	*Picea, Cathaya, Tsuga, Sciadopitys*
73	13	11,5	21,9	-0,1	13,6	23	28,3	735	1520	109	195	18	37	73	180	*Picea, Cathaya, Tsuga, Sciadopitys*
72	15	13,3	20,8	-0,1	13,3	23	27,9	619	1520	109	236	9	24	55	180	*Picea, Cathaya, Tsuga, Sciadopitys, Keteleeria, Cedrus*
71	16	13,3	20,5	-0,1	13,6	23	27,9	619	1520	109	236	8	24	55	141	*Picea, Cathaya, Tsuga, Sciadopitys, Keteleeria*
70	16	15,6	23,1	5	16,4	24,7	27,9	823	1520	204	245	8	24	79	180	*Picea, Cathaya, Tsuga, Sciadopitys, Keteleeria*
69	18	15,6	20,8	5	13,3	24,7	27,9	823	1520	109	236	18	24	79	180	*Picea, Cathaya, Tsuga, Sciadopitys*
68	18	15,6	20,8	5	13,3	24,7	28,1	823	1520	204	236	9	24	79	180	*Picea, Cathaya, Tsuga, Sciadopitys, Keteleeria*
67	18	15,6	21,9	5	13,6	24,7	28,1	823	1520	204	245	8	24	79	180	*Picea, Cathaya, Tsuga, Sciadopitys, Keteleeria*
66	19	15,6	20,8	5	13,3	24,7	27,9	823	1520	204	236	9	24	79	180	*Picea, Cathaya, Tsuga, Sciadopitys, Keteleeria*
65	17	15,6	20,8	5	13,3	24,7	27,9	823	1520	204	236	9	24	79	180	*Picea, Cathaya, Tsuga, Sciadopitys, Keteleeria*

sample	taxa anlaysed	MAT min (°C)	MAT max (°C)	CMT min (°C)	CMT max (°C)	WMT min (°C)	WMT max (°C)	MAP min (mm/yr)	MAP max (mm/yr)	Mpwet min (mm/m)	Mpwet max (mm/m)	Mpdry min (mm/m)	Mpdry max (mm/m)	Mpwarm min (mm/m)	Mpwarm max (mm/m)	excluded taxa
64	14	15,6	23,1	5	16,4	24,7	27,9	823	1520	204	245	8	24	79	172	*Picea, Cathaya, Tsuga, Sciadopitys, Keteleeria*
63	19	17,2	20,5	5	13,3	24,7	28,1	1187	1520	204	236	9	24	118	141	*Picea, Cathaya, Tsuga, Sciadopitys, Keteleeria*
62	17	13,6	23,1	1,8	16,4	23,6	27,9	619	1520	109	245	8	24	73	180	*Picea, Cathaya, Tsuga, Sciadopitys, Keteleeria*
61	19	15,6	20,8	5	13,3	24,7	27,9	823	1520	204	245	9	24	79	172	*Picea, Cathaya, Tsuga, Sciadopitys, Keteleeria*
60	22	17,2	21,9	5	13,6	24,7	27,9	1187	1520	204	245	8	24	118	172	*Picea, Cathaya, Sciadopitys, Ephedra, Myriophyllum*
59	22	15,6	21,9	5	13,6	24,7	27,9	823	1520	204	245	8	24	79	172	*Picea, Cathaya, Tsuga, Sciadopitys, Keteleeria, Ephedra*
58	23	13,3	20,8	-0,1	13,3	23	27,9	641	1520	109	236	9	24	55	172	*Picea, Cathaya, Tsuga, Sciadopitys*
57	18	15,6	20,8	5	13,3	24,7	27,9	823	1520	204	236	9	24	79	180	*Picea, Cathaya, Tsuga, Sciadopitys, Keteleeria*
56	17	15,6	20,8	5	13,6	24,7	27,9	823	1520	204	236	9	24	79	180	*Picea, Cathaya, Tsuga, Sciadopitys, Keteleeria*
55	22	15,6	21,9	5	13,6	24,7	27,9	823	1520	204	245	8	24	79	172	*Picea, Cathaya, Tsuga, Sciadopitys, Keteleeria*
54	25	15,6	20,5	5	13,3	24,7	27,9	823	1520	109	236	18	24	79	141	*Picea, Cathaya, Tsuga, Sciadopitys, Keteleeria*
53	18	15,6	23,1	5	16,4	24,7	27,9	823	1520	204	245	8	24	79	180	*Picea, Cathaya, Tsuga, Sciadopitys, Keteleeria, Cedrus*
52	22	15,6	20,8	5	13,3	24,7	27,9	823	1520	109	236	18	43	79	180	*Picea, Cathaya, Tsuga, Sciadopitys, Keteleeria, Ephedra*
51	24	15,6	20,8	5	13,3	24,7	28,1	823	1520	204	236	9	24	79	172	*Picea, Cathaya, Tsuga, Sciadopitys, Keteleeria*
50	14	15,7	21,9	9,6	15,6	23,6	28,1	619	1520	175	245	8	24	47	180	*Picea, Cathaya, Sciadopitys*
49	17	17,2	23,1	9,6	16,4	23,6	27,9	1187	1520	178	245	8	43	118	180	*Picea, Cathaya, Sciadopitys*
48	17	15,7	20,8	9,6	13,3	24,7	28,1	823	1520	204	236	9	43	79	176	*Picea, Cathaya, Sciadopitys, Keteleeria*
47	15	12,9	20,8	0,9	13,3	23,6	28,1	735	1520	109	195	18	24	51	180	*Picea, Cathaya, Sciadopitys, Keteleeria*
46	15	15,7	23,1	9,6	16,4	23,6	27,9	422	1520	175	245	8	24	55	180	*Picea, Cathaya, Sciadopitys*
45	17	13,3	20,8	0,9	13,3	23,6	27,9	422	1520	106	236	9	43	55	180	*Picea, Cathaya, Sciadopitys*
44	15	13,3	23,1	0,9	16,4	23,6	28,1	619	1520	109	245	8	24	51	176	*Picea, Cathaya, Sciadopitys, Ephedra*
43	15	15,6	21,9	5	15,6	24,7	28,1	823	1520	204	245	8	24	79	176	*Picea, Cathaya, Sciadopitys*
42	15	15,7	23,1	9,6	16,4	19,6	28,1	422	1520	175	245	8	24	45	180	*Picea, Cathaya, Sciadopitys, Keteleeria, Ephedra*
41	18	13,3	20,8	0,9	13,3	23,6	27,9	619	1520	109	236	9	43	55	176	*Picea, Cathaya, Sciadopitys*
40	16	11,5	20,8	-1	13,3	23	27,9	641	1520	109	236	9	24	55	180	*Picea, Cathaya, Sciadopitys*
39	15	9,1	20,8	-2,7	13,3	21,7	28,1	422	1520	92	236	9	24	66	176	*Picea, Cathaya, Sciadopitys*
38	15	11,5	20,8	-0,1	13,3	23	28,1	619	1520	109	236	9	43	47	180	*Picea, Cathaya, Sciadopitys, Keteleeria*
37	14	13,3	21,9	-0,1	15,6	23	28,3	619	1520	109	245	8	43	66	176	*Picea, Cathaya, Sciadopitys, Keteleeria*
36	18	15,6	20,8	5	13,3	24,7	28,1	823	1520	204	236	9	24	79	176	*Picea, Cathaya, Sciadopitys, Keteleeria*
35	15	11,5	21,9	-1	15,6	23	28,1	641	1520	109	245	8	24	47	180	*Picea, Cathaya, Sciadopitys, Keteleeria, Cedrus*
34	15	15,6	21,9	5	15,6	24,7	28,1	823	1520	204	245	8	24	79	180	*Picea, Cathaya, Sciadopitys, Ephedra*
33	19	11,5	21,9	-1	15,6	23	28,1	619	1520	109	245	8	24	47	172	*Picea, Cathaya, Sciadopitys, Keteleeria*
32	14	9,1	20,8	-2,7	13,3	19,6	27,9	373	1520	73	236	9	24	55	176	*Picea, Cathaya, Sciadopitys, Keteleeria*
31	15	13,6	21,9	1,8	15,6	23,6	28,1	505	1520	109	245	8	24	47	176	*Picea, Cathaya, Sciadopitys, Keteleeria*

sample	taxa anlaysed	MAT min (°C)	MAT max (°C)	CMT min (°C)	CMT max (°C)	WMT min (°C)	WMT max (°C)	MAP min (mm/yr)	MAP max (mm/yr)	Mpwet min (mm/m)	Mpwet max (mm/m)	Mpdry min (mm/m)	Mpdry max (mm/m)	Mpwarm min (mm/m)	Mpwarm max (mm/m)	excluded taxa
30	18	15,7	20,8	9,6	13,3	24,7	27,9	823	1520	204	236	9	24	79	176	*Picea, Cathaya, Sciadopitys, Keteleeria*
29	17	15,6	21,9	5	13,6	24,7	28,1	823	1520	204	245	8	24	79	172	*Picea, Cathaya, Sciadopitys, Keteleeria*
28	16	9,1	21,9	-2,7	13,6	21,7	27,9	422	1520	92	245	8	24	66	176	*Picea, Cathaya, Sciadopitys*
27	14	9,1	20,8	-2,7	13,3	19,3	27,9	422	1520	92	236	9	24	73	176	*Picea, Cathaya, Sciadopitys, Keteleeria*
26	19	15,7	20,8	9,6	13,3	24,7	27,9	823	1520	204	236	9	24	79	176	*Picea, Cathaya, Sciadopitys, Keteleeria*
25	16	15,6	20,8	5	13,3	24,7	28,1	823	1520	204	236	9	43	79	176	*Picea, Cathaya, Sciadopitys, Keteleeria*
24	17	9,1	20,8	-2,7	13,3	19,6	27,9	641	1520	98	236	9	24	55	176	*Picea, Cathaya, Sciadopitys, Keteleeria*
23	19	12,9	20,8	0,9	13,3	23,6	28,1	619	1520	109	236	9	24	51	176	*Picea, Cathaya, Sciadopitys*
22	19	15,7	20,8	9,6	13,3	24,7	27,9	823	1520	204	236	9	24	79	180	*Picea, Cathaya, Sciadopitys*
21	16	9,1	20,8	-2,7	13,3	21,7	28,1	422	1520	92	236	9	24	66	176	*Picea, Cathaya, Sciadopitys, Keteleeria*
20	17	15,7	20,8	9,6	13,3	24,7	28,1	823	1520	204	236	9	24	79	172	*Picea, Cathaya, Sciadopitys, Keteleeria, Cedrus*
19	20	15,6	21,9	5	13,6	24,7	27,9	823	1520	204	245	8	24	79	176	*Picea, Cathaya, Sciadopitys, Keteleeria*
18	14	12,9	21,9	0,9	15,6	23,6	28,3	641	1520	109	245	8	43	66	176	*Picea, Cathaya, Sciadopitys, Keteleeria*
17	17	15,6	20,8	5	13,3	24,7	27,9	823	1520	204	236	9	24	79	176	*Picea, Cathaya, Sciadopitys, Keteleeria*
16	13	9,1	21,9	-2,7	13,6	21,7	27,9	422	1520	73	245	8	24	55	172	*Picea, Cathaya, Sciadopitys, Keteleeria*
15	16	15,6	21,9	5	13,6	24,7	28,1	823	1520	204	245	8	24	79	176	*Picea, Cathaya, Sciadopitys, Keteleeria*
14	17	9,1	21,9	-2,7	13,6	21,7	28,3	473	1520	70	245	8	43	47	172	*Picea, Cathaya, Sciadopitys, Keteleeria*
13	16	15,6	20,8	5	13,3	24,7	28,1	823	1520	204	236	9	24	79	180	*Picea, Cathaya, Sciadopitys, Keteleeria*
12	18	11,5	21,9	-1	15,6	23	27,9	619	1520	109	245	8	24	73	176	*Picea, Cathaya, Sciadopitys, Keteleeria*
11	13	9,1	20,8	-2,7	13,3	19,6	28,1	422	1520	92	236	9	43	66	180	*Picea, Cathaya, Sciadopitys, Keteleeria*
10	20	15,7	21,9	9,6	15,6	24,7	28,1	823	1520	175	245	18	24	79	176	*Picea, Cathaya, Sciadopitys, Keteleeria*
9	17	11,5	21,9	-1	13,6	23	28,1	619	1520	109	245	8	24	73	176	*Picea, Cathaya, Sciadopitys, Keteleeria*
8	13	9,1	21,9	-2,7	15,6	19,6	27,9	581	1520	92	245	8	43	66	176	*Picea, Cathaya, Sciadopitys, Keteleeria*
7	14	15,6	21,9	5	15,6	24,7	28,1	823	1520	204	245	8	24	79	180	*Picea, Cathaya, Sciadopitys*
6	17	15,6	20,8	5	13,3	24,7	28,1	823	1520	204	236	9	24	79	180	*Picea, Cathaya, Sciadopitys, Keteleeria*
5	20	15,7	20,8	9,6	13,3	23	27,9	619	1520	175	236	9	37	73	176	*Picea, Cathaya, Sciadopitys*
4	20	17,2	21,9	9,6	15,6	24,7	28,1	1187	1520	204	204	8	43	118	176	*Picea, Cathaya, Sciadopitys*
3	19	15,7	21,9	9,6	15,6	23,6	27,9	735	1520	175	195	18	24	73	180	*Picea, Cathaya, Sciadopitys*
2	19	15,6	21,9	5	13,6	24,7	28,1	823	1520	204	245	8	24	79	176	*Picea, Cathaya, Sciadopitys*
1	20	15,7	20,8	9,6	13,3	24,7	28,1	823	1520	204	236	9	24	79	180	*Picea, Cathaya, Sciadopitys, Keteleeria*
all	43	17,2	20,5	9,6	13,3	24,7	27,9	1187	1520	178	236	18	24	118	141	all mentioned above

7.4. Supplementary material Chapter 4

7.4.1. Data sets: magnetic susceptibility. natural gamma radiation. ostracod abundance **(Table 4.1)**

Raw data (magnetic susceptibility. gamma radiation. ostracod abundance per 100 gram sediment) for all 600 samples. The 3-point mean is provided for the gamma radiation. Further. the root/arcsin-transformed values are given for all measurements/counts.

sample	mag. suszeptibility	mag. suszeptibility %. arcsin	gamma	gamma % arcsin	gamma 3-point	all ostracods (per 100g)	all ostracods % arcsin
941	0.56	0.0395	27	0.0378	31.3	1358.6	0.0747
942	0.49	0.0370	38	0.0448	30.7	1219.2	0.0708
943	0.50	0.0374	29	0.0392	30.0	1064.7	0.0661
944	0.54	0.0389	25	0.0364	27.7	1704.8	0.0837
945	0.58	0.0404	36	0.0436	26.7	432.1	0.0421
946	0.69	0.0437	22	0.0341	27.3	626.7	0.0507
947	0.71	0.0444	22	0.0341	28.7	1383.0	0.0754
948	0.71	0.0446	38	0.0448	30.7	1754.0	0.0849
949	0.74	0.0455	26	0.0371	30.0	1270.8	0.0723
950	0.75	0.0458	28	0.0385	33.0	1537.5	0.0795
951	0.75	0.0457	36	0.0436	34.3	2543.8	0.1023
952	0.72	0.0449	35	0.0430	32.7	1863.0	0.0875
953	0.72	0.0449	32	0.0411	32.7	2285.2	0.0970
954	0.70	0.0441	31	0.0405	33.3	2401.0	0.0994
955	0.70	0.0441	35	0.0430	33.7	2004.9	0.0908
956	0.72	0.0447	34	0.0424	34.3	2293.6	0.0971
957	0.73	0.0450	32	0.0411	34.0	1811.9	0.0863
958	0.76	0.0460	37	0.0442	33.3	1680.7	0.0831
959	0.74	0.0453	33	0.0418	32.0	3046.0	0.1120
960	0.71	0.0445	30	0.0398	29.7	2332.0	0.0980
961	0.66	0.0428	33	0.0418	28.3	1773.3	0.0854
962	0.67	0.0433	26	0.0371	28.7	1200.0	0.0702
963	0.61	0.0414	26	0.0371	28.0	1790.0	0.0858
964	0.60	0.0410	34	0.0424	29.7	1275.0	0.0724
965	0.54	0.0389	24	0.0356	31.0	564.7	0.0481
966	0.60	0.0409	31	0.0405	35.0	1314.7	0.0735
967	0.46	0.0359	38	0.0448	35.3	1082.1	0.0667
968	0.41	0.0340	36	0.0436	34.7	1642.5	0.0822
969	0.38	0.0325	32	0.0411	31.7	1460.0	0.0775
970	0.44	0.0350	36	0.0436	32.7	7247.4	0.1733
971	0.46	0.0356	27	0.0378	30.7	4746.8	0.1400
972	0.47	0.0363	35	0.0430	32.0	806.0	0.0575
973	0.51	0.0376	30	0.0398	31.0	794.4	0.0571
974	0.45	0.0353	31	0.0405	33.7	965.7	0.0630
975	0.47	0.0363	32	0.0411	29.7	1423.1	0.0765
976	0.51	0.0377	38	0.0448	28.3	2086.8	0.0926
977	0.57	0.0399	19	0.0317	24.7	2429.2	0.1000
978	0.61	0.0414	28	0.0385	30.3	1302.6	0.0732
979	0.60	0.0409	27	0.0378	31.0	399.0	0.0405
980	0.63	0.0418	36	0.0436	31.7	963.5	0.0629

sample	mag. suszeptibility	mag. suszeptibility %. arcsin	gamma	gamma % arcsin	gamma 3-point	all ostracods (per 100g)	all ostracods % arcsin
981	0.64	0.0424	30	0.0398	32.3	238.7	0.0313
982	0.62	0.0416	29	0.0392	30.0	71.4	0.0171
983	0.63	0.0419	38	0.0448	29.0	707.3	0.0539
984	0.65	0.0427	23	0.0349	26.3	1207.0	0.0704
985	0.78	0.0468	26	0.0371	29.0	422.8	0.0417
986	0.84	0.0485	30	0.0398	33.3	701.4	0.0537
987	0.88	0.0495	31	0.0405	34.3	1820.8	0.0865
988	0.84	0.0485	39	0.0454	36.0	809.2	0.0576
989	0.70	0.0443	33	0.0418	34.3	1118.1	0.0678
990	0.65	0.0425	36	0.0436	36.7	911.2	0.0612
991	0.63	0.0418	34	0.0424	34.0	1082.0	0.0667
992	0.66	0.0429	40	0.0460	30.3	1120.2	0.0678
993	0.66	0.0429	28	0.0385	22.3	1099.2	0.0672
994	0.65	0.0426	23	0.0349	22.7	679.2	0.0528
995	0.62	0.0417	16	0.0291	25.7	1024.6	0.0649
996	0.59	0.0405	29	0.0392	31.7	517.9	0.0461
997	0.54	0.0390	32	0.0411	33.3	588.7	0.0492
998	0.43	0.0346	34	0.0424	33.7	451.2	0.0430
999	0.48	0.0367	34	0.0424	31.7	137.0	0.0237
1000	0.45	0.0354	33	0.0418	31.3	67.0	0.0166
1001	0.44	0.0349	28	0.0385	30.7	655.9	0.0519
1002	0.41	0.0337	33	0.0418	34.0	880.3	0.0601
1003	0.43	0.0346	31	0.0405	30.7	709.4	0.0540
1004	0.41	0.0338	38	0.0448	30.7	1376.2	0.0752
1005	0.43	0.0347	23	0.0349	31.0	704.5	0.0538
1006	0.41	0.0339	31	0.0405	35.7	587.0	0.0491
1007	0.39	0.0330	39	0.0454	36.7	876.0	0.0600
1008	0.39	0.0329	37	0.0442	32.7	635.2	0.0511
1009	0.44	0.0349	34	0.0424	31.0	1146.8	0.0686
1010	0.48	0.0365	27	0.0378	29.7	1372.3	0.0751
1011	0.51	0.0376	32	0.0411	30.7	1530.2	0.0793
1012	0.51	0.0376	30	0.0398	29.7	833.3	0.0585
1013	0.55	0.0391	30	0.0398	33.3	1356.8	0.0747
1014	0.56	0.0395	29	0.0392	34.3	324.3	0.0365
1015	0.60	0.0409	41	0.0466	35.3	449.4	0.0429
1016	0.58	0.0403	33	0.0418	33.7	567.6	0.0483
1017	0.62	0.0417	32	0.0411	31.0	1027.8	0.0650
1018	0.64	0.0423	36	0.0436	33.0	1435.9	0.0768
1019	0.63	0.0419	25	0.0364	30.3	421.9	0.0416
1020	0.62	0.0415	38	0.0448	34.7	688.0	0.0531
1021	0.64	0.0421	28	0.0385	30.3	628.5	0.0508
1022	0.62	0.0416	38	0.0448	31.3	960.8	0.0628
1023	0.56	0.0397	25	0.0364	32.3	1004.2	0.0642
1024	0.52	0.0381	31	0.0405	35.3	299.1	0.0350
1025	0.64	0.0424	41	0.0466	41.0	405.7	0.0408
1026	0.65	0.0426	34	0.0424	34.7	706.6	0.0539
1026	0.65	0.0426	34	0.0424	34.7	706.6	0.0539
1027	0.60	0.0409	48	0.0504	37.3	1824.3	0.0866
1028	0.53	0.0386	22	0.0341	33.0	1663.6	0.0827
1029	0.47	0.0363	42	0.0471	37.3	378.2	0.0394
1030	0.42	0.0342	35	0.0430	34.7	363.3	0.0386

sample	mag. suszeptibility	mag. suszeptibility %. arcsin	gamma	gamma % arcsin	gamma 3-point	all ostracods (per 100g)	all ostracods % arcsin
1031	0.39	0.0330	35	0.0430	35.7	80.9	0.0182
1032	0.38	0.0324	34	0.0424	30.7	281.6	0.0340
1033	0.42	0.0341	38	0.0448	31.0	362.8	0.0386
1034	0.44	0.0350	20	0.0325	27.3	411.2	0.0411
1035	0.48	0.0364	35	0.0430	34.7	371.4	0.0390
1036	0.54	0.0388	27	0.0378	33.3	723.4	0.0545
1037	0.58	0.0402	42	0.0471	36.7	2.6	0.0033
1038	0.58	0.0402	31	0.0405	34.7	629.6	0.0508
1039	0.55	0.0393	37	0.0442	35.7	377.6	0.0394
1040	0.51	0.0378	36	0.0436	32.3	542.1	0.0472
1041	0.47	0.0362	34	0.0424	30.3	463.5	0.0436
1042	0.45	0.0354	27	0.0378	30.3	637.8	0.0512
1043	0.47	0.0361	30	0.0398	33.3	562.5	0.0480
1044	0.50	0.0374	34	0.0424	33.3	741.6	0.0552
1045	0.52	0.0381	36	0.0436	32.3	163.2	0.0259
1046	0.52	0.0381	30	0.0398	33.3	142.9	0.0242
1047	0.50	0.0375	31	0.0405	33.3	239.1	0.0313
1048	0.50	0.0373	39	0.0454	32.7	206.0	0.0291
1049	0.51	0.0378	30	0.0398	28.3	129.2	0.0230
1050	0.49	0.0371	29	0.0392	35.0	140.7	0.0240
1051	0.53	0.0385	26	0.0371	32.3	426.0	0.0418
1052	0.53	0.0386	50	0.0514	32.7	333.3	0.0370
1053	0.55	0.0392	21	0.0333	27.3	252.7	0.0322
1054	0.53	0.0386	27	0.0378	31.0	44.5	0.0135
1055	0.56	0.0395	34	0.0424	34.7	229.2	0.0307
1056	0.56	0.0394	32	0.0411	35.7	316.7	0.0360
1057	0.59	0.0406	38	0.0448	39.3	159.5	0.0256
1058	0.53	0.0386	37	0.0442	39.0	209.4	0.0293
1059	0.52	0.0383	43	0.0477	37.0	268.9	0.0332
1060	0.51	0.0377	37	0.0442	32.7	4.3	0.0042
1061	0.50	0.0373	31	0.0405	30.3	90.7	0.0193
1062	0.53	0.0384	30	0.0398	34.7	425.0	0.0418
1063	0.55	0.0390	30	0.0398	35.3	225.2	0.0304
1064	0.56	0.0397	44	0.0483	37.7	88.4	0.0190
1065	0.60	0.0408	32	0.0411	33.3	114.2	0.0216
1066	0.58	0.0401	37	0.0442	34.7	436.2	0.0423
1067	0.53	0.0385	31	0.0405	34.3	479.4	0.0444
1068	0.50	0.0374	36	0.0436	36.7	369.6	0.0389
1069	0.49	0.0368	36	0.0436	36.3	830.8	0.0584
1070	0.50	0.0374	38	0.0448	34.3	808.6	0.0576
1071	0.54	0.0389	35	0.0430	32.3	416.7	0.0414
1072	0.56	0.0394	30	0.0398	29.7	774.6	0.0564
1073	0.61	0.0412	32	0.0411	30.3	795.7	0.0572
1074	0.63	0.0419	27	0.0378	28.7	804.8	0.0575
1075	0.63	0.0418	32	0.0411	30.7	858.2	0.0594
1076	0.61	0.0414	27	0.0378	30.7	411.6	0.0411
1077	0.60	0.0408	33	0.0418	36.7	413.8	0.0412
1078	0.59	0.0405	32	0.0411	38.7	94.1	0.0196

sample	mag. suszeptibility	mag. suszeptibility %. arcsin	gamma	gamma % arcsin	gamma 3-point	all ostracods (per 100g)	all ostracods % arcsin
1079	0.60	0.0408	45	0.0488	38.3	456.3	0.0433
1080	0.58	0.0404	39	0.0454	33.7	480.0	0.0444
1081	0.60	0.0410	31	0.0405	32.3	134.9	0.0235
1082	0.62	0.0416	31	0.0405	32.3	91.5	0.0194
1083	0.62	0.0415	35	0.0430	30.0	155.4	0.0252
1084	0.65	0.0426	31	0.0405	29.0	532.3	0.0467
1085	0.67	0.0434	24	0.0356	30.3	665.4	0.0523
1086	0.69	0.0439	32	0.0411	30.3	607.5	0.0499
1087	0.68	0.0436	35	0.0430	29.7	864.4	0.0596
1088	0.66	0.0429	24	0.0356	28.3	945.5	0.0623
1089	0.61	0.0413	30	0.0398	32.7	1042.6	0.0654
1090	0.59	0.0404	31	0.0405	31.0	1097.4	0.0671
1091	0.59	0.0406	37	0.0442	36.3	560.0	0.0479
1092	0.70	0.0442	25	0.0364	35.0	873.4	0.0599
1093	0.63	0.0418	47	0.0499	41.7	481.7	0.0445
1094	0.62	0.0416	33	0.0418	37.7	377.7	0.0394
1095	0.60	0.0409	45	0.0488	39.3	265.2	0.0330
1096	0.57	0.0400	35	0.0430	34.0	483.4	0.0445
1097	0.56	0.0395	38	0.0448	33.7	427.4	0.0419
1098	0.54	0.0387	29	0.0392	30.7	164.0	0.0259
1099	0.57	0.0400	34	0.0424	37.0	397.6	0.0404
1100	0.63	0.0418	29	0.0392	33.3	294.6	0.0348
1101	0.64	0.0421	48	0.0504	35.7	410.1	0.0410
1102	0.65	0.0426	23	0.0349	30.3	346.7	0.0377
1103	0.65	0.0427	36	0.0436	32.7	336.8	0.0372
1104	0.60	0.0409	32	0.0411	35.7	346.0	0.0377
1105	0.58	0.0403	30	0.0398	39.3	533.9	0.0468
1106	0.55	0.0392	45	0.0488	40.7	451.2	0.0430
1107	0.55	0.0392	43	0.0477	34.7	250.0	0.0320
1108	0.57	0.0398	34	0.0424	31.7	1058.8	0.0659
1109	0.60	0.0409	27	0.0378	32.3	558.5	0.0479
1110	0.62	0.0416	34	0.0424	32.7	200.9	0.0287
1111	0.62	0.0415	36	0.0436	32.0	370.1	0.0390
1112	0.61	0.0414	28	0.0385	33.7	314.3	0.0359
1113	0.55	0.0393	32	0.0411	35.7	703.6	0.0537
1114	0.52	0.0379	41	0.0466	38.0	495.7	0.0451
1115	0.48	0.0367	34	0.0424	37.3	497.7	0.0452
1116	0.52	0.0381	39	0.0454	37.0	477.9	0.0443
1117	0.55	0.0393	39	0.0454	34.7	626.5	0.0507
1118	0.60	0.0409	33	0.0418	30.3	491.1	0.0449
1119	0.60	0.0411	32	0.0411	31.0	566.7	0.0482
1120	0.61	0.0414	26	0.0371	31.7	674.5	0.0526
1121	0.63	0.0420	35	0.0430	35.3	361.9	0.0385
1122	0.62	0.0417	34	0.0424	34.3	251.9	0.0322
1123	0.61	0.0414	37	0.0442	36.0	421.3	0.0416
1124	0.61	0.0412	32	0.0411	34.7	547.5	0.0474

sample	mag. suszeptibility	mag. suszeptibility %. arcsin	gamma	gamma % arcsin	gamma 3-point	all ostracods (per 100g)	all ostracods % arcsin
1125	0.65	0.0427	39	0.0454	35.7	284.0	0.0341
1126	0.67	0.0433	33	0.0418	33.3	409.5	0.0410
1127	0.67	0.0433	35	0.0430	31.7	542.4	0.0472
1128	0.68	0.0434	32	0.0411	30.0	622.5	0.0506
1129	0.65	0.0425	28	0.0385	33.7	1303.3	0.0732
1130	0.59	0.0405	30	0.0398	37.3	620.4	0.0505
1131	0.57	0.0397	43	0.0477	36.7	1000.0	0.0641
1132	0.53	0.0384	39	0.0454	30.3	403.5	0.0407
1133	0.53	0.0386	28	0.0385	31.3	263.4	0.0329
1134	0.52	0.0382	24	0.0356	29.3	568.3	0.0483
1135	0.49	0.0370	42	0.0471	31.7	747.9	0.0554
1136	0.48	0.0367	22	0.0341	30.7	495.7	0.0451
1137	0.51	0.0379	31	0.0405	35.3	517.4	0.0461
1138	0.53	0.0386	39	0.0454	36.3	255.7	0.0324
1139	0.59	0.0407	36	0.0436	35.3	374.6	0.0392
1140	0.66	0.0428	34	0.0424	32.7	119.0	0.0221
1141	0.70	0.0441	36	0.0436	35.3	151.3	0.0249
1142	0.62	0.0415	28	0.0385	32.3	71.4	0.0171
1143	0.63	0.0419	42	0.0471	34.0	259.0	0.0326
1144	0.58	0.0403	27	0.0378	33.0	51.6	0.0146
1145	0.56	0.0397	33	0.0418	34.7	515.8	0.0460
1146	0.59	0.0406	39	0.0454	35.3	456.6	0.0433
1147	0.73	0.0452	32	0.0411	34.0	219.2	0.0300
1148	0.65	0.0425	35	0.0430	36.3	323.8	0.0365
1149	0.73	0.0450	35	0.0430	37.7	178.0	0.0270
1150	0.81	0.0474	39	0.0454	38.7	218.1	0.0299
1151	0.91	0.0503	39	0.0454	38.3	860.8	0.0595
1152	0.97	0.0520	38	0.0448	37.3	392.9	0.0402
1153	0.85	0.0488	38	0.0448	35.3	831.8	0.0584
1154	0.83	0.0482	36	0.0436	32.7	346.3	0.0377
1155	0.71	0.0446	32	0.0411	32.7	723.1	0.0545
1156	0.69	0.0438	30	0.0398	35.0	403.0	0.0407
1157	0.64	0.0424	36	0.0436	33.0	653.5	0.0518
1158	0.59	0.0407	39	0.0454	28.7	327.5	0.0367
1159	0.59	0.0406	24	0.0356	23.0	55.6	0.0151
1160	0.58	0.0403	23	0.0349	26.0	64.4	0.0162
1161	0.58	0.0402	22	0.0341	25.0	87.8	0.0190
1162	0.59	0.0404	33	0.0418	29.0	153.5	0.0251
1163	0.57	0.0400	20	0.0325	28.3	159.2	0.0256
1164	0.56	0.0394	34	0.0424	29.3	58.8	0.0155
1165	0.57	0.0400	31	0.0405	30.3	150.2	0.0248
1166	0.59	0.0407	23	0.0349	31.7	175.4	0.0268
1167	0.63	0.0421	37	0.0442	33.3	134.8	0.0235
1168	0.62	0.0416	35	0.0430	29.7	204.2	0.0289
1169	0.62	0.0416	28	0.0385	28.0	119.8	0.0222
1170	0.60	0.0408	26	0.0371	28.0	121.1	0.0223

sample	mag. suszeptibility	mag. suszeptibility %. arcsin	gamma	gamma % arcsin	gamma 3-point	all ostracods (per 100g)	all ostracods % arcsin
1171	0.59	0.0407	30	0.0398	32.0	95.5	0.0198
1172	0.62	0.0416	28	0.0385	33.0	105.7	0.0208
1173	0.65	0.0425	38	0.0448	33.7	285.1	0.0342
1174	0.72	0.0449	33	0.0418	34.7	302.5	0.0352
1175	0.78	0.0466	30	0.0398	34.0	411.8	0.0411
1176	0.80	0.0473	41	0.0466	32.0	332.2	0.0369
1177	0.78	0.0466	31	0.0405	27.0	346.2	0.0377
1178	0.78	0.0467	24	0.0356	27.0	199.1	0.0286
1179	0.75	0.0456	26	0.0371	27.7	401.5	0.0406
1180	0.66	0.0430	31	0.0405	30.0	241.0	0.0314
1181	0.70	0.0442	26	0.0371	34.7	252.8	0.0322
1182	0.60	0.0410	33	0.0418	38.7	401.8	0.0406
1183	0.51	0.0376	45	0.0488	38.3	183.5	0.0274
1184	0.59	0.0406	38	0.0448	32.0	65.6	0.0164
1185	0.62	0.0415	32	0.0411	29.7	74.4	0.0175
1186	0.67	0.0433	26	0.0371	31.0	53.8	0.0149
1187	0.80	0.0473	31	0.0405	33.0	4.1	0.0041
1188	0.87	0.0492	36	0.0436	33.3	76.6	0.0177
1189	0.90	0.0502	32	0.0411	28.3	53.1	0.0148
1190	0.89	0.0498	32	0.0411	30.0	263.0	0.0328
1191	0.80	0.0473	21	0.0333	29.3	175.7	0.0268
1192	0.71	0.0444	37	0.0442	32.0	425.5	0.0418
1193	0.65	0.0426	30	0.0398	31.0	342.8	0.0375
1194	0.59	0.0407	29	0.0392	32.7	288.8	0.0344
1195	0.59	0.0406	34	0.0424	33.7	226.0	0.0304
1196	0.60	0.0410	35	0.0430	29.7	121.2	0.0223
1197	0.62	0.0414	32	0.0411	27.0	45.0	0.0136
1198	0.63	0.0420	22	0.0341	24.7	81.8	0.0183
1199	0.61	0.0413	27	0.0378	29.0	115.2	0.0217
1200	0.60	0.0409	25	0.0364	25.7	300.9	0.0351
1201	0.60	0.0409	35	0.0430	26.7	231.1	0.0308
1202	0.65	0.0425	17	0.0300	24.3	340.5	0.0374
1203	0.64	0.0424	28	0.0385	30.3	251.0	0.0321
1204	0.64	0.0424	28	0.0385	29.7	275.9	0.0336
1205	0.60	0.0409	35	0.0430	32.0	335.9	0.0371
1206	0.62	0.0415	26	0.0371	32.7	366.2	0.0388
1207	0.62	0.0416	35	0.0430	33.3	228.1	0.0306
1208	0.69	0.0439	37	0.0442	32.0	317.2	0.0361
1209	0.62	0.0416	28	0.0385	29.0	391.3	0.0401
1210	0.67	0.0432	31	0.0405	30.7	289.7	0.0345
1211	0.65	0.0427	28	0.0385	27.0	31.7	0.0114
1212	0.66	0.0430	33	0.0418	28.0	160.7	0.0257
1213	0.62	0.0417	20	0.0325	25.3	53.6	0.0148
1214	0.62	0.0414	31	0.0405	29.7	289.2	0.0344
1215	0.57	0.0399	25	0.0364	30.0	205.6	0.0290
1216	0.55	0.0391	33	0.0418	32.7	175.2	0.0268

sample	mag. suszeptibility	mag. suszeptibility %. arcsin	gamma	gamma % arcsin	gamma 3-point	all ostracods (per 100g)	all ostracods % arcsin
1217	0.56	0.0394	32	0.0411	35.0	217.6	0.0299
1218	0.58	0.0402	33	0.0418	39.0	97.7	0.0200
1219	0.59	0.0405	40	0.0460	36.3	168.1	0.0263
1220	0.67	0.0432	44	0.0483	30.7	315.0	0.0360
1221	0.77	0.0464	25	0.0364	25.3	330.5	0.0368
1222	0.82	0.0478	23	0.0349	28.7	262.5	0.0328
1223	0.84	0.0486	28	0.0385	30.7	249.0	0.0320
1224	0.80	0.0473	35	0.0430	30.7	250.8	0.0321
1225	0.71	0.0445	29	0.0392	28.3	243.7	0.0316
1226	0.63	0.0418	28	0.0385	28.7	227.3	0.0305
1227	0.59	0.0405	28	0.0385	29.0	70.9	0.0171
1228	0.59	0.0405	30	0.0398	29.7	1325.5	0.0738
1229	0.55	0.0393	29	0.0392	29.7	610.0	0.0500
1230	0.70	0.0443	30	0.0398	33.3	769.6	0.0562
1231	0.72	0.0448	30	0.0398	32.0	464.3	0.0437
1232	0.70	0.0441	40	0.0460	31.3	247.7	0.0319
1233	0.75	0.0456	26	0.0371	27.3	247.4	0.0319
1234	0.83	0.0481	28	0.0385	26.7	184.6	0.0275
1235	0.80	0.0474	28	0.0385	24.7	210.7	0.0294
1236	0.76	0.0461	24	0.0356	23.3	105.0	0.0208
1237	0.73	0.0452	22	0.0341	27.0	107.4	0.0210
1238	0.69	0.0438	24	0.0356	27.3	224.6	0.0304
1239	0.68	0.0435	35	0.0430	27.7	193.6	0.0282
1240	0.72	0.0449	23	0.0349	24.3	168.7	0.0263
1241	0.73	0.0450	25	0.0364	27.0	455.1	0.0432
1242	0.73	0.0450	25	0.0364	27.7	767.1	0.0561
1243	0.62	0.0417	31	0.0405	32.7	377.7	0.0394
1244	0.66	0.0428	27	0.0378	33.0	162.3	0.0258
1245	0.60	0.0409	40	0.0460	34.3	237.1	0.0312
1246	0.57	0.0400	32	0.0411	32.7	261.3	0.0327
1247	0.55	0.0392	31	0.0405	31.0	266.5	0.0331
1248	0.58	0.0403	35	0.0430	32.0	97.3	0.0200
1249	0.63	0.0420	27	0.0378	31.0	78.4	0.0179
1250	0.69	0.0439	34	0.0424	31.0	147.3	0.0246
1251	0.73	0.0450	32	0.0411	31.3	122.4	0.0224
1252	0.73	0.0451	27	0.0378	29.3	89.7	0.0192
1253	0.71	0.0445	35	0.0430	29.0	60.4	0.0157
1254	0.67	0.0431	26	0.0371	27.7	10.4	0.0065
1255	0.63	0.0421	26	0.0371	26.7	46.4	0.0138
1256	0.59	0.0406	31	0.0405	32.3	120.3	0.0222
1257	0.59	0.0406	23	0.0349	34.3	51.5	0.0145
1258	0.54	0.0389	43	0.0477	39.3	59.0	0.0156
1259	0.50	0.0372	37	0.0442	38.0	114.8	0.0217
1260	0.44	0.0349	38	0.0448	36.7	92.9	0.0195
1261	0.51	0.0376	39	0.0454	33.0	112.5	0.0215
1262	0.55	0.0393	33	0.0418	32.0	32.3	0.0115

sample	mag. suszeptibility	mag. suszeptibility %. arcsin	gamma	gamma % arcsin	gamma 3-point	all ostracods (per 100g)	all ostracods % arcsin
1263	0.54	0.0387	27	0.0378	30.0	91.9	0.0194
1264	0.55	0.0390	36	0.0436	30.0	126.6	0.0228
1265	0.54	0.0389	27	0.0378	25.3	159.6	0.0256
1266	0.57	0.0400	27	0.0378	26.7	72.6	0.0173
1267	0.61	0.0413	22	0.0341	28.7	187.5	0.0277
1268	0.66	0.0429	31	0.0405	36.7	229.4	0.0307
1269	0.66	0.0431	33	0.0418	40.0	200.0	0.0286
1270	0.70	0.0441	46	0.0493	39.7	221.5	0.0301
1271	0.63	0.0419	41	0.0466	32.7	105.5	0.0208
1272	0.61	0.0411	32	0.0411	28.0	195.1	0.0283
1273	0.57	0.0400	25	0.0364	28.0	75.7	0.0176
1274	0.58	0.0403	27	0.0378	28.7	190.1	0.0279
1275	0.56	0.0397	32	0.0411	28.3	53.5	0.0148
1276	0.55	0.0392	27	0.0378	28.0	76.0	0.0177
1277	0.54	0.0388	26	0.0371	32.7	171.1	0.0265
1278	0.55	0.0390	31	0.0405	35.7	311.1	0.0357
1279	0.56	0.0394	41	0.0466	36.0	232.9	0.0309
1280	0.57	0.0400	35	0.0430	32.3	167.3	0.0262
1281	0.57	0.0400	32	0.0411	30.7	205.3	0.0290
1282	0.59	0.0406	30	0.0398	30.0	111.2	0.0214
1283	0.59	0.0405	30	0.0398	26.3	11.8	0.0070
1284	0.58	0.0403	30	0.0398	28.3	136.9	0.0237
1285	0.60	0.0408	19	0.0317	33.7	84.7	0.0186
1286	0.58	0.0401	36	0.0436	37.7	348.2	0.0378
1287	0.56	0.0394	46	0.0493	36.7	1615.4	0.0815
1288	0.55	0.0392	31	0.0405	33.0	135.7	0.0236
1289	0.58	0.0402	33	0.0418	35.0	298.7	0.0350
1290	0.60	0.0409	35	0.0430	35.7	268.3	0.0332
1291	0.62	0.0416	37	0.0442	36.7	256.6	0.0324
1292	0.65	0.0427	35	0.0430	35.0	73.0	0.0173
1293	0.65	0.0427	38	0.0448	32.7	12.4	0.0071
1294	0.66	0.0430	32	0.0411	32.0	26.9	0.0105
1295	0.66	0.0428	28	0.0385	32.0	14.2	0.0076
1296	0.63	0.0418	36	0.0436	32.3	31.7	0.0114
1297	0.62	0.0415	32	0.0411	32.0	101.9	0.0204
1298	0.59	0.0407	29	0.0392	30.7	50.2	0.0143
1299	0.61	0.0412	35	0.0430	29.0	60.4	0.0157
1300	0.57	0.0399	28	0.0385	27.7	554.6	0.0477
1301	0.57	0.0398	24	0.0356	24.7	775.4	0.0564
1302	0.57	0.0399	31	0.0405	26.7	791.3	0.0570
1303	0.64	0.0423	19	0.0317	28.7	632.6	0.0510
1304	0.68	0.0435	30	0.0398	33.0	1496.0	0.0784
1305	0.69	0.0440	37	0.0442	33.0	534.2	0.0468
1306	0.77	0.0463	32	0.0411	32.0	427.9	0.0419
1307	0.71	0.0446	30	0.0398	30.3	448.5	0.0429
1308	0.68	0.0437	34	0.0424	31.7	715.2	0.0542

sample	mag. suszeptibility	mag. suszeptibility %. arcsin	gamma	gamma % arcsin	gamma 3-point	all ostracods (per 100g)	all ostracods % arcsin
1309	0.66	0.0428	27	0.0378	30.3	219.7	0.0300
1310	0.58	0.0403	34	0.0424	30.0	266.3	0.0331
1311	0.58	0.0402	30	0.0398	29.7	247.9	0.0319
1312	0.57	0.0398	26	0.0371	29.7	440.2	0.0425
1313	0.55	0.0390	33	0.0418	32.0	314.0	0.0359
1314	0.43	0.0348	30	0.0398	31.7	40.2	0.0128
1315	0.55	0.0391	33	0.0418	31.3	79.3	0.0180
1316	0.53	0.0383	32	0.0411	29.7	86.2	0.0188
1317	0.54	0.0389	29	0.0392	29.7	672.3	0.0525
1318	0.52	0.0383	28	0.0385	30.7	666.7	0.0523
1319	0.54	0.0388	32	0.0411	32.3	488.2	0.0448
1320	0.54	0.0388	32	0.0411	33.0	95.7	0.0198
1321	0.52	0.0380	33	0.0418	29.7	781.4	0.0566
1322	0.50	0.0373	34	0.0424	31.0	883.9	0.0602
1323	0.52	0.0380	22	0.0341	30.7	294.1	0.0347
1324	0.52	0.0380	37	0.0442	34.3	225.5	0.0304
1325	0.52	0.0380	33	0.0418	33.3	157.7	0.0254
1326	0.56	0.0396	33	0.0418	28.7	704.9	0.0538
1327	0.59	0.0404	34	0.0424	26.3	923.1	0.0616
1328	0.63	0.0420	19	0.0317	24.3	209.0	0.0293
1329	0.66	0.0429	26	0.0371	30.7	96.5	0.0199
1330	0.67	0.0434	28	0.0385	34.0	77.9	0.0179
1331	0.63	0.0419	38	0.0448	35.0	257.3	0.0325
1332	0.62	0.0416	36	0.0436	34.3	46.3	0.0138
1333	0.58	0.0404	31	0.0405	34.3	241.6	0.0315
1334	0.58	0.0402	36	0.0436	31.7	68.8	0.0168
1335	0.55	0.0392	36	0.0436	29.3	168.9	0.0263
1336	0.55	0.0391	23	0.0349	26.7	276.4	0.0337
1337	0.61	0.0411	29	0.0392	29.0	109.4	0.0212
1338	0.64	0.0421	28	0.0385	29.0	265.3	0.0330
1339	0.64	0.0422	30	0.0398	32.3	73.0	0.0173
1340	0.59	0.0406	29	0.0392	32.0	485.7	0.0446
1341	0.63	0.0419	38	0.0448	33.3	238.9	0.0313
1342	0.59	0.0406	29	0.0392	30.7	264.0	0.0329
1343	0.60	0.0408	33	0.0418	31.0	149.1	0.0247
1344	0.64	0.0422	30	0.0398	27.3	236.8	0.0312
1345	0.64	0.0421	30	0.0398	30.0	176.8	0.0269
1346	0.67	0.0432	22	0.0341	27.7	108.7	0.0211
1347	0.72	0.0448	38	0.0448	32.3	35.4	0.0120
1348	0.75	0.0459	23	0.0349	27.3	858.9	0.0594
1349	0.77	0.0463	36	0.0436	32.7	609.1	0.0500
1350	0.76	0.0462	23	0.0349	32.3	436.7	0.0423
1351	0.78	0.0467	39	0.0454	34.0	330.1	0.0368
1352	0.70	0.0443	35	0.0430	33.7	115.4	0.0218
1353	0.75	0.0459	28	0.0385	34.3	331.9	0.0369
1354	0.77	0.0463	38	0.0448	33.3	183.8	0.0275

sample	mag. suszeptibility	mag. suszeptibility %. arcsin	gamma	gamma % arcsin	gamma 3-point	all ostracods (per 100g)	all ostracods % arcsin
1355	0.72	0.0448	37	0.0442	32.3	315.8	0.0360
1356	0.67	0.0433	25	0.0364	28.0	324.8	0.0365
1357	0.67	0.0431	35	0.0430	28.3	112.0	0.0214
1358	0.65	0.0426	24	0.0356	27.0	123.6	0.0225
1359	0.63	0.0420	26	0.0371	29.3	183.1	0.0274
1360	0.65	0.0425	31	0.0405	27.0	10.7	0.0066
1361	0.69	0.0438	31	0.0405	24.3	38.9	0.0126
1362	0.69	0.0440	19	0.0317	27.0	119.3	0.0221
1363	0.70	0.0442	23	0.0349	33.0	55.1	0.0150
1364	0.73	0.0451	39	0.0454	37.0	75.6	0.0176
1365	0.68	0.0436	37	0.0442	33.7	207.0	0.0291
1366	0.70	0.0443	35	0.0430	32.7	347.8	0.0378
1367	0.70	0.0442	29	0.0392	36.0	503.9	0.0455
1368	0.68	0.0436	34	0.0424	43.7	222.8	0.0302
1369	0.66	0.0430	45	0.0488	46.0	221.3	0.0301
1370	0.64	0.0421	52	0.0525	39.7	120.0	0.0222
1371	0.63	0.0418	41	0.0466	34.0	108.2	0.0211
1372	0.60	0.0410	26	0.0371	30.3	655.3	0.0519
1373	0.61	0.0414	35	0.0430	33.0	37.4	0.0124
1374	0.60	0.0408	30	0.0398	28.3	18.2	0.0086
1375	0.62	0.0415	34	0.0424	28.3	72.6	0.0173
1376	0.63	0.0420	21	0.0333	24.7	111.9	0.0214
1377	0.64	0.0422	30	0.0398	29.3	150.0	0.0248
1378	0.67	0.0431	23	0.0349	30.7	305.9	0.0354
1379	0.67	0.0432	35	0.0430	37.0	69.4	0.0169
1380	0.64	0.0421	34	0.0424	33.0	271.4	0.0334
1381	0.61	0.0413	42	0.0471	32.7	333.3	0.0370
1382	0.63	0.0420	23	0.0349	34.3	263.9	0.0329
1383	0.65	0.0427	33	0.0418	40.3	279.9	0.0339
1384	0.70	0.0441	47	0.0499	40.0	173.6	0.0267
1385	0.73	0.0450	41	0.0466	30.3	213.0	0.0296
1386	0.73	0.0451	32	0.0411	27.3	195.1	0.0283
1387	0.71	0.0445	18	0.0309	25.3	276.2	0.0337
1388	0.95	0.0515	32	0.0411	30.0	176.7	0.0269
1389	0.65	0.0427	26	0.0371	27.7	386.4	0.0398
1390	0.65	0.0427	32	0.0411	29.3	284.6	0.0342
1391	0.66	0.0429	25	0.0364	30.7	268.8	0.0332
1392	0.69	0.0439	31	0.0405	35.0	306.8	0.0355
1393	0.70	0.0442	36	0.0436	33.3	65.5	0.0164
1394	0.71	0.0444	38	0.0448	34.0	195.3	0.0283
1395	0.70	0.0442	26	0.0371	34.3	192.3	0.0281
1396	0.68	0.0436	38	0.0448	35.0	277.6	0.0337
1397	0.69	0.0437	39	0.0454	34.0	16.4	0.0082
1398	0.68	0.0436	28	0.0385	30.0	143.5	0.0243
1399	0.67	0.0433	35	0.0430	30.7	234.9	0.0310
1400	0.66	0.0430	27	0.0378	28.0	44.7	0.0135

sample	mag. suszeptibility	mag. suszeptibility %. arcsin	gamma	gamma % arcsin	gamma 3-point	all ostracods (per 100g)	all ostracods % arcsin
1401	0.62	0.0417	30	0.0398	31.3	39.4	0.0127
1402	0.60	0.0410	27	0.0378	33.7	41.7	0.0131
1403	0.59	0.0405	37	0.0442	34.3	44.3	0.0135
1404	0.58	0.0402	37	0.0442	33.0	62.5	0.0160
1405	0.56	0.0397	29	0.0392	34.0	27.2	0.0106
1406	0.54	0.0388	33	0.0418	31.0	9.3	0.0062
1407	0.53	0.0384	40	0.0460	31.3	4.7	0.0044
1408	0.54	0.0388	20	0.0325	27.0	10.0	0.0064
1409	0.58	0.0403	34	0.0424	31.3	44.3	0.0135
1410	0.68	0.0435	27	0.0378	30.3	21.0	0.0093
1411	0.68	0.0437	33	0.0418	32.7	41.4	0.0130
1412	0.66	0.0428	31	0.0405	33.0	35.6	0.0121
1413	0.64	0.0422	34	0.0424	36.0	68.2	0.0167
1414	0.63	0.0419	34	0.0424	36.0	70.3	0.0170
1415	0.72	0.0449	40	0.0460	35.7	153.1	0.0251
1416	0.73	0.0450	34	0.0424	34.3	188.2	0.0278
1417	0.72	0.0447	33	0.0418	34.0	120.7	0.0223
1418	0.71	0.0446	36	0.0436	35.3	76.6	0.0177
1419	0.72	0.0448	33	0.0418	34.0	126.8	0.0228
1420	0.71	0.0446	37	0.0442	33.7	76.4	0.0177
1421	0.71	0.0446	32	0.0411	36.3	139.3	0.0239
1422	0.61	0.0412	32	0.0411	37.3	111.1	0.0213
1423	0.69	0.0440	45	0.0488	36.3	211.7	0.0295
1424	0.68	0.0436	35	0.0430	32.7	78.3	0.0179
1425	0.66	0.0430	29	0.0392	30.3	280.0	0.0339
1426	0.57	0.0397	34	0.0424	29.3	247.8	0.0319
1427	0.55	0.0392	28	0.0385	27.3	153.1	0.0251
1428	0.58	0.0401	26	0.0371	28.3	130.4	0.0231
1429	0.58	0.0404	28	0.0385	28.0	78.9	0.0180
1430	0.55	0.0393	31	0.0405	30.0	59.9	0.0157
1431	0.59	0.0407	25	0.0364	30.7	40.4	0.0129
1432	0.60	0.0411	34	0.0424	32.0	149.1	0.0247
1433	0.62	0.0417	33	0.0418	28.7	109.1	0.0212
1434	0.66	0.0431	29	0.0392	25.0	79.2	0.0180
1435	0.67	0.0431	24	0.0356	24.7	26.5	0.0104
1436	0.66	0.0430	22	0.0341	26.3	41.7	0.0131
1437	0.62	0.0417	28	0.0385	28.7	101.9	0.0204
1438	0.62	0.0415	29	0.0392	28.0	173.5	0.0267
1439	0.62	0.0416	29	0.0392	29.0	290.0	0.0345
1440	0.62	0.0416	26	0.0371	31.3	122.1	0.0224
1441	0.63	0.0420	32	0.0411	33.3	130.3	0.0231
1442	0.65	0.0427	36	0.0436	30.3	56.6	0.0152
1443	0.64	0.0422	32	0.0411	26.0	81.7	0.0183
1444	0.66	0.0430	23	0.0349	24.7	178.9	0.0271
1445	0.67	0.0431	23	0.0349	28.3	112.5	0.0215
1446	0.68	0.0435	28	0.0385	33.0	166.7	0.0261

sample	mag. suszeptibility	mag. suszeptibility %. arcsin	gamma	gamma % arcsin	gamma 3-point	all ostracods (per 100g)	all ostracods % arcsin
1447	0.65	0.0427	34	0.0424	32.3	205.7	0.0291
1448	0.65	0.0427	37	0.0442	30.3	87.9	0.0190
1449	0.63	0.0421	26	0.0371	26.0	114.6	0.0217
1450	0.61	0.0412	28	0.0385	26.0	317.9	0.0361
1451	0.60	0.0409	24	0.0356	26.3	101.9	0.0204
1452	0.60	0.0409	26	0.0371	25.0	134.1	0.0235
1453	0.58	0.0404	29	0.0392	24.3	121.7	0.0223
1454	0.57	0.0400	20	0.0325	24.7	64.2	0.0162
1455	0.55	0.0392	24	0.0356	24.3	49.2	0.0142
1456	0.57	0.0399	30	0.0398	23.7	26.7	0.0105
1457	0.54	0.0387	19	0.0317	22.7	79.2	0.0180
1458	0.54	0.0387	22	0.0341	27.0	26.7	0.0105
1459	0.54	0.0388	27	0.0378	28.3	35.9	0.0121
1460	0.54	0.0388	32	0.0411	30.7	252.3	0.0322
1461	0.55	0.0393	26	0.0371	27.7	212.3	0.0295
1462	0.64	0.0423	34	0.0424	27.7	183.5	0.0274
1463	0.64	0.0422	23	0.0349	28.0	298.6	0.0350
1464	0.65	0.0424	26	0.0371	34.0	42.1	0.0131
1465	0.65	0.0425	35	0.0430	36.3	67.3	0.0166
1466	0.67	0.0431	41	0.0466	30.0	286.9	0.0343
1467	0.66	0.0428	33	0.0418	26.7	300.0	0.0351
1468	0.69	0.0440	16	0.0291	26.7	286.3	0.0343
1469	0.66	0.0428	31	0.0405	30.7	58.0	0.0154
1470	0.64	0.0423	33	0.0418	30.0	46.9	0.0139
1471	0.64	0.0423	28	0.0385	29.0	57.6	0.0154
1472	0.63	0.0421	29	0.0392	29.0	83.3	0.0185
1473	0.63	0.0420	30	0.0398	29.0	115.7	0.0218
1474	0.62	0.0415	28	0.0385	32.0	273.6	0.0335
1475	0.60	0.0410	29	0.0392	32.7	39.8	0.0128
1476	0.59	0.0406	39	0.0454	32.3	76.1	0.0177
1477	0.55	0.0390	30	0.0398	29.7	19.5	0.0089
1478	0.59	0.0407	28	0.0385	29.0	200.7	0.0287
1479	0.58	0.0402	31	0.0405	28.3	126.9	0.0228
1480	0.56	0.0395	28	0.0385	26.7	148.5	0.0247
1481	0.52	0.0379	26	0.0371	28.7	40.6	0.0129
1482	0.49	0.0368	26	0.0371	30.3	53.2	0.0148
1483	0.47	0.0363	34	0.0424	33.3	48.4	0.0141
1484	0.47	0.0361	31	0.0405	32.0	82.6	0.0184
1485	0.47	0.0361	35	0.0430	31.3	95.6	0.0198
1486	0.48	0.0365	30	0.0398	31.7	123.8	0.0225
1487	0.42	0.0342	29	0.0392	31.7	60.1	0.0157
1488	0.48	0.0366	36	0.0436	33.0	12.9	0.0073
1489	0.47	0.0362	30	0.0398	33.7	43.9	0.0134
1490	0.46	0.0358	33	0.0418	34.7	28.4	0.0108
1491	0.44	0.0351	38	0.0448	35.3	148.8	0.0247
1492	0.40	0.0335	33	0.0418	32.0	29.9	0.0111

sample	mag. suszeptibility	mag. suszeptibility %. arcsin	gamma	gamma % arcsin	gamma 3-point	all ostracods (per 100g)	all ostracods % arcsin
1493	0.41	0.0337	35	0.0430	32.3	91.7	0.0194
1494	0.35	0.0312	28	0.0385	29.7	61.0	0.0158
1495	0.36	0.0315	34	0.0424	27.7	47.4	0.0139
1496	0.38	0.0324	27	0.0378	26.3	35.0	0.0120
1497	0.35	0.0314	22	0.0341	27.0	82.8	0.0184
1498	0.38	0.0324	30	0.0398	28.3	17.2	0.0084
1499	0.39	0.0330	29	0.0392	28.0	219.3	0.0300
1500	0.39	0.0331	26	0.0371	32.3	63.2	0.0161
1501	0.35	0.0314	29	0.0392	33.3	14.5	0.0077
1502	0.38	0.0327	42	0.0471	31.3	59.5	0.0156
1503	0.39	0.0332	29	0.0392	23.3	86.3	0.0188
1504	0.43	0.0345	23	0.0349	25.7	191.0	0.0280
1505	0.39	0.0331	18	0.0309	28.7	54.7	0.0150
1506	0.50	0.0372	36	0.0436	37.7	76.3	0.0177
1507	0.49	0.0371	32	0.0411	32.7	133.7	0.0234
1508	0.51	0.0377	45	0.0488	33.3	13.4	0.0074
1509	0.51	0.0377	21	0.0333	28.3	46.9	0.0139
1510	0.41	0.0338	34	0.0424	31.3	119.0	0.0221
1511	0.50	0.0375	30	0.0398	29.0	239.2	0.0313
1512	0.51	0.0378	30	0.0398	30.3	156.7	0.0254
1513	0.45	0.0353	27	0.0378	27.0	10.4	0.0065
1514	0.49	0.0371	34	0.0424	28.7	64.8	0.0163
1515	0.51	0.0377	20	0.0325	27.3	22.5	0.0096
1516	0.48	0.0365	32	0.0411	33.7	74.2	0.0174
1517	0.48	0.0364	30	0.0398	30.3	95.0	0.0197
1518	0.47	0.0363	39	0.0454	32.0	29.4	0.0110
1519	0.47	0.0362	22	0.0341	32.3	55.9	0.0151
1520	0.40	0.0334	35	0.0430	32.7	69.9	0.0169
1521	0.46	0.0357	40	0.0460	30.0	107.8	0.0210
1522	0.45	0.0355	23	0.0349	26.3	31.4	0.0113
1523	0.45	0.0355	27	0.0378	28.7	177.2	0.0270
1524	0.45	0.0355	29	0.0392	27.0	363.6	0.0386
1525	0.45	0.0355	30	0.0398	25.7	561.6	0.0480
1526	0.44	0.0349	22	0.0341	26.0	177.7	0.0270
1527	0.44	0.0352	25	0.0364	30.3	120.5	0.0222
1528	0.44	0.0351	31	0.0405	34.3	67.2	0.0166
1529	0.41	0.0340	35	0.0430	35.0	209.5	0.0293
1530	0.37	0.0320	37	0.0442	33.3	407.1	0.0409
1531	0.38	0.0327	33	0.0418	29.7	478.3	0.0443
1532	0.35	0.0311	30	0.0398	29.7	286.7	0.0343
1533	0.36	0.0319	26	0.0371	30.3	257.9	0.0325
1534	0.36	0.0319	33	0.0418	30.0	822.2	0.0581
1535	0.35	0.0312	32	0.0411	26.7	471.2	0.0440
1536	0.35	0.0314	25	0.0364	25.0	560.0	0.0479
1537	0.37	0.0320	23	0.0349	26.3	349.4	0.0379
1538	0.39	0.0330	27	0.0378	28.0	249.1	0.0320

sample	mag. suszeptibility	mag. suszeptibility %. arcsin	gamma	gamma % arcsin	gamma 3-point	all ostracods (per 100g)	all ostracods % arcsin
1539	0.37	0.0321	29	0.0392		185.8	0.0276
1540	0.33	0.0302	28	0.0385		232.6	0.0309

7.5. Supplementary material Chapter 5

7.5.1. Collection of all measurements and countings (Table 5.1)

All raw data of geochemistry. geophysics and ostracods/100 gram sediment are collected next to the percentage countings of palynomorths (dinoflagellate cysts and pollen)

sample	magnetic susceptibility	gamma radiation	ostracods (100g)	Total Carbon (%)	C in % acid	Carbonate equivalent	total S (%)	TOC/S ratio
1391	0.66	25	268.8	2.16	0.84	11.03	0.10	8.03
1392	0.69	31	306.8	2.13	0.82	10.93	0.10	8.29
1393	0.70	36	65.5	2.14	0.83	10.94	0.12	6.77
1394	0.71	38	195.3	2.07	0.84	10.23	0.10	8.35
1395	0.70	26	192.3	2.03	0.82	10.16	0.14	6.01
1396	0.68	38	277.6	2.10	1.19	7.58	0.09	12.67
1397	0.69	39	16.4	1.96	0.84	9.32	0.09	8.90
1398	0.68	28	143.5	1.95	0.82	9.46	0.07	11.88
1399	0.67	35	234.9	1.96	0.86	9.14	0.08	10.95
1400	0.66	27	44.7	1.89	0.81	8.98	0.10	8.04
1401	0.62	30	39.4	1.90	0.83	8.93	0.08	10.54
1402	0.60	27	41.7	1.88	0.89	8.26	0.07	12.59
1403	0.59	37	44.3	1.88	0.86	8.53	0.09	9.41
1404	0.58	37	62.5	1.94	0.85	9.07	0.25	3.36
1405	0.56	29	27.2	1.95	1.05	7.50	0.16	6.49
1406	0.54	33	9.3	1.94	1.02	7.68	0.08	12.45
1407	0.53	40	4.7	2.14	1.17	8.05	0.06	20.92
1408	0.54	20	10.0	1.93	0.96	8.12	0.11	8.64
1409	0.58	34	44.3	2.00	0.93	8.92	0.17	5.57
1410	0.68	27	21.0	2.01	0.92	9.05	0.10	9.01
1411	0.68	33	41.4	2.06	0.91	9.60	0.20	4.55
1412	0.66	31	35.6	2.01	0.95	8.85	0.16	5.87
1413	0.64	34	68.2	2.06	1.00	8.79	0.08	12.30
1414	0.63	34	70.3	2.12	1.09	8.65	0.07	16.53
1415	0.72	40	153.1	2.02	0.97	8.77	0.14	6.93
1416	0.73	34	188.2	1.99	0.96	8.57	0.10	9.91
1417	0.72	33	120.7	2.03	1.27	6.36	0.09	14.01
1418	0.71	36	76.6	2.05	1.27	6.52	0.10	13.21
1419	0.72	33	126.8	1.98	1.12	7.21	0.24	4.65
1420	0.71	37	76.4	2.00	1.10	7.57	0.19	5.71
1421	0.71	32	139.3	2.01	1.09	7.65	0.08	13.70
1422	0.61	32	111.1	1.98	1.01	8.12	0.13	7.86
1423	0.69	45	211.7	2.10	1.13	8.10	0.12	9.40
1424	0.68	35	78.3	1.96	0.98	8.21	0.09	11.03
1425	0.66	29	280.0	1.98	1.28	5.83	0.19	6.91
1426	0.57	34	247.8	1.97	1.01	8.02	0.08	13.37

sample	magnetic suszeptibility	gamma radiation	ostracods (100g)	Total Carbon (%)	C in % acid	Carbonate equivalent	total S (%)	TOC/S ratio
1427	0.55	28	153.1	1.90	0.98	7.68	0.12	7.96
1428	0.58	26	130.4	1.89	0.93	8.03	0.09	10.33
1429	0.58	28	78.9	2.18	1.21	8.09	0.08	15.00
1430	0.55	31	59.9	1.96	1.02	7.84	0.34	2.99
1431	0.59	25	40.4	1.96	1.04	7.70	0.52	2.02
1432	0.60	34	149.1	1.95	1.06	7.38	0.24	4.43
1433	0.62	33	109.1	2.00	1.04	7.96	0.43	2.40
1434	0.66	29	79.2	1.97	1.01	8.04	0.22	4.63
1435	0.67	24	26.5	2.00	0.98	8.53	0.21	4.66
1436	0.66	22	41.7	2.05	0.99	8.86	0.31	3.17
1437	0.62	28	101.9	2.27	0.99	10.61	0.29	3.38
1438	0.62	29	173.5	2.40	1.04	11.28	0.29	3.64
1439	0.62	29	290.0	2.43	1.08	11.31	0.29	3.65
1440	0.62	26	122.1	2.27	1.09	9.85	0.55	2.00
1441	0.63	32	130.3	2.17	1.09	9.07	0.42	2.56
1442	0.65	36	56.6	2.15	1.21	7.86	0.29	4.15
1443	0.64	32	81.7	2.26	0.83	11.94	0.10	8.33
1444	0.66	23	178.9	2.25	0.83	11.77	0.14	5.94
1445	0.67	23	112.5	2.27	0.86	11.77	0.17	5.01
1446	0.68	28	166.7	2.31	0.85	12.21	0.17	5.07
1447	0.65	34	205.7	2.34	0.88	12.14	0.18	4.79
1448	0.65	37	87.9	2.36	0.87	12.46	0.17	5.05
1449	0.63	26	114.6	2.39	0.87	12.71	0.14	6.04
1450	0.61	28	317.9	2.27	0.85	11.86	0.26	3.28
1451	0.60	24	101.9	2.20	0.84	11.38	0.24	3.52
1452	0.60	26	134.1	2.12	0.84	10.73	0.38	2.21
1453	0.58	29	121.7	2.12	0.81	10.88	0.24	3.42
1454	0.57	20	64.2	2.15	0.56	13.20	0.14	4.14
1455	0.55	24	49.2	2.19	0.89	10.90	0.17	5.12
1456	0.57	30	26.7	1.87	0.93	7.86	0.25	3.74
1457	0.54	19	79.2	2.01	0.97	8.68	0.27	3.58
1458	0.54	22	26.7	1.95	1.04	7.61	0.32	3.29
1459	0.54	27	35.9	1.96	0.94	8.53	0.26	3.62
1460	0.54	32	252.3	2.10	0.94	9.70	0.22	4.33
1461	0.55	26	212.3	2.09	0.97	9.32	0.28	3.46
1462	0.64	34	183.5	2.04	0.96	9.00	0.21	4.61
1463	0.64	23	298.6	1.94	0.96	8.14	0.27	3.51
1464	0.65	26	42.1	1.88	0.96	7.70	0.28	3.47
1465	0.65	35	67.3	1.92	0.96	7.93	0.35	2.75
1466	0.67	41	286.9	2.00	0.98	8.54	0.24	4.12
1467	0.66	33	300.0	1.99	1.02	8.13	0.40	2.56
1468	0.69	16	286.3	2.04	0.68	11.32	0.27	2.53
1469	0.66	31	58.0	1.97	0.96	8.47	0.29	3.29

sample	magnetic suszeptibility	gamma radiation	ostracods (100g)	Total Carbon (%)	C in % acid	Carbonate equivalent	total S (%)	TOC/S ratio
1470	0.64	33	46.9	1.96	1.04	7.70	0.29	3.54
1471	0.64	28	57.6	1.96	1.00	8.07	0.19	5.24
1472	0.63	29	83.3	1.97	0.98	8.25	0.33	2.99
1473	0.63	30	115.7	1.98	1.08	7.54	0.24	4.54
1474	0.62	28	273.6	1.95	0.93	8.47	0.32	2.92
1475	0.60	29	39.8	1.90	0.99	7.59	0.49	2.02
1476	0.59	39	76.1	1.83	0.92	7.60	4.60	0.49
1477	0.55	30	19.5	1.90	0.92	8.12	0.57	1.62
1478	0.59	28	200.7	1.99	0.92	8.98	0.25	3.65
1479	0.58	31	126.9	2.03	0.95	8.97	0.36	2.64
1480	0.56	28	148.5	2.01	0.95	8.88	0.76	1.24
1481	0.52	26	40.6	2.05	1.03	8.48	1.15	0.90
1482	0.49	26	53.2	2.04	1.02	8.54	0.34	2.96
1483	0.47	34	48.4	2.03	1.03	8.35	0.25	4.06
1484	0.47	31	82.6	2.06	0.66	11.72	0.35	1.88
1485	0.47	35	95.6	2.08	0.99	9.10	0.25	3.99
1486	0.48	30	123.8	2.01	0.97	8.65	0.25	3.93
1487	0.42	29	60.1	1.93	0.99	7.83	0.51	1.95
1488	0.48	36	12.9	1.81	0.97	7.00	0.39	2.49
1489	0.47	30	43.9	1.84	0.98	7.14	0.64	1.53
1490	0.46	33	28.4	1.88	1.09	6.64	0.92	1.18
1491	0.44	38	148.8	1.87	1.02	7.10	0.24	4.31
1492	0.40	33	29.9	2.09	1.07	8.44	0.89	1.21
1493	0.41	35	91.7	1.88	1.04	7.03	0.30	3.45
1494	0.35	28	61.0	1.89	0.94	7.93	0.47	2.01
1495	0.36	34	47.4	1.77	1.10	5.65	0.20	5.35
1496	0.38	27	35.0	1.78	0.94	6.97	0.32	2.98
1497	0.35	22	82.8	1.75	1.06	5.76	0.40	2.66
1498	0.38	30	17.2	1.82	0.99	6.94	0.58	1.70
1499	0.39	29	219.3	1.74	1.02	6.00	0.56	1.83
1500	0.39	26	63.2	1.77	1.03	6.15	0.32	3.20
1501	0.35	29	14.5	1.79	0.98	6.72	1.52	0.65
1502	0.38	42	59.5	1.79	1.01	6.44	0.31	3.29
1503	0.39	29	86.3	2.12	1.05	8.93	0.49	2.12
1504	0.43	23	191.0	1.88	0.94	7.86	0.29	3.19
1505	0.39	18	54.7	1.90	1.00	7.55	0.32	3.16
1506	0.50	36	76.3	1.91	0.97	7.82	0.34	2.84
1507	0.49	32	133.7	1.89	0.96	7.71	0.50	1.94
1508	0.51	45	13.4	1.88	0.92	8.05	0.99	0.93
1509	0.51	21	46.9	1.91	0.97	7.84	0.29	3.31
1510	0.41	34	119.0	1.86	0.94	7.67	0.51	1.86

sample	magnetic suszeptibility	gamma radiation	ostracods (100g)	Total Carbon (%)	C in % acid	Carbonate equivalent	total S (%)	TOC/S ratio
1511	0.50	30	239.2	1.92	0.93	8.22	0.33	2.82
1512	0.51	30	156.7	1.89	0.93	8.03	0.29	3.14
1513	0.45	27	10.4	1.97	0.93	8.69	0.53	1.77
1514	0.49	34	64.8	2.04	0.92	9.32	0.35	2.65
1515	0.51	20	22.5	1.94	0.88	8.83	1.25	0.70
1516	0.48	32	74.2	2.03	0.88	9.59	0.81	1.08
1517	0.48	30	95.0	1.90	0.60	10.85	0.26	2.27
1518	0.47	39	29.4	1.96	0.89	8.89	0.26	3.45
1519	0.47	22	55.9	1.95	0.88	8.90	0.26	3.33
1520	0.40	35	69.9	1.85	0.89	8.00	0.30	3.00
1521	0.46	40	107.8	1.87	0.87	8.40	0.52	1.65
1522	0.45	23	31.4	1.92	0.90	8.45	0.31	2.90
1523	0.45	27	177.2	1.97	0.88	9.09	0.39	2.26
1524	0.45	29	363.6	2.02	0.88	9.51	0.42	2.10
1525	0.45	30	561.6	2.08	0.94	9.47	0.37	2.54
1526	0.44	22	177.7	1.96	0.82	9.52	0.42	1.96
1527	0.44	25	120.5	1.99	0.80	9.94	0.29	2.75
1528	0.44	31	67.2	1.99	0.82	9.78	0.47	1.73
1529	0.41	35	209.5	2.24	0.84	11.63	0.38	2.23
1530	0.37	37	407.1	2.32	0.81	12.56	0.35	2.28
1531	0.38	33	478.3	2.34	0.82	12.69	0.47	1.73
1532	0.35	30	286.7	2.43	0.80	13.57	0.71	1.14
1533	0.36	26	257.9	2.56	0.87	14.13	0.64	1.35
1534	0.36	33	822.2	2.62	0.93	14.15	0.73	1.27
1535	0.35	32	471.2	2.39	0.91	12.31	0.74	1.23
1536	0.35	25	560.0	2.12	0.90	10.20	0.46	1.95
1537	0.37	23	349.4	2.12	0.99	9.36	0.15	6.43
1538	0.39	27	249.1	2.17	0.86	10.92	0.11	7.83
1539	0.37	29	185.8	2.50	1.20	10.86	0.19	6.44
1540	0.33	28	232.6	2.36	0.89	12.29	0.25	3.59

sample	Dinocysts/gm sediment	Spiniferites/Achomosphaera spp.	Impagidinium spp.	Selenopemphix spp.	Round brown cysts	Protoperidiniod	Pyxidinopsis psilata	other cysts	Heterotrophic cysts	Autotrophic cysts
1391	12102.9	39.7	32.8	4.4	8.8	9.8	3.4	1.0	23.53	76.47
1392	6674.4	30.0	26.0	12.0	10.0	17.0	5.0	0.0	39.00	61.00
1393	6674.4	40.5	23.5	4.5	10.0	15.0	6.0	0.5	30.00	70.00
1394	12877.6	44.9	23.9	3.4	7.8	14.6	4.9	0.5	25.85	74.15
1395	6163.3	41.1	29.7	2.0	5.0	17.3	4.5	0.5	24.75	75.25
1396	10221.3	37.3	31.3	4.5	8.0	9.5	8.5	1.0	22.89	77.11
1397	6674.4	41.0	31.5	5.0	7.5	10.5	3.5	1.0	24.00	76.00
1398	15637.1	46.3	42.4	0.0	2.0	6.3	2.9	0.0	8.29	91.71
1399	8714.1	39.2	42.6	2.5	4.9	9.3	1.5	0.0	16.67	83.33
1400	10044.9	45.0	21.5	1.0	9.0	22.0	1.5	0.0	32.00	68.00
1401	7647.6	34.6	28.0	0.5	15.9	19.6	0.9	0.5	35.98	64.02
1402	6951.4	37.1	30.7	4.0	7.4	13.9	5.9	1.0	26.24	73.76
1403	11788.6	49.3	29.1	1.0	3.4	15.3	2.0	0.0	19.70	80.30
1404	23392.7	42.1	26.6	3.7	5.6	15.0	6.1	0.9	24.77	75.23
1405	23502.0	44.2	33.0	1.4	5.1	11.2	4.7	0.5	17.67	82.33
1406	11751.0	42.8	29.3	2.3	8.8	10.7	5.1	0.9	22.79	77.21
1407	6324.2	43.6	30.3	1.9	6.6	11.8	5.7	0.0	20.38	79.62
1408	14366.1	41.3	29.9	1.5	7.5	18.9	1.0	0.0	27.86	72.14
1409	34378.6	39.6	28.4	0.9	4.5	21.2	3.6	1.8	28.38	71.62
1410	20647.8	40.0	24.0	2.5	8.0	23.0	1.5	1.0	34.50	65.50
1411	11262.4	31.5	38.5	3.0	3.5	17.0	5.0	1.5	25.00	75.00
1412	7947.2	28.4	29.4	4.0	12.9	22.4	2.5	0.5	39.80	60.20
1413	8002.1	47.9	20.9	0.0	6.6	21.8	2.4	0.5	28.91	71.09
1414	4386.5	40.4	32.0	2.5	10.8	10.8	2.5	1.0	25.12	74.88
1415	13671.8	30.1	21.4	2.4	13.6	25.7	3.4	3.4	45.15	54.85
1416	10025.0	30.2	15.6	5.4	18.0	25.4	0.5	4.9	53.66	46.34
1417	7396.8	38.4	32.0	3.0	8.9	16.3	0.0	1.5	29.06	70.94
1418	4704.6	36.0	30.5	3.0	9.0	17.0	3.5	1.0	30.00	70.00
1419	7469.6	31.7	24.4	2.4	8.3	28.3	4.4	0.5	39.51	60.49
1420	8424.3	37.3	27.5	3.9	5.9	23.5	2.0	0.0	33.33	66.67
1421	4364.8	36.6	24.8	3.0	5.9	28.2	0.5	1.0	38.12	61.88
1422	5884.6	36.4	27.8	2.4	8.1	21.1	2.9	1.4	33.01	66.99
1423	8065.8	41.2	14.2	4.9	11.8	23.0	4.4	0.5	40.20	59.80
1424	5273.6	44.8	28.6	2.4	4.3	15.7	1.0	3.3	22.86	77.14
1425	7290.3	44.6	39.2	0.5	2.0	8.3	4.4	1.0	11.27	88.73
1426	9338.0	60.7	18.9	1.5	6.0	9.0	3.0	1.0	16.92	83.08

sample	Dinocysts/gm sediment	Spiniferites/Achomosphaera spp.	Impagidinium spp.	Selenopemphix spp.	Round brown cysts	Protoperidiniod	Pyxidinopsis psilata	other cysts	Heterotrophic cysts	Autotrophic cysts
1427	7360.3	46.0	21.8	2.0	12.9	15.3	1.5	0.5	30.69	69.31
1428	8573.5	34.0	18.7	1.5	17.2	24.6	2.5	1.5	44.83	55.17
1429	9384.4	40.1	19.8	5.0	11.4	17.8	3.0	3.0	36.63	63.37
1430	6585.6	33.7	31.7	4.5	11.4	15.3	2.5	1.0	32.18	67.82
1431	10788.5	42.6	31.6	1.0	9.1	13.4	1.9	0.5	23.92	76.08
1432	8105.4	46.8	21.0	2.4	12.2	13.7	2.0	2.0	29.76	70.24
1433	9246.2	51.0	14.7	4.9	10.3	17.6	1.5	0.0	32.84	67.16
1434	8065.8	49.5	33.8	2.5	6.4	3.4	3.9	0.5	12.75	87.25
1435	5631.2	44.0	33.0	1.5	7.5	10.5	3.5	0.0	19.50	80.50
1436	7730.5	45.2	30.8	2.4	7.2	10.6	3.4	0.5	20.19	79.81
1437	5467.2	47.8	27.6	1.5	8.9	9.4	3.9	1.0	20.20	79.80
1438	9430.9	48.3	22.2	5.9	8.9	11.3	2.5	1.0	27.09	72.91
1439	10296.0	41.0	31.7	2.4	8.3	11.7	3.9	1.0	23.41	76.59
1440	10323.9	47.0	40.0	1.0	3.5	5.5	2.0	1.0	11.00	89.00
1441	9878.3	45.0	36.1	2.0	7.4	5.9	3.0	0.5	15.84	84.16
1442	6960.2	44.2	25.2	3.4	5.8	13.1	8.3	0.0	22.33	77.67
1443	9557.0	55.6	28.7	2.8	4.6	5.6	2.8	0.0	12.96	87.04
1444	11788.6	47.8	25.6	3.9	9.9	7.9	4.9	0.0	21.67	78.33
1445	8489.1	48.3	22.4	2.0	10.4	9.0	7.0	1.0	21.89	78.11
1446	4145.4	45.8	43.3	2.5	2.5	3.9	2.0	0.0	8.87	91.13
1447	8342.6	46.0	29.9	2.8	4.3	11.4	4.7	0.9	19.43	80.57
1448	8772.9	44.8	29.6	2.0	9.4	10.3	2.5	1.5	23.15	76.85
1449	4980.2	50.2	34.8	0.5	6.0	4.5	3.5	0.5	11.44	88.56
1450	10931.2	37.0	29.0	1.5	14.5	14.5	2.5	1.0	31.50	68.50
1451	8937.5	47.0	30.7	2.5	6.4	10.9	2.5	0.0	19.80	80.20
1452	7615.4	44.5	39.2	0.0	4.8	7.2	3.3	1.0	12.92	87.08
1453	6825.0	37.1	37.1	2.5	11.9	5.4	5.9	0.0	19.80	80.20
1454	7622.8	41.8	30.3	2.0	11.9	10.9	3.0	0.0	24.88	75.12
1455	9291.5	37.5	32.0	1.0	9.0	12.5	4.5	3.5	26.00	74.00
1456	5394.2	37.3	25.4	3.3	12.4	18.2	3.3	0.0	33.97	66.03
1457	5183.7	36.8	36.3	1.4	13.2	9.4	2.4	0.5	24.06	75.94
1458	10931.2	35.5	29.0	2.0	15.5	14.5	3.0	0.5	32.50	67.50
1459	12528.5	36.4	26.8	1.9	9.6	23.9	0.5	1.0	36.36	63.64
1460	6951.4	34.2	27.7	3.0	6.9	24.3	4.0	0.0	34.16	65.84
1461	8421.7	35.7	31.0	1.9	6.6	22.1	2.8	0.0	30.52	69.48
1462	7742.9	40.0	17.5	0.0	10.0	28.0	3.0	1.5	39.50	60.50
1463	7656.2	42.7	19.9	0.5	6.8	26.7	3.4	0.0	33.98	66.02
1464	8784.7	29.3	33.2	2.9	8.2	21.6	3.4	1.4	34.13	65.87
1465	7781.6	31.8	18.9	3.0	10.4	33.3	2.0	0.5	47.26	52.74
1466	12168.9	36.9	19.7	3.0	12.3	23.6	4.4	0.0	38.92	61.08
1467	11375.0	32.7	19.8	2.5	6.4	33.7	4.5	0.5	43.07	56.93
1468	14366.1	40.3	22.4	4.0	1.5	28.9	2.0	1.0	35.32	64.68
1469	11672.4	47.3	26.4	2.0	3.0	18.4	2.5	0.5	23.88	76.12

sample	Dinocysts/gm sediment	Spiniferites/Achomosphaera spp.	Impagidinium spp.	Selenopemphix spp.	Round brown cysts	Protoperidiniod	Pyxidinopsis psilata	other cysts	Heterotrophic cysts	Autotrophic cysts
1470	7781.6	55.7	21.9	1.5	6.5	11.9	2.5	0.0	19.90	80.10
1471	7907.7	51.0	23.0	3.5	4.0	15.0	2.5	1.0	23.50	76.50
1472	8079.6	45.5	30.5	1.5	5.0	13.0	4.0	0.5	19.50	80.50
1473	18583.0	50.5	26.5	2.5	3.0	12.5	4.5	0.5	18.50	81.50
1474	17698.1	46.0	25.5	1.5	4.0	20.0	2.5	0.5	26.00	74.00
1475	14866.4	48.0	24.0	0.0	0.0	26.0	1.0	1.0	27.00	73.00
1476	26547.1	39.0	36.5	1.0	1.5	21.0	1.0	0.0	23.50	76.50
1477	15535.4	46.9	24.4	0.0	2.4	23.0	3.3	0.0	25.36	74.64
1478	7433.2	31.5	32.0	3.5	4.0	24.0	5.0	0.0	31.50	68.50
1479	32019.9	47.8	20.1	0.9	4.5	25.0	0.9	0.9	30.36	69.64
1480	17569.4	44.2	27.9	1.4	5.3	19.2	1.9	0.0	25.96	74.04
1481	16320.7	45.0	26.7	0.0	1.5	23.3	3.0	0.5	25.25	74.75
1482	22081.0	42.1	35.6	0.5	1.5	14.4	5.9	0.0	16.34	83.66
1483	16451.4	36.9	23.6	2.3	5.6	29.6	2.0	0.0	37.54	62.46
1484	11040.5	46.0	20.8	2.5	4.5	24.3	1.5	0.5	31.19	68.81
1485	12574.5	43.3	32.0	1.0	4.4	15.3	3.0	1.0	21.67	78.33
1486	15795.6	41.7	34.3	2.5	4.9	13.7	2.5	0.5	21.57	78.43
1487	14940.7	40.8	25.9	0.5	2.0	26.9	4.0	0.0	29.35	70.65
1488	11256.0	36.8	35.4	2.4	3.3	16.5	5.7	0.0	22.17	77.83
1489	16492.4	50.2	25.4	0.9	3.3	18.3	1.4	0.5	23.00	77.00
1490	8341.7	41.6	27.2	0.5	5.4	19.8	5.0	0.5	26.24	73.76
1491	37723.5	33.5	26.1	1.0	3.9	33.5	2.0	0.0	38.42	61.58
1492	15640.7	50.0	15.3	1.0	1.0	31.2	1.5	0.0	33.17	66.83
1493	21862.4	40.0	34.0	1.5	4.5	18.5	1.5	0.0	24.50	75.50
1494	11614.4	38.0	26.5	1.0	5.0	28.0	1.5	0.0	34.00	66.00
1495	11989.0	46.0	30.5	0.5	3.5	19.0	0.5	0.0	23.00	77.00
1496	10073.9	45.6	35.0	0.0	1.9	15.5	1.9	0.0	17.48	82.52
1497	17062.6	45.0	32.7	0.0	0.0	18.3	3.5	0.5	18.81	81.19
1498	15684.1	38.9	39.3	0.0	3.8	15.6	2.4	0.0	19.43	80.57
1499	16159.1	42.5	27.0	2.0	9.0	17.0	2.0	0.5	28.50	71.50
1500	10931.2	51.0	26.0	2.5	3.5	13.5	3.5	0.0	19.50	80.50
1501	10323.9	38.5	29.5	1.0	4.5	21.0	4.5	1.0	27.50	72.50
1502	11149.8	45.1	36.8	2.0	2.9	12.3	1.0	0.0	17.16	82.84
1503	12636.4	39.7	28.9	2.0	6.4	21.1	2.0	0.0	29.41	70.59
1504	14866.4	43.0	18.0	2.0	10.5	24.0	2.5	0.0	36.50	63.50
1505	9955.2	48.7	24.3	2.7	8.0	14.0	2.0	0.3	25.00	75.00
1506	8446.8	37.7	40.0	0.7	7.7	10.7	2.7	0.7	19.67	80.33
1507	8576.8	34.3	42.0	1.0	8.3	11.3	1.7	1.3	22.00	78.00
1508	8710.8	33.3	48.0	1.3	3.7	12.7	1.0	0.0	17.67	82.33
1509	7636.8	40.3	28.0	1.3	13.0	14.7	2.0	0.7	29.67	70.33
1510	9780.5	44.3	34.3	1.0	2.7	14.3	1.3	2.0	19.33	80.67

sample	Dinocysts/gm sediment	Spiniferites/Achomosphaera spp.	Impagidinium spp.	Selenopemphix spp.	Round brown cysts	Protoperidiniod	Pyxidinopsis psilata	other cysts	Heterotrophic cysts	Autotrophic cysts
1511	11377.3	36.3	32.7	2.0	8.3	20.0	0.7	0.0	30.33	69.67
1512	7852.0	42.7	32.7	0.0	9.3	13.3	1.7	0.3	22.67	77.33
1513	17479.6	38.2	33.6	2.7	7.6	16.3	1.3	0.3	26.91	73.09
1514	12119.3	41.7	31.0	0.7	5.7	19.7	1.0	0.3	26.00	74.00
1515	13273.6	34.7	33.3	1.0	9.3	19.3	2.3	0.0	29.67	70.33
1516	8849.0	39.7	27.3	1.0	6.7	23.0	1.7	0.7	31.33	68.67
1517	17983.5	41.7	24.3	1.0	4.0	26.7	2.0	0.3	32.00	68.00
1518	13597.3	39.3	33.0	0.0	2.3	23.3	1.7	0.3	25.67	74.33
1519	13983.7	34.9	33.2	1.3	5.0	23.9	1.0	0.7	30.56	69.44
1520	16893.6	43.0	30.0	1.0	3.3	19.7	3.0	0.0	24.00	76.00
1521	15981.4	40.9	30.6	0.3	5.0	20.9	2.3	0.0	26.25	73.75
1522	15928.3	39.7	32.3	1.0	4.0	20.0	2.7	0.3	25.00	75.00
1523	8768.9	45.7	28.5	3.0	3.6	17.9	1.3	0.0	24.50	75.50
1524	13983.7	40.5	27.9	3.0	6.0	21.3	1.0	0.3	30.56	69.44
1525	9449.0	44.0	25.3	3.3	7.0	19.3	1.0	0.0	29.67	70.33
1526	11614.4	43.7	34.0	2.7	3.7	13.7	2.3	0.0	20.00	80.00
1527	9169.6	49.8	26.6	1.0	5.6	15.0	1.7	0.3	21.93	78.07
1528	13008.1	44.2	28.6	3.7	4.7	16.9	1.7	0.3	25.25	74.75
1529	14670.8	44.7	32.7	1.0	3.7	15.7	2.3	0.0	20.33	79.67
1530	15067.3	53.0	22.0	6.3	3.3	12.0	3.0	0.3	21.67	78.33
1531	16893.6	49.0	28.0	2.3	5.0	13.7	2.0	0.0	21.00	79.00
1532	20308.6	55.6	22.5	1.6	5.2	12.4	2.0	0.7	19.61	80.39
1533	9955.2	54.3	17.3	2.3	6.7	16.7	2.7	0.0	25.67	74.33
1534	11861.5	54.7	27.3	0.7	2.0	12.3	2.7	0.3	15.00	85.00
1535	9955.2	48.0	28.7	3.0	6.3	12.3	1.7	0.0	21.67	78.33
1536	14216.0	52.6	24.8	0.0	5.2	14.4	2.9	0.0	19.61	80.39
1537	5574.9	53.3	25.3	4.0	2.0	12.3	3.0	0.0	18.33	81.67
1538	11567.0	54.4	19.7	7.9	3.3	13.1	1.3	0.3	24.59	75.41
1539	7089.1	50.2	31.4	3.9	2.6	8.7	3.2	0.0	15.21	84.79
1540	8123.4	50.65	24.51	6.21	2.94	13.07	2.29	0.33	22.22	77.78

sample	pollen/gm sediment	pollen-diversity	*Abies*	*Cathaya*	*Picea*	*Sciadopitys*	Taxodioideae	*Tsuga*	gymnosperm<2%	Arecaceae	*Carya*	*Fagus*	*Poaceae*	*Pterocarya*	*Quercus*	*Sparganium/Typha*	*Ulmus*	angiosperm<2%
1391	24917.7	20	17.7	38.7	23.9	0.7	2.6	1.3	0.0	0.0	4.9	2.0	2.6	0.3	0.7	0.7	1.3	2.6
1392	29204.7	20	15.9	34.0	21.6	0.3	11.7	1.6	0.0	0.0	3.5	2.5	3.2	1.6	1.0	0.6	0.0	2.5
1393	27330.3	17	14.5	39.8	19.6	0.0	7.5	0.9	0.0	0.0	7.5	3.0	2.1	0.3	1.5	0.6	0.9	1.8
1394	48055.5	19	11.1	40.1	19.9	0.3	9.4	2.4	0.3	0.0	4.2	1.7	4.2	0.3	2.8	0.7	0.3	2.1
1395	33554.5	18	16.9	38.0	25.7	0.4	5.6	2.1	0.0	0.0	3.9	1.4	2.1	0.4	0.7	0.7	0.7	1.4
1396	37750.3	20	16.2	43.9	18.2	0.0	4.9	2.0	0.3	0.0	5.2	1.4	2.0	0.0	1.7	0.3	0.6	3.2
1397	16884.4	16	16.3	30.1	18.3	0.0	12.7	4.9	0.3	0.0	7.2	1.6	3.9	0.3	1.3	0.7	1.0	1.3
1398	30386.6	13	17.9	40.2	18.9	0.0	9.8	1.0	0.0	0.0	3.4	2.0	4.7	0.0	0.7	0.7	0.0	0.7
1399	19322.3	17	14.0	36.0	21.8	0.6	10.1	1.6	0.0	0.0	5.5	2.3	3.9	1.0	0.6	1.0	0.6	1.0
1400	77205.3	18	16.4	43.1	12.5	0.0	8.6	1.6	0.0	0.0	4.3	3.9	4.6	0.7	1.3	0.3	0.3	2.3
1401	29708.3	16	17.4	43.9	15.3	0.0	8.7	1.0	0.0	0.0	5.6	1.4	2.8	0.7	1.0	0.3	0.7	1.0
1402	19492.2	20	17.8	41.2	15.8	0.0	8.8	2.0	0.0	0.0	6.1	1.2	2.3	0.3	1.2	0.3	0.3	2.6
1403	24802.6	19	23.7	29.8	20.4	0.0	7.3	3.6	0.0	0.0	5.5	2.1	2.4	0.9	0.9	0.3	0.0	3.0
1404	37713.2	19	23.1	36.1	18.0	0.0	8.8	1.7	0.7	0.0	2.7	1.7	1.7	0.3	1.0	0.0	1.7	2.4
1405	22603.4	18	19.5	43.2	20.8	0.0	6.3	1.0	0.0	0.0	2.3	0.7	2.6	0.3	0.3	0.3	0.7	2.0
1406	24986.0	15	21.0	44.3	18.1	0.0	7.0	1.8	0.0	0.0	3.0	0.7	1.8	0.4	0.4	0.4	0.4	0.7
1407	12793.3	16	20.0	37.0	22.6	0.4	4.4	2.2	0.0	0.0	5.9	0.7	2.6	1.1	1.1	0.4	0.7	0.7
1408	24339.7	15	17.8	48.8	13.9	0.7	3.9	4.6	0.0	0.0	2.5	2.5	2.1	0.0	1.8	0.4	0.4	0.7
1409	21304.9	18	20.4	40.8	15.1	0.0	7.7	2.0	0.3	0.0	4.0	1.0	4.0	0.7	1.3	0.0	1.0	1.7
1410	24277.7	19	18.7	37.8	19.0	0.3	8.8	2.0	0.0	0.0	5.1	1.0	2.7	0.3	1.7	0.3	0.3	1.7
1411	12371.3	16	14.2	41.1	18.8	0.0	9.2	2.1	0.0	0.0	3.9	2.8	1.1	1.4	2.1	0.0	0.7	2.5
1412	19662.4	18	18.7	37.3	18.3	0.0	9.7	3.0	0.0	0.0	3.0	1.7	3.0	1.0	1.0	0.3	1.3	1.7
1413	19976.8	18	12.7	34.7	16.8	0.0	14.8	3.4	1.0	0.0	6.9	2.4	2.7	1.0	1.0	0.3	0.0	2.1
1414	19074.6	15	18.2	36.8	19.3	0.0	7.4	3.2	0.0	0.0	4.6	2.5	3.2	0.0	1.1	0.0	1.1	2.8
1415	34148.9	17	11.7	39.9	16.2	0.0	12.0	0.0	1.0	0.0	5.5	2.1	3.4	1.7	3.1	0.0	1.0	2.4
1416	36612.6	21	13.3	43.9	13.3	0.0	6.1	3.7	0.0	0.0	5.4	2.0	4.1	1.0	1.0	0.0	1.4	4.8
1417	19756.9	19	15.4	42.0	13.1	0.0	9.9	1.9	0.0	0.3	0.6	2.2	5.4	3.2	2.9	0.3	0.0	2.6
1418	18950.0	18	18.0	36.9	15.6	0.0	9.0	3.6	0.0	0.0	3.0	2.7	4.9	0.8	1.6	0.0	1.1	2.7
1419	24384.6	20	13.8	42.5	15.4	0.3	8.5	1.9	0.3	0.0	7.9	2.5	1.6	0.9	1.9	0.0	0.6	1.9
1420	22691.9	18	13.5	35.3	12.2	0.0	16.2	2.3	0.0	0.0	6.6	2.6	4.3	0.3	1.7	1.3	0.7	3.0
1421	16571.2	17	12.7	37.5	16.4	0.3	16.1	2.3	0.0	0.0	3.7	3.3	2.7	0.7	1.7	0.7	1.0	1.0
1422	16912.8	20	11.5	36.5	13.3	0.0	17.3	1.9	0.0	0.0	4.6	1.5	6.2	0.6	0.9	0.9	0.9	3.7
1423	13682.8	21	9.2	40.6	22.9	0.4	10.3	1.5	0.7	0.0	3.7	2.6	3.7	1.1	0.4	0.4	0.4	2.2
1424	14617.3	19	10.4	40.7	12.1	0.3	13.1	2.7	0.0	0.0	3.4	3.4	6.7	3.0	1.0	0.7	0.3	2.0
1425	17367.2	17	8.1	48.0	16.4	0.3	8.4	0.7	0.3	0.0	4.0	3.7	5.7	1.0	1.7	0.0	0.0	1.7
1426	23065.6	17	10.9	47.3	16.0	0.0	10.9	2.0	0.0	0.0	3.4	3.1	1.4	1.4	1.4	0.3	0.7	1.4

sample	**pollen/gm sediment**	**pollen-diversity**	***Abies***	***Cathaya***	***Picea***	***Sciadopitys***	**Taxodioideae**	***Tsuga***	**gymnosperm<2%**	**Arecaceae**	***Carya***	***Fagus***	***Poaceae***	***Pterocarya***	***Quercus***	***Sparganium/Typha***	***Ulmus***	**angiosperm<2%**
1427	16816.6	14	13.6	49.7	9.7	0.0	10.1	4.2	0.0	0.0	3.6	2.6	2.9	1.6	0.3	0.3	0.6	0.6
1428	20700.8	21	9.7	44.3	13.0	0.7	7.7	2.3	0.7	0.0	4.7	5.0	4.3	1.7	1.3	0.3	0.7	3.7
1429	26847.0	17	18.7	35.1	18.1	0.0	11.3	2.5	0.0	0.0	3.1	2.3	3.4	1.7	0.6	1.1	0.6	1.4
1430	24292.5	17	9.7	44.2	24.4	0.0	6.2	0.3	0.3	0.0	4.5	2.6	1.6	0.3	3.9	0.6	0.3	1.0
1431	19358.5	16	9.3	40.4	20.2	0.7	14.6	1.3	0.0	0.0	3.3	1.3	5.3	0.0	1.3	0.3	0.7	1.3
1432	16872.3	19	5.6	42.7	18.9	0.3	17.2	0.3	0.3	0.0	4.6	1.3	4.0	0.0	1.3	0.3	0.7	2.3
1433	25062.0	20	9.0	40.8	19.7	0.6	13.6	2.0	0.3	0.0	4.6	1.7	4.0	0.3	1.2	0.3	0.3	1.7
1434	22148.0	17	7.5	45.4	18.8	0.0	10.9	1.0	0.0	0.0	5.1	3.8	2.7	0.7	1.4	0.0	1.0	1.7
1435	19755.4	16	7.7	47.4	17.2	0.0	11.9	1.4	0.0	0.0	5.6	2.5	2.1	1.1	0.7	0.4	0.7	1.4
1436	27163.8	17	10.2	40.3	16.0	0.0	17.4	1.4	0.0	0.0	3.4	2.4	2.7	0.7	2.4	1.0	0.3	1.7
1437	16731.7	20	9.7	35.9	15.9	0.0	18.6	1.7	0.7	0.0	5.9	3.8	2.1	0.3	1.0	0.7	0.7	3.1
1438	21596.8	22	14.0	38.5	12.0	0.0	17.1	1.3	0.0	0.0	3.3	3.7	2.7	1.0	0.7	0.3	1.0	4.3
1439	20362.8	20	17.3	35.5	11.3	0.6	14.8	3.1	0.0	0.0	4.4	2.5	3.1	0.6	1.9	0.9	0.9	2.8
1440	17754.7	17	16.7	38.1	17.3	0.7	10.5	2.0	0.0	0.0	3.4	2.7	4.4	1.0	1.4	0.3	0.0	1.4
1441	12999.5	16	9.7	48.3	14.3	0.0	9.3	1.5	0.4	0.0	4.6	3.1	3.1	1.2	1.5	0.0	0.4	2.7
1442	22818.6	15	8.7	42.2	17.8	0.0	11.5	1.7	0.0	0.0	4.2	3.1	3.5	1.4	3.5	1.0	0.0	1.4
1443	30999.7	18	18.5	38.8	16.3	0.7	11.2	2.9	0.4	0.4	4.3	1.1	1.1	0.4	2.2	0.4	0.0	1.4
1444	22631.8	21	12.0	43.6	14.9	0.4	13.1	0.7	0.7	0.0	4.4	1.8	1.8	0.4	1.8	0.4	0.7	3.3
1445	45158.6	16	11.5	46.2	19.1	0.0	9.4	1.7	0.0	0.0	2.8	2.4	2.1	0.7	1.7	0.3	1.0	1.0
1446	23661.2	17	13.2	38.5	15.5	0.0	14.5	2.6	0.0	0.0	3.6	2.0	4.9	0.7	1.0	0.7	1.3	1.6
1447	32192.8	21	15.4	42.2	15.7	0.0	9.8	1.6	0.0	0.3	2.9	2.6	3.6	0.3	1.3	0.7	0.7	2.9
1448	24868.9	20	13.9	41.8	15.0	0.0	10.1	2.4	0.0	0.0	4.2	1.0	3.5	1.4	1.4	0.7	1.0	3.5
1449	30386.2	22	14.5	46.8	12.7	0.3	8.5	3.3	0.3	0.0	1.8	0.3	3.9	1.2	1.2	1.2	0.6	3.3
1450	27677.7	16	14.5	41.8	12.5	0.0	12.5	2.7	0.0	0.0	3.1	0.8	4.7	1.6	2.7	0.8	0.8	1.6
1451	22831.0	21	11.2	40.5	19.4	0.0	9.5	0.3	0.7	0.3	5.9	1.6	3.3	0.3	2.0	1.0	0.7	3.3
1452	25204.6	17	15.1	38.8	14.8	0.0	14.1	1.7	0.0	0.0	4.1	1.4	3.4	1.7	0.3	0.7	1.0	2.7
1453	28424.9	19	13.3	37.4	18.4	0.7	11.2	3.7	0.0	0.0	5.8	2.0	1.7	0.3	2.0	0.3	0.0	3.1
1454	26582.8	20	14.2	33.8	16.6	0.0	14.2	2.3	0.0	0.0	6.0	1.3	3.0	1.3	1.7	0.7	1.7	3.3
1455	21063.0	22	7.8	35.3	14.9	0.3	19.7	2.7	0.0	0.0	6.4	1.0	3.7	1.4	1.0	0.3	1.0	4.4
1456	22543.5	19	13.3	35.0	19.4	0.0	11.8	1.9	0.0	0.4	4.6	2.3	3.8	1.5	1.5	1.1	1.1	2.3
1457	28363.1	20	12.6	36.4	20.3	0.0	6.1	3.1	0.8	0.0	6.1	3.4	2.7	0.8	2.3	1.1	0.4	3.8
1458	34655.8	20	6.1	43.2	20.7	0.0	13.2	1.8	0.0	0.4	2.5	1.8	4.6	0.7	1.1	0.0	0.4	3.6
1459	51813.7	22	9.6	42.8	14.0	0.4	12.8	2.0	0.0	0.0	2.4	2.8	3.2	0.0	3.6	1.2	1.6	3.6
1460	25100.5	20	9.5	44.9	13.2	0.0	11.8	1.4	0.0	0.0	6.4	2.0	3.4	1.0	2.0	0.3	0.7	3.4
1461	31143.8	19	11.4	41.1	17.1	0.7	10.0	1.8	0.0	0.0	5.7	2.9	2.1	1.8	2.1	1.1	0.4	1.8
1462	22668.4	19	10.9	39.3	14.2	0.0	11.6	1.8	0.0	0.0	8.4	1.5	3.6	1.1	3.3	0.4	1.1	2.9
1463	25918.9	18	14.8	36.6	11.4	1.0	13.8	3.0	0.0	0.0	5.0	2.0	4.4	1.7	2.0	1.0	1.7	1.7
1464	28131.4	20	10.8	35.3	12.2	0.3	14.7	3.5	0.0	0.0	4.9	2.4	4.2	1.0	3.8	1.0	1.7	3.8
1465	22709.1	17	9.4	35.2	16.5	0.7	15.0	2.6	0.4	0.0	6.4	2.6	4.9	1.1	3.0	0.0	1.1	1.1
1466	37727.3	20	9.5	40.1	8.0	0.0	17.5	2.2	0.0	0.0	5.1	1.8	4.0	1.8	3.6	1.8	0.7	3.6
1467	25694.5	21	8.1	39.3	13.4	0.0	13.4	0.8	0.0	0.4	5.3	2.8	3.2	1.6	4.5	2.0	1.6	3.6
1468	22637.8	18	7.6	36.4	14.8	0.0	16.8	2.0	0.0	0.0	3.2	2.8	7.2	1.2	2.0	2.4	0.4	3.2
1469	21063.0	17	14.3	34.1	15.9	0.0	11.6	3.1	0.0	0.0	6.6	1.6	2.7	2.7	3.9	0.0	0.0	3.5

sample	**pollen/gm sediment**	**pollen-diversity**	***Abies***	***Cathaya***	***Picea***	***Sciadopitys***	**Taxodioideae**	***Tsuga***	**gymnosperm<2%**	**Arecaceae**	***Carya***	***Fagus***	***Poaceae***	***Pterocarya***	***Quercus***	***Sparganium/Typha***	***Ulmus***	**angiosperm<2%**
1470	40289.3	17	14.2	35.6	23.6	0.4	8.2	2.6	0.0	0.0	4.5	1.1	4.5	0.4	1.9	1.5	0.4	1.1
1471	34639.6	22	13.7	35.8	16.5	0.4	14.7	2.8	0.4	0.0	3.2	0.7	4.2	1.8	1.1	1.1	1.1	2.8
1472	40730.6	22	13.3	31.9	20.4	0.7	11.5	2.9	0.0	0.0	6.8	2.2	1.8	1.1	2.5	0.7	0.7	3.6
1473	34109.9	18	16.3	32.6	26.1	0.4	9.1	1.9	0.0	0.0	5.7	1.5	1.5	0.4	1.1	0.4	1.5	1.5
1474	44559.9	17	15.3	36.7	19.8	0.0	7.7	1.6	0.0	0.0	7.3	1.6	3.2	0.8	2.0	0.8	1.6	1.6
1475	35973.7	23	16.9	32.2	19.2	0.4	7.8	3.5	0.0	0.4	4.3	2.0	2.7	2.0	2.4	0.8	0.0	5.5
1476	49059.5	20	16.3	32.9	17.9	0.8	8.9	2.0	0.0	0.0	5.3	2.8	2.8	1.6	2.0	3.3	0.4	2.8
1477	33006.7	17	17.9	38.3	15.8	0.4	9.6	2.5	0.0	0.0	4.2	1.7	3.8	0.8	2.1	0.8	0.4	1.7
1478	23889.5	17	21.3	32.8	17.2	0.8	15.6	0.8	0.0	0.4	2.0	0.4	2.9	0.8	2.0	1.2	0.8	0.8
1479	62473.1	22	21.7	31.0	14.0	0.8	8.9	5.4	0.8	0.4	3.9	1.6	3.1	1.2	2.3	0.0	1.9	3.1
1480	26787.4	17	23.5	36.0	12.6	0.4	5.7	5.3	0.0	0.0	6.9	1.6	3.2	0.8	1.2	0.8	0.8	1.2
1481	27505.2	19	16.0	34.4	16.8	0.0	11.3	3.1	0.0	0.0	7.4	1.2	3.5	0.0	0.8	2.0	1.2	2.3
1482	59414.3	23	13.2	40.1	15.6	0.4	9.3	2.3	0.0	0.0	3.5	2.7	3.9	0.4	1.2	1.6	0.4	5.4
1483	36884.2	19	13.3	37.9	13.7	0.4	10.1	3.6	0.0	0.0	4.8	2.0	3.6	1.6	2.8	0.4	1.6	4.0
1484	33168.0	22	14.8	37.9	14.8	0.0	10.9	2.3	0.0	0.0	5.5	1.6	3.1	1.2	2.0	1.2	0.4	4.3
1485	24022.2	20	15.7	34.5	18.1	0.4	13.7	2.4	0.4	0.0	3.2	1.2	3.2	0.8	2.4	0.4	0.4	3.2
1486	59763.0	17	17.6	38.2	16.8	0.4	10.9	2.5	0.0	0.0	2.9	2.9	1.3	1.3	2.5	0.8	0.0	1.7
1487	36023.8	20	18.4	33.6	15.2	0.8	11.9	3.3	0.0	0.0	7.0	1.6	0.8	0.0	1.6	0.0	2.0	3.7
1488	31134.3	19	17.0	37.3	15.1	2.2	11.1	3.0	0.0	0.0	5.5	0.4	1.8	0.7	1.5	1.1	1.1	2.2
1489	24099.4	15	14.6	45.0	14.6	0.4	11.7	0.8	0.4	0.0	5.4	0.8	2.9	1.3	0.8	0.0	0.8	0.4
1490	37413.1	18	19.6	39.6	16.0	0.4	7.2	2.4	0.8	0.8	4.8	0.8	2.4	1.6	1.2	0.8	0.8	0.8
1491	59028.9	20	16.7	41.4	9.6	1.2	15.5	2.8	0.0	0.4	2.4	0.8	2.8	0.0	1.6	1.2	0.8	2.8
1492	38586.5	21	20.2	40.9	11.3	1.6	9.3	2.4	0.4	0.0	2.4	0.8	2.0	0.4	2.0	1.2	1.2	3.6
1493	25628.8	23	13.4	39.4	12.6	0.4	13.4	2.4	0.8	0.0	2.8	2.0	3.7	0.4	0.4	2.4	1.2	4.5
1494	49699.5	21	14.8	50.6	9.7	0.4	9.3	1.2	0.4	0.4	3.9	0.8	1.2	1.2	2.3	1.2	0.8	1.9
1495	25479.0	22	19.9	40.7	8.9	0.0	7.6	2.1	0.0	0.0	7.2	0.0	3.0	1.3	1.7	1.3	2.1	4.2
1496	34913.2	18	19.5	48.2	12.4	0.9	4.4	4.4	0.0	0.0	3.1	0.4	0.9	0.4	2.7	0.0	0.4	2.2
1497	32216.0	18	16.0	44.1	5.5	1.7	15.1	2.5	0.0	0.0	4.2	1.3	1.7	2.1	2.5	1.3	0.4	1.7
1498	55172.6	21	18.7	38.7	11.1	0.9	14.5	3.0	0.0	0.0	2.6	1.7	2.1	0.4	1.3	0.4	0.9	3.8
1499	35487.0	19	22.4	37.6	13.1	0.4	14.7	2.4	0.4	0.0	1.6	0.8	0.8	0.4	1.2	0.8	0.4	2.9
1500	97880.6	21	15.2	42.6	10.5	0.8	11.4	3.4	1.3	0.0	3.0	0.8	1.7	1.3	1.7	1.7	1.7	3.0
1501	47812.6	18	21.2	40.8	7.2	0.4	14.4	2.0	0.0	0.4	2.8	0.4	1.6	1.6	3.6	0.8	1.6	1.2
1502	41295.0	24	10.6	44.7	5.1	1.7	20.4	2.1	0.4	0.0	1.7	0.4	2.6	0.0	3.8	1.3	0.9	4.3
1503	24882.1	23	13.1	36.7	5.2	0.4	22.3	1.6	0.4	0.4	3.2	0.4	4.0	1.2	2.8	2.4	2.8	3.2
1504	30441.3	17	14.2	36.3	9.2	0.4	18.3	2.1	0.0	0.0	6.3	1.3	2.9	0.4	4.6	2.1	1.3	0.8
1505	29263.6	19	17.8	36.4	11.2	1.9	12.4	3.9	0.4	0.0	3.9	1.2	2.7	0.8	1.9	2.3	1.2	1.9
1506	34671.1	23	16.9	39.3	12.0	0.0	9.1	4.5	0.0	0.4	3.7	1.2	0.8	0.8	4.1	0.8	1.7	4.5
1507	44746.9	18	21.5	40.0	9.1	0.4	14.0	1.5	0.0	0.0	1.5	0.4	3.0	1.5	2.3	1.9	1.1	1.9
1508	28798.6	21	13.9	38.5	9.5	0.8	15.9	2.8	0.0	0.0	2.4	1.2	3.6	0.8	3.2	2.0	1.2	4.4
1509	26767.1	18	16.2	45.3	9.8	0.0	12.4	1.3	0.0	0.0	2.1	2.1	2.6	1.3	1.7	2.6	0.0	2.6
1510	46196.7	23	18.8	38.9	7.9	0.4	16.7	2.5	0.8	0.8	1.7	1.3	2.9	0.4	1.7	1.7	1.3	2.1

sample	pollen/gm sediment	pollen-diversity	*Abies*	*Cathaya*	*Picea*	*Sciadopitys*	Taxodioideae	*Tsuga*	gymnosperm<2%	Arecaceae	*Carya*	*Fagus*	*Poaceae*	*Pterocarya*	*Quercus*	*Sparganium/Typha*	*Ulmus*	angiosperm<2%
1511	34295.3	25	15.8	39.5	11.0	0.9	11.0	2.2	0.9	0.0	4.4	0.9	1.3	1.8	2.2	1.8	2.2	4.4
1512	36077.8	21	14.8	43.6	10.0	1.2	12.0	3.2	0.0	0.0	2.8	2.4	2.0	0.8	1.6	1.2	0.8	3.6
1513	27001.0	24	18.5	40.3	7.7	0.8	11.7	2.4	1.2	0.0	2.4	2.0	2.4	0.4	2.0	3.6	0.8	3.6
1514	23153.6	19	18.6	46.3	5.2	1.3	9.1	2.6	0.4	0.4	3.5	2.2	3.0	0.9	1.7	1.7	1.7	1.3
1515	40719.7	18	11.7	46.8	10.5	0.4	12.1	2.0	0.0	0.0	3.6	1.2	4.0	1.6	0.0	2.0	0.8	3.2
1516	35174.7	24	11.6	32.8	10.8	0.0	12.9	3.0	0.0	0.0	5.6	2.2	4.3	2.2	4.7	3.4	0.9	5.6
1517	39420.5	22	17.6	34.9	14.9	1.5	10.3	2.3	0.4	0.8	3.8	1.5	3.4	0.4	1.1	1.9	0.4	4.6
1518	31620.5	16	20.7	37.4	8.8	0.4	12.3	1.3	0.0	0.9	3.1	0.9	4.0	1.3	3.1	3.5	1.8	0.4
1519	39042.2	24	15.4	38.2	10.2	0.4	13.0	2.0	1.6	0.4	2.4	1.2	3.7	1.2	1.2	2.4	1.6	4.9
1520	50455.6	25	24.5	33.9	10.3	0.4	8.6	2.6	0.9	0.4	3.9	0.9	3.9	0.0	3.0	0.9	1.3	4.7
1521	60754.1	22	15.2	33.6	10.7	0.0	12.7	2.0	1.2	1.2	4.9	0.8	5.7	1.2	2.5	2.5	1.2	4.5
1522	44776.4	18	12.7	41.5	14.8	0.4	12.2	1.7	0.0	0.0	3.5	0.9	3.5	0.9	2.2	3.1	0.0	2.6
1523	33265.4	25	19.2	27.6	10.8	1.2	15.2	2.8	0.8	0.4	6.0	1.2	3.2	1.2	2.4	1.2	1.6	5.2
1524	37651.3	20	6.4	42.4	7.2	0.8	21.2	3.8	0.0	0.0	2.5	1.7	4.7	0.4	3.4	2.1	0.4	3.0
1525	45216.6	20	11.4	34.1	7.3	2.3	16.4	3.6	0.9	0.9	4.1	0.0	2.7	1.8	4.5	4.5	1.8	3.6
1526	28151.9	26	14.1	33.1	3.6	0.4	19.4	1.6	0.0	1.6	3.2	3.2	2.4	1.6	4.0	2.4	2.8	6.5
1527	30958.5	24	7.9	41.3	12.0	0.8	15.3	1.7	0.0	0.0	4.1	1.2	2.9	1.2	1.2	4.1	2.1	4.1
1528	28065.7	26	10.7	33.5	12.4	0.4	19.0	1.2	0.4	0.4	2.9	1.7	2.9	0.4	2.5	5.0	0.8	5.8
1529	37300.7	20	11.2	37.5	16.0	1.5	14.9	0.4	0.4	0.7	3.7	2.2	4.1	0.4	2.2	0.4	1.5	3.0
1530	20421.2	27	11.4	33.9	8.7	3.1	16.5	0.8	1.2	0.8	2.8	1.6	3.1	1.6	4.3	3.1	1.2	5.9
1531	24553.4	26	19.0	27.3	13.4	3.5	13.9	1.7	0.9	0.9	2.6	0.0	2.2	2.2	3.5	0.9	2.2	6.1
1532	38582.2	24	17.7	28.8	10.7	2.3	17.7	2.8	0.9	0.0	4.7	0.9	3.3	1.9	1.4	1.4	0.9	4.7
1533	28960.5	24	9.8	29.3	11.6	1.8	17.8	2.2	0.0	0.0	3.1	1.3	2.2	0.9	6.7	4.0	3.6	5.8
1534	27530.9	19	16.7	24.1	8.8	0.9	22.2	2.8	0.5	0.5	3.7	0.9	3.7	1.4	6.0	6.5	0.5	0.9
1535	19256.8	25	14.7	21.9	5.4	2.7	22.3	2.2	0.9	1.3	4.0	2.2	6.7	1.8	3.6	2.7	2.2	5.4
1536	25574.0	30	9.2	24.7	11.7	1.3	19.2	2.1	0.8	1.7	4.2	0.8	4.2	1.3	4.6	5.0	0.4	8.8
1537	20717.0	26	13.1	21.7	6.6	2.0	15.6	3.7	0.8	2.0	7.4	2.5	2.9	1.6	3.7	9.0	1.6	5.7
1538	18305.9	28	12.4	23.6	5.8	3.9	14.3	5.0	0.0	1.5	6.2	0.4	8.1	1.5	4.2	2.7	1.9	8.5
1539	16551.8	28	15.5	24.7	9.6	4.1	10.5	1.8	0.9	1.4	1.4	1.8	6.8	3.7	4.1	2.3	2.3	9.1
1540	34772.8	34	15.2	14.8	6.3	3.4	14.8	3.4	2.1	2.1	2.5	3.0	11.0	1.7	4.2	4.6	2.1	8.9

7.5.2. Coexistence Approach climatic data (Table 3.2)

Table 3.2 shows which taxa were selected for the Coexistance Appraoch and which were excluded. Further. an argument is listed for each of the not considered taxa.

NLR – Nearest Living Realtive.

Hennersdorf	NLR_reference_taxon		excluded
Abies	Abies sp..........	x	long distance
Cathaya	Cathaya sp..........		NLR limited
Cupressaceae	Cupressaceae........	x	
Ginkgo	Ginkgo biloba.......		NLR limited
Ephedra	Ephedra sp..........		long distance
Picea	Picea sp............		long distance
Sciadopitys	Sciadopitys verticil		NLR limited
Sequoia	Taxodiaceae.........	x	
Taxodioideae	Taxodiaceae.........	x	
Tsuga	Tsuga sp............		NLR limited
Acer	Acer sp.............	x	
Amaranthaceae	Amaranthaceae.......		single grain
Alnus	Alnus sp............	x	
Araliaceae	Araliaceae..........	x	
Arecaceae	Arecaceae...........	x	
Artemisia	Artemisia sp........	x	single grain
Asteraceae	Compositae..........	x	
Betula	Betula sp...........	x	
Buxus	Buxus sp............		single grain
Carpinus	Carpinus sp.........	x	
Carya	Carya sp............	x	
Caryophyllaceae	Caryophyllaceae.....	x	
Castanea-type	Castanea sp.........	x	
Celtis	Celtis sp...........	x	
Chenopodiaceae	Chenopodiaceae......	x	
Corylus	Corylus sp..........	x	
Cyperaceae	Cyperaceae..........	x	
Eleaegnus	Cyperaceae..........	x	
Engelhardia	Engelhardtia sp.....	x	
Ericaceae	Ericaceae...........	x	
Euphorbiaceae	Euphorbiaceae.......	x	
Fagus	Fagus sp............	x	
Fraxinus	Fraxinus sp.........	x	
Hamamelidaceae	Hamamelidaceae......		single grain
Ilex	Ilex sp.............		single grain
Juglans	Juglans sp..........	x	
Liquidambar	Liquidambar sp......	x	
Lonicera	Lonicera sp.........	x	
Lythraceae	Lythraceae..........	x	
Myrica	Myrica sp...........	x	
Nuphar	Nuphar sp...........		single grain
Nyssa	Nyssa sp............	x	
Platycarya	Platycarya sp.......	x	
Poaceae	Poaceae.............	x	
Pontamogeton	Potamogeton sp......	x	
Pterocarya	Pterocarya sp.......	x	

Quercus	Quercus sp..........	x
Rhus	Rhus sp.............	x
Rosaceae	Rosaceae............	x
Rubiaceae	Rubiaceae...........	x
Rutaceae	Ruta sp.............	x
Salix	Salix sp............	x
Sapotaceae	Sapotaceae..........	x
Sparganium	Sparganium sp.......	x
Symplocos	Symplocos sp........	x
Tilia	Tilia sp............	x
Typha	Typha sp............	x
Ulmus	Ulmus sp............	x
Vitaceae	Vitaceae............	x
Zelkova	Zelkova sp..........	x